

# **Tetraphenylethylene Luminogens: Design, Synthesis and Applications**

**Ph.D. Thesis**

*By*

**THAKSEN JADHAV**



**DISCIPLINE OF CHEMISTRY  
INDIAN INSTITUTE OF TECHNOLOGY INDORE  
NOVEMBER 2016**



# **Tetraphenylethylene Luminogens: Design, Synthesis and Applications**

**A THESIS**

*Submitted in partial fulfillment of the  
requirements for the award of the degree*

*of*

**DOCTOR OF PHILOSOPHY**

*By*

**THAKSEN JADHAV**



**DISCIPLINE OF CHEMISTRY  
INDIAN INSTITUTE OF TECHNOLOGY INDORE**

**NOVEMBER 2016**





# INDIAN INSTITUTE OF TECHNOLOGY INDORE

## CANDIDATE'S DECLARATION

I hereby certify that the work which is being presented in the thesis entitled "**Tetraphenylethylene Luminogens: Design, Synthesis and Applications**" in the partial fulfillment of the requirements for the award of the degree of **DOCTOR OF PHILOSOPHY** and submitted in the **DISCIPLINE OF CHEMISTRY, INDIAN INSTITUTE OF TECHNOLOGY INDORE**, is an authentic record of my own work carried out during the time period from JANUARY 2012 to NOVEMBER 2016 under the supervision of **Dr. RAJNEESH MISRA**, Associate Professor, Indian Institute of Technology Indore.

The matter presented in this thesis has not been submitted by me for the award of any other degree of this or any other institute.

**Signature of the student with date**  
**THAKSEN JADHAV**

This is to certify that the above statement made by the candidate is correct to the best of my/our knowledge.

Signature of Thesis Supervisor with date

**Dr. RAJNEESH MISRA**

**THAKSEN JADHAV** has successfully given his Ph.D. Oral Examination held on **<Date of PhD Oral Examination>**.

Signature(s) of Thesis Supervisor(s)

Date:

Convener, DPGC

Date:

Signature of PSPC Member #1

Date:

Signature of PSPC Member #1

Date:

Signature of External Examiner

Date:



# ACKNOWLEDGEMENTS

The work described in this thesis would not have been possible without numerous people who were always there when I required them the most. I take this opportunity to acknowledge them and extend my sincere gratitude for helping me and make this Ph.D. thesis possible.

I would like to express my sincere gratitude to my supervisor Dr. Rajneesh Misra for the continuous support during my Ph.D. study and research, for his patience, motivation, and enthusiasm. He has always guided me to acquire the best out of anything. It's his vigor and hunger to perform in adverse situation, which has inspired me to thrive for excellence and nothing less.

I express my gratitude to Dr. Shaikh M. Mobin for single crystal X-ray support and his valuable guidance. My sincere thanks also go to my PSpC members Dr. Chelvam Venkatesh, Dr. Sanjay K. Singh and Dr. Anand Parkash for their valuable suggestions and guidance. I would like to thank Dr. Biswarup Pathak, Dr. George Mathai, and Dr. Gourab Kanti Das for their guidance about theoretical study.

With great respect, I express my sincere thanks to Prof. Pradeep Mathur (Director, Indian Institute of Technology Indore) for his unending encouragement and providing all the facilities at Indian Institute of Technology Indore.

I am grateful to Dr. Satya S. Bulusu (Head, Discipline of Chemistry, Indian Institute of Technology Indore) for his suggestions and guidance in various aspects. I am also grateful to Dr. Suman Mukhopadhyay, Dr. Tridib K. Sarma, Dr. Anjan Chakraborty, Dr. Sampak Samanta, Dr. Tushar Mukharji, Dr. Apurba Das, Dr. Amrendra Kumar Singh and Dr. Deepa Dey for their guidance and help during various activities.

I would like to acknowledge all my teachers who have taught me in some or the other way since my childhood. I would have never achieved anything without

their guidance, blessing and support. I would like to extend my deepest gratitude to Dr. H. N. Gopi who guided me during my masters and also inspired me to pursue a career in research. I would also like to extend my sincere thanks to Dr. Wadia, Dr. G. C. Kulkarni, Dr. Chabukswar, Dr. Bahule, Dr. Hangarge, Dr. Nikam, Dr. Gokule, Mr. Borkar, Dr. Kamble, Mr. Kulkarni, Dr. Katte, Mr. Jadhav, Mr. Sonawane, Mr. Nevase, Mr. Lagad, Mr. Rahane, Mr. Mane, Mr. Jagtap, Mr. Shinde.

I personally extend my heartiest gratitude to Dr. Bhausaheb Dhokale for his constant guidance, help and support in all my ups and downs and during my initial days of the Ph. D. program. I extend my profound thanks to my group members, Dr. Prabhat, Dr. Rakesh Kumar Gupta, Dr. Pramod, Dr. Vijay, Mr. Ramesh, Mrs. Rekha, Mr. Yuvraj, Ms. Madhurima, Ms. Anupama, Mr. Jivan, Mr. Yogajivan, Mr. Bijesh, Mr. Rahul, Ms. Deepali, and Ms. Charu for their constant co-operation and help.

It has been wonderful to work with many friends and labmates together during my Ph.D., and I would like to record my thanks to Dr. N. Rajendra, Dr. Bhagwati, Dr. Tamalika, Dr. Dnyaneshwar, Dr. R. Thakur, Dr. Indrajit, Mr. Shivendra, Dr. Pradeep Kumar Jaiswal, Dr. Archana, Dr. Anvita, Dr. Veenu, Mr. Anupam, Ms. Sonam, Mr. Debashish, Mr. Maruthi, Mr. Biju, Ms. Anuradha, Mr. Rohit, Ms. Deepika, Ms. Kavita, Ms. Poulami Mandal Ms. Roopali, Mr. Akbar, Mr. Ajit, Mr. Anup, Mr. Arup Mahata, Mr. Kuber, Mr. Siddharth, Mr. Jonu and Mr. Ajay. My heart-felt thanks to my splendid juniors at IIT Indore for their generous co-operation and help. I am also thankful to all my friends who helped me directly or indirectly during my Ph. D.

I would also like to thank the technical staff of Sophisticated Instrumentation Center (SIC), IIT Indore, Ms. Sarita Batra, Mr. Kinny Pandey, Mr. Ghanshyam Bhavsar, Mr. Nitin Upadhyay, and Mr. Manish Kushwaha for their patience and timely technical support without which it was impossible to continue with my work. I would also like to thank Ms. Anjali Bandiwadekar, Mr. Gati Krishna Nayak, Mr. Rajesh Kumar, Mr. Lala Ram Ahirwar and other library staff and Mr.

Prahalad Singh Panwar, Mr. Manoj Pal, Mr. Nitin Bhate, and other technical and non-technical staff for their constant help, whenever required.

I would like to express my thanks to IIT Indore for infrastructure and University Grant Commission (UGC), New Delhi for my Fellowship.

I would like to express my heart filled thanks to all my friends Mr. Nitin Kadam, Mr. Bapu Kadam, Mr. Krishna Kadam, Mr. Mangesh Kadam, Mr. Yogesh Kadam, Mr. Ramdas Kadam, Mr. Santosh Kadam, Mr. Pradeep Kadam, Mr. Ajeet Jadhav, Mr. Santosh Jadhav, Mr. Yogesh Jadhav, Dr. Sandip Jadhav, Dr. Sachin Mali, Mr. Vikas Patil, Mr. Sarjerao Khochare, Mr. Shrikant Palwe, Mr. Yuvraj Kale, Mr. Ravi Salunkhe and Mr. Pratik Gore for their constant love and support.

I thank the Almighty for giving me the strength and patience to work through all these years.

Finally, I would like to acknowledge the people who mean the world to me, my parents, grandmother, brother and sisters. I don't imagine a life without their love and blessings.

**Thaksen Jadhav**  
**IIT Indore**



*DEDICATED TO MY FAMILY,  
TEACHERS, FRIENDS  
AND  
MY NATION.....INDIA*

**-THAKSEN**



# Synopsis

Design and synthesis of luminescent organic solids with different color emission have been continuously attracting the scientific community for various optoelectronic applications. However, most of the organic solids are non-emissive in the solid state due to the obstacle called aggregation caused quenching (ACQ). A great deal of efforts has been done to minimize the aggregate formation but have ended up with limited success. The formation of aggregates at high concentration or in solid state is an inherent phenomenon and difficult to prevent it. Tang *et al.* in 2001 utilized the aggregation phenomenon and developed an anti ACQ material which shows emission in the aggregated state and termed this concept as aggregation induced emission (AIE). The AIE materials are highly fluorescent in the solid state and work on the principle of restricted intramolecular rotations. Generally, the propeller shape molecule exhibits AIE behavior, and based on this concept various AIE active compounds have been developed.

The tetraphenylethylene (TPE) moiety has propeller shape molecular structure and exhibits AIE behavior. The TPE can be functionalized at various positions by changing the synthetic methodology. Owing to these properties TPE serves as an important luminogen in the field of solid state emission and being utilized in various applications such as organic light emitting diodes (OLEDs), metal ion sensors, mechano-sensors, supramolecular assemblies and in-vivo as well as in-vitro bio-imaging.

The fascinating properties of TPE derivatives inspired us to develop new TPE based luminogens which would be applicable in OLEDs and emerging area of mechano-sensors. We have coupled TPE to various chromophores such as phenanthroimidazole, pyrenoimidazole, benzothiadiazole and pyrazabole with varying degree of electronic structure and acceptor strength and further studied their photophysical, AIE and mechanochromic properties.

The main objectives of the present study are;

- To design and synthesize new TPE based AIE-active luminogens which can show different colored emission.
- To study the structure property relationship of the new TPE based luminogens.
- To explore the mechanochromic applications of the new TPE based AIE luminogens.
- To investigate mechanistic understanding of the AIE and mechanochromic effect.

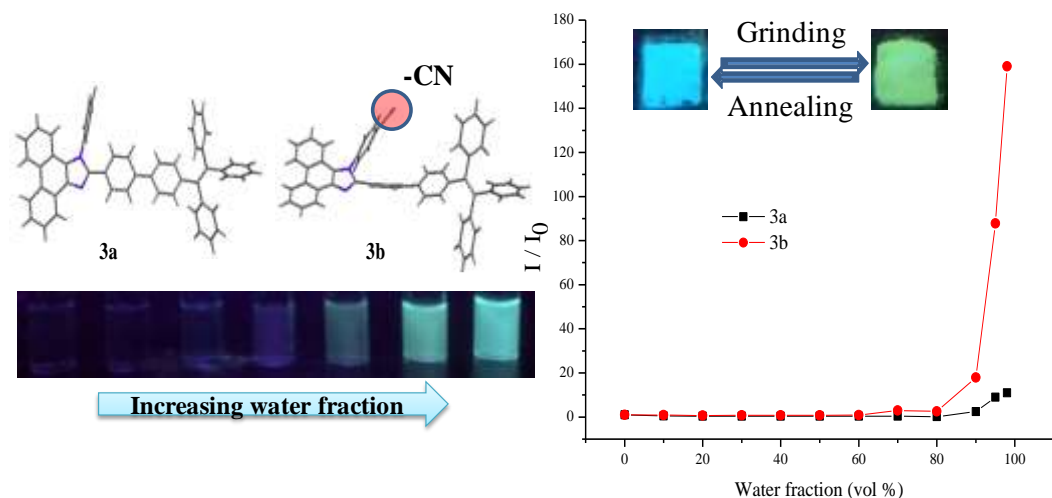
## **Chapter 1: Introduction**

This chapter describes how the AIE luminogens are important, followed by detailed discussion about synthesis, properties and applications of TPE based luminogens.

## **Chapter 2: Materials and experimental techniques**

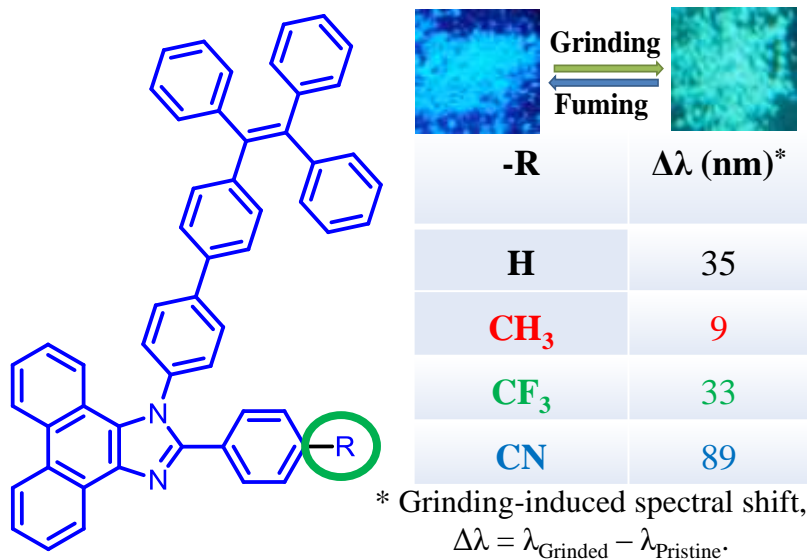
Chapter 2 summarizes the general experimental methods, characterization techniques and details of instruments used for characterization.

### Chapter 3: Tetraphenylethylene substituted phenanthroimidazole



In this chapter two TPE substituted phenanthroimidazoles **3a** and **3b** were synthesized by the Suzuki cross-coupling reaction. The molecule **3b** has additional cyano-group on the phenanthroimidazole ring. The single crystal structure, photophysical properties, AIE and mechanochromic properties are discussed. The crystal structure of **3a** and **3b** shows twisted geometries for TPE and phenyl rings and no  $\pi$ - $\pi$  stacking interaction in the crystal packing diagram. The presence of cyano-group in **3b** results in strong hydrogen bonding and higher extent of C-H $\cdots$  $\pi$  interactions which results in tight crystal packing in **3b** as compared to **3a**. The phenanthroimidazoles exhibit good thermal stability and cyano-group helps in further improvement of thermal stability. The cyano-group in phenanthroimidazole also enhances the AIE effect. The single crystal X-ray structure and packing analysis reveal that hydrogen bonding and strong supramolecular interactions are responsible for AIEE in **3b**. The **3a** and **3b** show reversible mechanochromic behavior with colors contrast between sky-blue and yellow green. The powder XRD study shows that destruction of crystalline state into amorphous state is associated with mechanochromism. The planarization induced enhanced conjugation may be the responsible for the mechanochromic behavior in TPE substituted phenanthroimidazoles.

## Chapter 4: Effect of end-groups on mechanochromism and electroluminescence in tetraphenylethylene substituted phenanthroimidazoles



In order to evaluate the positional effect of TPE unit and to study the effect on solid state emission and mechanochromism by changing different end groups on phenanthroimidazole, four TPE substituted phenanthroimidazoles **3a–3d** were designed. The phenanthroimidazoles **3a–3d** were synthesized by Suzuki coupling reaction of iodophenanthroimidazoles having different end groups (H, CH<sub>3</sub>, CF<sub>3</sub> and CN) with 4-(1,2,2-triphenylvinyl)phenylboronic acid pinacol ester in good yields. The single crystal structures of **2b**, **2c**, **3a** and **3d** are reported and show that the multiple phenyl rings in the TPE unit adopt non-planar orientation. Their photophysical, aggregation induced emission (AIE), mechanochromic, electrochemical and electroluminescence properties were studied. The phenanthroimidazoles **3a–3d** exhibit strong AIE effect. High color contrast reversible mechanochromism between blue and green color was observed for phenanthroimidazoles **3a–3d**. It was found that the solid state emission and mechanochromic behavior of tetraphenylethylene substituted phenanthroimidazoles **3a–3d** are function of the end group on phenanthroimidazole. The electroluminescence behavior of **3a** and **3d** was studied

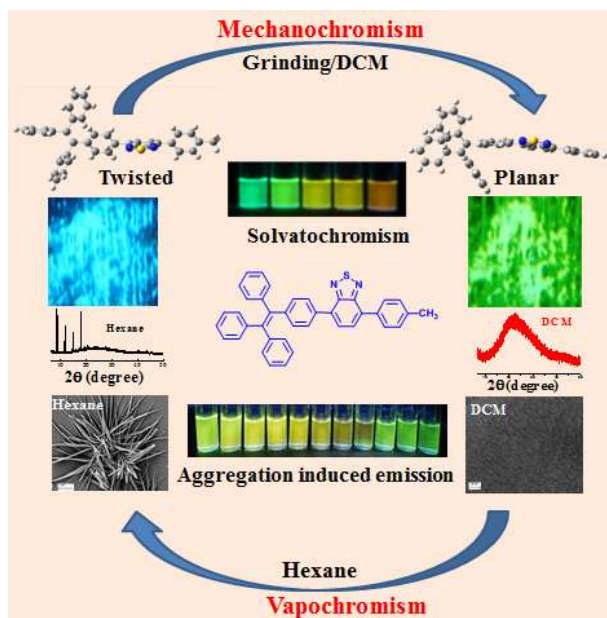
and performed well as non-doped blue emitters in the organic light-emitting diodes and exhibits 3.9% and 4.0% external quantum efficiency, respectively.

## Chapter 5: Tetraphenylethylene substituted phenanthroimidazole



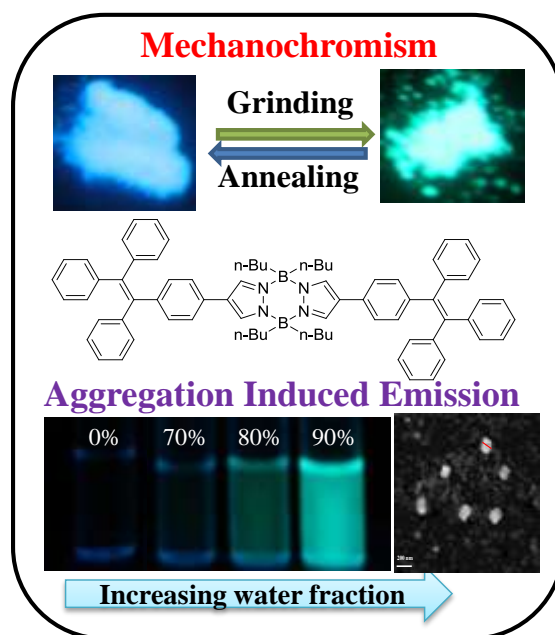
In order to evaluate the effect of increasing the conjugation on phenanthroimidazole, phenanthroimidazole was changed to pyrenoimidazole, along with the alteration in the TPE unit. Two pyrenoimidazole based luminogens **3a** and **3b** were designed and synthesized by the Pd-catalyzed Suzuki cross-coupling reaction of bromopyrenoimidazole with 4-(1,2,2-triphenylvinyl)phenylboronic acid pinacol ester and 2-(4-pinacoloboronphenyl)-3,3-diphenylacrylonitrile. The single crystal X-ray structure of **3a** was also studied and reveals the twisted conformation. Their photophysical, AIE and mechanochromic properties were studied. The pyrenoimidazoles **3a** and **3b** exhibit strong AIE. The **3b** show different colored emission with varying water fraction. The **3a** and **3b** exhibit reversible mechanochromic behavior with color contrast between blue and green. The enhanced conjugation and increasing amorphous nature after grinding are associated with mechanochromism in pyrenoimidazoles **3a** and **3b**.

## Chapter 6: Tetraphenylethylene substituted benzothiadiazole



In order to understand how the donor (D)/ acceptor (A) substituents and their substitution pattern affect the solution and solid-state optical properties, a series of symmetrical and unsymmetrical TPE substituted BTDs **3–8** were designed and synthesized by the Suzuki and Stille coupling reactions. Their solvatochromic, aggregation induced emission (AIE), mechanochromic, and vapochromic properties were studied and compared. The single crystal X-ray structures of BTDs **5** and **6** are reported. The BTDs **3–8** are highly fluorescent with tunable emissions. In BTDs **3–8**, solvent dependent emission was observed and their Lippert-Mataga plots showed a linear correlation of the Stokes shift with solvent polarity. The emission study in varying tetrahydrofuran (THF):water percentages showed enhanced emission in aggregates. The BTDs exhibit reversible multi-stimuli response towards mechanical force, solvent and heat. The detailed study using single crystal X-ray, photophysical properties, powder X-ray diffraction, scanning electron microscopy and theoretical calculation reveals that the planarization induced enhancement in conjugation and conversion of crystalline to amorphous state are responsible for mechanochromism and vapochromism.

## Chapter 7: Tetraphenylethylene substituted pyrazabole



In this chapter a TPE substituted pyrazabole was designed and synthesized by the Pd-catalyzed Suzuki cross-coupling reaction. The photophysical, AIE and mechanochromic properties of TPE substituted pyrazabole were studied. The pyrazabole TPE substituted pyrazabole exhibits strong aggregation induced emission (AIE) and the nanoaggregate formation was further characterized by dynamic light scattering (DLS) and scanning electron microscope (SEM). The reversible mechanochromic behavior with high color contrast between blue and green was observed. The powder XRD study shows that destruction of crystalline state into amorphous state is responsible for mechanochromism.



## LIST OF PUBLICATIONS

1. **Jadhav T.**, Dhokale B., Patil Y., Mobin S. M., Misra R.\* (2016), Multi-stimuli responsive donor–acceptor tetraphenylethylene substituted benzothiadiazoles, *J. Phys. Chem. C*, 120, 24030–24040 (DOI: 10.1021/acs.jpcc.6b09015).†
2. **Jadhav T.**, Dhokale B., Misra R.\* (2015), Effect of the cyano group on solid state photophysical behavior of tetraphenylethene substituted benzothiadiazoles. *J. Mater. Chem. C*, 2015, 3, 9063–9068 (DOI: 10.1039/C5TC01871D).†
3. **Jadhav T.**, Dhokale B., Mobin S. M., Misra R.\* (2015), Aggregation induced emission and mechanochromism in pyrenoimidazoles. *J. Mater. Chem. C*, 3, 9981–9988 (DOI: 10.1039/C5TC02181B).†
4. **Jadhav T.**, Choi J. M., Lee J. Y., Dhokale B., Mobin S. M., Misra R.\* (2016), Effect of end-groups on mechanochromism and electroluminescence in tetraphenylethylene substituted phenanthroimidazoles. *J. Phys. Chem. C*, 120, 18487–18495 (DOI: 10.1021/acs.jpcc.6b06277).†
5. Misra R.,\* **Jadhav T.**, Dhokale B., Mobin S. M. (2014), Reversible mechanochromism and enhanced AIE in tetraphenylethene substituted phenanthroimidazoles. *Chem. Commun.*, 50, 9076-9078 (DOI: 10.1039/C4CC02824D).†
6. **Jadhav T.**, Dhokale B., Patil Y., Misra R.\* (2015), Aggregation induced emission and mechanochromism in tetraphenylethene substituted pyrazabole. *RSC Adv.*, 5, 68187-68191 (DOI: 10.1039/C5RA12697E).†
7. **Jadhav T.**, Dhokale B., Mobin S. M., Misra R.\* (2015), Mechanochromism and aggregation induced emission in benzothiazole substituted tetraphenylethylenes: a structure function correlation, *RSC Adv.*, 5, 29878-29884 (DOI: 10.1039/C5RA04881H).

8. **Jadhav T.**, Choi J. M., Lee J. Y., Dhokale B., Misra R.\* (2016), Non-doped blue organic light emitting devices based on tetraphenylethylene- $\pi$ -imidazole derivatives, *Org. Electron.*, 37, 448–452 (DOI: 10.1016/j.orgel.2016.07.009)
9. Misra R.,\* **Jadhav T.**, Mobin S. M. (2014), Ferrocenyl pyrazaboles: design, synthesis, structure, and properties, *Dalt. Trans.*, 43, 2013–2022 (DOI: 10.1039/C3DT52315B).
10. **Jadhav T.**, Maragani R., Misra R.\* (2013), Design and synthesis of donor–acceptor pyrazabole derivatives for multiphoton absorption, *Dalt. Trans.*, 42, 4340 (DOI: 10.1039/c3dt33065f).
11. Misra R.,\* **Jadhav T.**, Dhokale B., Mobin S. M. (2015), Colorimetric and fluorimetric detection of fluoride and cyanide ions using tri and tetra coordinated boron containing chromophores, *Dalt. Trans.*, 44, 16052–16060 (DOI: 10.1039/C5DT02356D).
12. Misra R.,\* **Jadhav T.**, Dhokale B., Gautam P., Sharma R., Maragani R., Mobin S. M. (2014), Carbazole-BODIPY conjugates: design, synthesis, structure and properties, *Dalt. Trans.*, 43, 13076 (DOI: 10.1039/C4DT00983E)
13. **Jadhav T.**, Misra R.,\* Biswas S., Sharma G. D. (2015), Bulk heterojunction organic solar cells based on carbazole–BODIPY conjugate small molecules as donors with high open circuit voltage, *Phys. Chem. Chem. Phys.*, 17, 26580–26588 (DOI: 10.1039/C5CP04807A).
14. Misra R.,\* **Jadhav T.**, Mobin S. M. (2013), Aryl pyrazaboles: a new class of tunable and highly fluorescent materials, *Dalt. Trans.*, 42, 7246 (DOI: 10.1039/C3DT52154K).
15. Dhokale B., **Jadhav T.**, Patil Y., Misra R.\* (2016), Symmetrical and unsymmetrical ferrocenyl perylenediimides: Design, synthesis and properties, *Dye. Pigment.*, 134, 164–170 (DOI: 10.1016/j.dyepig.2016.07.006).
16. Patil Y., **Jadhav T.**, Dhokale B., Misra R.\* (2016), Tuning of the HOMO-LUMO gap of symmetrical and unsymmetrical ferrocenyl-substituted

- diketopyrrolopyrroles, *European J. Org. Chem.*, 733–738 (DOI: 10.1002/ejoc.201501123).
17. Misra R.,\* Dhokale B., **Jadhav T.**, Mobin S. M. (2014), The quenching of fluorescence as an indicator of donor-strength in *meso* arylethynyl BODIPYs, *Dalt. Trans.*, 43, 4854 (DOI: 10.1039/c3dt53056f).
  18. Dhokale B., **Jadhav T.**, Mobin S M., Misra R.\* (2016), Tetracyanobutadiene functionalized ferrocenyl BODIPY dyes, *Dalt. Trans.*, 45, 1476–1483 (DOI: 10.1039/C5DT04037J).
  19. Maragani R., **Jadhav T.**, Mobin S. M., Misra R.\* (2012), Synthesis, structure, photophysical, and electrochemical properties of donor–acceptor ferrocenyl derivatives, *Tetrahedron*, 68, 7302–7308 (DOI: 10.1016/j.tet.2012.06.094).
  20. Dhokale B., **Jadhav T.**, Mobin S. M., Misra R.\* (2015), Synergistic effect of donors on tetracyanobutadine (TCBD) substituted ferrocenyl pyrenes, *RSC Adv.*, 5, 57692–57699 (DOI: 10.1039/C5RA11433K).
  21. Sahu S. N., Gupta M. K., **Jadhav T.**, et al. (2014), Substituent dependent tunable fluorescence in thieno[3,2-c]pyrans, *RSC Adv.*, 4, 56779–56783 (DOI: 10.1039/C4RA11337C).
  22. Misra R.,\* Dhokale B., **Jadhav T.**, Mobin S. M. (2014), *meso*-Aryloxy and *meso*-arylaza linked BODIPY dimers: synthesis, structures and properties, *New J. Chem.*, 38, 3579 (DOI: 10.1039/C4NJ00354C)
  23. Dhokale B., **Jadhav T.**, Mobin S M., Misra R.\* (2015), *Meso* enyne substituted BODIPYs: synthesis, structure and properties, *Dalt. Trans.*, 44, 15803–15812 (DOI: 10.1039/C5DT00565E).
  24. Dhokale B., **Jadhav T.**, Mobin S. M., Misra R.\* (2014), *Meso* enamine substituted BODIPYs, *Chem. Commun.*, 50, 9119 (DOI: 10.1039/C4CC03857F).
  25. Misra R.,\* Dhokale B., **Jadhav T.**, Mobin S. M. (2014), Heteroatom-connected ferrocenyl BODIPYs: synthesis, structure, and properties, *Organometallics*, 33, 1867–1877 (DOI: 10.1021/om5002292).

26. Misra R.,\* Maragani R., **Jadhav T.**, Mobin S. M. (2014), Ferrocenyl end capped molecular rods: synthesis, structure, and properties, *New J. Chem.*, 38, 1446 (DOI: 10.1039/c3nj01244a).
27. Misra R.,\* Dhokale B., **Jadhav T.**, Mobin S. M. (2013), Donor–acceptor meso-alkynylated ferrocenyl BODIPYs: synthesis, structure, and properties, *Dalt. Trans.*, 42, 13658 (DOI: 10.1039/c3dt51374b).
28. Misra R.,\* Gautam P., **Jadhav T.**, Mobin S. M. (2013), Donor–acceptor ferrocenyl-substituted benzothiadiazoles: Synthesis, structure, and properties, *J. Org. Chem.*, 78, 4940–4948 (DOI: 10.1021/jo4005734).
29. Patil Y., **Jadhav T.**, Dhokale B., Misra R.\* (2016), Design and Synthesis of Low HOMO-LUMO Gap N- Phenylcarbazole-substituted diketopyrrolopyrroles, *Asian J. Org. Chem.*, 5, 1008–1014 (DOI: 10.1002/ajoc.201600194).
30. Maragani R., **Jadhav T.**, Mobin S. M., Misra R.\* (2013), C3 symmetric ferrocenyl triazines: synthesis, structure, and properties, *RSC Adv.*, 3, 2889 (DOI: 10.1039/c2ra23153k).
31. Dhokale B., **Jadhav T.**, Mobin S. M., Misra R.\* (2015), Meso alkynylated tetraphenylethylene (TPE) and 2,3,3-Triphenylacrylonitrile (TPAN) substituted BODIPYs, *J. Org. Chem.*, 80, 8018–8025 (DOI: 10.1021/acs.joc.5b01117).

†Papers pertaining to the thesis.

## **CONFERENCE AND WORKSHOPS PRESENTATION**

1. **Jadhav, T.**, Dhokale, B., Misra, R.,\* Mechanochromic and AIE active tetraphenylethene substituted phenanthroimidazoles, 8<sup>th</sup> Asian

- Photochemistry conference (APC-2014), Trivandrum, India (10-13th Nov, 2014); Poster presented.
2. **Jadhav, T.**, Dhokale, B., Misra, R.\* Ferrocenyl pyrazaboles: design, synthesis, structure, and properties, Frontier Lecture Series in Chemistry (FLSC-2014), Indore, India (30-31<sup>st</sup> Jan, 2014); Poster presented.
  3. **Jadhav, T.**, Dhokale, B., Misra, R.,\* Tetraphenylethene substituted benzothiadiazoles: Aggregation induced emission and mechanochromism, Aggregation Induced Emission: Faraday Discussion, Guangzhou, China (18-20<sup>th</sup> Nov, 2016); Poster Accepted.
  4. International Winter School on “Organic Electronic Materials and Devices” (OMED-2013), NITK Surathkal, Mangalore, India (19-21<sup>th</sup> Dec, 2013)(Workshop).
  5. Global Initiative on Academic Network Indian Institute of Technology Indore on “Introduction to principles of Green Chemistry” Indore, India (17-24<sup>st</sup> Jun, 2016) (Workshop).
  6. Workshop on Introduction to Gaussian: Theory and practice Delhi, India (17-21<sup>th</sup> Dec, 2012).
  7. Workshop on Introduction to Gaussian: Theory and practice Delhi, India (6-10<sup>th</sup> Jan, 2014).
  8. Workshop on Laboratory Health and Safety Workshop, IIT Indore, India(4<sup>th</sup> April 2014).



# TABLE OF CONTENTS

<b>LIST OF FIGURES</b>	<b>XXVII</b>
<b>LIST OF SCHEMES</b>	<b>XXXIII</b>
<b>LIST OF TABLES</b>	<b>XXXIV</b>
<b>LIST OF ACRONYMS</b>	<b>XXXVII</b>
<b>LIST OF NOMENCLATURE</b>	<b>XXXIX</b>

## **1. Chapter 1** 1-30

### **General introduction and background**

1.1	Background	1
1.2	Aggregation-Induced Emission (AIE)	2
1.3	Luminogens with Aggregation-Induced Emission Characteristics	4
1.4	Tetraphenylethylene (TPE)	5
1.5	Synthesis of Tetraphenylethylene	6
1.6	Applications of Tetraphenylethylene Derivatives	8
1.6.1	Organic Light Emitting Diodes (OLEDs)	8
1.6.2	Fluorescent Sensors	10
1.6.2.1	Metal Ion Sensing	10
1.6.2.2	Bio Sensing	11
1.6.2.3	Nitro Sensing	12
1.6.3	Liquid crystalline materials from TPE derivatives	13
1.6.4	TPE derivative in metal organic frameworks and complexes	14
1.6.5	Stimuli Responsive Materials	15
1.6.5.1	Mechanochromic Materials	15

1.6.6	Biological Imaging	18
1.7	Organization of thesis	19
1.8	Reference	20
<b>2.</b>	<b>Chapter 2</b>	<b>31-34</b>
	<b>Materials and experimental techniques</b>	
2.1	Introduction	31
2.2	Chemicals used for synthesis	31
2.3	Spectroscopic Measurements	32
2.4	Electrochemical Studies	32
2.5	Powder XRD	32
2.6	Computational Calculations	32
2.7	Single Crystal X-ray Diffraction Studies	33
2.8	Scanning electron microscopy (SEM)	33
2.9	Thermogravimetric analysis (TGA)	33
2.10	Dynamic light scattering (DLS)	33
2.11	Mechanochromism study	33
2.12	References	34
<b>3.</b>	<b>Chapter 3</b>	<b>35-52</b>
	<b>Reversible mechanochromism and enhanced AIE in tetraphenylethene substituted phenanthroimidazoles</b>	
3.1	Introduction	35
3.2	Results and discussion	36
3.2.1	Synthesis	36
3.2.2	Thermogravimetric analysis	37
3.2.3	Photophysical properties	38

3.2.4	Mechanochromic property	40
3.2.5	Theoretical Calculations	42
3.2.6	Single crystal X-ray diffraction studies	44
3.3	Experimental Section	46
3.4	Conclusion	48
3.5	References	48
<b>4.</b>	<b>Chapter 4</b>	<b>53-75</b>
	<b>Effect of end-groups on mechanochromism in tetraphenylethylene substituted phenanthroimidazoles</b>	
4.1	Introduction	53
4.2	Results and discussion	54
4.2.1	Synthesis	54
4.2.2	Thermogravimetric analysis	55
4.2.3	Photophysical properties	55
4.2.4	Mechanochromic property	58
4.2.5	Electrochemical properties	62
4.2.6	Theoretical Calculations	63
4.2.7	Single crystal X-ray diffraction studies	65
4.3	Experimental Section	68
4.4	Conclusion	71
4.5	References	71
<b>5.</b>	<b>Chapter 5</b>	<b>77-98</b>

## **Aggregation induced emission and mechanochromism in pyrenoimidazoles**

5.1	Introduction	77
5.2	Results and discussion	78
5.2.1	Synthesis	78
5.2.2	Thermogravimetric analysis	79
5.2.3	Photophysical properties	79
5.2.4	Mechanochromic property	85
5.2.5	Theoretical Calculations	87
5.2.6	Single crystal X-ray diffraction studies	88
5.3	Experimental Section	90
5.4	Conclusion	92
5.5	References	93

## **6. Chapter 6** 99-136

### **Multi-stimuli responsive donor-acceptor tetraphenylethylene substituted benzothiadiazoles**

6.1	Introduction	99
6.2	Results and discussion	101
6.2.1	Synthesis	101
6.2.2	Single crystal X-ray diffraction studies	102
6.2.3	Thermogravimetric analysis	105
6.2.4	Theoretical Calculations	106
6.2.5	Photophysical properties	108

6.2.6	Mechanochromic property	113
6.2.7	Vapochromic property	120
6.3	Experimental Section	122
6.4	Conclusion	125
6.5	References	126
<b>7.</b>	<b>Chapter 7</b>	<b>137-149</b>
	<b>Aggregation induced emission and mechanochromism in tetraphenylethene substituted pyrazabole</b>	
7.1	Introduction	137
7.2	Results and discussion	138
7.2.1	Synthesis	138
7.2.2	Thermogravimetric analysis	138
7.2.3	Theoretical Calculations	139
7.2.4	Photophysical properties	140
7.2.5	Mechanochromic property	142
7.3	Experimental Section	143
7.4	Conclusion	144
7.5	References	144
<b>8.</b>	<b>Chapter 8</b>	<b>151-155</b>
	<b>Conclusions and future scope</b>	<b>151-155</b>
8.1	Introduction	151
8.2	Results and discussion	153



# LIST OF FIGURES

<b>Figure 1.1</b>	Schematic presentation of ACQ effect of planar pyrene molecule.	2
<b>Figure 1.2</b>	Fluorescence photographs of HPS in acetonitrile/water mixtures with different water fractions.	3
<b>Figure 1.3</b>	Schematic presentation of mechanism involving AIE as restricted intramolecular rotation in hexaphenylsilole (HPS) luminogen.	4
<b>Figure 1.4</b>	Structure of tetraphenylethylene.	6
<b>Figure 1.5</b>	Configuration of WOLED constructed from TTPEPy and BTPETTD and photos of the B, R, and WOLEDs.	10
<b>Figure 1.6</b>	Schematic diagram of detection of Hg <sup>2+</sup> ion.	11
<b>Figure 1.7</b>	Fluorescence “turn-on” probe for specific detection of glucose.	12
<b>Figure 1.8</b>	(A) TPE esters used in the study (B) Polarizing microscopy image of tetrakis[4-(trisalkyloxybenzoyloxy)phenyl]ethenes showing fan shaped texture (C) Possible arrangement of tetrakis[4-(trisalkyloxybenzoyloxy)phenyl]ethenes in the hexagonal columnar mesophase.	14
<b>Figure 1.9</b>	Multicomponent coordination driven self-assembly of tetragonal prisms.	15
<b>Figure 1.10</b>	The molecular structure of TPE substituted luminogen and their reversible mechanochromic behavior, annealing sample (a) and pressing sample (b) under 365 nm UV light.	16
<b>Figure 1.11</b>	ESPy–Zn taken at room temperature under ambient light (left) and UV light (right). Samples: bas, as-synthesized sample; Gb1, ground sample; Fb1, fumed sample (ground sample in methanol vapor for five	17

	minutes); Ab1, annealed sample (the ground sample was annealed at 300 °C for 1 hour and cooled down at room temperature); Gb2, re-ground sample; Fb2, re-fumed sample; Ab2, re-annealed sample.	
<b>Figure 1.12</b>	Fluorescent images of the HeLa cells stained by (A) benzothiazolium and (B) pyridinium salts.	19
<b>Figure 3.1</b>	Thermogravimetric analysis of <b>3a</b> and <b>3b</b> , measured at a heating rate of 10 °C/ min under nitrogen atmosphere.	38
<b>Figure 3.2</b>	(A) Electronic absorption spectra of <b>3a</b> and <b>3b</b> recorded in dichloromethane. Fluorescence spectra of <b>3a</b> (B), and <b>3b</b> (C) in THF-water mixtures with different water fractions. (D) Plot of Photoluminescence intensity (PL) vs. % of water fraction ( $f_w$ ). Luminogen concentration: 10 $\mu$ M; excitation wavelength: 340 nm; intensity calculated at $\lambda_{max}$ .	39
<b>Figure 3.3</b>	Fluorescence pictures of <b>3b</b> solutions with different water fractions under UV (365 nm) light.	39
<b>Figure 3.4</b>	Solid state absorption spectra of <b>3a</b> in crystalline (left) and its grinded (right) form.	40
<b>Figure 3.5</b>	Solid state absorption spectra of <b>3b</b> in crystalline (left) and its grinded (right) form.	40
<b>Figure 3.6</b>	(A) Emission spectra of (A) <b>3a</b> and (B) <b>3b</b> as pristine, grinded and fumed solids and photograph taken under 365 nm UV illumination.	41
<b>Figure 3.7</b>	Repeated switching of the solid-state fluorescence of <b>3a</b> and <b>3b</b> by repeated grinding and fuming cycles.	42
<b>Figure 3.8</b>	The XRD patterns of (A) <b>3a</b> and (B) <b>3b</b> as synthesized, grinded and heated solids.	42
<b>Figure 3.9</b>	HOMO and LUMO frontier molecular orbitals of <b>3a</b>	43

and **3b** at the B3LYP/6-31G (d) level.

<b>Figure 3.10</b>	Crystal structures of <b>3a</b> and <b>3b</b> and Crystal packing of <b>3b</b> .	44
<b>Figure 3.11</b>	Crystal packing of <b>3a</b> and <b>3b</b> .	44
<b>Figure 4.1</b>	Thermogravimetric analysis of phenanthroimidazoles <b>3a–3d</b> measured at a heating rate of 10 °C/ min under nitrogen atmosphere.	55
<b>Figure 4.2</b>	UV-vis absorption spectra of phenanthroimidazoles <b>3a–3d</b> in THF–water mixtures with different water fractions.	57
<b>Figure 4.3</b>	Fluorescence spectra of <b>3a</b> (A), <b>3b</b> (B), <b>3c</b> (A) and <b>3d</b> (D) in THF–water mixtures with different water fractions (10 $\mu$ M). (E) Plot of photoluminescence intensity (PL) vs. % of water fraction ( $f_w$ ). Luminogen concentration: 10 $\mu$ M; intensity calculated at $\lambda_{\max}$ .	58
<b>Figure 4.4</b>	Emission spectra of (A) <b>3a</b> , (B) <b>3b</b> , (C) <b>3c</b> and (D) <b>3d</b> as Synthesized, Grinded and Fumed solids and photograph taken under 365 nm UV illuminations.	59
<b>Figure 4.5</b>	Solid state absorption spectra of <b>3a</b> in crystalline and its grinded form.	60
<b>Figure 4.6</b>	Solid state absorption spectra of <b>3b</b> in crystalline and its grinded form.	60
<b>Figure 4.7</b>	Solid state absorption spectra of <b>3c</b> in crystalline and its grinded form.	60
<b>Figure 4.8</b>	Solid state absorption spectra of <b>3d</b> in crystalline and its grinded form.	61
<b>Figure 4.9</b>	PXRD curves of <b>3a</b> (A), <b>3b</b> (B), <b>3c</b> (C) and <b>3d</b> (D) in Synthesized, Grinded and Fumed form.	62
<b>Figure 4.10</b>	Cyclic voltammetry (CV) plots of <b>3a–3d</b> .	63
<b>Figure 4.11</b>	HOMO and LUMO frontier molecular orbitals of	64

	phenanthroimidazoles <b>3a–3d</b> at the B3LYP/6-31G (d) level.	
<b>Figure 4.12</b>	(A) Crystal structure of <b>3a</b> . (B) Crystal structure of <b>3c</b> having two molecules in asymmetric unit.	65
<b>Figure 4.13</b>	Crystal packing diagram of <b>3a</b> .	66
<b>Figure 4.14</b>	Crystal packing diagram of <b>3c</b> .	66
<b>Figure 5.1</b>	Thermogravimetric analysis of <b>3a</b> , and <b>3b</b> measured at a heating rate of 10 °C/ min under nitrogen atmosphere.	79
<b>Figure 5.2</b>	(A) Electronic absorption spectra of pyrenoimidazoles <b>3a</b> and <b>3b</b> recorded in THF. Absorption spectra of <b>3a</b> (B) and <b>3b</b> (C) in different solvents with varying polarities. Photoluminescence spectra of <b>3a</b> (D) and <b>3b</b> (E) in different solvents with varying polarities (excitation wavelength or $\lambda_{\text{ex}} = 340$ nm).	80
<b>Figure 5.3</b>	(A) Fluorescence spectra of <b>3a</b> , and (B) <b>3b</b> in THF–water mixtures with different water fractions. (C) Plot of fluorescence intensity (PL) vs. % of water fraction ( $f_w$ ). Luminogen concentration: 10 $\mu\text{M}$ ; excitation wavelength: 340 nm; intensity calculated at $\lambda_{\text{max}}$ .	82
<b>Figure 5.4</b>	Photographs of <b>3a</b> (A) and <b>3b</b> (B) in THF–water mixtures with different water fractions (10 $\mu\text{M}$ ) under 365 nm UV illumination.	83
<b>Figure 5.5</b>	The particle size distributions of <b>3a</b> in THF–water mixture (A) at 90% ( $f_w$ ) and <b>3b</b> in THF–water mixture (B) at 70% ( $f_w$ ) and (C) at 95% ( $f_w$ ).	84
<b>Figure 5.6</b>	UV-vis absorption spectra of <b>3a</b> (left) and <b>3b</b> (right) in THF–water mixtures with different water fractions; Luminogen concentration: 10 $\mu\text{M}$ .	85
<b>Figure 5.7</b>	Emission spectra of <b>3a</b> (left) and <b>3b</b> (right) as Pristine, Ground and Heated solids and photograph taken under 365 nm UV illumination.	86

<b>Figure 5.8</b>	Solid state absorption spectra of <b>3a</b> (left) and <b>3b</b> (right) in crystalline and its ground form.	86
<b>Figure 5.9</b>	PXRD curves of <b>3a</b> (left) and <b>3b</b> (right) in Pristine, Ground and Fumed form.	87
<b>Figure 5.10</b>	Correlation diagram showing the HOMO, and LUMO wave functions and energies of the pyrenoimidazoles <b>3a</b> (left) and <b>3b</b> (right).	88
<b>Figure 5.11</b>	Crystal structure (left) and C-H--- $\pi$ interactions assisted crystal packing (right) of <b>3a</b> .	90
<b>Figure 6.1</b>	Crystal structure of BTDs <b>5</b> and <b>6</b> (i) Front view, (ii) Side view.	104
<b>Figure 6.2</b>	Crystal packing diagram of BTD <b>5</b> along <i>b</i> -axis.	104
<b>Figure 6.3</b>	Crystal packing diagram of BTD <b>6</b> along tilted <i>a</i> -axis.	105
<b>Figure 6.4</b>	Thermogravimetric analysis of the BTDs <b>3–9</b> , measured at a heating rate of 10 °C/ min under nitrogen atmosphere.	106
<b>Figure 6.5</b>	Frontier molecular orbitals HOMO and LUMO of the BTDs <b>3–9</b> .	107
<b>Figure 6.6</b>	Correlation diagram showing the HOMO, and LUMO energies of the BTDs <b>3–9</b> , as determined at the B3LYP/6-31G(d) level.	108
<b>Figure 6.7</b>	(A) Normalized absorption spectra and (B) Fluorescence spectra of BTDs <b>3–9</b> recorded in dichloromethane.	108
<b>Figure 6.8</b>	Normalized absorption spectra of BTDs <b>3(A)</b> , <b>4(B)</b> , <b>5(C)</b> , <b>6(D)</b> , <b>7(E)</b> , <b>8(F)</b> and <b>9(G)</b> in different solvents with different polarities.	109
<b>Figure 6.9</b>	Photoluminescence spectra of BTDs <b>3(A)</b> , <b>4(B)</b> , <b>5(C)</b> , <b>6(D)</b> , <b>7(E)</b> , <b>8(F)</b> and <b>9(G)</b> in different solvents with different polarities (concentration = $1 \times 10^{-5}$ M, excitation = 370 nm). (H) Stokes Shift ( $\Delta\nu$ ) of BTDs	110

	3–9 as a function of the solvent polarity parameter ( $\Delta f$ ).	
<b>Figure 6.10</b>	Fluorescence spectra of BTDs <b>3</b> (A), <b>4</b> (B), <b>5</b> (C), <b>6</b> (D), <b>7</b> (E), <b>8</b> (F) and <b>9</b> (G) in THF–Water mixtures with different water fractions (10 $\mu$ M). (H) Plot of fluorescence intensity (PL) vs. % of water fraction ( $f_w$ ). Luminogen concentration: 10 $\mu$ M; intensity calculated at $\lambda_{\text{max}}$ of BTDs <b>3–9</b> .	112
<b>Figure 6.11</b>	(A) Photograph of synthesized solid of BTDs <b>3–9</b> under 365 nm UV illumination. (B) Photograph of BTD <b>9</b> in THF–water mixtures with different water fractions (10 $\mu$ M) under 365 nm UV illumination.	113
<b>Figure 6.12</b>	Emission spectra of <b>3</b> (A), <b>4</b> (B), <b>5</b> (C), <b>6</b> (D), <b>7</b> (E), <b>8</b> (F) and <b>9</b> (G) as Pristine, Grinded and Fumed solids and photographs taken under 365 nm UV illumination.	114
<b>Figure 6.13</b>	photograph taken under 365 nm UV illumination of BTDs <b>3</b> (A), <b>4</b> (B), <b>5</b> (C), <b>6</b> (D), <b>7</b> (E), <b>8</b> (F) and <b>9</b> (G) as pristine and ground solids.	115
<b>Figure 6.14</b>	Absorption spectra of BTDs <b>3</b> (A), <b>4</b> (B), <b>5</b> (C), <b>6</b> (D), <b>7</b> (E), <b>8</b> (F) and <b>9</b> (G) as pristine and grinded solids.	117
<b>Figure 6.15</b>	Correlation diagram showing the HOMO, LUMO and HOMO-LUMO gap energies of BTD <b>5</b> , twisted BTD <b>6</b> (BTD <b>6T</b> ) and planar BTD <b>6</b> (BTD <b>6P</b> ), determined at the B3LYP/6-31G(d) level.	118
<b>Figure 6.16</b>	Powder XRD patterns of BTDs <b>3</b> (A), <b>4</b> (B), <b>5</b> (C), <b>6</b> (D), <b>7</b> (E), <b>8</b> (F) and <b>9</b> (G) in the state of as-prepared solid, after grinding and solvent fumigation treatment.	119
<b>Figure 6.17</b>	Emission spectra of BTDs <b>3</b> (A), <b>4</b> (B), <b>5</b> (C), <b>6</b> (D), <b>7</b> (E), <b>8</b> (F) and <b>9</b> (G) as solids from Hexane and dichloromethane (DCM).	121
<b>Figure 6.18</b>	Emission spectra of BTD <b>6</b> (left) and BTD <b>8</b> (right) as	122

	solids from Hexane and dichloromethane and photograph taken under 365 nm UV illumination.	
<b>Figure 6.19</b>	The SEM of thin films of BTD <b>6</b> from (A) Hexane solution and from (B) DCM solution; (C) PXRD graph of thin films of BTD <b>6</b> from Hexane solution and DCM.	122
<b>Figure 7.1</b>	Thermogravimetric analysis of <b>2</b> , measured at a heating rate of 10 °C/ min under nitrogen atmosphere.	139
<b>Figure 7.2</b>	Energy optimized structure of pyrazabole <b>2</b> at the B3LYP/6-31G (d) level.	140
<b>Figure 7.3</b>	(A) Fluorescence spectra of pyrazabole <b>2</b> in THF-water mixtures with different water fractions, (B) Plot of Photoluminescence intensity (PL) vs % of water fraction ( $f_w$ ). Luminogen concentration: 10 $\mu$ M; excitation wavelength: 340 nm; intensity calculated at $\lambda_{max}$ . Inset photograph of <b>2</b> in THF–water mixtures with different water fractions (10 $\mu$ M) under 365 nm UV illumination.	141
<b>Figure 7.4</b>	UV-Vis absorption spectra of <b>2</b> in THF–water mixtures with different water fractions.	141
<b>Figure 7.5</b>	The particle size distributions of <b>2</b> in THF–water mixture (10:90, v:v) (Left) and SEM image (right).	142
<b>Figure 7.6</b>	(A) Emission spectra of <b>2</b> as pristine, grinded and fumed solids; Photograph taken under 365 nm UV illumination. (B) Repeated switching of the solid-state fluorescence of <b>2</b> by repeated grinding and fuming cycles.	143
<b>Figure 7.7</b>	PXRD curves of <b>2</b> in pristine, grinded and fumed form.	143

## LIST OF SCHEMES

<b>Scheme 1.1</b>	Synthesis of TPE by using Knoevenagel like condensation reaction.	6
<b>Scheme 1.2</b>	Synthesis of TPE by using McMurry like condensation reaction.	7
<b>Scheme 1.3</b>	Synthesis of TPE by using selenobenzophenones with diphenyldiazomethane.	7
<b>Scheme 1.4</b>	Synthesis of TPE from diphenyldichloromethane.	8
<b>Scheme 1.5</b>	The reversible fluorescence quenching mechanism of SNF with PA based on photoinduced electron transfer and/or energy transfer.	13
<b>Scheme 3.1</b>	Synthetic route to intermediate <b>5</b> .	36
<b>Scheme 3.2</b>	Synthetic route for the phenanthroimidazoles <b>3a</b> and <b>3b</b> .	37
<b>Scheme 4.1</b>	Synthesis of heteroatom connected ferrocenyl BODIPYs <b>2a</b> , <b>2b</b> , <b>3c</b> and <b>3d</b> .	54
<b>Scheme 5.1</b>	Synthetic route for the pyrenoimidazoles <b>3a</b> and <b>3b</b> .	78
<b>Scheme 6.1</b>	Synthetic route for BTDs <b>2</b> and <b>3</b> .	101
<b>Scheme 6.2</b>	Synthetic route for BTD <b>4</b> .	101
<b>Scheme 6.3</b>	Synthetic route for BTDs <b>5–9</b> .	102
<b>Scheme 7.1</b>	Synthetic route for the TPE substituted pyrazabole <b>2</b> .	138

## LIST OF TABLES

<b>Table 3.1</b>	Photophysical, and thermal properties of the <b>3a</b> and <b>3b</b> .	38
------------------	--	----

<b>Table 3.2</b>	Computed vertical transitions and their oscillator strengths and configurations.	43
<b>Table 3.3</b>	Crystal data and structure refinement parameters.	45
<b>Table 4.1</b>	Photophysical and thermal properties of the <b>3a–3d</b> .	56
<b>Table 4.2</b>	Peak emission wavelengths ( $\lambda$ , in nm) of <b>3a–3d</b> under various external stimuli.	58
<b>Table 4.3</b>	Computed vertical transitions and their oscillator strengths and configurations of <b>3a–3d</b> .	64
<b>Table 4.4</b>	Crystal data and structure refinement for <b>2b</b> , <b>2c</b> , <b>3a</b> and <b>3c</b> .	67
<b>Table 4.5</b>	Important distance of intermolecular interactions of <b>3a</b> and <b>3c</b> .	68
<b>Table 5.1</b>	Photophysical, and thermal properties of the <b>3a</b> and <b>3b</b> .	81
<b>Table 5.2</b>	Photophysical properties of <b>3a</b> and <b>3b</b> in different solvents.	82
<b>Table 5.3</b>	Crystal data and structure refinement for <b>3a</b> .	88
<b>Table 6.1</b>	Crystal data and structure refinement for BTD <b>5</b> and <b>6</b> .	103
<b>Table 6.2</b>	Photophysical properties of BTDs <b>3–9</b> in different solvents.	111
<b>Table 6.3</b>	Slopes of Lippert-Mataga plot for the BTDs <b>3–9</b> .	111
<b>Table 6.4</b>	Absorption and emission wavelengths of solid BTDs <b>3–9</b> under various external stimuli.	116
<b>Table 6.5</b>	Emission wavelengths of solid BTDs <b>3–9</b> after exposure to hexane and dichloromethane vapours.	121

## LIST OF CHARTS

<b>Chart 1.1</b>	Various molecules exhibiting aggregation induced emission phenomenon.	5
<b>Chart 6.1</b>	The TPE substituted BTDs <b>3–9</b> .	100



# ACRONYMS

TPE	Tetraphenylethylene
AIE	Aggregation Induced Emission
OLED	Organic Light Emitting Diode
ACQ	Aggregation Caused Quenching
TGA	Thermogravimetric Analysis
NMR	Nuclear Magnetic Resonance
PXRD	Powder X-ray diffraction
AFM	Atomic force microscopy
DCM	Dichloromethane
UV-vis	UV-Visible Spectroscopy
ESI-MS	Electrospray Ionization- Mass Spectrometry
CDCl <sub>3</sub>	Chloroform- <i>d</i>
Calcd.	Calculated
DLS	Dynamic Light Scattering
DMF	Dimethylformamide
Ph	Phenyl
SCXRD	Single Crystal X-ray Diffraction
PPh <sub>3</sub>	Triphenylphosphine
EtOH	Ethanol
MeOH	Methanol
THF	Tetrahydrofuran
TLC	Thin Layer Chromatography

TEA	Triethylamine
TOF-MS	Time-of-flight mass spectrometry
AcOH	Acetic acid
ACN	Acetonitrile

# NOMENCLATURE

$\alpha$	Alpha
$\beta$	Beta
$\gamma$	Gamma
$\phi$	Quantum Yield
$\text{\AA}$	Angstrom
$\lambda$	Wavelength
$\mu$	Micro
$\pi$	Pi
nm	Nanometer
mM	Milli Molar
$\mu\text{M}$	Micro Molar
$\epsilon$	Molar Extinction coefficient
cm	Centimeter
$^{\circ}$	Degree
mL	Milliliter
$\mu\text{L}$	Microliter
a. u.	Arbitrary Unit
$\lambda_{\text{ex}}$	Excitation Wavelength
$\lambda_{\text{em}}$	Emission Wavelength



# Chapter 1

## General introduction and background

### 1.1. Background

Organic  $\pi$ -conjugated materials have been proved as promising candidate for organic light emitting diodes (OLEDs),<sup>[1]</sup> organic fluorescent chemosensors,<sup>[2]</sup> flat panel displays<sup>[3]</sup> organic solid-state lasers,<sup>[4]</sup> and bioprobes<sup>[5]</sup> owing to their luminescence property. In order to increase the luminescence efficiency of organic luminogens, a simple and efficient plan is to extend the  $\pi$ -conjugation by connecting aromatic rings. The implementation of this plan resulted in organic luminogens having highly emissive nature in dilute solution. The luminescence behavior of such luminogens had been examined in solution state for laboratory purpose. Although in real world applications, luminogens are practically used in solid state. Unfortunately, most of these conventional luminogens in solid state or in high concentration weakens or quenches their emission, a result conventional luminogens are ineffective in applications. This quenching effect was first discovered by Forster and Kasper in 1954 for pyrene molecule. The fluorescence intensity of the pyrene molecule decreases upon increasing the solution concentration.<sup>[6]</sup> Eventually the quenching effect was recognized to be a common occurrence for most aromatic compounds. In the classic book of Birks on "*Photophysical Properties of Aromatic Molecules*" mentioned about this effect as "known to be common to most aromatic hydrocarbon and their derivatives".<sup>[7]</sup> This was an outcome of the strong interactions between ground state and excited molecules which triggered the formation of sandwich shaped excimers and exciplexes. The absence of solvent forces in concentrated state results solute molecules to be in close proximity. The large aromatic frameworks of luminogens particularly disc shaped molecules experience a strong  $\pi$ - $\pi$  stacking interaction leading to formation of random or ordered aggregates. The excited states of these aggregates form excimer or exciplexes and are

prone to decay *via* non radiative pathway. This phenomenon is commonly known as Aggregation caused quenching (ACQ) of light emission.<sup>[8]</sup>

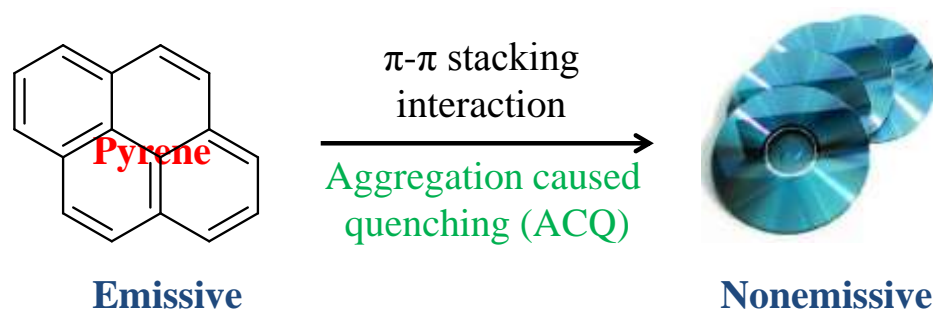


**Figure 1.1.** Schematic presentation of ACQ effect of planar pyrene molecule.

The ACQ effect is usual for many organic molecules and forces the researchers for using these luminogens in very dilute solutions. However multiple problems were encountered by using dilute solutions of luminogens such as emissions from dilute solutions are often weak, leading to poor sensitivity in fluorescence sensory systems, quick photo bleaching of dye molecules in dilute solutions when a harsh laser beam is employed as the excitation light source. Furthermore, many applications like OLEDs, full color displays, lighting, solid state lasers, mechano-sensors *etc.* require organic luminescent materials to be used in solid state.<sup>[8]</sup> The ACQ effect is a thorny obstacle and to minimize this, researchers have developed various chemical, physical and engineering approaches. The commonly used chemical approaches are use of branched alkyl chains, bulky substituents and spiro linkages to barricade/obstruct the aggregate formation.<sup>[9]</sup> During device fabrication ACQ effect is minimized by physical passivation *via* surfactant encapsulation (e.g. sodium dodecylsulfate) or blending non-conjugated polymers such as poly(methyl methacrylate) (PMMA).<sup>[10]</sup> Regardless of the attempts made, only limited success was achieved. The development of a system in which aggregation constructively enhances the emission of system is necessary. This would make development of emissive luminophores easier because aggregation now turns to advantage and no extra efforts would be required to artificially interrupt the natural process of luminophore aggregation.<sup>[11]</sup>

## 1.2. Aggregation-Induced Emission (AIE)

In 2001, Tang *et al.* reported an exciting phenomenon termed as aggregation induced emission (AIE). This was totally contradictory to the ACQ phenomenon, in which light emission was enhanced by aggregation. This unusual phenomenon was first observed for hexaphenylsilole (HPS) (Figure 1.2) derivatives, which are non-emissive in dilute solutions of good solvents (acetonitrile, tetrahydrofuran (THF) and chloroform).<sup>[12]</sup> Water being a poor solvent for HPS; the addition of large amount of water into the acetonitrile solution of HPS results in the formation of aggregates which are highly emissive. This kind of enhancement of emission induced by aggregation was termed as aggregation induced emission.<sup>[12]</sup>

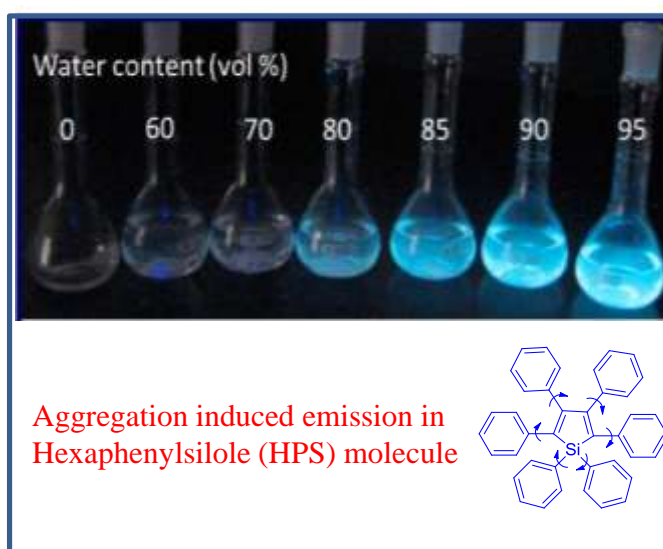


**Figure 1.2.** Fluorescence photographs of HPS in acetonitrile/water mixtures with different water fractions.

The AIE phenomenon was further studied by fluorescence spectroscopic analysis technique. The fluorescence of the HPS solution in acetonitrile was negligible (Figure 1.2) with a quantum yield ( $\Phi_F$ ) 0.22%.<sup>[13]</sup> After gradual increase in water percentage up to 50%, the  $\Phi_F$  value remains constant and beyond that increases promptly. The poor fluorescence of HPS in acetonitrile was enhanced in aggregated suspension (99% water fraction) by 255-folds ( $\Phi_F$ -56%). The AIE effect makes HPS highly fluorescent in the solid state. The absorption spectra of different acetonitrile and water concentration mixtures having high water concentration show absorption tails extending well

into the long wavelength region, this is due to the light scattering effect of nano-aggregates. This effect is well known in case of nanoparticles and termed as Mie effect.<sup>[14]</sup> The particle size analyses of HPS solution in the solvent mixtures with 80% and 90% water reveal the existence of particles with average sizes of 190 nm and 130 nm, respectively. This confirmed the HPS molecules aggregated into nanoparticles.

The six phenyl rings of HPS have non-planar geometry resulting in a propeller shaped molecule in the dilute solution of HPS. The phenyl rings exhibit intramolecular rotations through the single bond which act as a non radiative relaxation channel for the excited state. At higher concentration or in aggregated state the intramolecular rotations became restricted and consequently restricted the excited state decay by the radiative pathway. Tang's *et al.* has proposed this restriction of intramolecular rotation (RIR) in the aggregates is a main cause for the AIE effect (Figure 1.3). Since HPS has propeller shape, it does not exhibit  $\pi$ - $\pi$  stacking interactions in the aggregate form. The validity of the RIR hypothesis was proved by series of experiments where RIR process was modulated internally and externally.<sup>[15,16]</sup> The external RIR was proved by increasing the solution viscosity, lowering the temperature and pressurization which resulted boost in the emission of AIE molecules efficiently.<sup>[16]</sup> The structural perturbation turning the AIE active molecule to AIE inactive proves the RIR internally.<sup>[15]</sup>

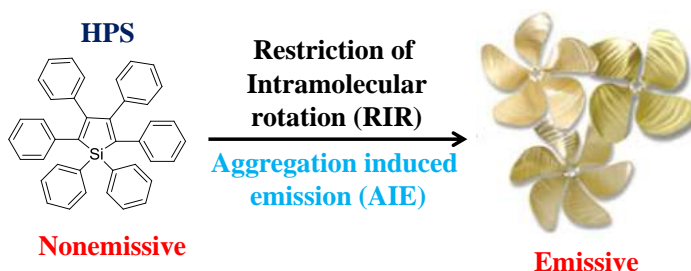


**Figure 1.3.** Schematic presentation of mechanism involving AIE as restricted intramolecular rotation in hexaphenylsilole (HPS) luminogen.

### 1.3. Luminogens with Aggregation-Induced Emission Characteristics

Fascinated by the exciting phenomenon and its broad outlooks, more and more researchers have done a large amount of outstanding work. Guided

by the basic understanding, researchers have synthesized different kinds of molecules with a structural feature of propeller-shape, consisting of multiple phenyl rotors and olefinic or aromatic stators to suppress intermolecular interactions. Some examples of the AIEgens are summarized in Chart 1.1. [12a,15b,17] The promising and efficient strategy to convert ACQ fluorophore to AIEgen is by decorating an AIEgen onto an ACQ fluorophore. For example, anthracene and pyrene show typical ACQ effects due to their unavoidable  $\pi$ - $\pi$  stacking in the aggregate states. Decorating them with AIE luminophore converts these ACQphores to AIE active luminogens. By using this strategy the developed luminogens show emission color covering entire visible region. We were interested in design and synthesis of various AIE active luminogens containing tetraphenylethylene unit.

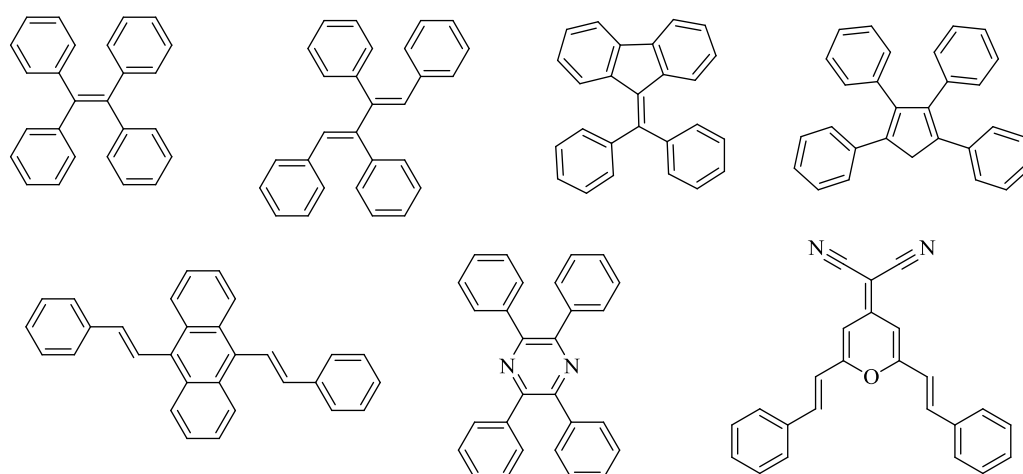


**Chart 1.1.** Various molecules exhibiting aggregation induced emission phenomenon.

#### 1.4. Tetraphenylethylene (TPE)

Tetraphenylethylene (TPE) (Figure 1.4) represents a family of polyaromatic compounds where an olefin is flanked by four phenyl rings. The crystal structure of TPE was reported by Hong *et al.*, which reveals four phenyl rings adopt propeller like conformations.<sup>[18]</sup> The phenyl rings are twisted geometry with  $\sim 50^\circ$  twisting angle corresponds to central olefin. This propeller like conformation minimizes a direct  $\pi$ - $\pi$  stacking interaction which was observed in the molecular packing. The weak C-H $\cdots$  $\pi$  interactions are

present in between hydrogen atoms of phenyl rings of one TPE molecule and the  $\pi$ -electrons of the phenyl rings of the adjacent molecule. This weak C-H $\cdots$  $\pi$  interactions can further lock the molecular conformation in the solids. The absence of  $\pi$ - $\pi$  stacking interaction and locking of intramolecular rotations of phenyl rings makes TPE as an AIE active molecule.<sup>[19]</sup> The synthesis of various functionalized TPE derivatives is a facile process which makes TPE a very attractive and useful molecule in generating new luminogens with AIE characteristics. The halogenated TPE can be synthesized very easily by using halogenated precursors for TPE synthesis.

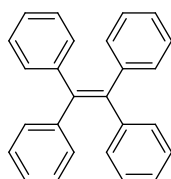
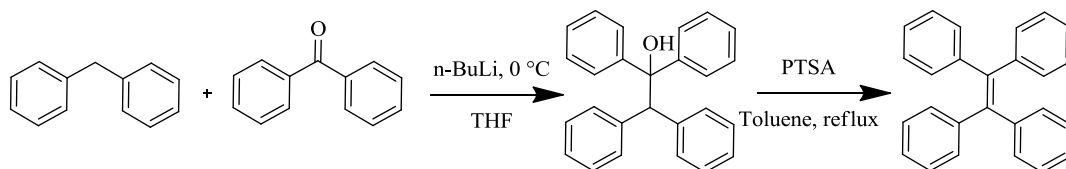


**Figure 1.4.** Structure of tetraphenylethylene.

### 1.5. Synthesis of Tetraphenylethylene (TPE)

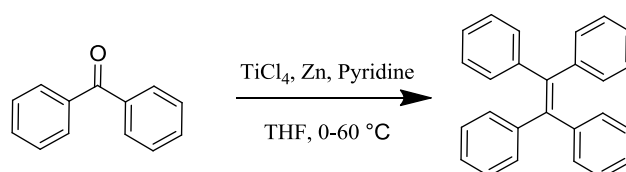
The synthesis of TPE and its derivatives were achieved by various routes. The commonly used retrosynthetic pathway is from the central olefin, along with this sometimes C-C bonds is also constructed between olefin and phenyl ring during the synthesis of TPE derivatives. The very first synthesis of TPE was performed by de Boissieu back in 1888 by dry distillation of diphenylmethane in the presence of bromine.<sup>[20]</sup> Subsequently various synthetic routes are available in the literature for preparation of TPE (Scheme 1.1-1.4). Some of these routes are also suitable for building functionalized TPE's.



**Scheme 1.1.** Synthesis of TPE by using Knoevenagel like condensation reaction.

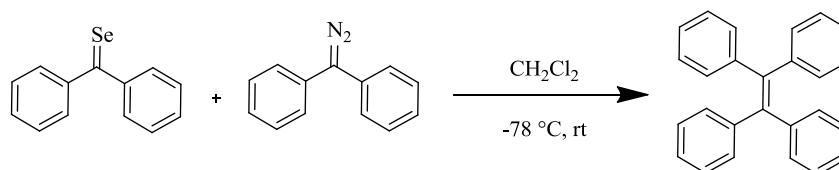
The Knoevenagel like condensation reaction was used by Wang *et al.* for synthesis of TPE (Scheme 1.1). The diphenylmethane was first

deprotonated using n-BuLi in THF at 0 °C to which benzophenone was added slowly to yield tetraphenylethanol.<sup>[21]</sup> The dehydration of resulting tertiary alcohol was carried using catalytic *para*-toluene sulphonic acid (PTSA) and water was removed using Dean-Stark apparatus *via* azeotropic mixture with toluene which results the desired TPE. This synthetic methodology is also important in synthesizing various functionalized TPEs, including halogenated TPE. This methodology has limitations in terms of substituents on diphenylmethane as well as benzophenone such as it is not applicable with electron donating substituents on diphenylmethane unit due to formation of unstable anion.



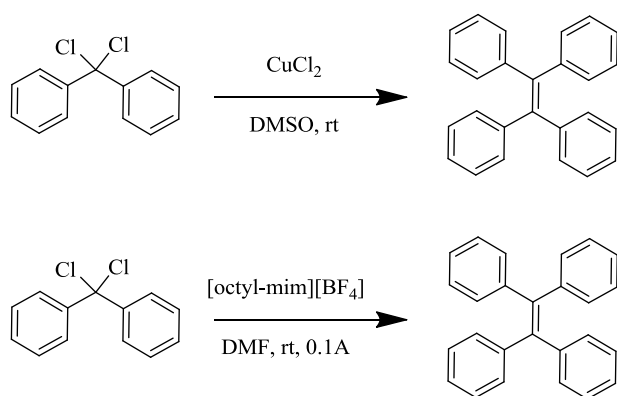
**Scheme 1.2.** Synthesis of TPE by using McMurry like condensation reaction.

Second important method of synthesizing TPE and its derivatives is the McMurry coupling. In this the two ketones (benzophenone) are coupled in presence of Ti(III) and Ti(IV) salts and reducing agent Zn to TPE (Scheme 1.2).<sup>[22]</sup> Symmetrically substituted TPE's can also be prepared as this reaction is tolerant to alkyl, halogen, ether, amine, alcohol, and phenol substituents. This reaction has also been extended to cross-coupling of two benzophenones with different substituents to yield unsymmetrically substituted TPEs.



**Scheme 1.3.** Synthesis of TPE by using selenobenzophenones with diphenyldiazomethane.

The reaction of selenobenzophenones with diphenyldiazomethane in dichloromethane at -40 °C resulted in the formation of TPE as described in Scheme 1.3.<sup>[23]</sup> This reaction is believed to proceed *via* a 1,3,4-selenadiazoline intermediate followed by deselenization and evolution of nitrogen gas. This strategy can also be extended to afford unsymmetrical TPE derivatives.



**Scheme 1.4.** Synthesis of TPE from diphenyldichloromethane.

Diphenyldichloromethane was found to undergo an exothermic reaction with stoichiometric copper metal in DMSO to yield TPE (Scheme 1.4).<sup>[24]</sup> This reaction is believed to proceed *via* a copper carbenoid intermediate. Barhadi *et al.* developed similar electrochemical coupling reactions of diphenyldichloromethane using nickel catalyst at room temperature ionic liquids (Scheme 1.4).<sup>[25]</sup>

## 1.6. Applications of Tetraphenylethylene Derivatives

The TPE luminophores have been explored for a wide variety of application due to the high emission efficiency in the solid state, which differentiates them from the conventional luminophores. Some of the common applications are discussed below:

### 1.6.1. Organic Light Emitting Diodes (OLEDs)

The development of organic light-emitting diodes (OLEDs) has gained extensive research interest since Tang and VanSlyke introduced the first electroluminescence (EL) device by vapor deposition.<sup>[26]</sup> considerable attempts have been made for the development of efficient OLEDs.<sup>[27]</sup> The conventional luminogens suffer from the ACQ due to  $\pi$ - $\pi$  stacking interactions in the planar luminogens, which limits their applicability in the efficient OLEDs. Now days, the use of AIEgens to decorate ACQphores is comes out to be a famous strategy used to overcome from ACQ. The TPE has been widely explored for generating AIEgens as well as for the development of OLED materials.<sup>[28]</sup>

The full-color displays can be accomplished with emission colors covering the whole visible range with the help of TPE. The well-known pyrene ACQphore is converted in to the AIEphore by attaching TPE to the periphery of pyrene. The OLED device fabricated with configuration as, ITO/NPB/**TTPEPy**/TPBi/LiF/Al, where ITO = indium tin oxide, NPB = *N,N'*-bis(1-naphthalenyl)-*N,N'*-bis(phenyl)benzidine and TPBi = 1,3,5-tris(1-phenyl-1*H*-benzo[*d*]imidazol-2-yl)-benzene, which emits a sky blue light of 488 nm with a turn-on voltage of 3.6 V, maximum luminance ( $L_{\max}$ ) of 36300  $\text{cd m}^{-2}$ , current efficiencies of 12.3  $\text{cd A}^{-1}$ , power efficiencies of 7.0  $\text{lm W}^{-1}$ , and its high  $\eta_{\text{EL}}$  of (5.0%).<sup>[29]</sup>

The luminogen developed from coupling TPE with benzo-2,1,3-thiadiazole emits orange red emission. The OLED device fabricated with a configuration of ITO/NPB (60 nm)/BTPETTD (20 nm)/TPBi (10 nm)/Alq<sub>3</sub> (30 nm)/LiF (1 nm)/Al (100 nm). The EL device of BTPETTD shows EL with  $L_{\max}$ ,  $\eta_{\text{C,max}}$  and  $\eta_{\text{ext,max}}$  of 8330  $\text{cd m}^{-2}$ , 6.4  $\text{cd A}^{-1}$  and 3.1%, respectively, which are much higher than attained by most non-doped fluorescent red OLEDs.<sup>[30]</sup> Non-doped fluorescent white organic light emitting diodes (WOLEDs) based on AIE emitters have been explored using TTPEPy as the blue emitter and BTPETTD as the red emitter (Figure 1.5). The device emits white light with Commission Internationale de l'Eclairage (CIE) coordinates of (0.38, 0.41), a turn-on voltage of 6.0 V, maximum current efficiency of 7.4  $\text{cd A}^{-1}$ , and power efficiency of 4.0  $\text{lm W}^{-1}$ .<sup>[31]</sup>

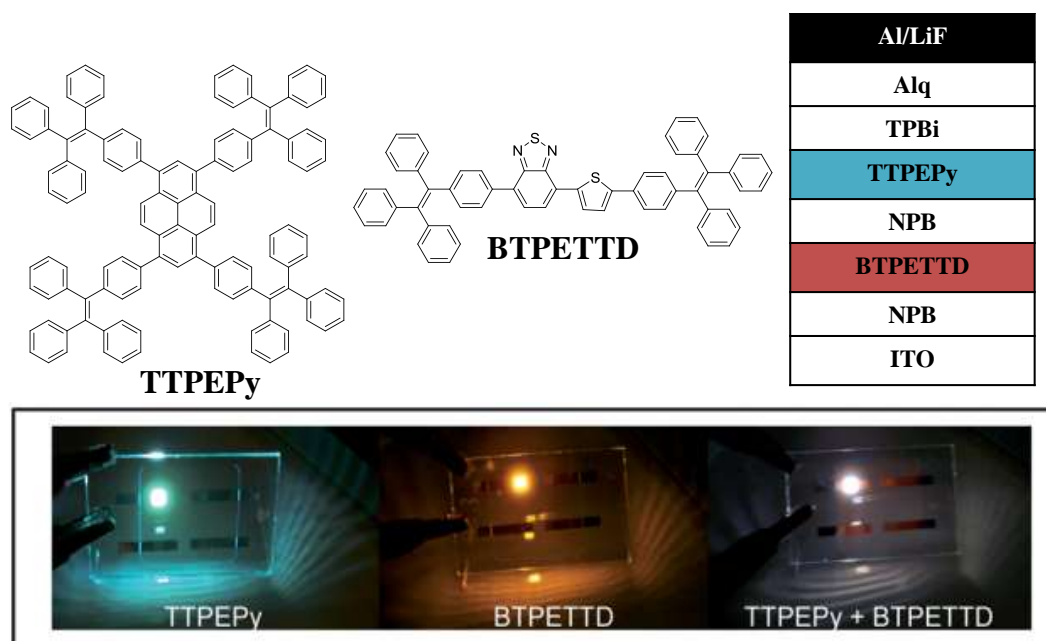


**Figure 1.5.** Configuration of WOLED constructed from TTPEPy and BTPETTD and photos of the B, R, and WOLEDs.

### 1.6.2. Fluorescent Sensors

In the recent years the design and synthesis of TPE based molecules for developing fluorescent sensors has gained attention. The TPE based luminogens are used to develop both turn-on and turn-off type sensors for detection of various environment pollutants, metal ions and biological systems. The TPE can be functionalized on various binding ligands and used for detection of desired species. The main benefit in designing the TPE based sensors is that they can be used in both solution and solid state.

#### 1.6.2.1. Metal Ion Sensing

Ions are undoubtedly important component of systems as well as surroundings. Ions are essential for biological, physiological and environmental process, their adequate amount sustains, whereas excess destroy the process. Various TPE based AIEgens were developed for cation as well as anion sensing.<sup>[32]</sup>

Mercury ion ( $\text{Hg}^{2+}$ ) is a severe environmental pollutant and a toxicant to the human body which can cause nausea, vomiting, stomach ache, Minamata disease, and damages of liver, kidney, as well as brain. Tang *et al.* has developed selective and sensitive turn-on fluorescent sensor for  $\text{Hg}^{2+}$  in aqueous solution by using the TPE-functionalized benzothiazolium salt with

iodide as counter ion.<sup>[33]</sup> The high selectivity of TPE-functionalized benzothiazolium salt towards  $\text{Hg}^{2+}$  ion is due to the high affinity of  $\text{Hg}^{2+}$  ion towards I and S atom of benzothiazolium unit. The enhancement in the light emission after  $\text{Hg}^{2+}$  ion is firstly due to the  $\text{Hg}^{2+}$  ion displaces the I ion and forms  $\text{HgI}_2$  and secondly is due the formation of fluorescent nano-aggregates by complexation of  $\text{Hg}^{2+}$  with S-atom of benzothiazolium unit as shown in below Figure 1.6.

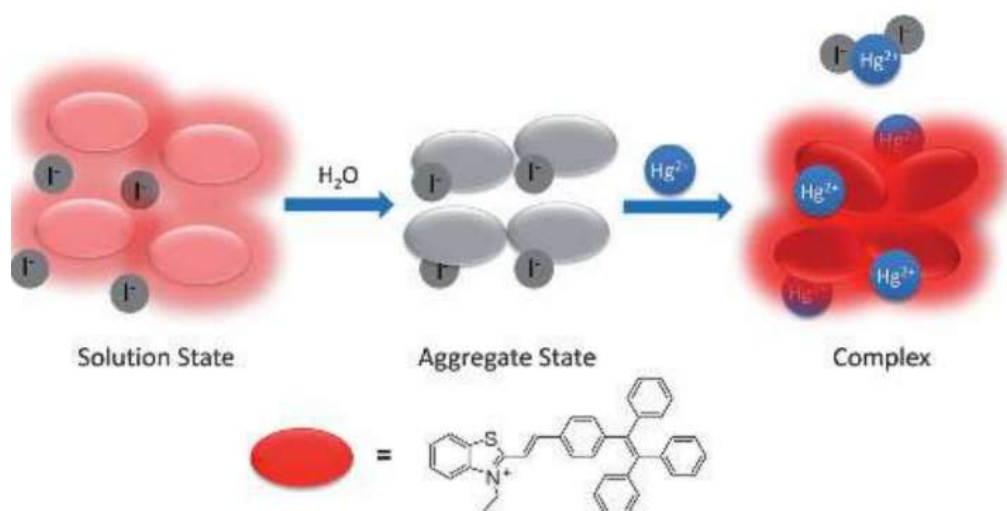


**Figure 1.6.** Schematic diagram of detection of  $\text{Hg}^{2+}$  ion.

### 1.6.2.2. Bio Sensing

The development of luminescent biosensors is of great significance in the biological science, due to their usefulness as powerful analytical tools for studying biological events in living systems. TPE was extensively studied in the field of bio sensing. For example, the TPE based glucose sensor was developed by carrying two boronic acids on the TPE unit (DBTPE).<sup>[34]</sup> The glucose molecules are readily reactive towards boronic acid functionality. The oligomerization reaction of two diol units in glucose with two boronic acids of DBTPE forms rigid oligomers. The rigid oligomers further restrict the intramolecular rotations of the phenyl rings of TPE, which enhances the fluorescence intensity. The DBTPE acts as turn-on probe for specific detection of glucose sensing (Figure 1.7).

Liu *et al.* designed and synthesized TPE luminogen probe by functionalizing a TPE with two phosphate groups (TPE-phos) for the detection

of alkaline phosphatase (ALP) and its enzymatic activity based on the specific interaction between the probe and ALP.<sup>[35]</sup> The TPE-phos are highly water soluble and non-luminescent in the aqueous medium due to non-radiative decay. The ALP recognizes and cleaves the phosphate groups in TPE-phos, which gives a water-insoluble enzymatic residue. The insoluble residue is highly luminescent due to the activated AIE process.

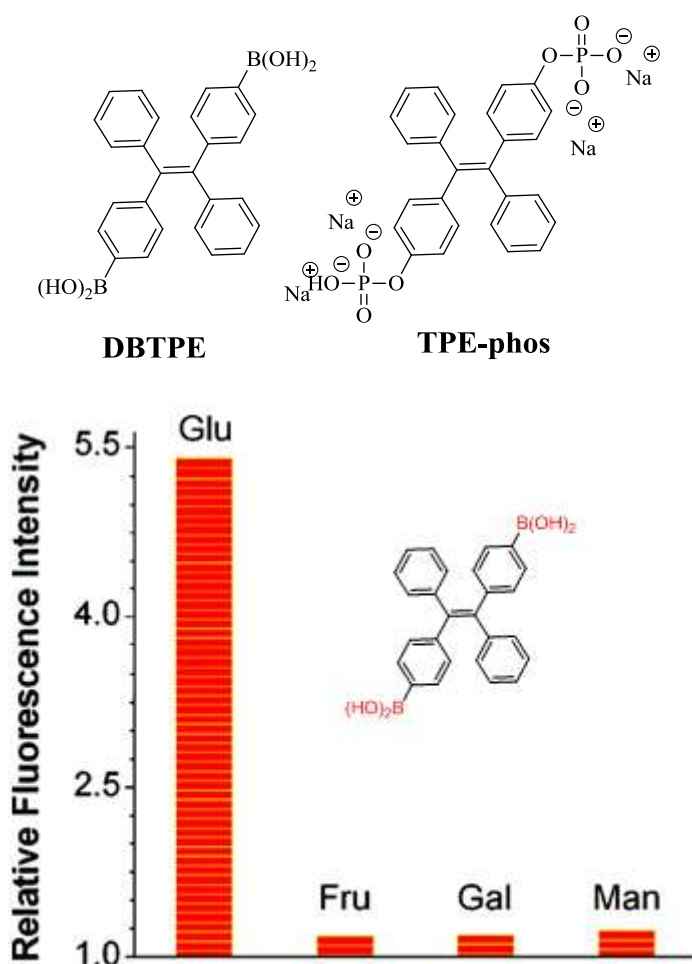


**Figure 1.7.** Fluorescence “turn-on” probe for specific detection of glucose.

### 1.6.2.3. Nitro Sensing

In recent year development of highly selective and sensitive explosive sensor become increasingly important and urgent issue due to its antiterrorism applications in both national security and environmental protection. The TPE based luminogens are used to develop highly sensitive nitro aromatic fluorescent probes. The Tang and Yu *et al.* have developed various TPE based nitro aromatic sensors. For example, mesoporous SBA-15 functionalized with



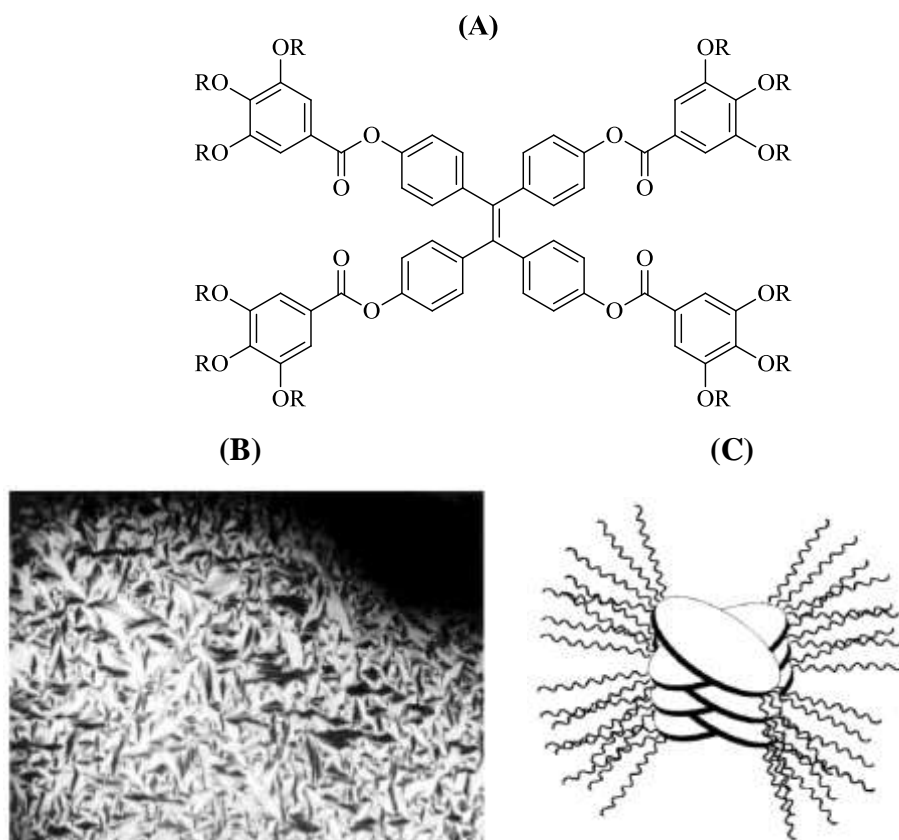


**Figure 1.8.** (A) TPE esters used in the study (B) Polarizing microscopy image of tetrakis[4-(trisalkoxybenzoyloxy)phenyl]ethenes showing fan shaped texture (C) Possible arrangement of tetrakis[4-(trisalkoxybenzoyloxy)phenyl]ethenes in the hexagonal columnar mesophase.

#### 1.6.4. TPE derivative in metal organic frameworks and complexes

In order to design organic as well as metal organic assemblies, the inbuilt geometrical traits of the TPE core could be exploited for their further use in field of crystal engineering. A tetragonal prism was designed using multicomponent coordination-driven self-assembly by Stang *et al.* as illustrated in Figure 1.9.<sup>[38]</sup> Tetra(4-pyridylphenyl)ethylene containing four pyridine groups along the TPE periphery was formulated to function as the faces of a tetragonal prism during the self-assembly event, whereas the linear donors 4,4'-bipyridine or *trans*-1,2-di(4-pyridyl)ethylene and platinum triflate were designated as pillars and corners of the tetragonal prism, respectively.<sup>[38]</sup> The formation of tetragonal prism was presumed by reaction of the three building blocks in stoichiometric ratio of 1:2:4 as shown in Figure 1.9.

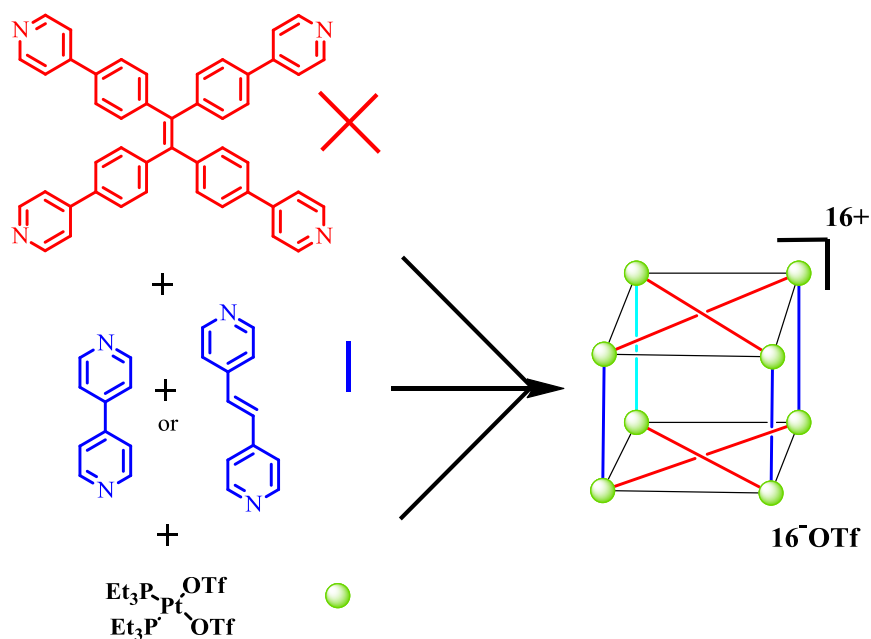


**Figure 1.9.** Multicomponent coordination driven self-assembly of tetragonal prisms.<sup>[38]</sup>

### 1.6.5. Stimuli Responsive Materials

Stimuli responsive materials show responses to different stimuli like mechanical strain, heat, light, pH, electric and magnetic field, pressure and solvent vapors which change their dynamic molecular architectures resulting change in their absorption or emission properties.<sup>[39]</sup> Consequently, design of materials that respond to multiple stimuli in a distinct way is very important in practical applications and has gained significant interest. Particularly, various stimuli-responsive materials such as mechanochromic, vapochromic, thermochromic, and acidchromic materials have reported which adopt different mechanisms to response the stimulus. Particularly, mechanochromic and vapochromic materials have been developed for their applications in mechano-sensors, vapo-sensor, environmental monitors, chemical sensors, optical data storage, and security papers. Various mechanochromic materials have been successfully synthesized from the TPE.

#### 1.6.5.1. Mechanochromic Materials

Mechanochromic luminescent materials are a class of *smart* materials. They change their emission colors in response to external mechanical stimuli (grinding, rubbing or crushing). These materials can be degenerated to their original state by another external stimuli. The mechanochromic luminescent

materials are widely used in mechano-sensors, security papers, and memory chips.<sup>[39]</sup> The mechanochromism can be achieved by either chemical or physical structural change. The chemical structural changes such as bond formation or bond breaking at the molecular level are induced using chemical reactions. To achieve this relatively high pressure is necessary to stimulate the chemical reactions. The incomplete conversion, irreversibility of reactions, or loss of luminescence ability of the luminophores can commonly occur in chemical structural reactions and thus considered as drawback.<sup>[40]</sup>

On the other hand, the luminescent properties of the solid-state compounds found to be dependent on the molecular arrangement, and intermolecular interactions. The mode of the molecular packing and/or conformation of the compound would affect the molecular stacking mode and effective conjugation which alter the fluorescent properties. Thus, controlling the mode of molecular packing becomes interesting and important in tuning the photophysical properties. In contrast to chemical structural change, physical structural change is more efficient and easier methodology to apply in realizing the dynamic control and reversible solid state fluorescence.<sup>[39-41]</sup>

The AIEphores overcomes the ACQ and are highly fluorescent in the solid state. The AIEphores exhibit highly twisted geometry results in loose packing in the solid state. This allows the luminogens to change their solid state arrangement upon mechanical stimuli. Recently, TPE based AIEgens has become an attractive research object for researchers interested in the development of mechanochromic materials.<sup>[39-41]</sup>

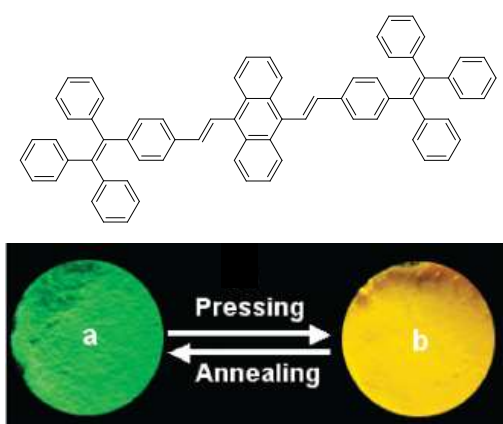


**Figure 1.10.** The molecular structure of TPE substituted luminogen and their reversible mechanochromic behavior, annealing sample (a) and pressing sample (b) under 365 nm UV light.



Recently, tetraphenylethylene substituted terpyridine ligand and their zinc ion complex was reported as first mechanochromic AIE complex.<sup>[43]</sup> They show multi-stimuli responses such as grinding, heating, solvent-fuming, as well as exposing to acid and base (Figure 1.11). The pristine solid of complex show blue emission at 474 nm. After grinding using mortar and pestle it changes emission to 555 nm. These spectral changes are reversible and can be achieved by solvent vapor fumigation. The solvent fumigated solid emits at 476 nm which is close to the pristine solid. However the annealed solids show green luminescence at 501 nm. The different stimuli based behavior shown in schematic Figure 1.11.<sup>[43]</sup>

### 1.6.6. Biological Imaging

Biological imaging is the technique which provides the visual representation of interior of a cell, tissue, or body for biological or clinical analysis and medical intervention. The various imaging models are available such as fluorescence imaging, magnetic resonance imaging (MRI), bioluminescence imaging, etc. Among these imaging techniques, fluorescence imaging has been attracting more research interest due to their advantages such as, the large variety of fluorescent reagents, strong labeling capability, intense output signal, high temporal and spatial resolution, low cost, and wide applicability. The most important requirement for fluorescence imaging is the highly luminescent imaging reagents i.e., luminogens. The frequently used fluorescence imaging reagents comprise organic dyes and proteins (e.g., green fluorescent protein) and inorganic quantum dots (QDs). However, the molar absorptivity and photobleaching resistance of currently available organic dyes or protein-based fluorescence imaging reagents are low. Moreover, the ACQ effect of conventional fluorogens also prevents them from being good players in biological imaging. The AIEphores such as TPE luminogens are come out to be the effective methodology and therefore various TPE based luminogens have been used in the bio imaging.<sup>[32,44]</sup>

Various light-up probes specific to mitochondria were developed by Tang *et al.*<sup>[45,46]</sup> Each of these two AIEgens is composed of a large lipophilic/hydrophobic moiety donated by TPE motif and other  $\pi$ -conjugate groups, together with a positively charged head. Moreover, with well-extended

electronic conjugation and strong D-A effect, the nanoaggregates of TPE substituted benzothiazolium (TPE-Bz) and pyridinium (TPE-Py) salts in mitochondria emit yellow and red fluorescence, respectively (Figure 1.12). It is noteworthy that the images of mitochondria stained by TPE substituted benzothiazolium and pyridinium salts show good resolution this might be due to the auto fluorescence from the cells is avoided due to the mismatch in the excitation wavelength.

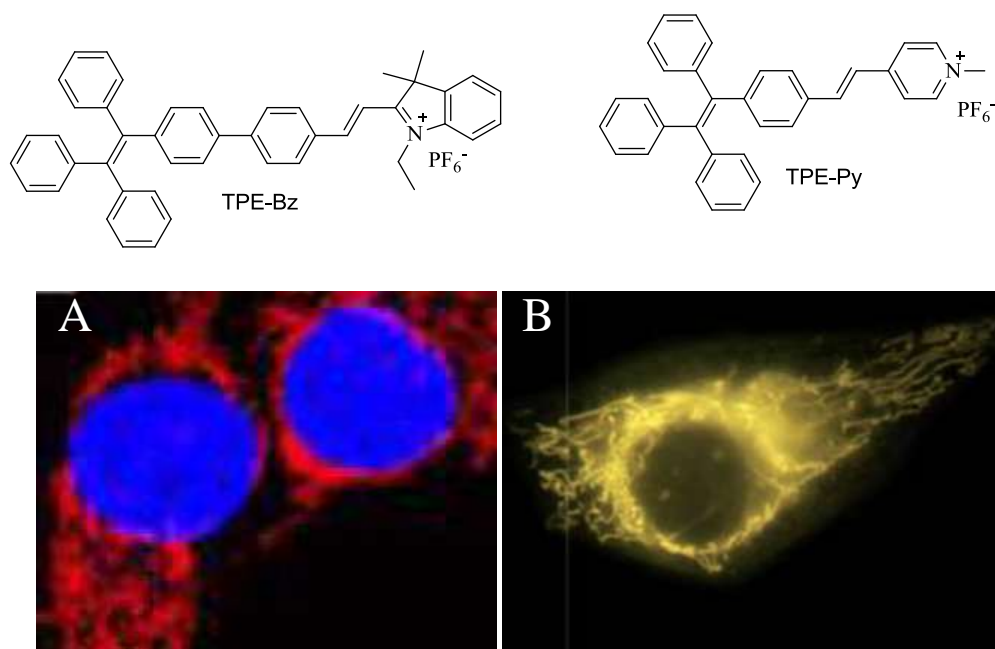


**Figure 1.12.** Fluorescent images of the HeLa cells stained by (A) benzothiazolium and (B) pyridinium salts.

## 1.7. Organization of thesis

**Chapter 1** describes how the AIE luminogens are important, followed by detailed discussion about synthesis, properties and applications of TPE based luminogens.

**Chapter 2** Summarizes the instrumentation and general methods used for the present study.

In **Chapter 3** two TPE substituted phenanthroimidazoles **3a** and **3b** were synthesized by the Suzuki cross-coupling reaction. Their crystal structure, AIE and mechanochromic properties were described. The cyano-group induced enhanced AIE behavior was described which is ascribed to the hydrogen-bonding assisted tight packing of nano-aggregates. They show

reversible mechanochromic behavior with colors contrast between sky-blue and yellow green.

In **Chapter 4**, the positional effect of TPE unit was studied. Along with that the effect on solid state emission and mechanochromism is studied by changing different end groups on phenanthroimidazole. To achieve this four TPE substituted phenanthroimidazoles **3a-3d** were designed and synthesized. The substituent dependent solid state emission and mechanochromic properties were described.

In **Chapter 5** the effect of variation on AIE and mechanochromism is studied by changing phenanthroimidazole unit to pyrenoimidazole and along with that the TPE unit was also changed to triphenylacrylonitrile (TPAN), the two pyrenoimidazole based luminogens **3a** and **3b** were designed. The **3a** and **3b** exhibit AIE and reversible mechanochromism.

In **Chapter 6** a series of symmetrical and unsymmetrical TPE substituted BTDs **3-9** were designed and synthesized to understand how the donor (D)/ acceptor (A) substituents and their substitution pattern affect the solution and solid-state optical properties. The BTDs **3-9** were synthesized by the Suzuki and Stille coupling reactions. Their solvatochromic, aggregation induced emission (AIE), mechanochromic, and vapochromic properties were studied and compared.

In **Chapter 7** TPE substituted pyrazabole was designed and synthesized by the Pd-catalyzed Suzuki cross-coupling reaction. The photophysical, AIE and mechanochromic properties of TPE substituted pyrazabole were described. The good color contrast and reversible mechanochromic behavior between blue and green color was observed.

## 1.8. References

- [1] (a) Yersin H., (2008) Highly efficient OLEDs with phosphorescent materials, Wiley VCH, Weinheim. (b) Müllen K., Scherf U., (2006) Organic light-emitting devices, synthesis properties and applications, Wiley-VCH, Weinheim. (c) Kafafi Z. H., (2005) Organic electroluminescence, Taylor& Francis, Boca Raton.
- [2] (a) Meaney M. S., McGuffin V. L., (2008), Luminescence-based methods for sensing and detection of explosives., *Anal. Bioanal. Chem.*, 391, 2557–2576 (DOI: 10.1007/s00216-008-2194-6). (b)

- Samuel W. Thomas III., Guy D. Joly Swager T M. (2007), Chemical sensors based on amplifying fluorescent conjugated polymers, (DOI: 10.1021/CR0501339). (c) Basabe-Desmonts L., Reinhoudt D N., Crego-Calama M., Albert K J., Walt D R., Colton R J., Russell J N., Yang J S., Swager T M., Czarnik A W., et al. (2007), Design of fluorescent materials for chemical sensing, *Chem. Soc. Rev.*, 36, 993 (DOI: 10.1039/b609548h). (d) Wolfbeis O S., (2005), Materials for fluorescence-based optical chemical sensors, *J. Mater. Chem.*, 15, 2657 (DOI: 10.1039/b501536g). (e) Ramon M-M., Sancenón F. (2003), Fluorogenic and chromogenic chemosensors and reagents for anions, *Chem. Rev.*, 103, 4419–4476 (DOI: 10.1021/CR010421E). (f) Sreejith S., Divya K. P., Ajayaghosh A., (2008), Detection of zinc ions under aqueous conditions using chirality assisted solid-state fluorescence of a bipyridyl based fluorophore, *Chem. Commun.*, 271, 2903 (DOI: 10.1039/b802958j). (g) Zhang S-W., Swager T. M. (2003), Fluorescent detection of chemical warfare agents: Functional group specific ratiometric chemosensors, *J. Am. Chem. Soc.*, 125, 3420–3421 (DOI: 10.1021/JA029265Z).
- [3] (a) Zaumseil J., Sirringhaus H. (2007), Electron and ambipolar transport in organic field-effect transistors, *Chem. Rev.*, 107, 1296–1323 (DOI: 10.1021/CR0501543). (b) Cicoira F. and Santato C. (2007), Organic light emitting field effect transistors: Advances and perspectives, *Adv. Funct. Mater.*, 17, 3421–3434 (DOI: 10.1002/adfm.200700174).
- [4] (a) Samuel I. D. W., Turnbull G. A. (2007), Organic semiconductor lasers, *Chem. Rev.*, 107, 1272–1295 (DOI: 10.1021/CR050152I). (b) Scherf U., Riechel S., Lemmer U., Mahrt R. (2001), Conjugated polymers: lasing and stimulated emission, *Curr. Opin. Solid State Mater. Sci.*, 5, 143–154 (DOI: 10.1016/S1359-0286(01)00010-9). (c) McGehee M. D., Heeger A. J. (2000), Semiconducting (conjugated) polymers as materials for solid-state lasers, *Adv. Mater.*, 12, 1655–1668 (DOI: 10.1002/1521-4095(200011)12:22<1655::AID-ADMA1655>3.0.CO;2-2). (d) Kranzelbinder G., Leising G., (2000), Organic solid-state lasers, *Reports Prog. Phys.*, 63, 729–762 (DOI:

- 10.1088/0034-4885/63/5/201). (e) Dodabalapur A., Chandross E. A., Berggren M., Slusher R. E. (1997), Organic solid-state lasers: Past and future, *Science*, 277, 1787 (DOI: 10.1126/science.277.5333.1787)
- [5] (a) Nathaniel L. R., Mirkin C. A. (2005), Nanostructures in biodiagnostics, *Chem. Rev.*, 105, 1547–1562 (DOI: 10.1021/CR030067F). (b) Burns A., Ow H., Wiesner U. (2006), Fluorescent core–shell silica nanoparticles: towards “Lab on a Particle” architectures for nanobiotechnology, *Chem. Soc. Rev.*, 35, 1028–1042 (DOI: 10.1039/B600562B). (c) Que E. L., Domaille D. W., Chang C. J. (2008), Metals in neurobiology: Probing their chemistry and biology with molecular imaging, *Chem. Rev.*, 108, 1517–1549 (DOI: 10.1021/cr078203u). (d) Nolan E M. and Lippard S J. (2009), Small-molecule fluorescent sensors for investigating zinc metalloneurochemistry, *Acc. Chem. Res.*, 42, 193–203 (DOI: 10.1021/ar8001409) (e) Feng X., Liu L., Wang S., Zhu D., (2010), Water-soluble fluorescent conjugated polymers and their interactions with biomacromolecules for sensitive biosensors, *Chem. Soc. Rev.*, 39, 2411 (DOI: 10.1039/b909065g).
- [6] Th. Förster and K. Kasper, *Z. Phys. Chem.* (Munich), 1954, 1, 275.
- [7] J. B. Birks, *Photophysics of Aromatic Molecules*, Wiley, London, 1970.
- [8] (a) Samuel W. Thomas III., Guy D. J., Swager T M. (2007), Chemical sensors based on amplifying fluorescent conjugated polymers, *Chem. Rev.*, 2007, 107, 1339–1386 (DOI: 10.1021/CR0501339). (b) Belletete M., Bouchard J., Leclerc M., Durocher G., (2005), Photophysics and solvent-induced aggregation of 2,7-carbazole-based conjugated polymers, *Macromolecules*, 38, 880–887 (DOI: 10.1021/MA048202T). (c) Menon A., Galvin M., Walz K A. and Rothberg L. (2004), Structural basis for the spectroscopy and photophysics of solution-aggregated conjugated polymers, *Synth. Met.*, 141, 197–202 (DOI: 10.1016/j.synthmet.2003.09.021). (d) Chen C-T. (2004), Evolution of red organic light-emitting diodes: Materials and devices, (DOI: 10.1021/CM049679M). (e) Jakubiak R., Collison C. J., Wan W. C., Rothberg L. J., Hsieh B. R. (1999), Aggregation quenching of luminescence in electroluminescent conjugated polymers, *J. Phys.*

- Chem. A*, 103, 2394–2398 (DOI: 10.1021/JP9839450). (f) Lemmer U., Heun S., Mahrt R. F., Scherf U., Hopmeier M., Siegner U., Göbel E. O., Mullen K., Bäessler H. (1995), Aggregate fluorescence in conjugated polymers, *Chem. Phys. Lett.*, 240, 373–378 (DOI: 10.1016/0009-2614(95)00512-3).
- [9] (a) Lee Y-T., Chiang C-L., Chen C-T., Chen C-T., Wu W-C., Yeh H-C., Chan L-H., Chen C-T., Yeh H-C., Yeh S-J., et al. (2008), Solid-state highly fluorescent diphenylaminospirobifluorenylfumaronitrile red emitters for non-doped organic light-emitting diodes, *Chem. Commun.*, 16, 217–219 (DOI: 10.1039/B711157F). (b) Wu C.-W., Tsai C.-M., Lin H-C. (2006), Synthesis and characterization of poly(fluorene)-based copolymers containing various 1,3,4-oxadiazole dendritic pendants, *Macromolecules*, 39, 4298–4305 (DOI: 10.1021/MA060743Q). (c) Wang J., Zhao Y., Dou C., Sun H., Xu P., Ye K., Zhang J., Jiang S., Li F., Wang Y. (2007), Alkyl and dendron substituted quinacridones: synthesis, structures, and luminescent properties, *J. Phys. Chem. B*, 111, 5082–5089 (DOI: 10.1021/JP068646M). (d) Lim S-F., Friend R. H., Rees I. D., Li J., Ma Y., Robinson K., Holmes A. B., Hennebicq E., Beljonne D., Cacialli F. (2005), Suppression of green emission in a new class of blue-emitting polyfluorene copolymers with twisted biphenyl moieties, *Adv. Funct. Mater.*, 15, 981–988 (DOI: 10.1002/adfm.200400457). (e) Setayesh S., Grimsdale A. C., Weil T., Enkelmann V., Müllen K., Meghdadi F., List E. J. W., Leising G. (2001), Polyfluorenes with polyphenylene dendron side chains: toward non-aggregating, light-emitting polymers, *J. Am. Chem. Soc.*, 123, 946–953 (DOI: 10.1021/JA0031220). (f) Hecht S., Fréchet J. M. J. (2001), Dendritic encapsulation of function: applying nature’s site isolation principle from biomimetics to materials science, *Angew. Chemie Int. Ed.*, 40, 74–91 (DOI: 10.1002/1521-3773(20010105)40:1<74::AID-ANIE74>3.0.CO;2-C). (g) Jakubiak R., Bao Z., Rothberg L. (2000), Dendritic sidegroups as three-dimensional barriers to aggregation quenching of conjugated polymer fluorescence, *Synth. Met.*, 114, 61-4 (DOI: 10.1016/S0379-6779(00)00225-3).
- [10] (a) Nguyen B. T., Gautrot J. E., Ji C., Brunner P.-L., Nguyen M. T.,

- Zhu X. X. (2006), Enhancing the photoluminescence intensity of conjugated polycationic polymers by using quantum dots as antiaggregation reagents, *Langmuir*, 22, 4799–4803 (DOI: 10.1021/LA053399J). (b) Kulkarni, A. P., Jenekhe S. A. (2003), Blue light-emitting diodes with good spectral stability based on blends of poly(9,9-dioctylfluorene): interplay between morphology, photophysics, and device performance, *macromolecules*, 36, 5285–5296 (DOI: 10.1021/MA0344700). (c) Abe S., Chen L. (2003), Tuning the photophysical properties of an ionic conjugated polymer through interactions with conventional polyelectrolytes, *J. Polym. Sci. Part B Polym. Phys.*, 41, 1676–1679 (DOI: 10.1002/polb.10521). (d) Gaylord B. S., Wang S., Heeger A. J., Bazan G C. (2001), Water-soluble conjugated oligomers: effect of chain length and aggregation on photoluminescence-quenching efficiencies, *J. Am. Chem. Soc.*, 2001, 123, 6417–6418 (DOI: 10.1021/JA010373F). (e) Chen L., Xu S., McBranch D., Whitten D. (2000), Tuning the properties of conjugated polyelectrolytes through surfactant complexation, *J. Am. Chem. Soc.*, 2000, 122, 9302–9303 (DOI: 10.1021/JA001248R). (f) Taylor P. N., O’Connell M. J., McNeill L. A., Hall M. J., Aplin R. T., Anderson H. L. (2000), Insulated molecular wires: synthesis of conjugated polyrotaxanes by suzuki coupling in water, *Angew. Chemie*, 39, 3456–3460 (DOI: 10.1002/1521-3773(20001002)39:19<3456::AID-ANIE3456>3.0.CO;2-0). (g) Sainova D., Miteva T., Nothofer H. G., Scherf U., Glowacki I., Ulanski J., Fujikawa H. and Neher D. (2000), Control of color and efficiency of light-emitting diodes based on polyfluorenes blended with hole-transporting molecules, *Appl. Phys. Lett.*, 76, 1810 (DOI: 10.1063/1.126173).
- [11] (a) Kokado K., Chujo Y. (2009), Emission via aggregation of alternating polymers with *o*-carborane and *p*-phenylene-ethynylene sequences, *Macromolecules*, 42, 1418–1420 (DOI: 10.1021/ma8027358). (b) Dong J., Solntsev K. M., Tolbert L. M. (2009), Activation and tuning of green fluorescent protein chromophore emission by alkyl substituent-mediated crystal packing, *J. Am. Chem. Soc.*, 131, 662–670 (DOI: 10.1021/ja806962e). (c) Tang W., Xiang Y.,

Tong A. (2009), Salicylaldehyde azines as fluorophores of aggregation-induced emission enhancement characteristics, *J. Org. Chem.*, 74, 2163–2166 (DOI: 10.1021/jo802631m). (d) Yao H., Yamashita M., Kimura K. (2009), Organic styryl dye nanoparticles: synthesis and unique spectroscopic properties, *Langmuir*, 25, 1131–1137 (DOI: 10.1021/la802879e). (e) Pu K-Y., Liu B. (2009), Conjugated polyelectrolytes as light-up macromolecular probes for heparin sensing, *Adv. Funct. Mater.*, 19, 277–284 (DOI: 10.1002/adfm.200800960). (f) Wang M., Zhang D., Zhang G., Zhu D. (2008), The convenient fluorescence turn-on detection of heparin with a silole derivative featuring an ammonium group, *Chem. Commun.*, 19, 4469 (DOI: 10.1039/b808877b). (h) Lv J., Jiang L., Li C., Liu X., Yuan M., Xu J., Zhou W., Song Y., Liu H., Li Y., et al. (2008), Large Third-order optical nonlinear effects of gold nanoparticles with unusual fluorescence enhancement, *Langmuir*, 24, 8297–8302 (DOI: 10.1021/la801000c). (i) Liu Y., Tao X., Wang F., Dang X., Zou D., Ren Y., Jiang M. (2008), Aggregation-induced emissions of fluorenonearylamine derivatives: a new kind of materials for nondoped red organic light-emitting diodes, *J. Phys. Chem. C*, 112, 3975–3981 (DOI: 10.1021/JP7117373). (j) Davis R., Kumar N. S. S., Abraham S., Suresh C. H., Rath N. P., Tamaoki N., Das S. (2008), Molecular packing and solid-state fluorescence of alkoxy-cyano substituted diphenylbutadienes: structure of the luminescent aggregates, *J. Phys. Chem. C*, 112, 2137–2146 (DOI: 10.1021/JP710352M). (k) Zhao Q., Li L., Li F., Yu M., Liu Z., Yi T., Huang C. (2008), Aggregation-induced phosphorescent emission (AIPE) of iridium( iii ) complexes, *Chem. Commun.*, 107, 685–687 (DOI: 10.1039/B712416C). (l) Ning Z., Chen Z., Zhang Q., Yan Y., Qian S., Cao Y., Tian H. (2007), Aggregation-induced emission (AIE) active starburst triarylamine fluorophores as potential non-doped red emitters for organic light-emitting diodes and  $\text{Cl}_2$  gas chemodosimeter, *Adv. Funct. Mater.*, 17, 3799–3807 (DOI: 10.1002/adfm.200700649).

- [12] (a) Luo J., Xie Z., Lam J W Y., Cheng L., Tang B Z., Chen H., Qiu C., Kwok H S., Zhan X., Liu Y., et al. (2001), Aggregation-induced

- emission of 1-methyl-1,2,3,4,5-pentaphenylsilole, *Chem. Commun.*, 397, 1740–1741 (DOI: 10.1039/b105159h). (b) Tang B Z., Zhan X., Yu G., Sze Lee P P., Liu Y., Zhu D. (2001), Efficient blue emission from siloles, *J. Mater. Chem.*, 11, 2974–2978 (DOI: 10.1039/b102221k).
- [13] Chen J., Law C. C. W., Lam J. W. Y., Dong Y., Lo S. M. F., Williams I. D., Zhu D., Tang B. Z. (2003), Synthesis, light emission, nanoaggregation, and restricted intramolecular rotation of 1,1-substituted 2,3,4,5-tetraphenylsiloles, *Chem. Mater.*, 15, 1535–1546 (DOI: 10.1021/CM021715Z).
- [14] Tang B. Z., Geng Y., Lam J. W. Y., Li B. (1999), Processible nanostructured materials with electrical conductivity and magnetic susceptibility: preparation and properties of maghemite/polyaniline nanocomposite films, *Chem. Mater.*, 11, 1581–1589 (DOI: 10.1021/CM9900305).
- [15] (a) Chen J., Law C. C. W., Lam J. W. Y., Dong Y., Lo S. M. F., Williams I. D., Zhu Daoben., Tang B. Z. (2003), Synthesis, light emission, nanoaggregation, and restricted intramolecular rotation of 1,1-substituted 2,3,4,5-tetraphenylsiloles, *Chem. Mater.*, 15, 1535–1546 (DOI: 10.1021/CM021715Z). (b) Li Z., Dong Y., Mi B., Tang Y., Häußler M., Tong H., Dong Y., Lam J. W. Y., Ren Y., Sung H. H. Y., et al. (2005), Structural control of the photoluminescence of silole regioisomers and their utility as sensitive regiodiscriminating chemosensors and efficient electroluminescent materials, *J. Phys. Chem. B*, 109, 10061–10066 (DOI: 10.1021/JP0503462).
- [16] Fan X., Sun J., Wang F., Chu Z., Wang P., Dong Y., Hu R., Tang B Z., Zou D. (2008), Photoluminescence and electroluminescence of hexaphenylsilole are enhanced by pressurization in the solid state, *Chem. Commun.*, 124, 2989 (DOI: 10.1039/b803539c).
- [17] (a) Tong H., Dong Y., Häußler M., Hong Y., Lam J W Y., Sung H H-Y., Williams I D., Kwok H S., Tang B Z. (2006), Molecular packing and aggregation-induced emission of 4-dicyanomethylene-2,6-distyryl-4H-pyran derivatives, *Chem. Phys. Lett.*, 428, 326–30 (DOI: 10.1016/j.cplett.2006.06.113). (b) Tong H., Dong Y., Matthias Häußler ab., Lam Y. J. W., Sung H. H-Y., Williams I. D., Sun J., Tang B. Z.

- (2006) Tunable aggregation-induced emission of diphenyldibenzofulvenes, *Chem. Commun.*, 1133-1135 (DOI: 10.1039/b515798f). (c) Tong H., Dong Y., Hong Y., Häussler M., Lam J. W. Y., Sung H. H.-Y., Yu X., Sun J., Williams I. D., Kwok H.S. et al. (2007), Aggregation-induced emission: effects of molecular structure, solid-state conformation, and morphological packing arrangement on light-emitting behaviors of diphenyldibenzofulvene derivatives, *J. Phys. Chem. C*, 111, 2287–2294 (DOI: 10.1021/JP0630828). (d) He J., Xu B., Chen F., Xia H., Li K., Ye L., Tian W. (2009), Aggregation-induced emission in the crystals of 9,10-distyrylanthracene derivatives: the essential role of restricted intramolecular torsion, *J. Phys. Chem. C*, 113, 9892–9899 (DOI: 10.1021/jp900205k).
- [18] Rathore R., Lindeman S. V., Kumar A. S., Kochi J. K. (1998), Disproportionation and Structural Changes of Tetraarylethylene Donors upon Successive Oxidation to Cation Radicals and to Dications, *J. Am. Chem. Soc.*, 120, 6931–6939 (DOI: 10.1021/JA981095W).
- [19] (a) Hong Y., Lam J W Y., Tang B Z. (2009), Aggregation-induced emission: phenomenon, mechanism and applications, *Chem. Commun.*, 1, 4332 (DOI: 10.1039/b904665h). (b) Cheng K. H., Zhong Y., Xie B. Y., Dong Y. Q., Hong Y., Sun J. Z., Tang B. Z., Wong K. S. (2008), Fabrication of and ultraviolet lasing in tpe/pmma polymer nanowires, *J. Phys. Chem. C*, 112, 17507–17511 (DOI: 10.1021/jp805158b).
- [20] Anon (1888), Organic chemistry, *J. Chem. Soc. Abstr.*, 54, 928 (DOI: 10.1039/ca8885400928).
- [21] Wang W., Lin T., Wang M., Liu T-X., Ren L., Chen D., Huang S. (2010), Aggregation emission properties of oligomers based on tetraphenylethylene, *J. Phys. Chem. B*, 114, 5983–5988 (DOI: 10.1021/jp911311j).
- [22] Schreivogel A., Maurer J., Winter R., Baro A., Laschat S. (2006), Synthesis and electrochemical properties of tetrasubstituted tetraphenylethenes, *European J. Org. Chem.*, 2006, 3395–3404 (DOI: 10.1002/ejoc.200600123).
- [23] Okuma K., Kojima K., Oyama K., Kubo K., Shioji K. (2004), Selenobenzophenones and diazoalkanes: isolation of tetraarylethenes

- by the reaction of benzophenone hydrazones with diselenium dibromide, *European J. Org. Chem.*, 2004, 820–825 (DOI: 10.1002/ejoc.200300510).
- [24] Minato M., Yamamoto K., Tsuji J. (1990), Osmium tetroxide catalyzed vicinal hydroxylation of higher olefins by using hexacyanoferrate(III) ion as a cooxidant, *J. Org. Chem.*, 55, 766–768 (DOI: 10.1021/jo00289a066).
- [25] Barhdadi R., Courtinard C., Nédélec J Y., Troupel M. (2003), Room-temperature ionic liquids as new solvents for organic electrosynthesis. The first examples of direct or nickel-catalysed electroreductive coupling involving organic halides, *Chem. Commun.*, 1434–1435 (DOI: 10.1039/B302944A).
- [26] Tang C. W., VanSlyke S. A. (1987), Organic electroluminescent diodes, *Appl. Phys. Lett.*, 51, 913 (DOI: 10.1063/1.98799).
- [27] Farinola G M., Ragni R. (2011), Electroluminescent materials for white organic light emitting diodes, *Chem. Soc. Rev.*, 40, 3467 (DOI: 10.1039/c0cs00204f).
- [28] Yang J., Huang J., Li Q., Li Z. (2016), Blue AIEgens: approaches to control the intramolecular conjugation and the optimized performance of OLED devices, *J. Mater. Chem. C*, 4, 2663–2684 (DOI: 10.1039/C5TC03262H).
- [29] Zhao Z., Chen S., Lam J. W. Y., Lu P., Zhong Y., Wong K. S., Kwok H. S., Tang B. Z. (2010), Creation of highly efficient solid emitter by decorating pyrene core with AIE-active tetraphenylethene peripheriesw, (DOI: 10.1039/b921451h).
- [30] Zhao Z., Deng C., Chen S., Lam J W Y., Qin W., Lu P., Wang Z., Kwok H S., Ma Y., Qiu H., et al. (2011), Full emission color tuning in luminogens constructed from tetraphenylethene, benzo-2,1,3-thiadiazole and thiophene building blocks, *Chem. Commun.*, 47, 8847 (DOI: 10.1039/c1cc12775f).
- [31] Chen S., Zhao Z., Tang B. Z., Kwok H S. (2010), Non-doped white organic light-emitting diodes based on aggregation-induced emission, *J. Phys. D. Appl. Phys.*, 43, 95101 (DOI: 10.1088/0022-3727/43/9/095101).

- [32] Mei J., Leung N. L. C., Kwok R. T. K., Lam J. W. Y., Tang B. Z. (2015), Aggregation-induced emission: together we shine, united we soar!, *Chem. Rev.*, 115, 11718–11940 (DOI: 10.1021/acs.chemrev.5b00263).
- [33] Zhao N., Lam J. W. Y., Sung H. H. Y., Su H. M., Williams I. D., Wong K. S., Tang B. Z. (2014), Effect of the counterion on light emission: a displacement strategy to change the emission behaviour from aggregation-caused quenching to aggregation-induced emission and to construct sensitive fluorescent sensors for  $\text{Hg}^{2+}$  detection, *Chem. - A Eur. J.*, 20, 133–138 (DOI: 10.1002/chem.201303251).
- [34] Liu Y., Deng C., Tang L., Qin A., Hu R., Sun J Z., Tang B Z. (2011), specific detection of d -glucose by a tetraphenylethene-based fluorescent sensor, *J. Am. Chem. Soc.*, 133, 660–663 (DOI: 10.1021/ja107086y).
- [35] Liang J., Kwok R T K., Shi H., Tang B Z., Liu B. (2013), Fluorescent light-up probe with aggregation-induced emission characteristics for alkaline phosphatase sensing and activity study, *ACS Appl. Mater. Interfaces*, 5, 8784–8789 (DOI: 10.1021/am4026517).
- [36] Li D., Liu J., Kwok R T K., Liang Z., Zhong Tang B., Yu J. (2012), Supersensitive detection of explosives by recyclable AIE luminogen-functionalized mesoporous materials, *Chem. Commun. Chem. Commun*, 48, 7167–7169 (DOI: 10.1039/c2cc31890c).
- [37] Schultz A., Diele S., Laschat S., Nimtz M. (2001), Novel columnar tetraphenylethenes via mcmurry coupling, *Adv. Funct. Mater.*, 11, 441 (DOI: 10.1002/1616-3028(200112)11:6<441::AID-ADFM441>3.0.CO;2-8).
- [38] Wang M., Zheng Y-R., Ghosh K., Stang P. J. (2010), Metallosupramolecular tetragonal prisms via multicomponent coordination-driven template-free self-assembly, *J. Am. Chem. Soc.*, 132, 6282–6283 (DOI: 10.1021/ja100889h).
- [39] Chi Z., Zhang X., Xu B., Zhou X., Ma C., Zhang Y., Liu S., Xu J. (2012), Recent advances in organic mechanofluorochromic materials, *Chem. Soc. Rev.*, 41, 3878 (DOI: 10.1039/c2cs35016e).
- [40] Sagara Y., Yamane S., Mitani M., Weder C. and Kato T. (2016),

- Mechanoresponsive luminescent molecular assemblies: an emerging class of materials, *Adv. Mater.*, 28, 1073–1095 (DOI: 10.1002/adma.201502589).
- [41] Xue S., Qiu X., Sun Q., Yang W. (2016), Alkyl length effects on solid-state fluorescence and mechanochromic behavior of small organic luminophores, *J. Mater. Chem. C*, 4, 1568–1578 (DOI: 10.1039/C5TC04358A).
- [42] Zhang X., Chi Z., Li H., Xu B., Li X., Zhou W., Liu S., Zhang Y., Xu J. (2011), Piezofluorochromism of an aggregation-induced emission compound derived from tetraphenylethylene, *Chem. - An Asian J.*, 6, 808–811 (DOI: 10.1002/asia.201000802).
- [43] Xu B., Chi Z., Zhang X., Li H., Chen C., Liu S., Zhang Y., Xu J. (2011), A new ligand and its complex with multi-stimuli-responsive and aggregation-induced emission effects, *Chem. Commun.*, 47, 11080 (DOI: 10.1039/c1cc13790e).
- [44] Yan L., Zhang Y., Xu B., Tian W. (2016), Fluorescent nanoparticles based on AIE fluorogens for bioimaging, *Nanoscale*, 8, 2471–2487 (DOI: 10.1039/C5NR05051K).
- [45] Zhao N., Li M., Yan Y., Lam J W Y., Zhang Y L., Zhao Y S., Wong K S., Tang B. Z. (2013), A tetraphenylethene-substituted pyridinium salt with multiple functionalities: synthesis, stimuli-responsive emission, optical waveguide and specific mitochondrion imaging, *J. Mater. Chem. C*, 1, 4640 (DOI: 10.1039/c3tc30759j).
- [46] Liang J., Shi H., Tang B Z., Liu B. (2013), specific light-up bioprobes with aggregation-induced emission characteristics for protein sensing, *Aggregation-Induced Emission: Fundamentals* (Chichester, United Kingdom: John Wiley and Sons Ltd) pp 239–258 (DOI: 10.1002/9781118735183.ch29).

## Chapter 2

# Materials and Experimental Techniques

---

### 2.1. Introduction

In this chapter the materials used, general synthetic procedures, characterization techniques and the instrumentation employed in this thesis are discussed.

### 2.2. Chemicals for synthesis

Common solvents used for syntheses were purified according to known procedures.<sup>[1]</sup> 4-bromobenzophenone, diphenyl methane, ammonium acetate, phenanthroquinone, benzaldehyde, pyrene, were obtained from Spectrochem India. 4,7-Dibromobenzo[c]-1,2,5-thiadiazole, 4-iodopyrazole, tributylborane solution, *n*-BuLi, dry THF, CuI, Pd(PPh<sub>3</sub>)<sub>4</sub>, PdCl<sub>2</sub>(PPh<sub>3</sub>)<sub>2</sub>, ferrocene, and tetrabutylammonium hexafluorophosphate (TBAPF<sub>6</sub>), were procured from Aldrich chemicals USA. Aluminum oxide (neutral) and silica gel (100 – 200 mesh and 230 – 400 mesh) were purchased from Rankem chemicals, India. TLC pre-coated silica gel plates (Kieselgel 60F254, Merck) were obtained from Merck, India.

Dry solvents dichloromethane, chloroform, tetrahydrofuran (THF), *N,N*-dimethylformamide (DMF), dioxane and methanol were obtained from spectrochem and S.D.Fine chem. Ltd. All oxygen or moisture sensitive reactions were performed under nitrogen/argon atmosphere.

The solvents and reagents were used as received unless otherwise indicated. Photophysical and electrochemical studies were performed with spectroscopic grade solvents.

### 2.3. Spectroscopic Measurements

#### 2.3.1. NMR Spectroscopy

<sup>1</sup>H NMR (400 MHz), and <sup>13</sup>C NMR (100 MHz) spectra were recorded on the Bruker Avance (III) 400 MHz, using CDCl<sub>3</sub> and acetone-*d*<sub>6</sub> as solvent. Chemical shifts in <sup>1</sup>H, and <sup>13</sup>C spectra were reported in parts per million (ppm). In <sup>1</sup>H NMR chemical shifts are reported relative to the residual solvent peak (CDCl<sub>3</sub>, 7.26 ppm). Multiplicities are given as: s (singlet), d (doublet), t (triplet), q (quartet), dd (doublet of doublets), m (multiplet), and the coupling constants *J*, are given in Hz. <sup>13</sup>C NMR chemical shifts are reported relative to the solvent residual peak (CDCl<sub>3</sub>, 77.36 ppm).

### 2.3.2. Mass Spectrometry

High resolution mass spectra (HRMS) were recorded on Bruker-Daltonics, microTOF-Q II mass spectrometer using positive and negative mode electrospray ionizations.

### 2.3.3. UV-vis Spectroscopy

UV-Vis absorption spectra were recorded using a Varian Cary100 Bio UV-Vis and PerkinElmer LAMBDA 35 UV/Vis spectrophotometer. The measurements were performed at 25 °C and path length of 1 cm quartz cuvette. The 2.0 mL volume of luminogen solutions were used for study. The solid state absorption spectra were recorded using BaSO<sub>4</sub> as standard

### 2.3.4. Fluorescence Spectroscopy

Fluorescence emission spectra were recorded upon specific excitation wavelength on a Horiba Scientific Fluoromax-4 spectrophotometer. The slit width for the excitation and emission was set at 2 nm. The measurements were performed at 25 °C and path length of 1 cm quartz cuvette. The 2.0 mL volume of luminogen solutions were used for study. The solid state fluorescence measurements were performed on glass slide and front face sample holder accessory were used in fluorimeter.

#### *The fluorescence quantum yields ( $\Phi_F$ )*

The fluorescence quantum yields ( $\Phi_F$ ) of luminogens were calculated by the steady-state comparative method using following equation,

$$\Phi_F = \Phi_{st} \times S_u/S_{st} \times A_{st} / A_u \times n_{Du}^2/n_{Dst}^2 \dots\dots\dots (Eq. 1)$$

Where  $\Phi_F$  is the emission quantum yield of the sample,  $\Phi_{st}$  is the emission quantum yield of the standard,  $A_{st}$  and  $A_u$  represent the absorbance of the standard and sample at the excitation wavelength, respectively, while  $S_{st}$  and  $S_u$  are the integrated emission band areas of the standard and sample, respectively, and  $n_{Dst}$  and  $n_{Du}$  the solvent refractive index of the standard and sample, u and st refer to the unknown and standard, respectively.

## 2.4. Electrochemical Studies

Cyclic voltamograms (CVs) and Differential Pulse Voltamograms (DPVs) were recorded on CHI620D electrochemical analyzer using Glassy carbon or platinum as working electrode, Pt wire as the counter electrode, and Saturated Calomel Electrode (SCE) or Ag/AgCl as the reference electrode. The scan rate was 100 mVs<sup>-1</sup>. A solution of tetrabutylammonium hexafluorophosphate (TBAPF<sub>6</sub>) in CH<sub>2</sub>Cl<sub>2</sub> (0.1 M) was employed as the supporting electrolyte.

## 2.5. Powder XRD (PXRD)

Powder X-ray Diffraction (PXRD) analyses were performed on the Rigaku SmartLab, Automated Multipurpose x-ray Diffractometer.

## 2.6. Computational Calculations

The density functional theory (DFT) calculation were carried out at the B3LYP/6-31G\*\* level in the Gaussian 09 program.<sup>[2]</sup>

## 2.7. Single Crystal X-ray Diffraction Studies

Single crystal X-ray diffraction studies were performed on SUPER NOVA diffractometer. The strategy for the Data collection was evaluated by using the CrysAlisPro CCD software. The data were collected by the standard 'phi-omega scan techniques, and were scaled and reduced using CrysAlisPro RED software. The structures were solved by direct methods using SHELXS-97, and refined by full matrix least-squares with SHELXL-97, refining on  $F^2$ . The positions of all the atoms were obtained by direct methods. All non-hydrogen atoms were refined anisotropically. The remaining hydrogen atoms were placed in geometrically constrained positions, and refined with isotropic temperature factors, generally  $1.2U_{eq}$  of their parent atoms. The CCDC numbers contain the respective supplementary crystallographic data. These data can be obtained free of charge via [www.ccdc.cam.ac.uk/conts/retrieving.html](http://www.ccdc.cam.ac.uk/conts/retrieving.html) (or from the Cambridge Crystallographic Data Centre, 12 union Road, Cambridge CB21 EZ, UK; Fax: (+44) 1223-336-033; or [deposit@ccdc.cam.ac.uk](mailto:deposit@ccdc.cam.ac.uk)).

## 2.8. Scanning electron microscopy (SEM)

The SEM images were collected on Carl Zeiss supra 55 and Field emission JSM-7001F (JEOL) operated at 15 kV after sputtering with gold. The samples for SEM were prepared by drop casting AIE solution of luminogens.

## 2.9. Thermogravimetric analysis (TGA)

Thermogravimetric analyses were performed on the Metler Toledo thermal analysis system. The measurements were done at heating rate of 10 °C/minute and heated upto 800 °C.

## 2.10. Dynamic light scattering (DLS)

The dynamic light scattering (DLS) studies were done on a Micromeritics Nanoplus 3 instrument. The samples for DLS study was used as it is AIE solution of luminogens.

## 2.11. Mechanochromism study

The mechanochromic properties were studied mainly by grinding, fuming and annealing. The grinded samples were prepared by taking the pristine/synthesized sample into a mortar and grinding it manually for

approximately 10 minutes by using a pestle. Annealing was done by heating the grinded samples in oven in open atmosphere at respective temperatures. In order to perform fumigation, the grinded samples were taken on a glass plate. The glass plate was further placed in a solvent chamber saturated with the vapors of the particular solvent.

## 2.12. References

---

- [1] (a) Vogel, A. I., Tatchell, A. R., Furnis, B. S., Hannaford, A. J., & Smith, P. W. G. (1996). *Vogel's Textbook of Practical Organic Chemistry (5th Edition)* (5th ed.); (b) Wei Ssberger, A. Proskraner, E. S. Riddick, J. A. Toppos Jr., E. F. (1970). *Organic Solvents in Techniques of Organic Chemistry*, Vol. IV, 3rd Edition, Inc. New York.
- [2] (a) Lee, C., Yang, W., & Parr, R. G. (1988). Development of the Colle-Salvetti correlation-energy formula into a functional of the electron density. *Physical Review B*, 37(2), 785–789. **DOI:** 10.1103/PhysRevB.37.785; (b) A.D. Becke (1993). A new mixing of Hartree-Fock and local density-functional theories. *J. Chem. Phys.* 98 (2), 1372–377. **DOI:** 10.1063/1.464304.

## Chapter 3

# Reversible mechanochromism and enhanced AIE in tetraphenylethene substituted phenanthroimidazoles

---

---

### 3.1. Introduction

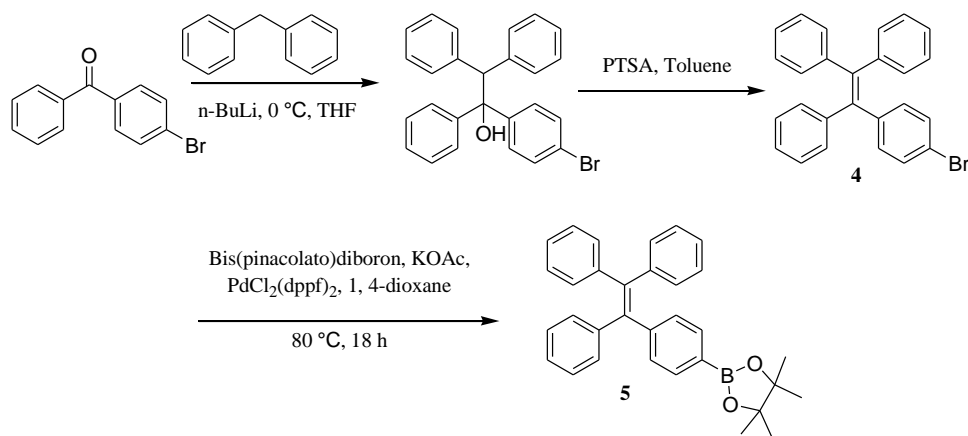
The development of mechanochromic luminescent materials have gained substantial attention due to their potential applications in mechano-sensors, security papers, data storage, and optoelectronic devices.<sup>[1-5]</sup> High contrast and solid state emission are key requirements for mechanochromic luminescent materials.<sup>[6]</sup> The conventional fluorescent molecules suffers from aggregation caused quenching (ACQ), which leads to poor solid state emission.<sup>[7-9]</sup> Tang *et al* introduced an effective methodology to overcome ACQ, which is called aggregation induced emission (AIE).<sup>[10]</sup> The AIE active molecules are highly fluorescent in the solid state, which is essential requirement for mechanochromism. The tetraphenylethene (TPE) derivatives show AIE phenomenon and mechanochromic effect.<sup>[11-17]</sup> The literature reveals that the incorporation of electronegative groups (F, CN) in AIE active fluorophores result in aggregation induced enhanced emission (AIEE) which improves the solid state emission.<sup>[18-21]</sup>

Phenanthroimidazoles based molecular systems have been explored in optoelectronics and molecular biology.<sup>[22-24]</sup> In this chapter, we wish to report synthesis of novel mechanochromic compounds **3a** and **3b**, which exhibits strong solid-state fluorescence and reversible mechano-response. Grinding of **3a** and **3b** results in change in fluorescence, which can be fully restored to its original color upon heating or exposure to solvent vapors. The destruction of solid state packing in the crystalline state to the amorphous state is responsible for the change in emission. The incorporation of cyano group in phenanthroimidazole leads to hydrogen bonding assisted tight packing in the solid-state which results in improved thermal stability and AIEE.

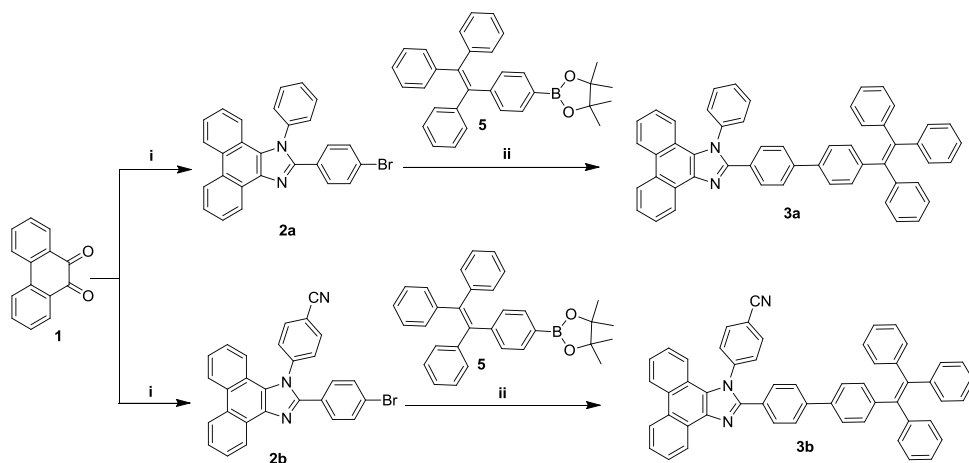
## 3.2. Results and discussion

### 3.2.1. Synthesis

The TPE substituted phenanthroimidazoles **3a** and **3b** were synthesized by the Suzuki cross-coupling reaction of 4-(1,2,2-triphenylvinyl)phenylboronic acid pinacol ester (**5**) with corresponding bromo-phenanthroimidazoles **2a** and **2b** using  $\text{Pd}(\text{PPh}_3)_4$  as catalyst in 67% and 78% yields, respectively (Scheme 3.2). The 4-(1,2,2-triphenylvinyl)phenylboronic acid pinacol ester (**5**) was synthesized from bromo-tetraphenylethene (TPE-Br) (**4**) (Scheme 3.1). The condensation reaction of 9,10-phenanthroquinone **1** with 4-bromobenzaldehyde and aniline (for **2a**)/4-aminobenzonitrile (for **2b**) resulted 2-(4-Bromo-phenyl)-1-phenyl-1H-phenanthro[9,10-d]imidazole (**2a**) and 4-[2-(4-Bromo-phenyl)-phenanthro[9,10-d]imidazol-1-yl]-benzonitrile (**2b**) in 91% and 76% yields, respectively.<sup>[22-24]</sup> The phenanthroimidazoles **3a** and **3b** were purified by column chromatography followed by crystallization. The TPE substituted phenanthroimidazoles **3a** and **3b** were well characterized by  $^1\text{H}$  NMR,  $^{13}\text{C}$  NMR, high resolution mass spectrometry (HRMS), and single crystal X-ray analysis.



**Scheme 3.1.** Synthetic route to intermediate **5**.



**Scheme 3.2.** Synthetic route for the phenanthroimidazoles **3a** and **3b**.

(i) Aniline (for **2a**)/ 4-aminobenzonitrile (for **2b**), 4-bromo benzaldehyde, acetic acid; (ii)  $K_2CO_3$ ,  $Pd(PPh_3)_4$ , Toluene:Ethanol:Water (10.0 mL:4.0 mL:0.5 mL).

### 3.2.2. Thermogravimetric analysis

Thermal stability of the materials is key requirement for mechanochromic effect.<sup>[25]</sup> The thermal stability of **3a** and **3b** were evaluated by thermogravimetric analysis (TGA) (Figure 3.1). The thermal decomposition temperatures ( $T_d$ ) corresponding to 5% weight loss under nitrogen atmosphere are 330 °C, and 445 °C for **3a** and **3b** respectively, which reflects that the incorporation of cyano-group improves the thermal stability.

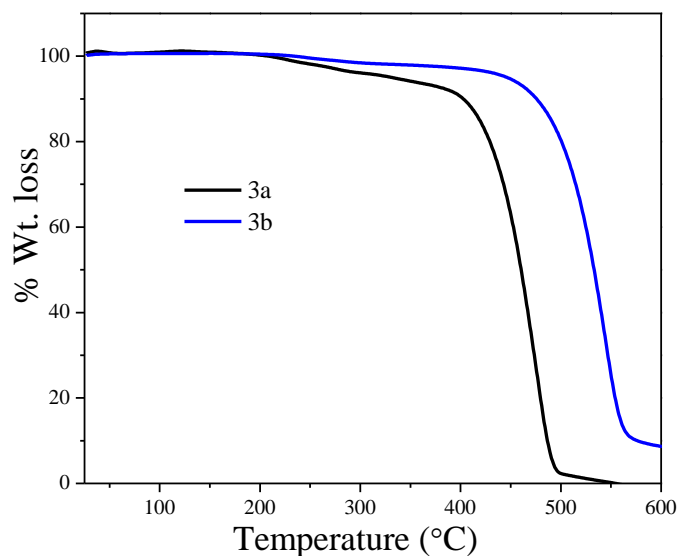


**Figure 3.1.** Thermogravimetric analysis of **3a** and **3b**, measured at a heating rate of 10 °C/ min under nitrogen atmosphere.

### 3.2.3. Photophysical properties

The electronic absorption and fluorescence spectra of **3a** and **3b** in dichloromethane solution are shown in Figure 3.2 and corresponding data are listed in Table 3.1. TPE substituted phenanthroimidazoles **3a** and **3b** exhibits sharp absorption band at 261 nm and broad absorption between 300-370 nm and poor emission at 415 and 458 nm respectively. The loss of excited state energy by intramolecular rotations of tetraphenylethene (TPE) unit makes them poorly fluorescent in solution.

**Table 3.1 Photophysical, and thermal properties of the 3a and 3b.**

Compounds	$\lambda_{\text{max}}$ [nm] ( $\epsilon$ [Lmol <sup>-1</sup> cm <sup>-1</sup> ]) <sup>a</sup>	$\lambda_{\text{em}}$ .(nm)	$\Phi_{\text{f}}$ <sup>b</sup>	Optical band gap (eV)	Theoretical band gap (eV) <sup>c</sup>	T <sub>d</sub> (°C)
<b>3a</b>	260 (52389)					
	344 (33215)	415	0.009	3.12	4.08	330
	363 (29321)					
<b>3b</b>	257 (51452)					
	346 (28593)	458	0.004	3.04	3.31	445
	360 (27064)					

<sup>a</sup>Measured in dichloromethane. <sup>b</sup>The fluorescence quantum yields using 9, 10-diphenylanthracene as a standard in ethanol solution were performed. <sup>c</sup>Theoretical values at B3LYP/6-31G(d) level.

The aggregation induced emission (AIE) is the characteristic property of TPE containing fluorophores.<sup>[26-28]</sup> The AIE active molecules are fluorescent in their aggregated state. The TPE substituted phenanthroimidazoles **3a** and **3b** are highly soluble in THF, and sparingly soluble in water. The small aggregates of molecules were prepared by gradual increase in the percentage of water in THF. The poor fluorescence of **3a** and **3b** in THF was enhanced in aggregated suspension (98% aqueous mixture) by 12 and 159 folds, respectively (Figure 3.2 and Figure 3.3).

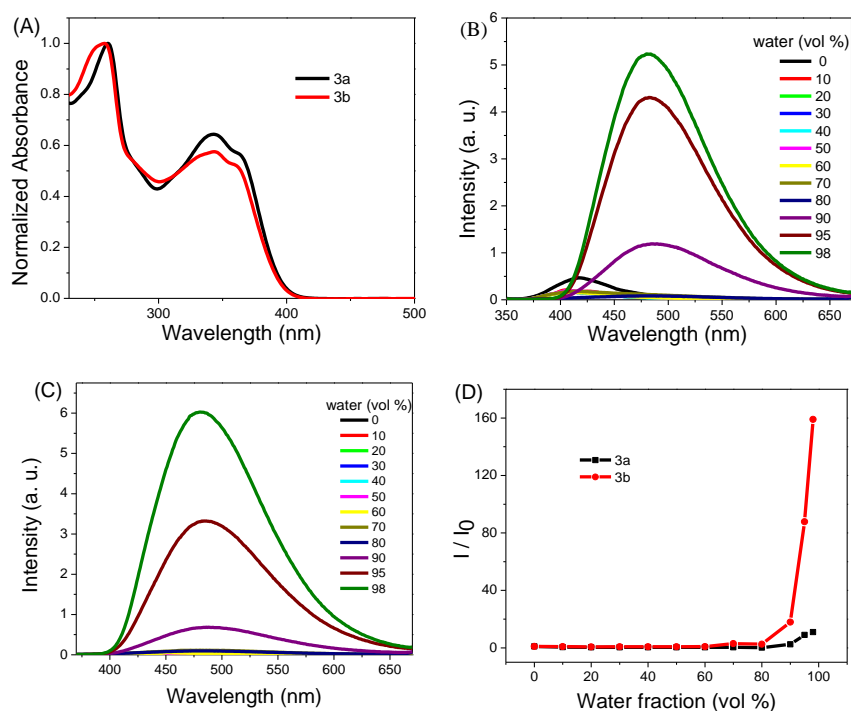


**Figure 3.2.** (A) Electronic absorption spectra of **3a** and **3b** recorded in dichloromethane. Fluorescence spectra of **3a**(B), and **3b** (C) in THF-water mixtures with different water fractions. (D) Plot of Photoluminescence intensity (PL) vs. % of water fraction ( $f_w$ ). Luminogen concentration: 10  $\mu$ M; excitation wavelength: 340 nm; intensity calculated at  $\lambda_{max}$ .



**Figure 3.3.** Fluorescence pictures of **3b** solutions with different water fractions under UV (365 nm) light.

The quantitative enhancement in emission of **3a** and **3b** were evaluated by the fluorescence quantum yields, using 9,10-diphenylanthracene as standard. In pure THF solution **3a** and **3b** show quantum yield of 0.005 and 0.004 respectively this increased to 0.207 and 0.327 in the aggregated state (98 % aqueous). In the aggregated state, the free molecular rotations in the TPE unit decreases and results in increase in fluorescence intensity. Tang *et al.* termed this phenomenon as restricted intramolecular rotation (RIR).<sup>[10]</sup> The high fold increment in AIE intensity of **3b** compared to **3a** can be attributed to tight packing of molecules in the aggregated state, due to more number of C-H--- $\pi$  interactions and additional C(4)-H(4)---N(3) interaction, which is evident from the crystal packing.<sup>[18-21]</sup>

### 3.2.4. Mechanochromic property

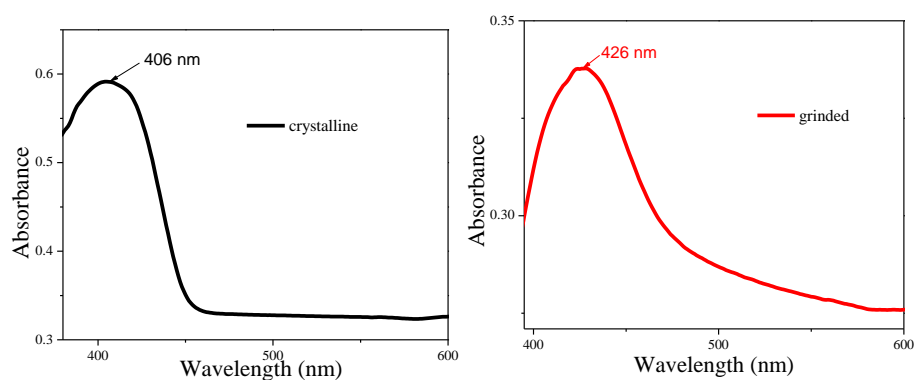


**Figure 3.4.** Solid state absorption spectra of **3a** in crystalline (left) and its grinded (right) form.

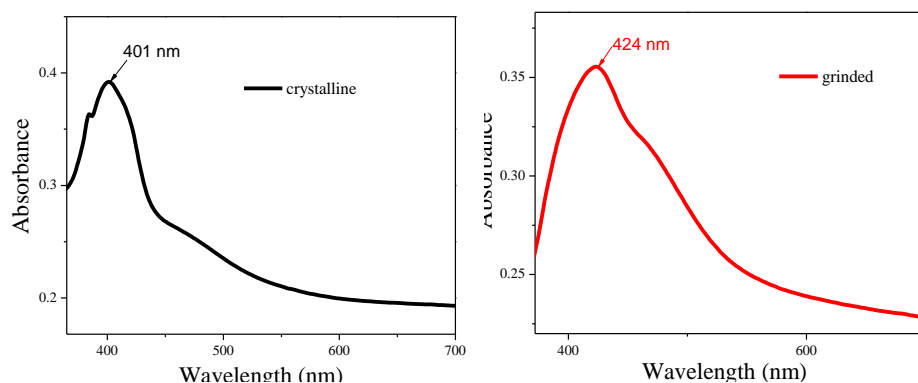


**Figure 3.5.** Solid state absorption spectra of **3b** in crystalline (left) and its grinded (right) form.

The mechanochromic effect of TPE substituted phenanthroimidazoles **3a**

and **3b** were explored by absorption and emission studies. The crystalline form of **3a** and **3b** absorbs at 406 nm and 401 nm respectively (Figure 3.4 and Figure 3.5). Upon grinding **3a** and **3b** exhibits bathochromic shift and absorbs at 426 nm and 424 nm, respectively. The **3a** and **3b** show sky blue emission at 460 nm and 450 nm respectively. Upon grinding using a spatula or pestle the sky blue emitting solids were converted to a yellowish green emitting solids and the emission peak was red-shifted to broad band around 509 nm and 508 nm, respectively (Figure 3.6). The mechanochromic effect can be reverted to its original color by annealing or fuming with solvent vapor. The grinded sample of **3b** upon annealing at 160 °C for 15 min or fuming with dichloromethane vapor for 2 min, restored to the original blue emission, whereas **3a** required high annealing temperature up to 200 °C for 30 min. or fuming with dichloromethane (DCM) vapor for 3 min. This mechanochromic conversion can be repeated between blue and yellowish green emission (10 times) as these stimuli does not cause any chemical change (Figure 3.7).

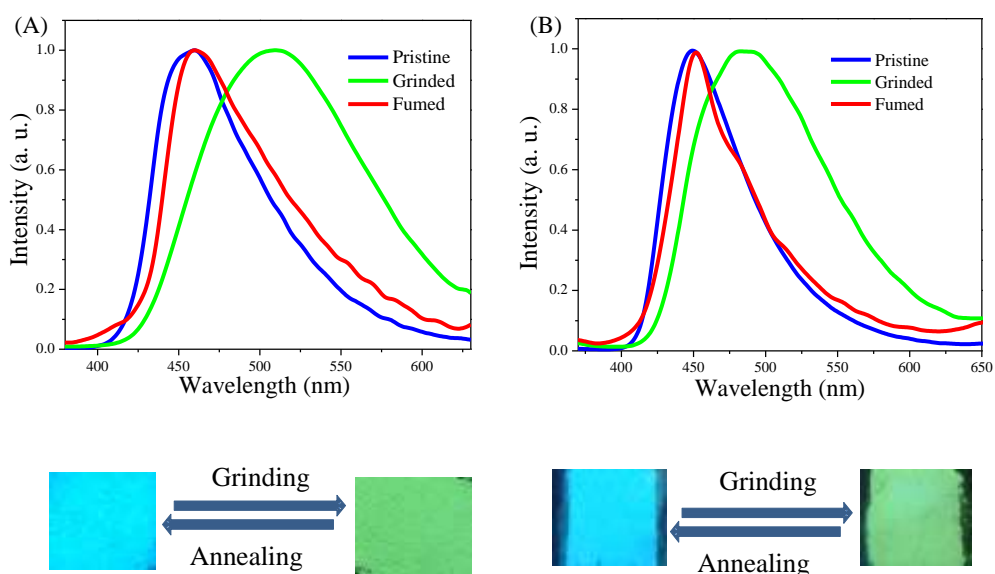


**Figure 3.6.** (A) Emission spectra of (A) **3a** and (B) **3b** as pristine, grinded and fumed solids and photograph taken under 365 nm UV illumination.

In order to understand the mechanism of mechanochromism, we studied **3a** and **3b** at different solid states by powder X-ray diffraction (XRD). The XRD diffractogram of the samples exhibit sharp diffraction peaks, indicative of their crystalline nature (Figure 3.8). After grinding, the sharp peak vanishes and

only a diffuse band was observed suggesting amorphous nature of solids. The grinded powder when heated or fumigated with solvent vapor restores the sharp diffraction peaks. This implies that the amorphous powder restored its crystallinity upon heating or solvent fumigation. This study clearly concludes that the mechanochromism in **3a** and **3b** are associated with the morphology change from the crystalline state to the amorphous state and vice versa.<sup>5</sup> The bathochromic shift in absorption and emission spectra can be attributed to the transformation of twisted crystalline state to planar amorphous state reflecting enhanced conjugation.

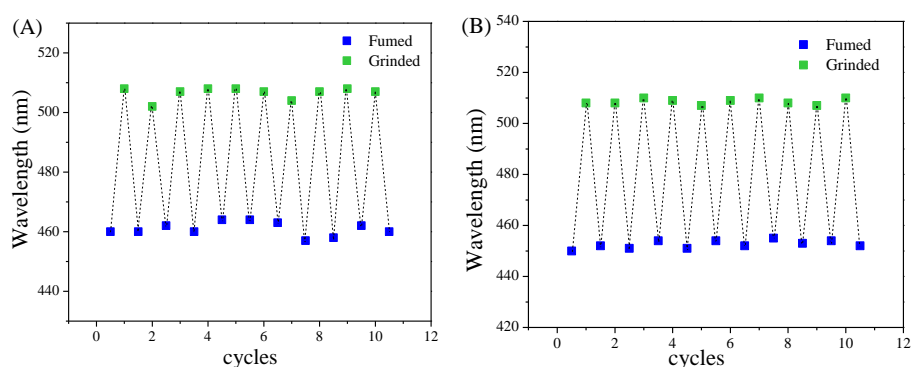


**Figure 3.7.** Repeated switching of the solid-state fluorescence of **3a** and **3b** by repeated grinding and fuming cycles.

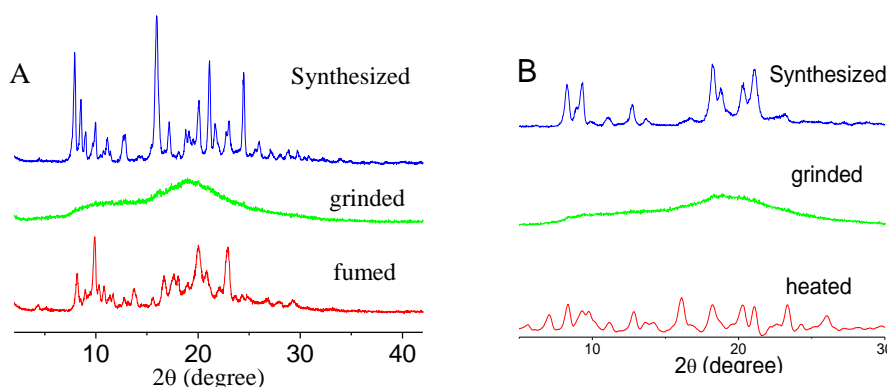


**Figure 3.8.** The XRD patterns of (A) **3a** and (B) **3b** as synthesized, grinded and heated solids.

### 3.2.5. Theoretical calculations

In order to understand the geometry and electronic structure of **3a** and **3b**, density functional theory (DFT) calculations were carried out. The energy

minimized structures for **3a** and **3b** show twisted conformation. The HOMO energy level of **3a** and **3b** are distributed on the entire molecule (Figure 3.9). The LUMO energy level in **3a** is mainly distributed over imidazole and TPE unit. The LUMO of **3b** was distributed on 4-cyanophenyl and imidazole ring. The incorporation of cyano group increases the acceptor strength of imidazole in **3b**. The theoretical band gap for **3a** and **3b** are 4.08 eV and 3.31 eV respectively. The lower band-gap in **3b** suggests bathochromic shift in the electronic absorption spectra, which was not observed. To analyze the origin of absorption bands in the **3b** TD-DFT calculations were performed. The TD-DFT calculations show good agreement with the experimental spectra, and reveals that the main transition ( $\lambda_{\max}$ ) in **3b** is from HOMO→LUMO+1 (Table 3.2).

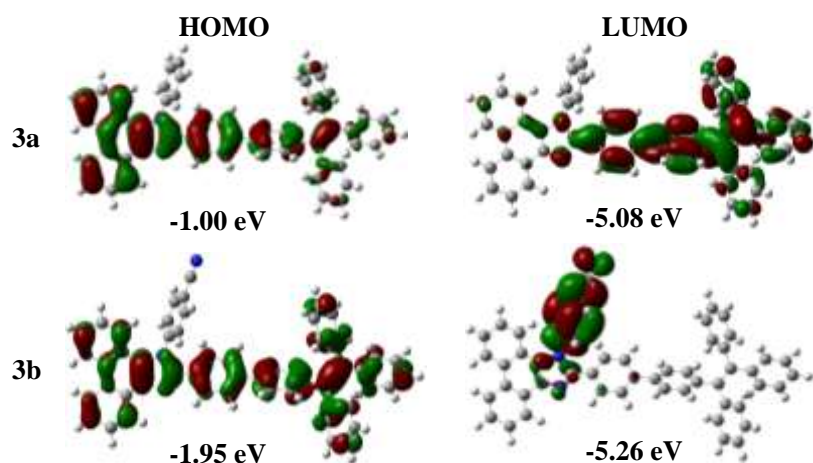


**Figure 3.9.** HOMO and LUMO frontier molecular orbitals of **3a** and **3b** at the B3LYP/6-31G (d) level.

**Table 3.2.** Computed vertical transitions and their oscillator strengths and configurations.

Compound	DCM		
	$\lambda_{\max}$ [nm]	$F$	Configuration
<b>3b</b>	436.39	1.9068	HOMO→LUMO+1 (-0.69633)
	375.67	0.1205	HOMO-1→LUMO+1 (0.68106)
			HOMO→LUMO+2 (0.14759)
	356.25	0.1155	HOMO→LUMO+3 (0.64780)
			HOMO→LUMO+4 (-0.16147)
HOMO-1→LUMO+2 (-0.15729)			

### 3.2.6. Single crystal X-ray diffraction studies

The single crystal X-ray structure of **3a** and **3b** provide insight into the AIE and mechanochromic mechanisms. The single crystal of **3a** and **3b** were obtained by slow diffusion of ethanol into the dichloromethane solution. The crystal structure of **3a** and **3b** exhibits twisted conformation of phenyl rings (Figure 3.10). This twisted conformation support active intramolecular rotations in solution leading to poor fluorescence. In the packing diagram of **3a**, the two mutual C-H $\cdots$  $\pi$  (2.938 Å) and C-H $\cdots$  $\pi$  (2.799 Å) interactions were observed (Figure 3.11). The packing diagram of **3b** reveals tight packing than those of **3a**. The **3b** shows moderate C-H $\cdots$ N hydrogen bonding interactions in the solid state. **3b** form a dimeric structure via two mutual hydrogen bonding interaction between the -CN group and the hydrogen of phenanthroimidazole [C(4)-H(4) $\cdots$ N(3) (2.728 Å)]. Further, C(16)-H(16) $\cdots$  $\pi$  (3.156 Å), C(17)-H(17) $\cdots$  $\pi$  (3.309 Å), and C(40)-H(40) $\cdots$  $\pi$  (3.026 Å) interactions in **3b** stabilize the packing (Figure 3.11).

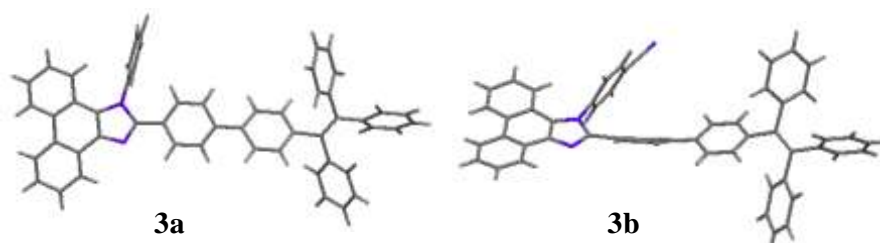


**Figure 3.10.** Crystal structures of **3a** and **3b**.

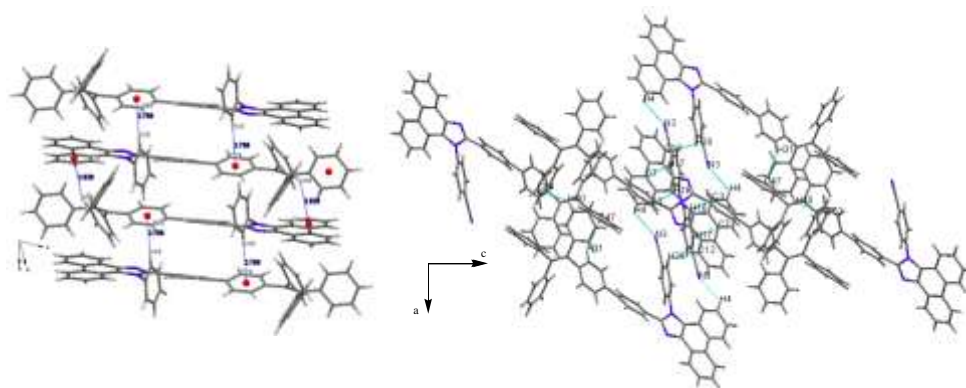


**Figure 3.11.** Crystal packing of **3a** and **3b**.

**Table 3.3.** Crystal data and structure refinement parameters.

Parameter	3a	3b
Identification code	rm104	rm121a
Empirical formula	C <sub>53</sub> H <sub>36</sub> N <sub>2</sub>	C <sub>54</sub> H <sub>35</sub> N <sub>3</sub>
Formula weight	700.84	725.85
Temperature	150(2) K	150(2) K
Wavelength(A)	1.5418	0.71073
Crystal system, space group	Triclinic, P -1	Monoclinic, P 21/n
<i>a</i> / (Å)	9.4287(9)	9.0367(4)
<i>b</i> / (Å)	12.0253(11)	11.5650(8)
<i>c</i> / (Å)	21.1903(15)	38.221(2)
$\alpha$ / (°)	75.864(7)	90
$\beta$ / (°)	86.937(7)	94.875(4)
$\gamma$ / (°)	74.600(8)	90
Volume	2246.0(3) Å <sup>3</sup>	3980.0(4) Å <sup>3</sup>
Z, Calculated density (mg m <sup>-3</sup> )	2, 1.036	4, 1.211
Absorption coefficient /(mm <sup>-1</sup> )	0.457	0.071
F(000)	736	1520
Crystal size	0.23 x 0.18 x 0.13 mm	0.21 x 0.17 x 0.13 mm
$\theta$ range for data collection/(°)	3.93 to 74.82	2.95 to 25.00
Reflections collected / unique	16015 / 8638 [R(int) = 0.0333]	32887 / 7009 [R(int) = 0.1083]
Completeness to theta	$\theta = 74.82$ ; 93.4 %	$\theta = 25.00$ ; 99.8 %
Absorption correction	Semi-empirical from equivalents	Semi-empirical from equivalents
Max. and min. transmission	0.9430 and 0.9021	0.9909 and 0.9853
Refinement method	Full-matrix least-squares on F <sup>2</sup>	Full-matrix least-squares on F <sup>2</sup>
Data / restraints / parameters	8638 / 0 / 497	7009 / 0 / 514
Goodness-of-fit on F <sup>2</sup>	0.980	1.005
Final R indices [I>2sigma(I)]	R1 = 0.1095, wR2 = 0.3502	R1 = 0.0652, wR2 = 0.1371
R indices (all data)	R1 = 0.1834, wR2 = 0.3960	R1 = 0.1526, wR2 = 0.1803
Largest diff. peak and hole (eÅ <sup>-3</sup> )	0.253 and -0.279	0.297 and -0.163

### 3.3. Experimental Section

Compound **4** was prepared according to the synthetic route shown in Scheme 3.1. Details can be found in the previous publication.<sup>[29]</sup> The intermediate **2a** was prepared according to the reported procedure.<sup>[22]</sup>

#### Synthesis and characterization of intermediates **5** and **2b**:

**5**: Pd(dppf)Cl<sub>2</sub>(0.12 mmol) was added to a well degassed solution of bromotetraphenylethene (2.4 mmol), bis(pinacolato)diboron (3.84 mmol) and KOAc (7.2 mmol) in anhydrous 1,4-dioxane (20 mL). The resulting mixture was stirred at 90 °C for 16 h under argon atmosphere. After cooling, the mixture was evaporated to dryness and taken up with CH<sub>2</sub>Cl<sub>2</sub>. The organic layer was washed with H<sub>2</sub>O, dried over MgSO<sub>4</sub>, filtered and evaporated to dryness. Column chromatography (SiO<sub>2</sub>, Hexane/CH<sub>2</sub>Cl<sub>2</sub> 95:5) gave compound **5** as a colorless solid in 68% yield. <sup>1</sup>H NMR (400 MHz, CDCl<sub>3</sub>, 25 °C): δ 7.53–7.55 (m, 2H), 7.07–7.10 (m, 9H), 6.98–7.04 (m, 8H), 1.31 (s, 12H); <sup>13</sup>C NMR (100 MHz, CDCl<sub>3</sub>, 25 °C): δ 146.8, 143.7, 143.6, 143.5, 141.4, 140.9, 134.1, 131.4, 131.3, 131.3, 130.7, 127.7, 127.6, 126.5, 126.5, 126.4, 83.7, 24.9, 0.0 ppm; HRMS (ESI): calcd. for C<sub>32</sub>H<sub>31</sub>BO<sub>2</sub>: 459.2495 (M+H)<sup>+</sup>, found 459.2491.

**2b**: The 9,10-phenanthrenequinone (9.6 mmol), 4-bromobenzaldehyde (9.6 mmol), 4-aminobenzonitrile (14.4 mmol), and ammonium acetate (96.1 mmol) in glacial acetic acid (50 mL) refluxed for 4 h under an argon atmosphere. After cooling to room temperature, a pale yellow mixture was obtained and poured into a methanol solution under stirring. The separated solid was filtered off, washed with 30ml water, and dried to gave compound **2b** as a pale yellow solid. <sup>1</sup>H NMR (400 MHz, CDCl<sub>3</sub>, 25 °C): δ 8.82 (dd, 1H, *J*=1.6, 8 Hz), 8.79 (d, 1H, *J*=8 Hz), 8.71 (d, 1H, *J*=8 Hz), 7.92 (dt, 2H, *J*=2, 8 Hz), 7.74–7.78 (m, 1H), 7.63–7.71 (m, 3H), 7.54–7.58 (m, 1H), 7.47 (dt, 2H, *J*=2.4, 8 Hz), 7.29–7.37 (m, 3H), 7.09 (dd, 1H, *J*=0.8, 8 Hz) ppm; HRMS (ESI): calcd. for C<sub>28</sub>H<sub>16</sub>BrN<sub>3</sub>: 474.0600 (M+H)<sup>+</sup>, found 474.0593.

#### Synthesis and Characterization of **3a-3b**:

**3a**: Pd(PPh<sub>3</sub>)<sub>4</sub> (0.004 mmol) was added to a well degassed solution of 2-(4-Bromo-phenyl)-1-phenyl-1H-phenanthro[9,10-d]imidazole (**2a**) (0.4 mmol), **5**

(0.48 mmol),  $K_2CO_3$ (1.2 mmol) in a mixture of toluene (12 mL)/ ethanol (4.0 mL)/  $H_2O$  (1.0 mL). The resulting mixture was stirred at 80 °C for 24 h under argon atmosphere. After cooling, the mixture was evaporated to dryness and the residue subjected to column chromatography on silica (Hexane-DCM 80:20 in vol.) to yield the desired product **3a** as colorless powder. The compound was recrystallized from DCM:ethanol (8:2) mixtures as colorless needle like crystals. Yield: 67.0%.  $^1H$  NMR (400 MHz,  $CDCl_3$ , 25 °C):  $\delta$  8.89 (dd, 4H,  $J=0.8$ , 8 Hz), 8.78 (d, 1H,  $J=8$  Hz), 8.71 (d, 1H,  $J=8$  Hz), 7.73-7.77 (m, 1H), 7.59-7.68 (m, 6H), 7.47-7.55 (m, 5H), 7.34 (dt, 2H,  $J=2$ , 8 Hz) 7.24-7.29 (m, 1H), 7.18 (dd, 1H,  $J=0.8$ , 8 Hz) 7.02-7.14 (m, 17H) ppm;  $^{13}C$  NMR (100 MHz,  $CDCl_3$ , 25 °C):  $\delta$  150.6, 143.7, 143.7, 143.6, 143.6, 143.2, 141.2, 140.7, 140.4, 138.8, 137.8, 137.5, 131.8, 131.4, 131.3, 130.2, 129.8, 129.6, 129.2, 129.2, 129.1, 128.2, 128.2, 127.8, 127.7, 127.6, 127.3, 127.2, 126.5, 126.5, 126.4, 126.4, 126.1, 125.6, 124.8, 124.1, 123.1, 123.0, 122.7, 120.8, 0.0 ppm; HRMS (ESI): calcd. for  $C_{53}H_{36}N_2$ : 701.2951 (M+H) $^+$ , found 701.2953.

**3b**:  $Pd(PPh_3)_4$  (0.004 mmol) was added to a well degassed solution of 4-[2-(4-Bromo-phenyl)-phenanthro [9,10-d]imidazol-1-yl]-benzotrile (**2b**) (0.4 mmol), **5** (0.48 mmol),  $K_2CO_3$ (1.2 mmol) in a mixture of toluene (12 mL)/ ethanol (4.0 mL)/  $H_2O$  (1.0 mL). The resulting mixture was stirred at 80 °C for 24 h under argon atmosphere. After cooling, the mixture was evaporated to dryness and the residue subjected to column chromatography on silica (Hexane-DCM 70:30 in vol.) to yield the desired product **3b** as colorless powder. The compound was recrystallized from DCM:ethanol (8:2) mixtures as colorless niddle like crystals. Yield: 78.0%.  $^1H$  NMR (400 MHz,  $CDCl_3$ , 25 °C):  $\delta$  8.86 (dd, 1H,  $J=1.2$ , 8 Hz), 8.80 (d, 1H,  $J=8$  Hz) 8.72 (d, 1H,  $J=8$  Hz), 7.91 (dt, 2H,  $J=2$ , 8.8 Hz) 7.74-7.78 (m, 1H), 7.66-7.70 (m, 3H), 7.49-7.57 (m, 5H), 7.30-7.36 (m, 3H) 7.02-7.15 (m, 18H) ppm;  $^{13}C$  NMR (100 MHz,  $CDCl_3$ , 25 °C):  $\delta$  150.5, 143.6, 143.6, 143.5, 142.8, 141.3, 141.3, 140.3, 137.9, 137.5, 134.0, 131.9, 131.4, 131.3, 131.3, 130.2, 129.7, 129.4, 128.4, 128.3, 127.8, 127.7, 127.6, 127.5, 126.9, 126.7, 126.5, 126.5, 126.5, 126.1, 126.0, 125.2, 124.4, 123.1, 122.8, 122.4, 120.4, 117.7, 113.8, 0.0 ppm; HRMS (ESI): calcd. for  $C_{54}H_{35}N_3$ : 726.2904 (M+H) $^+$ , found 726.2923.

### 3.4. Conclusions

In conclusion, we have designed and synthesized high color contrast mechanochromic tetraphenylethene substituted phenanthroimidazoles **3a** and **3b**. The powder XRD results indicate the destruction of solid state packing from crystalline to amorphous state is responsible for mechanochromism. The cyano-group in phenanthroimidazole improves the thermal stability and enhances the AIE. The single crystal X-ray and packing analysis reveals that hydrogen bonding and strong supramolecular interactions are responsible for AIEE in **3b**. The results obtained here will help in design of new AIEE and mechanochromic molecules for various optoelectronic applications.

**Note:** This is copyrighted material from Royal Society of Chemistry, *Chem. Commun.*, 2014, 50, 9076-9078 (DOI: 10.1039/C4CC02824D).

### 3.5. References

- [1] Sagara Y., Kato T. (2009), Mechanically induced luminescence changes in molecular assemblies, *Nat. Chem.*, 1, 605–610 (DOI: 10.1038/nchem.411).
- [2] Davis D A., Hamilton A., Yang J., et al. (2009), Force-induced activation of covalent bonds in mechanoresponsive polymeric materials, *Nature*, 459, 68–72 (DOI: 10.1038/nature07970).
- [3] Dong Y., Xu B., Zhang J., et al. (2012), piezochromic luminescence based on the molecular aggregation of 9,10-bis((*e*)-2-(pyrid-2-yl)vinyl)anthracene, *Angew. Chemie Int. Ed.*, 51, 10782–10785 (DOI: 10.1002/anie.201204660).
- [4] Luo X., Li J., Li C., Heng L., Dong Y Q., Liu Z., Bo Z., Tang B Z. (2011), Reversible switching of the emission of diphenyldibenzofulvenes by thermal and mechanical stimuli, *Adv. Mater.*, 23, 3261–3265 (DOI: 10.1002/adma.201101059).
- [5] Best Q A., Sattenapally N., Dyer D J., Scott C N., McCarroll M E.

- (2013), pH-Dependent Si-fluorescein hypochlorous acid fluorescent probe: spirocycle ring-opening and excess hypochlorous acid-induced chlorination, *J. Am. Chem. Soc.*, 135, 13365–13370 (DOI: 10.1021/ja401426s).
- [6] Kwon M S., Gierschner J., Yoon S-J., Park S Y. (2012), Unique piezochromic fluorescence behavior of dicyanodistyrylbenzene based donor-acceptor-donor triad: mechanically controlled photo-induced electron transfer (et) in molecular assemblies, *Adv. Mater.*, 24, 5487–5492 (DOI: 10.1002/adma.201202409).
- [7] J. B. Birks, *Photophysics of Aromatic Molecules*, Wiley, London, UK, 1970;
- [8] Jayanty S., Radhakrishnan T P. (2004), Enhanced fluorescence of remote functionalized diaminodicyanoquinodimethanes in the solid state and fluorescence switching in a doped polymer by solvent vapors, *Chem. - A Eur. J.*, 10, 791–797 (DOI: 10.1002/chem.200305123).
- [9] Henry J. T., Jerome L. M., Wim T. K., James A. M., Judith H., Scott W., Isaac R., Watts K. (2005), Enhanced photoluminescence from group 14 metalloles in aggregated and solid solutions, *Inorg. Chem.*, 44, 2003–2011 (DOI: 10.1021/IC049034O).
- [10] Luo J., Xie Z., Lam J W Y., et al. (2001), Aggregation-induced emission of 1-methyl-1,2,3,4,5-pentaphenylsilole, *Chem. Commun.*, 397, 1740–1741 (DOI: 10.1039/b105159h).
- [11] Dong Y., Lam J W Y., Qin A., Liu J., Li Z., Tang B Z., Sun J., Kwok H S. (2007), Aggregation-induced emissions of tetraphenylethene derivatives and their utilities as chemical vapor sensors and in organic light-emitting diodes, *Appl. Phys. Lett.*, 91, 11111 (DOI: 10.1063/1.2753723).
- [12] Huang J., Yang X., Wang J., et al. (2012), New tetraphenylethene-based efficient blue luminophors: aggregation induced emission and partially controllable emitting color, *J. Mater. Chem.*, 22, 2478–2484

(DOI: 10.1039/C1JM14054J).

- [13] Zhao N., Yang Z., Lam J W Y., et al. (2012), Benzothiazolium-functionalized tetraphenylethene: an AIE luminogen with tunable solid-state emission, *Chem. Commun.*, 48, 8637 (DOI: 10.1039/c2cc33780k).
- [14] Wang J., Mei J., Hu R., Sun J Z., Qin A., Tang B Z. (2012), Click synthesis, aggregation-induced emission, *e / z* isomerization, self-organization, and multiple chromisms of pure stereoisomers of a tetraphenylethene-cored luminogen, *J. Am. Chem. Soc.*, 134, 9956–9966 (DOI: 10.1021/ja208883h).
- [15] Zhao N., Li M., Yan Y., Lam J W Y., Zhang Y L., Zhao Y S., Wong K S., Tang B Z., Xiao L., Chen Z., et al. (2013), A tetraphenylethene-substituted pyridinium salt with multiple functionalities: synthesis, stimuli-responsive emission, optical waveguide and specific mitochondrion imaging, *J. Mater. Chem. C*, 1, 4640 (DOI: 10.1039/c3tc30759j).
- [16] Xu B., Xie M., He J., Xu B., Chi Z., Tian W., Jiang L., Zhao F., Liu S., Zhang Y., et al. (2013), An aggregation-induced emission luminophore with multi-stimuli single- and two-photon fluorescence switching and large two-photon absorption cross section, *Chem. Commun.*, 49, 273–275 (DOI: 10.1039/C2CC36806D).
- [17] Xu B., Chi Z., Zhang X., Li H., Chen C., Liu S., Zhang Y., Xu J., Beyer M K., Clausen-Schaumann H., et al. (2011), A new ligand and its complex with multi-stimuli-responsive and aggregation-induced emission effects, *Chem. Commun.*, 47, 11080 (DOI: 10.1039/c1cc13790e).
- [18] Byeong-Kwan A., Soon-Ki K., Sang-Don J., and Park S Y. (2002), Enhanced emission and its switching in fluorescent organic nanoparticles, *J. Am. Chem. Soc.*, 124, 14410–14415 (DOI: 10.1021/JA0269082).

- [19] Liu J., Meng Q., Zhang X., Lu X., He P., Jiang L., Dong H., Hu W., Jenekhe S A., Osaheni J A., et al. (2013), Aggregation-induced emission enhancement based on 11,11,12,12,-tetracyano-9,10-anthraquinodimethane, *Chem. Commun.*, 49, 1199 (DOI: 10.1039/c2cc38817k).
- [20] Shi Z., Davies J., Jang S-H., Kaminsky W., Jen A K-Y., Burroughes J H., Bradley D D C., Brown A R., Marks R N., Mackay K., et al. (2012), Aggregation induced emission (AIE) of trifluoromethyl substituted distyrylbenzenes, *Chem. Commun.*, 48, 7880 (DOI: 10.1039/c2cc32380j).
- [21] Gong Y., Tan Y., Liu J., Lu P., Feng C., Yuan W Z., Lu Y., Sun J Z., He G., Zhang Y., et al. (2013), Twisted D- $\pi$ -A solid emitters: efficient emission and high contrast mechanochromism, *Chem. Commun.*, 49, 4009 (DOI: 10.1039/c3cc39243k).
- [22] Zhang Y., Lai S-L., Tong Q-X., Lo M-F., Ng T-W., Chan M-Y., Wen Z-C., He J., Jeff K-S., Tang X-L., et al. (2012), High efficiency nondoped deep-blue organic light emitting devices based on imidazole- $\pi$ -triphenylamine derivatives, *Chem. Mater.*, 24, 61–70 (DOI: 10.1021/cm201789u).
- [23] Zhang S., Li W., Yao L., Pan Y., Shen F., Xiao R., Yang B., Ma Y., Baldo M A., O'Brien D F., et al. (2013), Enhanced proportion of radiative excitons in non-doped electro-fluorescence generated from an imidazole derivative with an orthogonal donor-acceptor structure, *Chem. Commun.*, 49, 11302 (DOI: 10.1039/c3cc47130f).
- [24] Eseola A O., Adepitan O., Görls H., Plass W., Angell S E., Rogers C W., Zhang Y., Wolf M O., Jr. W E J., Pradeep C P., et al. (2012), Electronic/substituents influence on imidazole ring donor-acceptor capacities using 1H-imidazo[4,5-f][1,10]phenanthroline frameworks, *New J. Chem.*, 36, 891 (DOI: 10.1039/c2nj20880f).
- [25] Li H., Zhang X., Chi Z., Xu B., Zhou W., Liu S., Zhang Y. and Xu J. (2011), New thermally stable piezofluorochromic aggregation-induced

- emission compounds, *Org. Lett.*, 13, 556–559 (DOI: 10.1021/ol102872x).
- [26] Hong Y., Lam J W Y., Tang B Z., III S W T., Joly G D., Swager T M., Hoeben F J M., Jonkheijm P., Meijer E W., Schenning A P H J., et al. (2011), Aggregation-induced emission, *Chem. Soc. Rev.*, 40, 5361 (DOI: 10.1039/c1cs15113d).
- [27] Chen F., Zhang J., Wan X. (2012), Design and synthesis of piezochromic materials based on push-pull chromophores: a mechanistic perspective, *Chem. - A Eur. J.*, 18, 4558–4567 (DOI: 10.1002/chem.201102929).
- [28] Qi Q., Zhang J., Xu B., Li B., Zhang S X-A., Tian W. (2013), Mechanochromism and polymorphism-dependent emission of tetrakis(4-(dimethylamino)phenyl)ethylene, *J. Phys. Chem. C*, 117, 24997–25003 (DOI: 10.1021/jp407965a).
- [29] Hu R., Maldonado J L., Rodriguez M., Deng C., Jim C K W., Lam J W Y., Yuen M M F., Ramos-Ortiz G., Tang B Z. (2012), Luminogenic materials constructed from tetraphenylethene building blocks: Synthesis, aggregation-induced emission, two-photon absorption, light refraction, and explosive detection, *J. Mater. Chem.*, 22, 232–240 (DOI: 10.1039/C1JM13556B).

## Chapter 4

# Effect of end-groups on mechanochromism in tetraphenylethylene substituted phenanthroimidazoles

---

### 4.1. Introduction

Design and synthesis of mechanochromic materials and emitters for organic light-emitting diode (OLED) are gaining considerable attention of scientific community due to their potential applications in the field of mechano-sensors, optical recording, security papers and optoelectronic devices.<sup>[1-3]</sup> The emission property of organic materials is governed by number of factors such as, effective conjugation length, planarity, and their interactions with surrounding environment. The molecular arrangement of materials in solid state is one of the important factors which control the emission of solids. The control over the solid state emission is a great challenge in designing the mechanochromic materials. Several attempts have been made to control over molecular arrangement and planarity by using electronegative elements and varying number and position of alkyl substituents and their chain lengths.<sup>[4-13]</sup>

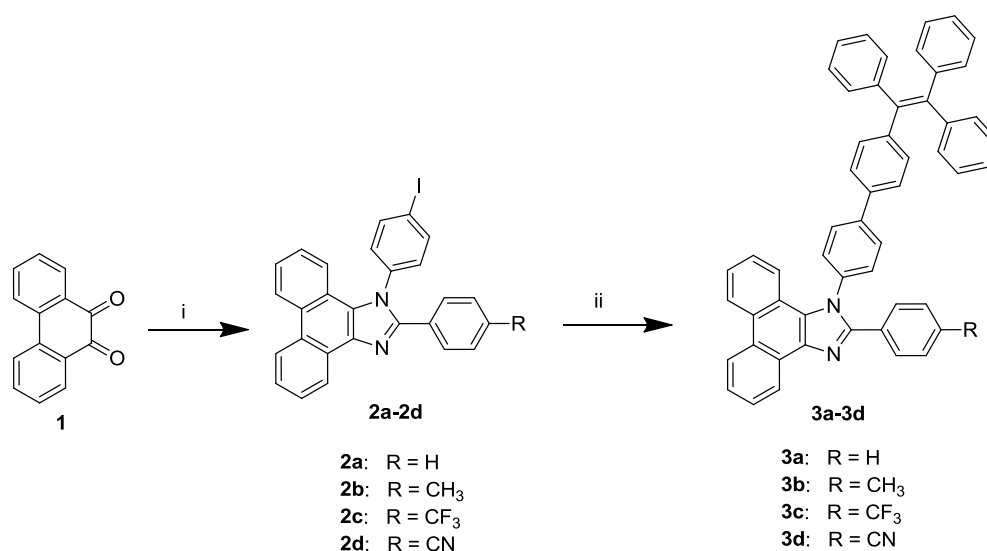
To develop good mechanochromic material and achieve high performance full color displays, highly efficient solid state emitters with outstanding stability are essential. The traditional dyes are non-emissive in solid state due to notorious effect called aggregation caused quenching (ACQ).<sup>[14-16]</sup> To overcome this, the new family of molecules was developed called aggregation induced emission (AIE) active molecules, they are highly fluorescent in the solid state.<sup>[17-20]</sup> The tetraphenylethylene (TPE) is AIE active molecule and frequently used in developing mechanochromic materials.<sup>[21-28]</sup> The TPE based AIE type emitters are also ideal as non-doped emitters in the OLEDs because ACQ effect frequently observed in common emitters can be avoided.<sup>[29]</sup>

Our group is involved in the design and synthesis of mechanochromic materials based on TPE.<sup>[30-32]</sup> Previous chapter, we have discussed TPE substituted phenanthroimidazoles as efficient mechanochromic material.<sup>[33]</sup>

We were further interested to study the positional effect of TPE unit by altering the position of TPE and phenyl unit on imidazole. The effect of different end groups on phenanthroimidazoles on its solid state emission and mechanochromism was studied. In this chapter we have designed four mechanochromic materials **3a–3d** by integrating tetraphenylethylene (TPE), a typical AIE luminogen to phenanthroimidazole having different (H, CH<sub>3</sub>, CF<sub>3</sub> and CN) substituents. It was found that the emission properties of phenanthroimidazoles **3a–3d** were dependent upon the substituent on phenanthroimidazole. The phenanthroimidazoles **3a–3d** show reversible mechano-response between blue and green.

## 4.2. Results and Discussion

### 4.2.1. Synthesis



**Scheme 4.1.** Synthetic route for the phenanthroimidazoles **3a–3d**. (i) 4-iodoaniline, benzaldehyde (for **2a**)/tolualdehyde(for **2b**)/4-trifluoromethyl benzaldehyde(for **2c**)/4-cyanobenzaldehyde(for **2d**), acetic acid; (ii) 4-(1,2,2-triphenylvinyl)phenylboronic acid pinacol ester, K<sub>2</sub>CO<sub>3</sub>, Pd(PPh<sub>3</sub>)<sub>4</sub>, Toluene:Ethanol:Water (10.0 mL:4.0 mL:0.5 mL).

The synthesis of TPE substituted phenanthroimidazoles **3a–3d** are shown in Scheme 4.1. The 9,10-phenanthroquinone **1** on condensation reaction with 4-iodoaniline and respective aldehydes (benzaldehyde for **2a**, tolualdehyde for **2b**, 4-trifluoromethyl benzaldehyde for **2c**, and 4-cyanobenzaldehyde for **2d**)

resulted **2a–2d** in 91%, 80%, 86% and 76% yields, respectively. The Suzuki cross-coupling reaction of 4-(1,2,2-triphenylvinyl)phenylboronic acid pinacol ester with corresponding iodophenanthroimidazoles **2a–2d** using Pd(PPh<sub>3</sub>)<sub>4</sub> as catalyst resulted **3a–3d** in 71% , 70%, 75% and 78% respectively. The TPE substituted phenanthroimidazoles **3a–3d** were well characterized by <sup>1</sup>H NMR, <sup>13</sup>C NMR, and high resolution mass spectrometry (HRMS). The phenanthroimidazoles **2b**, **2c**, **3a** and **3c** were also characterized by single crystal X-ray analysis.

#### 4.2.2. Thermogravimetric analysis

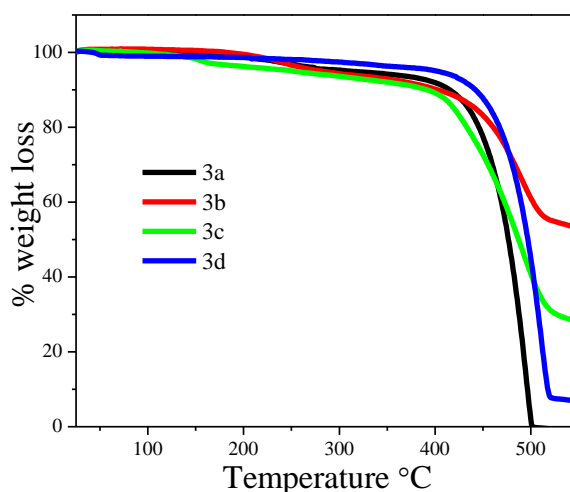


**Figure 4.1.** Thermogravimetric analysis of phenanthroimidazoles **3a–3d** measured at a heating rate of 10 °C/ min under nitrogen atmosphere.

To check the thermal stability of phenanthroimidazoles **3a–3d**, the thermogravimetric analysis (TGA) was performed (Figure 4.1). The thermal decomposition temperatures ( $T_d$ ) corresponding to 5% weight loss under nitrogen atmosphere are summarized in Table 4.1, and are 311 °C, 283 °C, 252 °C and 402 °C for **3a**, **3b**, **3c** and **3d** respectively. The thermal stability of the phenanthroimidazoles **3a–3d** follows the order **3d** > **3a** > **3b** > **3c**. This reveals that, the thermal stability of the phenanthroimidazoles **3a–3d** decreases with bulkiness of substituent on phenanthroimidazole unit.

### 4.2.3. Photophysical properties

The phenanthroimidazoles **3a–3d** exhibits good solubility in common organic solvents such as tetrahydrofuran (THF), dichloromethane, chloroform, etc., but they are insoluble in water and methanol due to the hydrophobic aromatic rings. The electronic absorption spectra of **3a–3d** in THF solutions are displayed in Figure 4.2 and corresponding data are listed in Table 4.1. The strong absorption around 250–261 nm and weak broad absorption band between 300–370 nm was observed. The phenanthroimidazoles **3a–3d** are weakly fluorescent in THF solutions. This may be due to the non radiative decay of the excited state energy through molecular rotations of phenyl rings.

**Table 4.1.** Photophysical and thermal properties of the **3a–3d**.

Compounds	$\lambda_{\text{max}}$ [nm] ( $\epsilon$ [Lmol <sup>-1</sup> cm <sup>-1</sup> ]) <sup>a</sup>	$\lambda_{\text{em}}$ (nm)	T <sub>d</sub> (°C)
<b>3a</b>	261 (109413)	370	311
	317 (58290)		
<b>3b</b>	261 (85759)		283
	317 (46170)		
<b>3c</b>	260 (106592)	402	252
	329 (59964)		
<b>3d</b>	254 (99272)	420	402
	335 (51618)		

<sup>a</sup> Measured in tetrahydrofuran.

The TPE is AIE active unit, so the AIE property of phenanthroimidazoles was studied by preparing small aggregates of molecules. The aggregates were prepared by gradual increase in the percentage of water in THF. The concentrations of phenanthroimidazoles **3a–3d** were kept at 10  $\mu$ M. The AIE property was studied with the help of the absorption and fluorescence spectroscopy. The absorption spectra of AIE studies show almost similar absorption band upto 60% water fraction. Above 60% water fraction light scattering or Mie effect was observed due to the formation of nanoaggregate suspension (Figure 4.2).

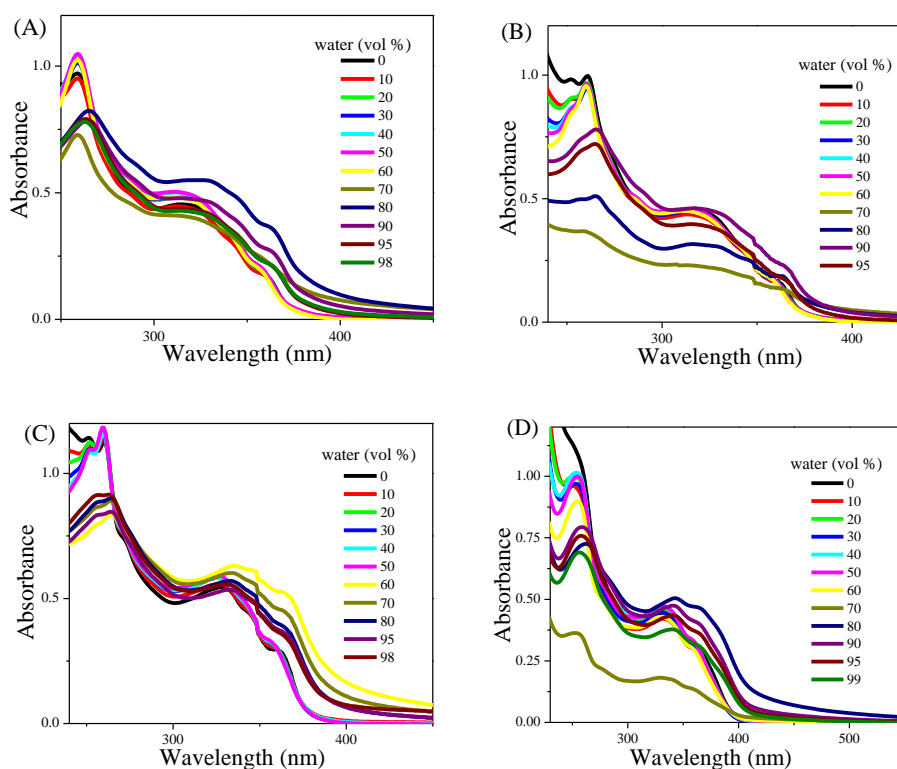


**Figure 4.2.** UV-vis absorption spectra of phenanthroimidazoles **3a–3d** in THF–water mixtures with different water fractions.

Similar trend was observed in fluorescence spectra and no distinct change in emission wavelength and intensity was observed upto 60% water fraction whereas above 60% water fraction, emission was red shifted with enhanced intensity (Figure 4.3). The free rotations of phenyl rings are suppressed in the aggregated state which reduces the non-radiative excited state energy loss leading to enhancement in emission intensity. The poor fluorescence of phenanthroimidazoles **3a–3d** in THF was enhanced in aggregated suspension (98% aqueous mixture) by 98, 12, 33 and 9 folds, respectively (Figure 4.3). The phenanthroimidazoles **3a–3d** at 60% – 70% water fractions show vibronic fluorescence spectra which may be due to formation of different sized aggregates.

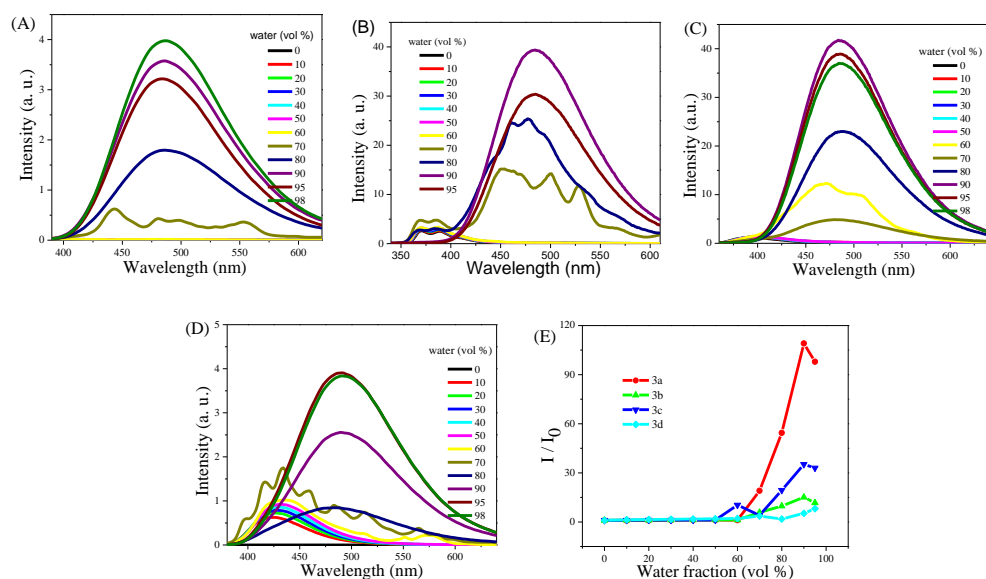


**Figure 4.3.** Fluorescence spectra of **3a**(A), **3b**(B), **3c**(A) and **3d**(D) in THF–water mixtures with different water fractions (10  $\mu$ M). (E) Plot of photoluminescence intensity (PL) vs. % of water fraction ( $f_w$ ). Luminogen concentration: 10  $\mu$ M; intensity calculated at  $\lambda_{\text{max}}$ .

#### 4.2.4. Mechanochromism

**Table 4.2.** Peak emission wavelengths ( $\lambda$ , in nm) of **3a–3d** under various external stimuli.

Compound	Emission			Absorption	
	$\lambda_{\text{Pristine}}$ (nm)	$\lambda_{\text{Grinded}}$ (nm)	$\Delta\lambda$ (nm) <sup>a</sup>	$\lambda_{\text{Pristine}}$ (nm)	$\lambda_{\text{Grinded}}$ (nm)
<b>3a</b>	456	491	35	428	439
<b>3b</b>	484	493	9	346	407
<b>3c</b>	462	495	33	404	419
<b>3d</b>	421	510	89	398	417

<sup>a</sup> Grinding-induced spectral shift,  $\Delta\lambda = \lambda_{\text{Grinded}} - \lambda_{\text{Pristine}}$ .

The mechanochromic properties of phenanthroimidazoles **3a–3d** were studied by absorption and emission spectroscopy. The emission spectra of **3a–3d** under various external stimuli are shown in Figure 4.4 and the corresponding spectroscopic data are summarized in Table 4.2. All the phenanthroimidazoles **3a–3d** show good color contrast reversible mechanochromic behavior which is dependent on the nature and size of substituent on the phenanthroimidazole unit. The phenanthroimidazoles **3a–3d** in pristine states emit at 456 nm, 484 nm, 462 nm, and 421 nm which upon grinding with mortar and pestle show red shifted emission at 491 nm, 493 nm,

495 nm, and 510 nm respectively. The phenanthroimidazoles **3a–3d** show grinding induced spectral shift ( $\Delta\lambda$ ) of 35 nm, 9 nm, 33 nm and 89 nm respectively. This indicates that the size and nature of substituent on the phenanthroimidazole unit plays a key role in deciding the emission in pristine as well as grinded forms. The reversible nature of mechanochromism was studied by using solvent fuming and annealing at high temperature. The solvent fumigation with dichloromethane for 2 minutes shows good reversibility for **3a**, **3c** and **3d** whereas **3b** show partial reversibility. The grinded samples annealed upto 240 °C and show partially reversible nature.

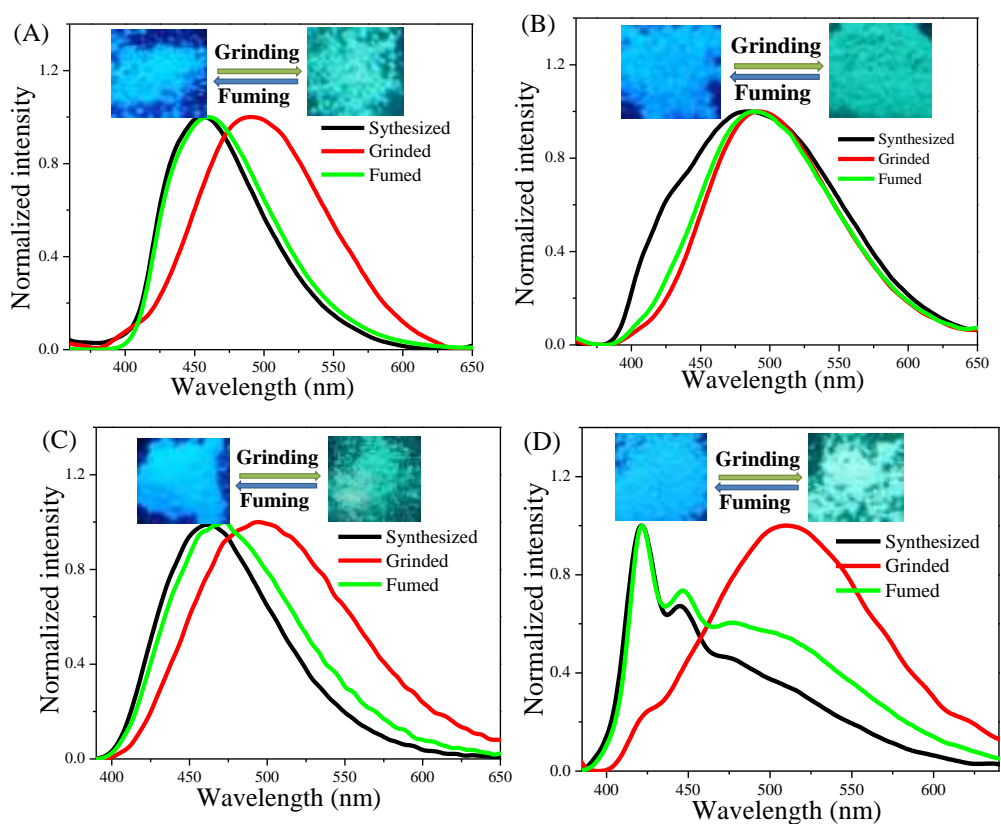


**Figure 4.4.** Emission spectra of (A) **3a**, (B) **3b**, (C) **3c** and (D) **3d** as Synthesized, Grinded and Fumed solids and photograph taken under 365 nm UV illuminations.

In order to understand more about emission behavior under different stimuli the solid state absorption spectra (Figure 4.5-4.8) of **3a–3d** were recorded in synthesized and grinded forms, the data are summarized in Table 4.2. The grinded phenanthroimidazoles **3a–3d** show bathochromic shift in the

absorption spectra compared to their pristine form. The grinding induced red shift in solid state absorption spectra may be due to planarization or enhanced conjugation

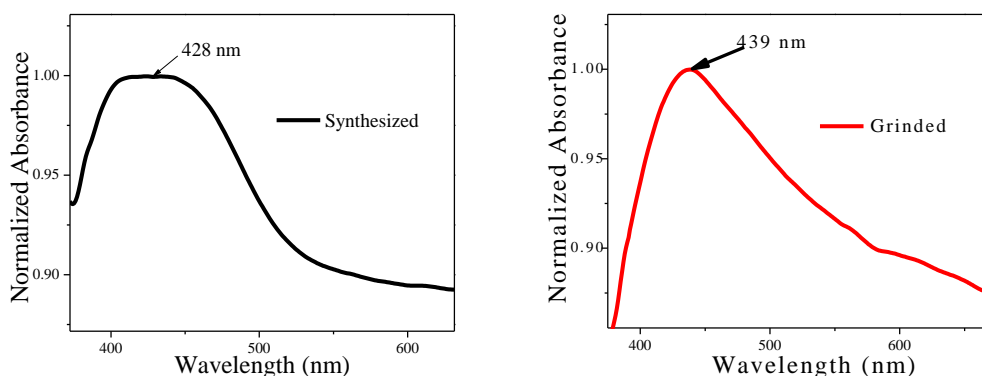


**Figure 4.5.** Solid state absorption spectra of **3a** in crystalline and its grinded form.

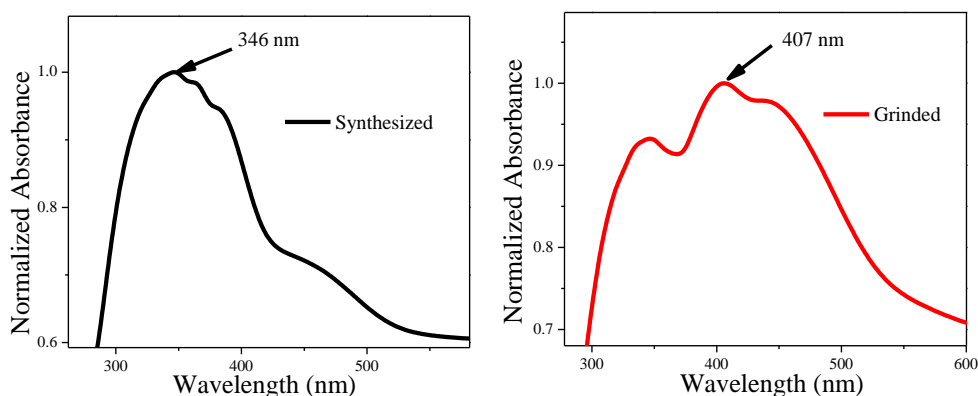


**Figure 4.6.** Solid state absorption spectra of **3b** in crystalline and its grinded form.

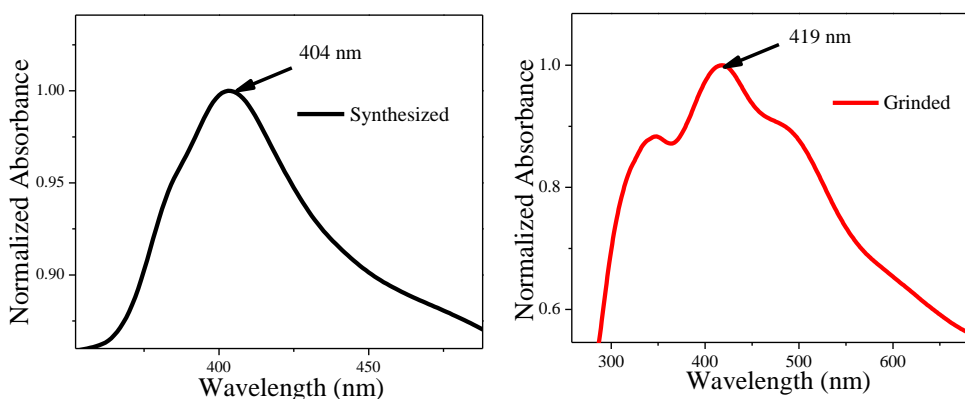


**Figure 4.7.** Solid state absorption spectra of **3c** in crystalline and its grinded form.

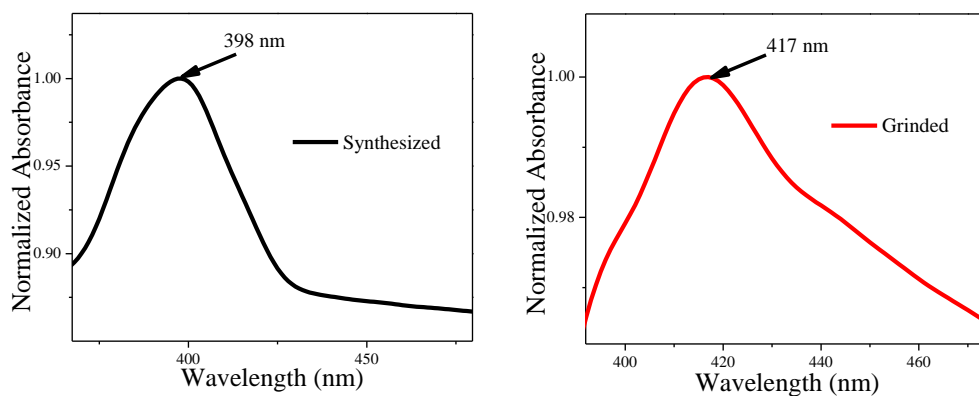


**Figure 4.8.** Solid state absorption spectra of **3d** in crystalline and its grinded form.

To get more insight into the mechanochromic behavior, we have studied the powder X-ray diffractions (PXRD) of pristine as well as grinded form of samples. The pristine samples show sharp diffraction pattern which indicates crystalline nature, whereas in grinded samples broad diffuse band was observed suggesting amorphous nature of solids (Figure 4.9). After fumigation or annealing, they restore crystalline nature and sharp peaks were regenerated in the diffractogram. The PXRD study reveals that the morphological change from the crystalline state to the amorphous state and *vice versa* was associated with the mechanochromism in phenanthroimidazoles.

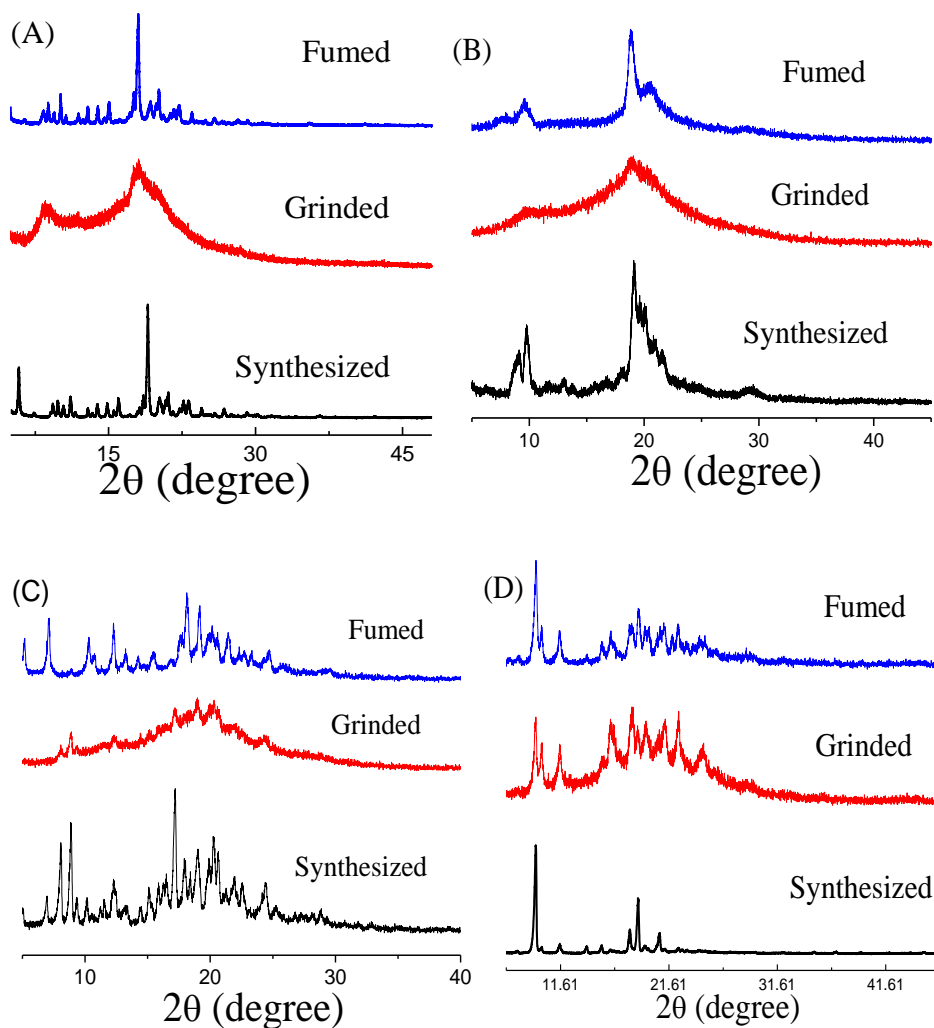


**Figure 4.9.** PXRD curves of **3a**(A), **3b**(B), **3c**(C) and **3d**(D) in Synthesized, Grinded and Fumed form.

#### 4.2.5. Electrochemical properties

To determine the energy levels, cyclic voltammetry (CV) measurement was performed in dichloromethane (DCM) solution with tetrabutylammonium hexafluorophosphate (TBAPF<sub>6</sub>) as supporting electrolyte. The cyclic voltammograms of **3a–3d** are presented in Figure 4.10. Based on the onset oxidation voltages ( $E_{\text{onset}}$ ), the energy levels of highest occupied molecular orbital (HOMO) were estimated and the values for **3a** and **3d** are -5.60 and -5.61 eV respectively. Their LUMO values were obtained by addition of the HOMO value to band gap ( $E_g$ ) estimated from the onset absorption. The calculated LUMOs are -2.53 and -2.51 eV for **3a** and **3d**, respectively.

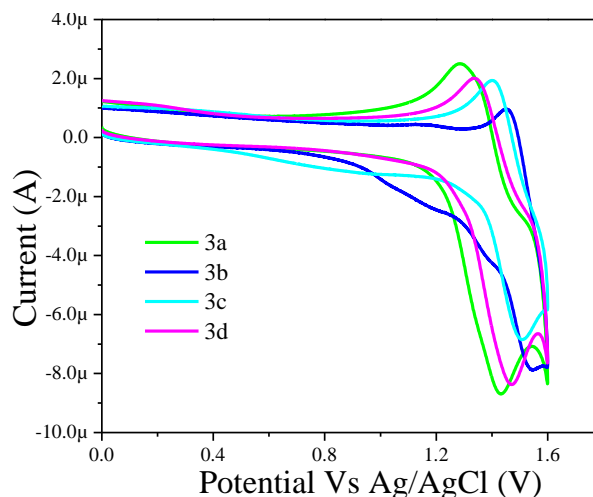


**Figure 4.10.** Cyclic voltammetry (CV) plots of **3a–3d**.

#### 4.2.6. Theoretical calculations

To understand the geometry and electronic structures of **3a–3d**, density functional theory (DFT) calculations were carried out. The DFT calculations were performed at the B3LYP/6-31G(d) level.<sup>[34-36]</sup> The energy minimized structures for **3a–3d** show twisted conformation of phenyl rings of TPE unit. The Figure 4.11 depicts the frontier molecular orbitals (FMO) of the **3a–3d**. The highest occupied molecular orbital (HOMO) of **3a**, **3b** and **3d** are distributed on phenanthroimidazole part whereas in **3c** it is distributed on whole molecule. The lowest unoccupied molecular orbitals (LUMO) in **3a** and **3b** is mainly distributed over TPE unit, while in case of **3c** along with TPE some part is distributed on 4-trifluorophenyl and imidazole ring. The LUMO orbital in **3d** is mainly distributed on 4-cyanophenyl and phenanthroimidazole. The LUMO distribution reveals that the electron withdrawing trifluoro and cyano group shifted the LUMO orbital distribution. The theoretical HOMO-LUMO gap for **3a**, **3b**, **3c** and **3d** are 3.58 eV, 3.80 eV, 3.90 eV and 3.66 eV respectively.

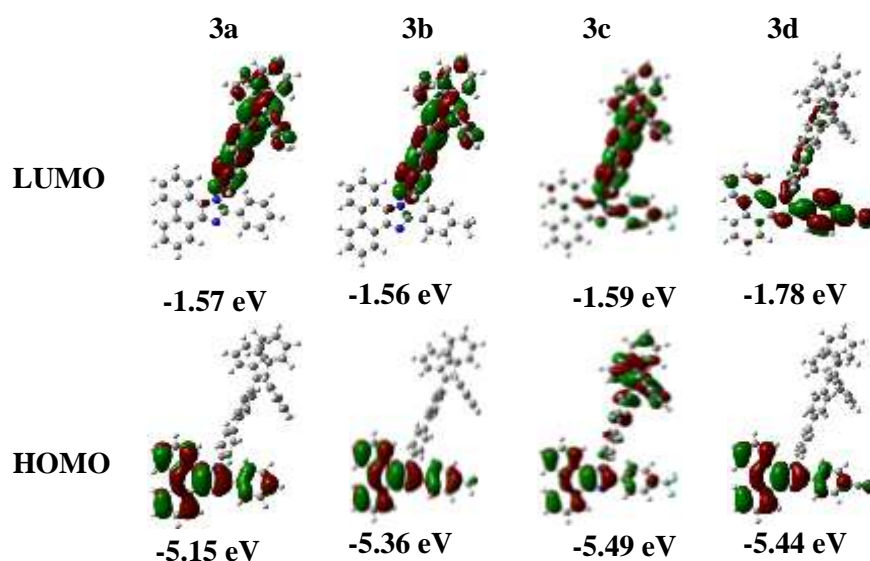


**Figure 4.11.** HOMO and LUMO frontier molecular orbitals of phenanthroimidazoles **3a–3d** at the B3LYP/6-31G (d) level.

The difference in the trend of HOMO-LUMO gap from UV-visible and theoretical study suggests the different nature of transitions. To analyze the origin of absorption bands in the **3a–3d**, TD-DFT calculations were performed. The computed vertical transitions, their oscillator strengths and configurations are shown in Table 4.3. The TD-DFT calculations show good agreement with the experimental spectra and reveals different origins of absorption bands in **3a–3d**.

**Table 4.3.** Computed vertical transitions and their oscillator strengths and configurations of **3a–3d**.

Compounds	$\lambda_{\max}$ [nm]	<i>F</i>	Configuration
<b>3a</b>	360.81	0.6341	HOMO-1→LUMO (0.70296)
	333.11	0.2315	HOMO→LUMO+1 (0.39449)
			HOMO→LUMO+2 (0.37922) HOMO→LUMO+2 (0.33203)
<b>3b</b>	357.49	1.0273	HOMO-1→LUMO (0.70301)
	332.86	0.1966	HOMO→LUMO+2 (0.46925)
			HOMO→LUMO+3 (0.38415)
320.63	0.1630	HOMO→LUMO+2 (-0.44977) HOMO→LUMO+3 (0.49581)	
<b>3c</b>	359.48	0.6074	HOMO-1→LUMO (0.69990)

	345.44	0.5020	HOMO→LUMO+1 (0.68154)
<b>3d</b>	375.36	0.333	HOMO→LUMO (0.66316) HOMO→LUMO+1 (-0.18545)
	366.00	0.6876	HOMO-1→LUMO (-0.43668) HOMO-1→LUMO+1 (0.49070)
	365.34	0.1142	HOMO→LUMO+1 (0.63246) HOMO→LUMO (0.15057) HOMO-1→LUMO+1 (0.17579)

#### 4.2.7. Single crystal X-ray diffraction studies

The single crystals of **2b**, **2c**, **3a** and **3c** were obtained by slow diffusion of ethanol into dichloromethane solution of the compounds. The collected crystals were good enough for single crystal X-ray diffraction analysis, and the data are summarized in Table 4.4. The crystal structures reveal that the phenyl rings in the molecular structure adopt a non-planar orientation (Figure 4.12). This twisted conformation promotes intramolecular rotations in solution phase leading to weak fluorescence and also suppresses the  $\pi$ - $\pi$  stacking interaction in solid state. The density of the solvent-free crystals of **2b**, **2c**, **3a** and **3c** are  $1.512 \text{ mg m}^{-3}$ ,  $1.610 \text{ mg m}^{-3}$ ,  $1.224 \text{ mg m}^{-3}$ , and  $1.259 \text{ mg m}^{-3}$  respectively. This reveals that the **3c** has less density compared to their intermediate **2c**, this may be due the highly twisted TPE unit resulted loose crystal packing. The crystal structure of **3c** consists of two molecules in an asymmetric unit which differs in the bond length and bond angles (Figure 4.12).

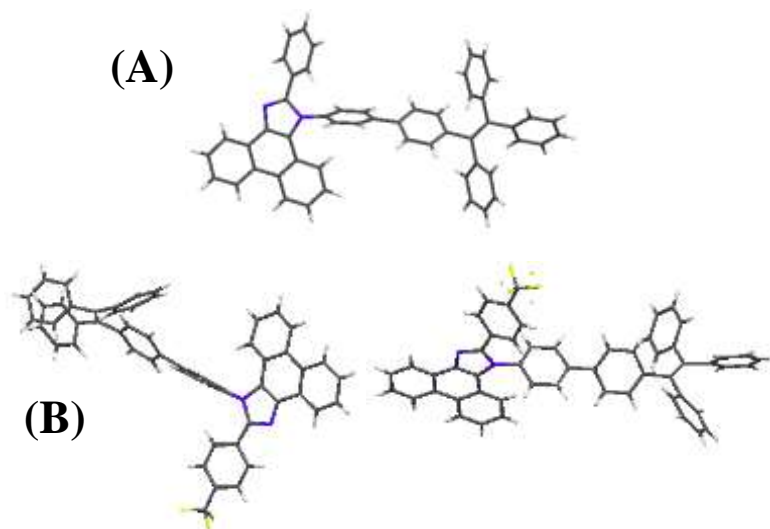


**Figure 4.12.** (A) Crystal structure of **3a**. (B) Crystal structure of **3c** having two molecules in asymmetric unit.



**Table 4.4.** Crystal data and structure refinement for **2b**, **2c**, **3a** and **3c**.

Parameter	<b>2b</b>	<b>2c</b>	<b>3a</b>	<b>3c</b>
Identification code	RM186	RM184	rm140	rm142a
Empirical formula	C <sub>28</sub> H <sub>19</sub> I N <sub>2</sub>	C <sub>28</sub> H <sub>16</sub> F <sub>3</sub> IN <sub>2</sub>	C <sub>53</sub> H <sub>36</sub> N <sub>2</sub>	C <sub>12</sub> H <sub>7.78</sub> F <sub>0.67</sub> N <sub>0.44</sub>
Formula weight	510.35	564.33	700.84	170.85
Temperature	293(2) K	293(2)	293(2) K	293(2) K
Wavelength(Å)	0.71073	0.71073	1.5418	1.5418
Crystal system, space group	Orthorhombic, P b c a	Orthorhombic, P b c a	Triclinic, P -1	Monoclinic, P 21/c
<i>a</i> / (Å)	16.1014(4)	19.9382(4)	10.2369(6)	9.5686(4)
<i>b</i> / (Å)	14.4742(4)	9.1720(2)	12.3813(9)	21.5894(9)
<i>c</i> / (Å)	19.2392(5)	25.4565(7)	15.6606(11)	22.1168(7)
$\alpha$ /(°)	90	90	88.882(6)	114.219(3)
$\beta$ /(°)	90	90	79.205(5)	100.897(3)
$\gamma$ /(°)	90	90	77.326(6)	92.228(3)
Volume	4483.8(2)	4655.31(19)	1901.8(2)Å <sup>3</sup>	4056.9(3)
Z, Calculated density (mg m <sup>-3</sup> )	8, 1.512	8, 1.610	2, 1.224	18, 1.259
Absorption coefficient /(mm <sup>-1</sup> )	1.446	1.419	0.540	0.662
F(000)	2032	2224	736	1600
Crystal size	0.210 x 0.170 x 0.140 mm	0.230 x 0.180 x 0.130 mm	0.33 x 0.26 x 0.21 mm	0.33 x 0.26 x 0.21 mm
$\theta$ range for data collection/(°)	2.895 to 24.999	2.922 to 24.996	2.87 to 71.45	3.81 to 71.23
Reflections collected / unique	39240 / 3945 [R(int) = 0.0449]	43380 / 4093 [R(int) = 0.0595]	12938 / 7201 [R(int) = 0.0220]	27182 / 15363 [R(int) = 0.0325]
Completeness to theta	$\theta = 24.999$ ; 99.8 %	$\theta = 24.996$ ; 99.9 %	$\theta = 71.45$ ; 97.1%	$\theta = 71.23$ ; 97.6%
Absorption correction	Semi-empirical from equivalents	Semi-empirical from equivalents	Analytical	Semi-empirical from equivalents
Max. and min. transmission	1.00000 and 0.37955	1.00000 and 0.35300	0.8951 and 0.8419	0.8734 and 0.8111
Refinement method	Full-matrix least-squares on F <sup>2</sup>	Full-matrix least-squares on F <sup>2</sup>	Full-matrix least-squares on F <sup>2</sup>	Full-matrix least-squares on F <sup>2</sup>
Data / restraints / parameters	3945 / 0 / 282	4093 / 321 / 335	7201 / 0 / 496	15363 / 0 / 1092
Goodness-of-fit on F <sup>2</sup>	1.064	1.032	1.064	1.067
Final R indices [I > 2 $\sigma$ (I)]	R1 = 0.0479, wR2 = 0.1275	R1 = 0.0428, wR2 = 0.1118	R1 = 0.0474, wR2 = 0.1306	R1 = 0.0874, wR2 = 0.2514
R indices (all data)	R1 = 0.0543, wR2 = 0.1345	R1 = 0.0538, wR2 = 0.1222	R1 = 0.0632, wR2 = 0.1438	R1 = 0.1076, wR2 = 0.2694
Largest diff. peak and hole (eÅ <sup>-3</sup> )	1.761 and -1.325	0.913 and -0.732	0.169 and -0.201	0.456 and -0.459

**Table 4.5.** Important distance of intermolecular interactions of **3a** and **3c**.

Interaction	Distance (Å)
<b>3a</b>	
C(20)-H(20)--- $\pi$ (C42,C43,C44,C45,C46,C47)	3.461
C(11)-H(11)--- $\pi$ (C16,C17,C18,C19,C20,C21)	2.918
C(52)-H(52)--- $\pi$ (N1,N2,C1,C14,C15)	2.821
C(4)-H(4)--- $\pi$ (C2,C3,C4,C5,C6,C7)	3.961
<b>3c</b>	
C(6)-H(6)--- $\pi$ (C91,C92,C93,C94,C95,C96)	2.889
C(82)-H(82)--- $\pi$ (N3,N4,C55,C56,C69)	2.646
C(24)-H(24)--- $\pi$ (C9,C10,C11,C12,C13,C14)	2.668
C(25)-H(25)--- $\pi$ (C3,C4,C5,C6,C7,C8)	2.849
C(66)-H(66)--- $\pi$ (C9,C10,C11,C12,C13,C14)	3.154
C(18)-H(18)--- $\pi$ (C97,C98,C99,C100,C101,C102)	3.663
C(39)-H(39)--- $\pi$ (C43,C44,C45,C46,C47)	3.320
C(79)-H(79)--- $\pi$ (C56,C57,C62,C63,C68,C69)	2.897
C(59)-H(59)--- $\pi$ (C103,C104,C105,C106,C107,C108)	2.961
C(54)-H(54)--- $\pi$ (C103,C104,C105,C106,C107,C108)	3.862
C(98)-H(98)--- $\pi$ (C43,C44,C45,C46,C47,C48)	3.737
C(60)-H(60)--- $\pi$ (C38,C39,C40,C41,C42,C43)	2.878
C(93)-H(93)--- $\pi$ (C103,C104,C105,C106,C107,C108)	3.165

### 4.3. Experimental section

#### Synthesis and characterization of intermediates **2a–2d**:

**General procedure for intermediates 2a–2d:** The 9,10-phenanthrenequinone (9.6 mmol), 4-iodoaniline (14.4 mmol), ammonium acetate (96.1 mmol) and respective benzaldehydes (9.6 mmol) in glacial acetic acid (50 mL) refluxed for 4 h under an argon atmosphere. After cooling to room temperature, a pale yellow mixture was obtained and poured it into a methanol solution under stirring. The separated solid was filtered off, washed with 30 mL water, and dried to give intermediates **2a–2d**.

**2a:** Yield: 91.0%.  $^1\text{H}$  NMR (400 MHz,  $\text{CDCl}_3$ , 25 °C):  $\delta$  8.86 (dd, 1H,  $J=1.2$ , 8 Hz), 8.78 (d, 1H,  $J=8$  Hz) 8.71 (d, 1H,  $J=8$  Hz), 7.92 (d, 2H,  $J=8$  Hz) 7.72-7.76 (m, 1H), 7.64-7.68 (m, 1H), 7.52-7.56 (m, 3H), 7.31-7.36 (m, 4H) 7.22-7.26 (m, 3H) ppm;  $^{13}\text{C}$  NMR (100 MHz,  $\text{CDCl}_3$ , 25 °C):  $\delta$  150.9, 139.3, 138.4, 137.5, 130.9, 130.2, 129.5, 129.3, 129.0, 128.3, 128.3, 127.8, 127.3, 127.1, 126.4, 125.7, 125.0, 124.2, 123.1, 122.8, 120.7, 95.3 ppm; HRMS (ESI): calcd. for  $\text{C}_{27}\text{H}_{17}\text{N}_2\text{I}$ : 497.0509 ( $M+H$ ) $^+$ , found 497.0517.

**2b:** Yield: 80.0%. <sup>1</sup>H NMR (400 MHz, CDCl<sub>3</sub>, 25 °C): δ 8.86 (d, 1H, *J*= 8 Hz), 8.78 (d, 1H, *J*=8 Hz), 8.71 (d, 1H, *J*= 8 Hz), 7.92 (d, 2H, *J*= 8 Hz), 7.66-7.74 (m, 2H), 7.13-7.53 (m, 9H) ppm; <sup>13</sup>C NMR (100 MHz, CDCl<sub>3</sub>, 25 °C): δ 151.1, 139.3, 139.0, 138.5, 137.4, 130.9, 129.3, 129.2, 129.0, 128.2, 127.7, 127.3, 127.1, 126.3, 125.6, 124.9, 124.1, 123.0, 122.8, 120.6, 95.2, 21.3 ppm; HRMS (ESI): calcd. for C<sub>28</sub>H<sub>19</sub>N<sub>2</sub>I: 511.0666 (*M+H*)<sup>+</sup>, found 511.0681.

**2c:** Yield: 86.0%. <sup>1</sup>H NMR (400 MHz, CDCl<sub>3</sub>, 25 °C): δ 8.84 (d, 1H, *J*= 8 Hz), 8.78 (d, 1H, *J*= 8 Hz), 8.71 (d, 1H, *J*= 8 Hz), 7.97 (d, 2H, *J*= 8 Hz), 7.54-7.78 (m, 7H), 7.34 (t, 1H, *J*= 8 Hz), 7.21-7.28 (m, 3H) ppm; <sup>13</sup>C NMR (100 MHz, CDCl<sub>3</sub>, 25 °C): δ 148.9, 139.5, 138.0, 137.6, 133.6, 130.8, 130.7, 130.4, 129.4, 128.3, 128.2, 127.4, 126.9, 126.5, 126.0, 125.3, 125.3, 125.2, 125.2, 124.2, 123.1, 122.7, 122.6, 122.5, 120.7, 95.7 ppm; HRMS (ESI): calcd. for C<sub>28</sub>H<sub>16</sub>F<sub>3</sub>I N<sub>2</sub>: 565.0383 (*M+H*)<sup>+</sup>, found 565.0418.

**2d:** Yield: 76.0%. <sup>1</sup>H NMR (400 MHz, CDCl<sub>3</sub>, 25 °C): δ 8.78 (d, 1H, *J*= 8 Hz), 8.70 (d, 1H, *J*=8 Hz), 7.98 (dt, 2H, *J*=2.4, 8 Hz), 7.73-7.78 (m, 1H), 7.66-7.70 (m, 3H), 7.54-7.62 (m, 3H), 7.32-7.36 (m, 1H) 7.25-7.29 (m, 2H), 7.21 (d, 1H, *J*=8 Hz) ppm; <sup>13</sup>C NMR (100 MHz, CDCl<sub>3</sub>, 25 °C): δ 148.3, 139.7, 137.9, 137.8, 134.4, 132.1, 130.6, 129.6, 129.5, 128.5, 128.4, 127.5, 126.8, 126.6, 126.1, 125.6, 124.3, 123.2, 122.6, 122.5, 120.8, 118.4, 112.3, 96.0, 53.4 ppm; HRMS (ESI): calcd. for C<sub>28</sub>H<sub>16</sub>N<sub>3</sub>I: 544.0281 (*M+Na*)<sup>+</sup>, found 544.0257.

### Synthesis and characterization of phenanthroimidazoles **3a–3d**:

**General procedure for phenanthroimidazoles **3a–3d**:** Pd(PPh<sub>3</sub>)<sub>4</sub> (0.004 mmol) was added to a well degassed solution of corresponding iodophenanthroimidazoles **2a–2d** (0.4 mmol), 4-(1,2,2-triphenylvinyl)phenylboronic acid pinacol ester (0.48 mmol), K<sub>2</sub>CO<sub>3</sub> (1.2 mmol) in a mixture of toluene (12 mL)/ ethanol (4.0 mL)/ H<sub>2</sub>O (1.0 mL). The resulting mixture was stirred at 80 °C for 24 h under argon atmosphere. After cooling, the mixture was evaporated to dryness and the residue subjected to column chromatography on silica (hexane-DCM 50:50 in vol.) to yield the desired phenanthroimidazoles **3a–3d** as colorless powders. The compounds were recrystallized from DCM:ethanol (8:2) mixtures as colorless crystals.

**3a:** Yield: 71.0%. <sup>1</sup>H NMR (400 MHz, CDCl<sub>3</sub>, 25 °C): δ 8.88 (d, 1H, *J*= 8 Hz), 8.78 (d, 1H, *J*=8 Hz), 8.71 (d, 1H, *J*= 8 Hz), 7.72-7.78 (m, 3H), 7.60-

7.67 (m, 3H), 7.50-7.53 (m, 5H), 7.28-7.32 (m, 4H), 7.05-7.20 (m, 18H) ppm;  $^{13}\text{C}$  NMR (100 MHz,  $\text{CDCl}_3$ , 25 °C):  $\delta$  151.0, 143.8, 143.6, 143.6, 141.7, 141.5, 140.1, 137.5, 137.4, 137.0, 132.1, 131.3, 131.3, 130.5, 129.4, 129.3, 129.2, 128.8, 128.2, 128.2, 128.2, 128.1, 127.8, 127.8, 127.7, 127.2, 127.2, 126.6, 126.6, 126.5, 126.3, 126.3, 125.6, 124.9, 124.1, 123.1, 123.1, 123.0, 122.7, 120.9 ppm; HRMS (ESI): calcd. for  $\text{C}_{53}\text{H}_{36}\text{N}_2$ : 701.2951 ( $M+H$ )<sup>+</sup>, found 701.2952.

**3b**: Yield: 70.0%.  $^1\text{H}$  NMR (400 MHz,  $\text{CDCl}_3$ , 25 °C):  $\delta$  8.87 (d, 1H,  $J=8$  Hz), 8.78 (d, 1H,  $J=8$  Hz), 8.71 (d, 1H,  $J=8$  Hz), 7.72-7.79 (m, 3H), 7.65 (t, 1H,  $J=8$  Hz), 7.49-7.53 (m, 7H), 7.27-7.30 (m, 2H), 7.05-7.20 (m, 19H), 2.33 (s, 3H) ppm;  $^{13}\text{C}$  NMR (100 MHz,  $\text{CDCl}_3$ , 25 °C):  $\delta$  151.2, 143.9, 143.6, 143.6, 143.6, 141.7, 141.5, 140.2, 138.8, 137.7, 137.4, 137.1, 132.1, 131.4, 131.3, 129.3, 129.3, 129.2, 129.0, 128.2, 128.2, 128.0, 127.9, 127.8, 127.7, 127.6, 127.2, 127.2, 126.6, 126.6, 126.6, 126.3, 125.5, 124.7, 124.1, 123.1, 123.1, 122.7, 120.8, 21.3 ppm; HRMS (ESI): calcd. for  $\text{C}_{54}\text{H}_{38}\text{N}_2$ : 715.3108 ( $M+H$ )<sup>+</sup>, found 715.3107.

**3c**: Yield: 75.0%.  $^1\text{H}$  NMR (400 MHz,  $\text{CDCl}_3$ , 25 °C):  $\delta$  8.86 (d, 1H,  $J=8$  Hz), 8.78 (d, 1H,  $J=8$  Hz), 8.72 (d, 1H,  $J=8$  Hz), 7.82 (d, 2H,  $J=8$  Hz), 7.75 (d, 3H,  $J=8$  Hz), 7.68 (t, 1H,  $J=8$  Hz), 7.52-7.57 (m, 7H), 7.30 (s, 1H), 7.08-7.21 (m, 17H) ppm;  $^{13}\text{C}$  NMR (100 MHz,  $\text{CDCl}_3$ , 25 °C):  $\delta$  149.2, 144.1, 143.6, 143.6, 143.5, 142.2, 141.6, 140.1, 137.6, 137.2, 136.8, 132.1, 131.4, 131.3, 129.5, 129.2, 128.5, 128.5, 128.4, 127.9, 127.8, 127.7, 127.4, 127.1, 126.7, 126.6, 126.6, 126.4, 126.3, 125.9, 125.3, 125.2, 125.2, 125.2, 124.2, 123.2, 122.9, 122.7, 121.2, 121.0 ppm; HRMS (ESI): calcd. for  $\text{C}_{54}\text{H}_{35}\text{F}_3\text{N}_2$ : 769.2825 ( $M+H$ )<sup>+</sup>, found 769.2827.

**3d**: Yield: 78.0%.  $^1\text{H}$  NMR (400 MHz,  $\text{CDCl}_3$ , 25 °C):  $\delta$  8.84 (d, 1H,  $J=8$  Hz), 8.78 (d, 1H,  $J=8$  Hz), 8.71 (d, 1H,  $J=8$  Hz), 7.83 (d, 2H,  $J=8$  Hz), 7.52-7.78 (m, 11H), 7.28-7.29 (m, 2H), 7.05-7.22 (m, 17H) ppm;  $^{13}\text{C}$  NMR (100 MHz,  $\text{CDCl}_3$ , 25 °C):  $\delta$  148.4, 144.2, 143.6, 143.5, 143.5, 142.4, 141.6, 140.1, 137.7, 137.0, 136.6, 134.8, 132.2, 132.0, 131.4, 131.3, 131.3, 129.6, 129.5, 129.0, 128.8, 128.6, 128.4, 127.9, 127.8, 127.7, 127.5, 126.9, 126.7, 126.6, 126.5, 126.3, 126.0, 125.4, 124.2, 123.2, 122.8, 122.6, 121.0, 118.5, 112.1 ppm; HRMS (ESI): calcd. for  $\text{C}_{54}\text{H}_{35}\text{N}_3$ : 726.2904 ( $M+H$ )<sup>+</sup>, found 726.2902.

#### 4.4. Conclusion

In conclusion, we have synthesized novel mechanochromic tetraphenylethylene substituted phenanthroimidazoles **3a–3d** by Pd-catalyzed Suzuki cross-coupling reaction. The phenanthroimidazoles **3a–3d** show good thermal stability and introduction of cyano-group helps to improve thermal stability. The phenanthroimidazoles **3a–3d** are weakly emissive in solutions whereas strong emission was observed in the aggregated state due to the aggregation induced emission (AIE). The reversible mechanochromism with good color contrast between blue and green color was observed in all phenanthroimidazoles **3a–3d**. It is shown that the changing the end group is effective strategy to tune the solid state emission and mechanochromism. We believe that this study will help in designing the new mechanochromic materials with desired properties.

**Note:** This is copyrighted material from American Chemical Society, *J. Phys. Chem. C*, 2016, 120, 18487–18495 (DOI: 10.1021/acs.jpcc.6b06277).

#### 4.5. References

- [1] Chi Z., Zhang X., Xu B., Zhou X., Ma C., Zhang Y., Liu S. and Xu J. (2012), Recent advances in organic mechanofluorochromic materials, *Chem. Soc. Rev.*, 41, 3878–3896 (DOI: 10.1039/C2CS35016E).
- [2] Luo X., Li J., Li C., Heng L., Dong Y Q., Liu Z., Bo Z. and Tang B Z. (2011), Reversible switching of the emission of diphenyldibenzofulvenes by thermal and mechanical stimuli, *Adv. Mater.*, 23, 3261–3265 (DOI: 10.1002/adma.201101059).
- [3] Wang L., Wang K., Zou B., Ye K., Zhang H. and Wang Y. (2015), Luminescent chromism of boron diketonate crystals: distinct responses to different stresses, *Adv. Mater.*, 27, 2918–2922 (DOI: 10.1002/adma.201500589).
- [4] Yoshii R., Hirose A., Tanaka K. and Chujo Y. (2014), Functionalization of boron diimines with unique optical properties: multicolor tuning of crystallization-induced emission and introduction into the main chain of

- conjugated polymers, *J. Am. Chem. Soc.*, 136, 18131–18139 (DOI: 10.1021/ja510985v).
- [5] Xue S., Liu W., Qiu X., Gao Y. and Yang W. (2014), Remarkable isomeric effects on optical and optoelectronic properties of N-Phenylcarbazole-Capped 9,10-Divinylanthracenes, *J. Phys. Chem. C*, 118, 18668–18675 (DOI: 10.1021/jp505527f).
- [6] Seki T., Takamatsu Y. and Ito H. (2016), A screening approach for the discovery of mechanochromic gold(i) isocyanide complexes with crystal-to-crystal phase transitions, *J. Am. Chem. Soc.*, 138, 6252–6260 (DOI: 10.108347/jacs.6b02409).
- [7] Sase M., Yamaguchi S., Sagara Y., Yoshikawa I., Mutai T. and Araki K. (2011), Piezochromic luminescence of amide and ester derivatives of tetraphenylpyrene-role of amide hydrogen bonds in sensitive piezochromic response, *J. Mater. Chem.*, 21, 8347–8354 (DOI: 10.1039/C0JM03950K).
- [8] Nguyen N D., Zhang G., Lu J., Sherman A E. and Fraser C L. (2011), Alkyl chain length effects on solid-state difluoroboron [small beta]-diketonate mechanochromic luminescence, *J. Mater. Chem.*, 21, 8409–8415 (DOI: 10.1039/C1JM00067E).
- [9] Han T., Zhang Y., Feng X., Lin Z., Tong B., Shi J., Zhi J. and Dong Y. (2013), Reversible and hydrogen bonding-assisted piezochromic luminescence for solid-state tetraaryl-butadiene, *Chem. Commun.*, 49, 7049–7051 (DOI: 10.1039/C3CC42644K).
- [10] Kumar N S S., Varghese S., Suresh C H., Rath N P. and Das S. (2009), Correlation between solid-state photophysical properties and molecular packing in a series of indane-1,3-dione containing butadiene derivatives, *J. Phys. Chem. C*, 113, 11927–11935 (DOI: 10.1021/jp902482r).
- [11] Liu Q., Liu W., Yao B., Tian H., Xie Z., Geng Y. and Wang F. (2007), Synthesis and chain-length dependent properties of monodisperse Oligo(9,9-di-n-octylfluorene-2,7-vinylene)s, *Macromolecules*, 40, 1851–1857 (DOI: 10.1021/ma0628073).
- [12] Bu L., Sun M., Zhang D., et al. (2013), Solid-state fluorescence properties and reversible piezochromic luminescence of aggregation-

- induced emission-active 9,10-bis[(9,9-dialkylfluorene-2-yl)vinyl]anthracenes, *J. Mater. Chem. C*, 1, 2028 (DOI: 10.1039/c3tc00017f).
- [13] Zhang X., Chi Z., Xu B., et al. (2012), Multifunctional organic fluorescent materials derived from 9,10-distyrylanthracene with alkoxy endgroups of various lengths, *Chem. Commun.*, 48, 10895 (DOI: 10.1039/c2cc36263e).
- [14] Birks J. B. *Photophysics of Aromatic Molecules*, Wiley, London, U.K., 1970.
- [15] Jayanty S., and Radhakrishnan T P. (2004), Enhanced fluorescence of remote functionalized diaminodicyanoquinodimethanes in the solid state and fluorescence switching in a doped polymer by solvent vapors, *Chem. - A Eur. J.*, 10, 791–797 (DOI: 10.1002/chem.200305123).
- [16] Henry J. T., Jerome L. M., Wim T. K., James A. M., Judith H., Scott W., Isaac R., and Watts K., (2005), Enhanced photoluminescence from group 14 metalloles in aggregated and solid solutions, *Inorg. Chem.*, 44, 2003–2011 (DOI: 10.1021/IC049034O).
- [17] Luo J., Xie Z., Lam J. W. Y., et al. (2001), Aggregation-induced emission of 1-methyl-1,2,3,4,5-pentaphenylsilole, *Chem. Commun.*, 397, 1740–1741 (DOI: 10.1039/b105159h).
- [18] Li Y., Liu T., Liu H., Tian M-Z. and Li Y. (2014), Self-assembly of intramolecular charge-transfer compounds into functional molecular systems, *Acc. Chem. Res.*, 47, 1186–1198 (DOI: 10.1021/ar400264e).
- [19] Liu H., Xu J., Li Y. and Li Y. (2010), Aggregate nanostructures of organic molecular materials., *Acc. Chem. Res.*, 43, 1496–1508 (DOI: 10.1021/ar100084y).
- [20] Hong Y., Lam J W Y., Tang B Z., et al. (2011), Aggregation-induced emission, *Chem. Soc. Rev.*, 40, 5361 (DOI: 10.1039/c1cs15113d).
- [21] Dong Y., Lam J W Y., Qin A., Liu J., Li Z., Tang B Z., Sun J. and Kwok H S. (2007), Aggregation-induced emissions of tetraphenylethene derivatives and their utilities as chemical vapor sensors and in organic light-emitting diodes, *Appl. Phys. Lett.*, 91, 11111 (DOI: 10.1063/1.2753723).
- [22] Huang J., Yang X., Wang J., et al. (2012), New tetraphenylethene-based

- efficient blue luminophors: aggregation induced emission and partially controllable emitting color, *J. Mater. Chem.*, 22, 2478–2484 (DOI: 10.1039/C1JM14054J).
- [23] Zhao N., Yang Z., Lam J W Y., et al. (2012), Benzothiazolium-functionalized tetraphenylethene: an AIE luminogen with tunable solid-state emission, *Chem. Commun.*, 48, 8637 (DOI: 10.1039/c2cc33780k).
- [24] Wang J., Mei J., Hu R., Sun J Z., Qin A. and Tang B Z. (2012), Click synthesis, aggregation-induced emission, *e / z* isomerization, self-organization, and multiple chromisms of pure stereoisomers of a tetraphenylethene-cored luminogen, *J. Am. Chem. Soc.*, 134, 9956–9966 (DOI: 10.1021/ja208883h).
- [25] Zhao N., Li M., Yan Y., et al. (2013), A tetraphenylethene-substituted pyridinium salt with multiple functionalities: synthesis, stimuli-responsive emission, optical waveguide and specific mitochondrion imaging, *J. Mater. Chem. C*, 1, 4640 (DOI: 10.1039/c3tc30759j).
- [26] Xu B., Xie M., He J., et al. (2013), An aggregation-induced emission luminophore with multi-stimuli single- and two-photon fluorescence switching and large two-photon absorption cross section, *Chem. Commun.*, 49, 273–275 (DOI: 10.1039/C2CC36806D)
- [27] Xu B., Chi Z., Zhang X., et al. (2011), A new ligand and its complex with multi-stimuli-responsive and aggregation-induced emission effects, *Chem. Commun.*, 47, 11080 (DOI: 10.1039/c1cc13790e).
- [28] Yuan H., Wang K., Yang K., Liu B. and Zou B. (2014), Luminescence properties of compressed tetraphenylethene: the role of intermolecular interactions, *J. Phys. Chem. Lett.*, 5, 2968–2973 (DOI: 10.1021/jz501371k).
- [29] Yang J., Huang J., Li Q., et al. (2016), Blue AIEgens: approaches to control the intramolecular conjugation and the optimized performance of OLED devices, *J. Mater. Chem. C*, 4, 2663–2684 (DOI: 10.1039/C5TC03262H).
- [30] Jadhav T., Dhokale B., Mobin S M., et al. (2015), Mechanochromism and aggregation induced emission in benzothiazole substituted tetraphenylethylenes: a structure function correlation, *RSC Adv.*, 5, 29878–29884 (DOI: 10.1039/C5RA04881H).

- [31] Jadhav T., Dhokale B., Mobin S M., et al. (2015), Aggregation induced emission and mechanochromism in pyrenoimidazoles, *J. Mater. Chem. C*, 3, 9981–9988 (DOI: 10.1039/C5TC02181B).
- [32] Jadhav T., Dhokale B., patil Y., et al. (2015), Aggregation induced emission and mechanochromism in tetraphenylethene substituted pyrazabole, *RSC Adv.*, 5, 68187–68191 (DOI: 10.1039/C5RA12697E).
- [33] Misra R., Jadhav T., Dhokale B., et al. (2014), Reversible mechanochromism and enhanced AIE in tetraphenylethene substituted phenanthroimidazoles, *Chem. Commun.*, 50, 9076 (DOI: 10.1039/C4CC02824D).
- [34] Frisch, M. J.; Trucks, G. W.; Schlegel, G. W.; Scuseria, G. E.; Robb, M. A.; Cheeseman, J. R.; Scalmani, G.; Barone, V.; Mennucci, B.; Petersson, G. A.; Nakatsuji, G. A.; Caricato, M.; Li, X.; Hratchian, H. P.; Izmaylov, A. F.; Bloino, J.; Zheng, G.; Sonnenberg, J. L.; Hada, M.; Ehara, M.; Toyota, K.; Fukuda, R.; Hasegawa, J.; Ishida, M.; Nakajima, T.; Honda, Y.; Kitao, O.; Nakai, H.; Vreven, T.; Montgomery, J. A. Jr.; Peralta, J. E.; Ogliaro, F.; Bearpark, M.; Heyd, J. J.; Brothers, E.; Kudin, K. N.; Staroverov, V. N.; Kobayashi, R.; Normand, J.; Raghavachari, K.; Rendell, A.; Burant, J. C.; Iyengar, S. S.; Tomasi, J.; Cossi, M.; Rega, N.; Millam, N. J.; Klene, M.; Knox, J. E.; Cross, J. B.; Bakken, V.; Adamo, C.; Jaramillo, J.; Gomperts, R.; Stratmann, R. E.; Yazyev, O.; Austin, A. J.; Cammi, R.; Pomelli, C.; Ochterski, J. W.; Martin, R. L.; Morokuma, K.; Zakrzewski, V. G.; Voth, G. A.; Salvador, P.; Dannenberg, J. J.; Dapprich, S.; Daniels, A. D.; Farkas, O.; Foresman, J. B.; Ortiz, J. V.; Cioslowski, J.; Fox, D. J.; Gaussian 09, revision A.02; Gaussian, Inc.: Wallingford, CT, 2009.
- [35] Lee C., Yang W. and Parr R G. (1988), Development of the Colle-Salvetti correlation-energy formula into a functional of the electron density, *Phys. Rev. B*, 37, 785–789 (DOI: 10.1103/PhysRevB.37.785).
- [36] Becke A D. (1993), A new mixing of Hartree–Fock and local density-functional theories, *J. Chem. Phys.*, 98, 1372 (DOI: 10.1063/1.464304).



## Chapter 5

# Aggregation induced emission and mechanochromism in pyrenoimidazoles

---

### 5.1. Introduction

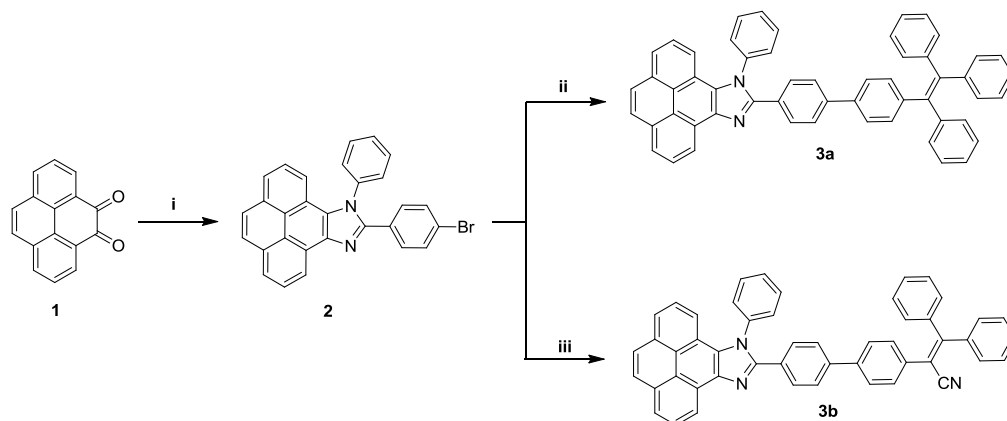
In recent years the research on fluorescent organic solids has gained momentum due to their wide range of applications in organic light emitting diodes (OLEDs), non-linear optics (NLO), organic lasers, and fluorescent sensors.<sup>[1-9]</sup> The fluorescent organic materials are extensively used in designing stimuli responsive solids called mechanochromic materials due to their applications in mechano-sensors, optical data storage, and security papers.<sup>[10-13]</sup> Pyrene is highly studied fluorophore for variety of applications due to its pure blue fluorescence with high quantum yield, exceptionally long fluorescence lifetime, excellent thermal stability, and high charge carrier mobility.<sup>[14-18]</sup> In addition, pyrene shows characteristic excimer formation in concentrated solutions and in the solid state, due to extensive  $\pi$ - $\pi$  stacking of planar pyrene rings.<sup>[19-21]</sup> However pyrene excimer exhibits red shifted emission with decreased fluorescence quantum yield, which is big hurdle in solid state applications.<sup>[22-24]</sup> The use of sterically hindered pyrenes is promising strategy to overcome the problem of  $\pi$ - $\pi$  stacking.<sup>[25-28]</sup> In this attempt Tang et al. has established a milestone by introducing the concept of aggregation induced emission (AIE). The propeller shape AIE active molecules are highly fluorescent in the solid state.<sup>[29,30]</sup> The tetraphenylethene (TPE) and triphenylacrylonitrile (TPAN) are AIE active molecules.<sup>[31-38]</sup>

Our group is involved in the design and synthesis of mechanochromic materials.<sup>[39-41]</sup> In the previous chapter, we have discussed mechanochromic property of tetraphenylethene substituted phenanthroimidazoles.<sup>[42]</sup> We were further interested to study the effect of variation in phenanthroimidazole and TPE unit on the AIE and mechanochromic properties. Therefore we have designed and synthesized pyrene based solid state emitters **3a** and **3b** by substituting TPE and TPAN units on pyrenoimidazole, respectively. The **3a**

and **3b** exhibit strong solid-state fluorescence and reversible mechano-response between blue and green.

## 5.2. Results and Discussion

### 5.2.1. Synthesis



**Scheme 5.1.** Synthetic route for the pyrenoimidazoles **3a** and **3b**.

(i) Aniline, 4-bromo benzaldehyde, ammonium acetate, acetic acid; (ii) 4-(1,2,2-triphenylvinyl)phenylboronic acid pinacol ester,  $K_2CO_3$ ,  $Pd(PPh_3)_4$ , Toluene:Ethanol:Water (12.0 mL:4.0 mL:1.0 mL); (iii) 2-(4-pinacolatoboronphenyl)-3,3-diphenylacrylonitrile,  $K_2CO_3$ ,  $Pd(PPh_3)_4$ , Toluene:Ethanol:Water (12.0 mL:4.0 mL:1.0 mL).

The condensation reaction of pyrene-4,5-dione **1** with 4-bromobenzaldehyde and aniline resulted 10-(4-bromophenyl)-9-phenyl-9H-pyreno[4,5-d]imidazole **2** in 91% yield.<sup>[43]</sup> The pyrenoimidazoles **3a** and **3b** were synthesized by the Suzuki cross-coupling reaction of bromopyrenoimidazole **2** with 4-(1,2,2-triphenylvinyl)phenylboronic acid pinacol ester and 2-(4-pinacolatoboronphenyl)-3,3-diphenylacrylonitrile using  $Pd(PPh_3)_4$  as catalyst in 89%, and 73% yields, respectively (Scheme 5.1). The 4-(1,2,2-triphenylvinyl)phenylboronic acid pinacol ester and 2-(4-pinacolatoboronphenyl)-3,3-diphenylacrylonitrile were synthesized by using reported procedures.<sup>[31-38]</sup> The pyrenoimidazoles **3a** and **3b** were purified by column chromatography followed by recrystallization. The pyrenoimidazoles **3a** and **3b** were well characterized by  $^1H$  NMR,  $^{13}C$  NMR and high resolution

mass spectrometry (HRMS) techniques. The pyrenoimidazole **3a** was also characterized by single crystal X-ray analysis.

### 5.2.2. Thermogravimetric analysis

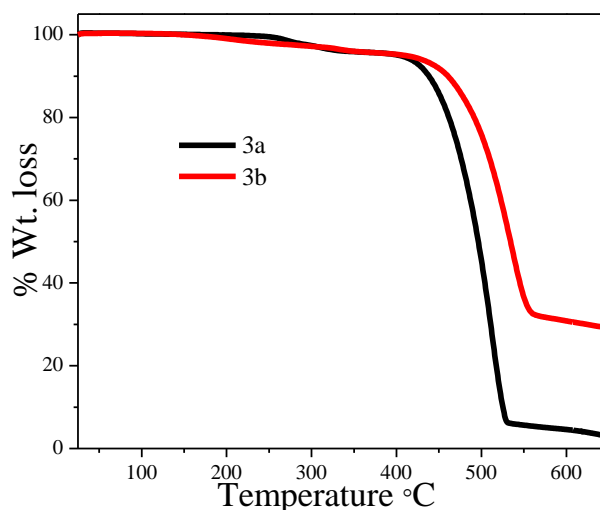


**Figure 5.1.** Thermogravimetric analysis of **3a**, and **3b** measured at a heating rate of 10 °C/ min under nitrogen atmosphere.

The thermal stability of pyrenoimidazoles **3a** and **3b** were investigated by thermogravimetric analysis (TGA). The pyrenoimidazoles **3a** and **3b** exhibits high thermal stability. The thermal decomposition temperatures ( $T_d$ ) corresponding to 5% weight loss under nitrogen atmosphere are 404 °C, and 412 °C for **3a** and **3b** respectively. This reflects the incorporation of cyano-group improves the thermal stability (Figure 5.1).

### 5.2.3. Photophysical properties

The electronic absorption spectra of the pyrenoimidazoles **3a** and **3b** are shown in Figure 5.2, and the data are summarized in Table 5.1. The pyrenoimidazoles **3a** and **3b** exhibit similar absorption behavior with small red shift in absorption spectra of **3b**. The absorption spectra of **3a** and **3b** show broad absorption band between 230–400 nm with absorption maxima around 243 nm, 292 nm, 350 nm and 387 nm. The absorption band between 310–410 nm corresponds to  $\pi$ - $\pi^*$  transitions localized on the pyrenoimidazoles.<sup>[44]</sup> This

long wavelength absorption band is significantly red shifted than corresponding TPE substituted phenanthroimidazole derivative.<sup>[42]</sup>

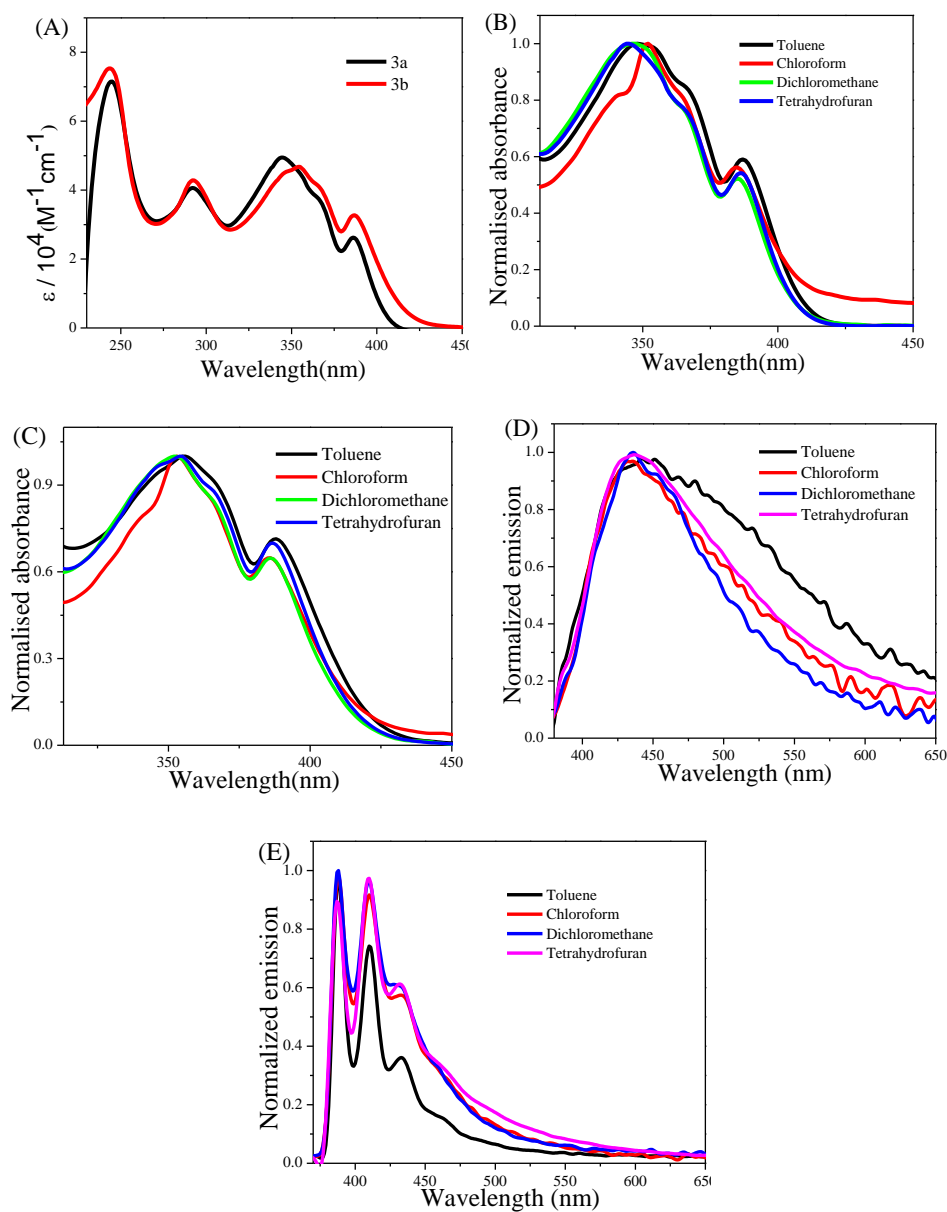


**Figure 5.2.** (A) Electronic absorption spectra of pyrenoimidazoles **3a** and **3b** recorded in THF. Absorption spectra of **3a** (B) and **3b** (C) in different solvents with varying polarities. Photoluminescence spectra of **3a** (D) and **3b** (E) in different solvents with varying polarities (excitation wavelength or  $\lambda_{\text{ex}} = 340$  nm).

**Table 5.1.** Photophysical, and thermal properties of the **3a** and **3b**.

Compounds	$\lambda_{\text{max}}[\text{nm}]$ ( $\epsilon[\text{Lmol}^{-1}\text{cm}^{-1}]$ ) <sup>a</sup>	$\lambda_{\text{em}}$ (nm)	$\Phi_f$ <sup>b</sup>	Optical band gap (eV)	Theoretical band gap (eV) <sup>c</sup>	$T_d$ (°C)
<b>3a</b>	245 (71366)					
	292 (40354)	438	0.0017	3.06	3.48	404
	344 (49592)					
	386 (26260)					
245 (75325)						
<b>3b</b>	293 (42756)	387,	0.0043	2.95	3.01	412
	355 (46715)	409,				
		432				
	387 (32859)					

<sup>a</sup>Measured in tetrahydrofuran. <sup>b</sup>The fluorescence quantum yields using 9, 10-diphenylanthracene as a standard in ethanol solution were performed. <sup>c</sup>Theoretical values at B3LYP/6-31G(d) level.

The pyrenoimidazoles **3a** and **3b** are weakly fluorescent in solutions, this can be ascribed to nonradiative decay of excited state due to free molecular rotations of tetraphenylethylene unit in solution. The fluorescence spectra of pyrenoimidazole **3b** shows vibronic pattern whereas the vibronic pattern disappears in pyrenoimidazole **3a**. The effect of solvent polarities on the absorption and fluorescence spectra was studied in solvents toluene, chloroform, dichloromethane, and tetrahydrofuran. The pyrenoimidazoles **3a** and **3b** are insoluble in highly polar (acetonitrile) and non-polar (cyclohexane) solvents. The solvatochromic study shows negligible changes on both absorption and fluorescence spectra (Figure 5.2 and Table 5.2). This reveals that there is less charge polarization in ground as well as excited state.

**Table 5.2.** Photophysical properties of **3a** and **3b** in different solvents.

Compounds	Solvents	$\lambda_{\text{abs.}}$ (nm)	$\lambda_{\text{em.}}$ (nm)
<b>3a</b>	Toluene	349, 387	442
	Chloroform	352, 385	436
	Dichloromethane	347, 385	436
	Tetrahydrofuran	345, 386	436
<b>3b</b>	Toluene	355, 388	388, 410, 432
	Chloroform	353, 386	388, 410, 432
	Dichloromethane	353, 386	388, 410, 432
	Tetrahydrofuran	354, 387	387, 410, 432

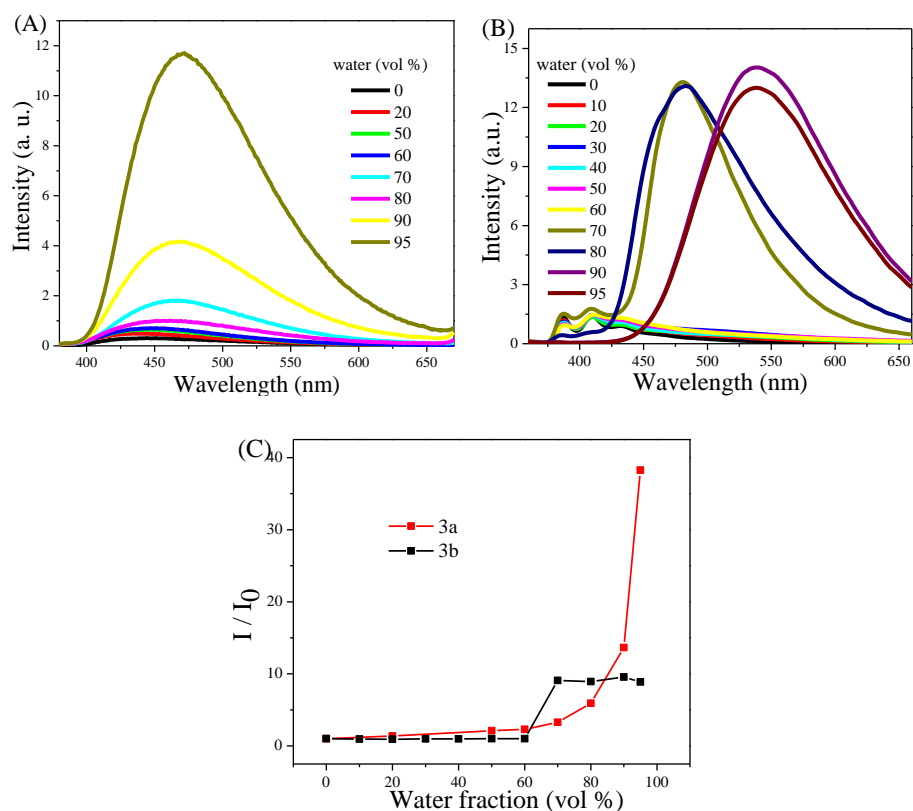


**Figure 5.3.** (A) Fluorescence spectra of **3a**, and (B) **3b** in THF-water mixtures with different water fractions. (C) Plot of fluorescence intensity (PL) vs. % of water fraction ( $f_w$ ). Luminogen concentration: 10  $\mu\text{M}$ ; excitation wavelength: 340 nm; intensity calculated at  $\lambda_{\text{max}}$ .

To check the AIE behavior of pyrenoimidazoles **3a** and **3b**, the absorption and fluorescence spectra in THF–water mixtures with different water fraction were studied. The small aggregates were prepared in THF by gradual increase in the water fraction. The pyrenoimidazoles **3a** and **3b** are weakly fluorescent in pure tetrahydrofuran and becomes highly fluorescent at higher water fraction which reveals these pyrenoimidazoles are AIE active (Figure 5.3). The different percentage of water fraction was required for pyrenoimidazoles **3a** and **3b** to start AIE effect. The pyrenoimidazole **3a** requires more than 80% water fraction, whereas pyrenoimidazole **3b** requires more than 60% water fraction. The poor fluorescence of pyrenoimidazoles **3a** and **3b** in THF was enhanced in aggregated suspension (95% water fraction) by 38 and 9 folds, respectively (Figure 5.3). The quantitative estimation of the AIE process was obtained by calculating the fluorescence quantum yields, in the mixture of water and THF in various proportions, using 9,10-diphenylanthracene as standard. In pure THF solution, pyrenoimidazoles **3a** and **3b** exhibit poor fluorescence with quantum yield 0.0017 and 0.0043 respectively, which was increased to 0.0460 and 0.0927 in the aggregated state (95 % aqueous).

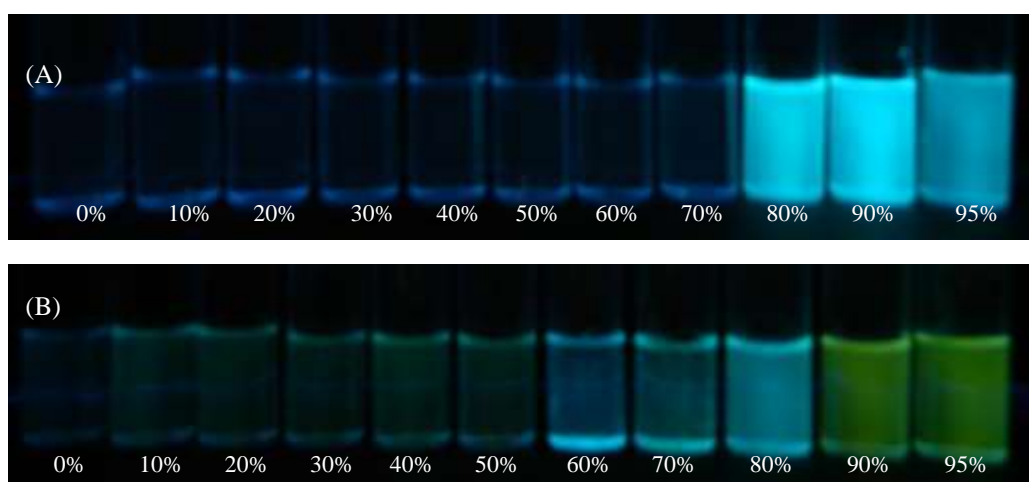


**Figure 5.4.** Photographs of **3a** (A) and **3b** (B) in THF–water mixtures with different water fractions (10  $\mu$ M) under 365 nm UV illumination.

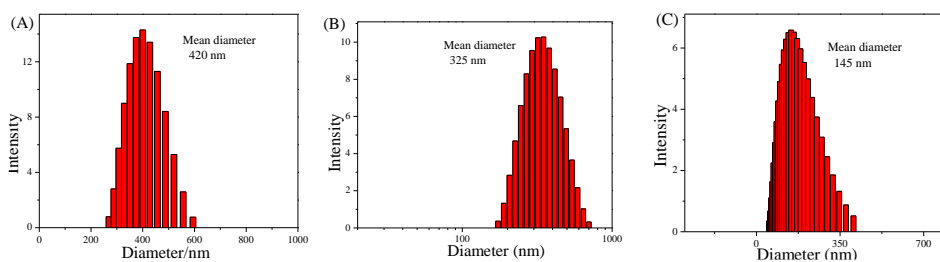


**Figure 5.5.** The particle size distributions of **3a** in THF–water mixture (A) at 90% ( $f_w$ ) and **3b** in THF–water mixture (B) at 70% ( $f_w$ ) and (C) at 95% ( $f_w$ ).

The images of pyrenoimidazoles **3a** and **3b** in THF–water mixture with different water fractions under UV illumination are shown in Figure 5.4. The pyrenoimidazole **3b** emits different color light at different water fraction, the aggregates formed at 70-80% water fraction emits blue color light ( $\lambda = 482$  nm), whereas aggregates formed at more than 90% water fraction emits yellow light ( $\lambda = 539$  nm). The size of different nano-aggregates of pyrenoimidazoles **3a** and **3b** at different water fraction was studied by dynamic light scattering (DLS). The DLS study of **3b** shows average diameter of 325 nm at 70% water fraction and 145 nm at 95% water fraction (Figure 5.5). The nano-aggregates of **3a** exhibit average diameter of 420 nm at 90% water fraction which is larger compared to **3b** (Figure 5.5). The larger average diameter of **3a** nano-aggregates compared to **3b** may leads to the lower quantum yield in **3a**. This may be due to the decrease in number of particles on the surface which leads to less contribution of molecules on the surface of the nano-aggregates in the emission intensity.<sup>[44]</sup> The AIE behavior was further explored by studying the absorption spectra in the THF–water mixtures (10  $\mu\text{M}$ ) (Figure 5.6). The absorption spectra of pyrenoimidazole **3a** at 80% water fraction, whereas pyrenoimidazole **3b** at 60% water fraction started to show light scattering by the nanoaggregate suspension in the THF–water mixtures.

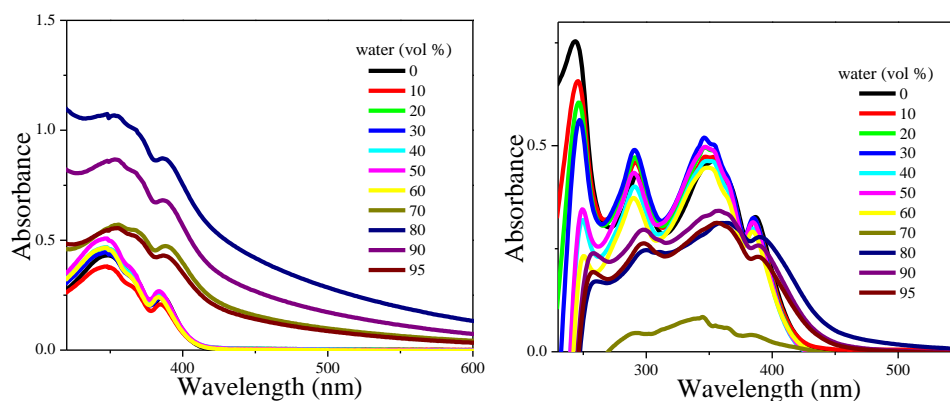


**Figure 5.6.** UV-vis absorption spectra of **3a** (left) and **3b** (right) in THF–water mixtures with different water fractions; Luminogen concentration: 10  $\mu$ M.

#### 5.2.4. Mechanochromic Property

The mechanochromic properties of pyrenoimidazoles **3a** and **3b** were studied by solid state emission spectroscopy. In the pristine form **3a** shows blue light emission at 461 nm, and **3b** show sky blue emission at 473 nm. Upon grinding using a spatula or pestle **3a** and **3b** solids exhibit drastic change in the emission behavior and exhibit yellowish green emission with emission maxima at 499 nm and 510 nm respectively (Figure 5.7). This mechanochromic effect is highly reversible in nature and can be reverted to its original color by annealing or fuming with solvent vapors. The ground sample of **3a** upon annealing at 200 °C for 15 min or fuming with dichloromethane vapor for 2 min, restored to the original blue emission. Whereas in ground sample of **3b**, annealing at 220 °C was required for 15 min to restore the original blue emission whereas fuming with solvent vapor does not restore to its original color completely.

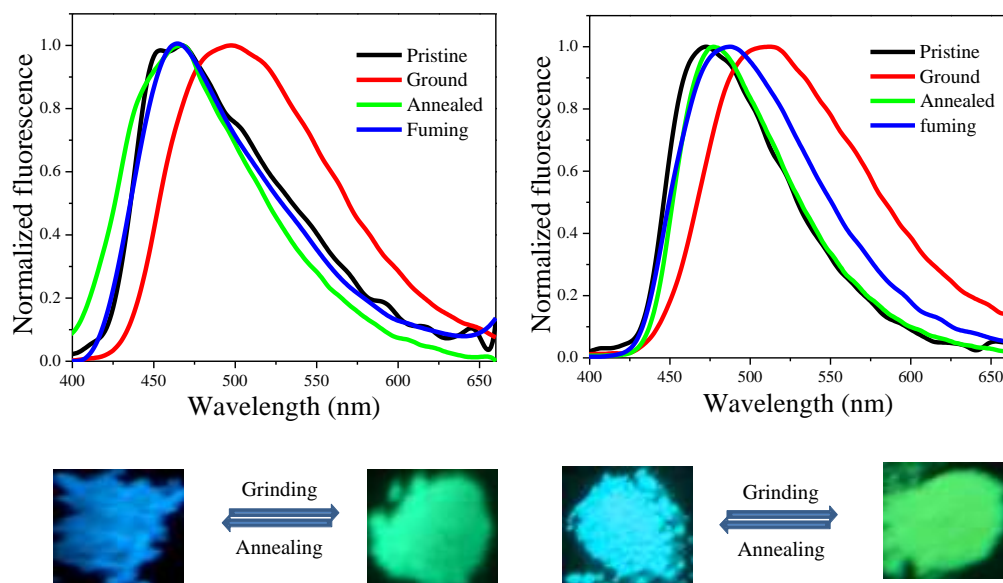


**Figure 5.7.** Emission spectra of **3a** (left) and **3b** (right) as Pristine, Ground and Heated solids and photograph taken under 365 nm UV illumination.

In order to understand the emission behavior under different stimuli, we have recorded absorption spectra in the solid state (Figure 5.8). The pristine form of pyrenoidimidazole **3a** and **3b** absorbs at 417 nm and 427 nm respectively which upon grinding exhibits bathochromic shift and absorbs at 446 nm and 437 nm, respectively. The bathochromic shift in absorption and emission suggests the enhanced conjugation, which can be attributed to the transformation of twisted conformation in pristine form to comparatively planar conformation in the ground form.

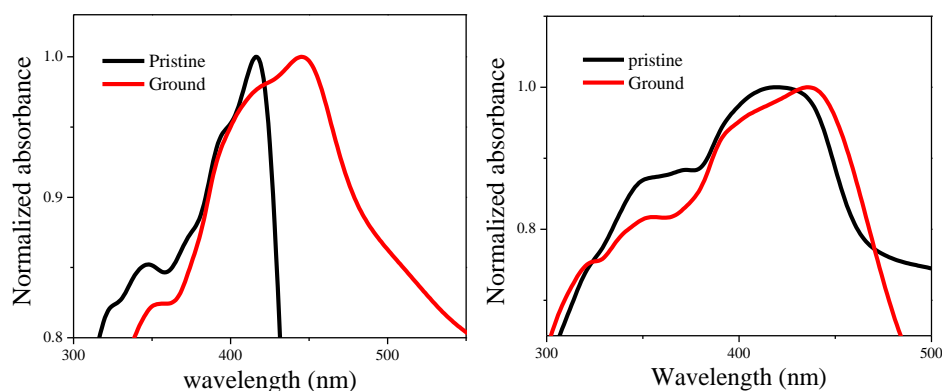


**Figure 5.8.** Solid state absorption spectra of **3a** (left) and **3b** (right) in crystalline and its ground form.

The pristine, ground and fumed forms of pyrenoimidazoles **3a** and **3b** were studied using powder X-ray diffraction (PXRD) (Figure 5.9). The diffraction patterns for pristine samples show sharp peaks, which is characteristic property of the crystalline state. The pristine samples upon grinding show broad diffuse band for **3a** and peak broadening in **3b** which indicates increased amorphous nature. The ground samples after fuming with dichloromethane restore the sharp peaks, suggesting regeneration of the crystalline nature. The PXRD study reveals that the morphological change from the crystalline state to the amorphous state and vice versa is associated with the mechanochromism in pyrenoimidazoles **3a** and **3b**.

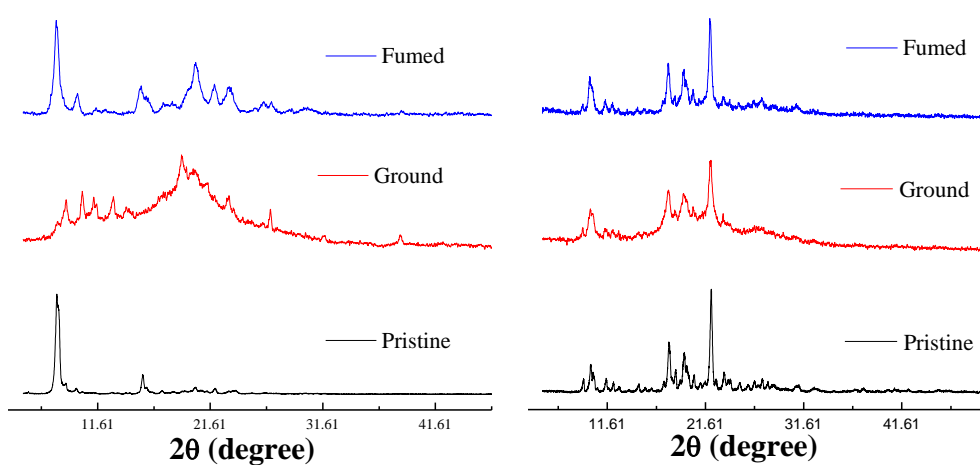


**Figure 5.9.** PXRD curves of **3a** (left) and **3b** (right) in Pristine, Ground and Fumed form.

### 5.2.5. Theoretical calculations

The geometry optimized and electronic structures of the pyrenoimidazoles **3a** and **3b** were obtained by density functional theory (DFT) calculations. The DFT calculations were performed at the B3LYP/6-31G(d) level.<sup>[45,46]</sup> The geometry optimized structures show highly twisted conformation. The contours of the highest occupied molecular orbital (HOMO) and lowest unoccupied molecular orbital (LUMO) of pyrenoimidazoles **3a** and **3b** are shown in Figure 5.10. The HOMO orbitals are localized over pyrenoimidazole part in **3a** and **3b**. In case of **3a** the LUMO orbital is localized on the TPE, imidazole and some part on pyrene unit, whereas in **3b** the LUMO orbital is localized only on the triphenylacrylonitrile. The replacement of phenyl in TPE with cyano-group in

**3b** leads to stabilization of both the HOMO and LUMO. The extent of stabilization of LUMO is more pronounced compared to HOMO, which leads to low HOMO-LUMO gap in **3b** compared to **3a**. This indicates the stronger donor-acceptor interaction in **3b** compared to **3a**.

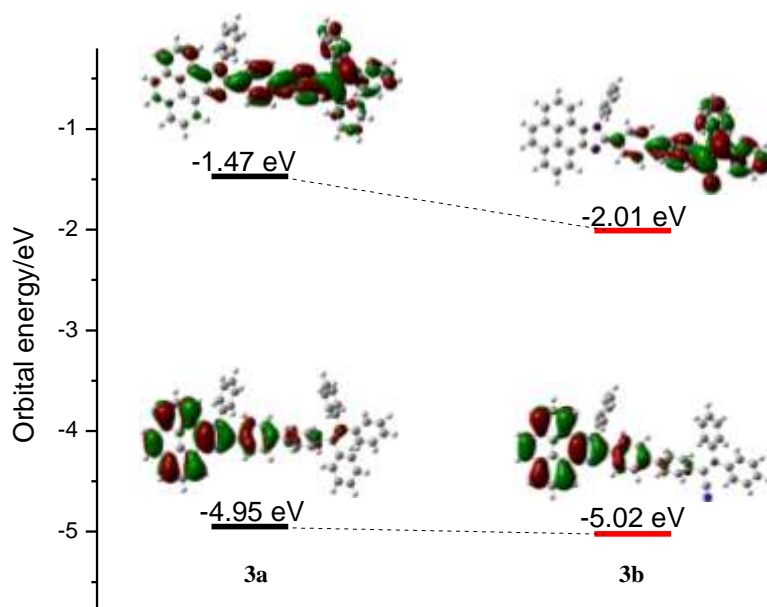


**Figure 5.10.** Correlation diagram showing the HOMO, and LUMO wave functions and energies of the pyrenoimidazoles **3a** (left) and **3b** (right).

### 5.2.6. Single crystal X-ray diffraction studies

**Table 5.3.** Crystal data and structure refinement for **3a**.

Parameter	<b>3a</b>
Identification code	rm172
Empirical formula	C <sub>11</sub> H <sub>7.20</sub> N <sub>0.40</sub>
Formula weight	144.97
Temperature	150(2) K
Wavelength(Å)	1.5418
Crystal system, space group	Triclinic, P -1
<i>a</i> / (Å)	9.4209(6)
<i>b</i> / (Å)	12.0079(11)
<i>c</i> / (Å)	21.6114(18)

$\alpha$ / (°)	75.523(8)
$\beta$ / (°)	85.392(6)
$\gamma$ / (°)	73.484(7)
<b>Volume</b>	2269.4(3) Å <sup>3</sup>
<b>Z, Calculated density (mg m<sup>-3</sup>)</b>	10, 1.061
<b>Absorption coefficient / (mm<sup>-1</sup>)</b>	0.468
<b>F(000)</b>	760
<b>Crystal size</b>	0.230 x 0.190 x 0.130 mm
<b><math>\theta</math> range for data collection / (°)</b>	3.953 to 49.989
<b>Reflections collected / unique</b>	9573 / 4648 [R(int) = 0.0408]
<b>Completeness to theta</b>	$\theta = 49.989$ ; 99.9 %
<b>Absorption correction</b>	Semi-empirical from equivalents
<b>Max. and min. transmission</b>	1.00000 and 0.85897
<b>Refinement method</b>	Full-matrix least-squares on F <sup>2</sup>
<b>Data / restraints / parameters</b>	4648 / 0 / 516
<b>Goodness-of-fit on F<sup>2</sup></b>	1.153
<b>Final R indices [I &gt; 2<math>\sigma</math>(I)]</b>	R1 = 0.1041, wR2 = 0.3147
<b>R indices (all data)</b>	R1 = 0.1268, wR2 = 0.3349
<b>Largest diff. peak and hole (eÅ<sup>-3</sup>)</b>	0.348 and -0.253

The single crystal X-ray structure of **3a** provides insight into the AIE. Generally, the pyrene unit containing fluorophores were known for planar and extensive  $\pi$ --- $\pi$  stacking interactions, but the crystal structure of **3a** exhibits twisted conformation of phenyl rings of TPE unit (Figure 5.11). This twisted conformation suppresses the  $\pi$ --- $\pi$  stacking effect of pyrene and supports AIE active nature, also twisting in phenyl rings supports the intramolecular rotations in solution leading to poor fluorescence. The packing diagram of **3a** exhibits intermolecular C-H--- $\pi$  interactions. Two mutual C-H--- $\pi$  interactions between two molecule via C(45)-H(45)--- $\pi$ (pyrene) And C(19)-H(19)--- $\pi$ (phenyl) to form a dimeric framework in head to tail fashion. Such dimers are connected to each other via C-H--- $\pi$  interaction C(42)-H(42)--- $\pi$ (pyrene) forming 2D staircase shaped framework (Figure 5.11). Thus, packing diagram reveals the absence of strong  $\pi$ --- $\pi$  stacking in pyrene unit.

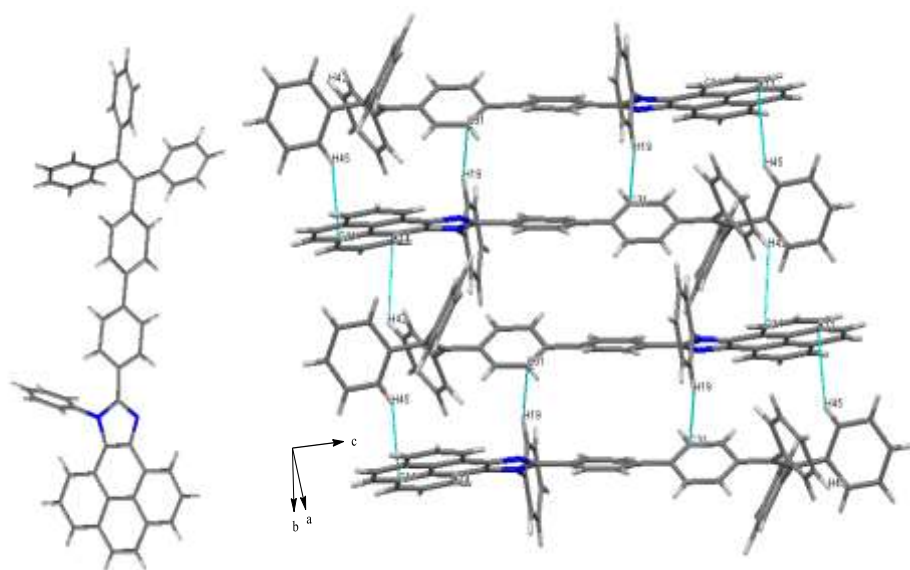


**Figure 5.11.** Crystal structure (left) and C-H... $\pi$  interactions assisted crystal packing (right) of **3a**.

### 5.3. Experimental section

#### Synthesis and characterization of intermediate **2**

**2:** The pyrene-4,5-dione (9.6 mmol), 4-bromobenzaldehyde (9.6 mmol), aniline (14.4 mmol), and ammonium acetate (96.1 mmol) in glacial acetic acid (50 mL) refluxed for 12 h under an argon atmosphere. After cooling to room temperature, a pale yellow mixture was obtained and poured into a methanol solution under stirring. The separated solid was filtered off, washed with 30 ml water, and dried to give compound **2** as off white solid. Yield: 91.0 %.  $^1\text{H}$  NMR (400 MHz,  $\text{CDCl}_3$ , 25 °C):  $\delta$  9.09 (dd, 1H,  $J=1.2, 8$  Hz), 8.21 (dd, 1H,  $J=1.2, 8$  Hz), 8.10-8.16 (m, 2H), 8.03-8.06 (m, 2H), 7.63-7.71 (m, 4H), 7.58-7.61 (m, 2H), 7.53 (dt, 2H,  $J=2, 8$  Hz), 7.45 (dt, 2H,  $J=2, 8$  Hz), 7.39 (dd, 1H,  $J=0.8, 8$  Hz) ppm; HRMS (ESI): calcd. for  $\text{C}_{19}\text{H}_{17}\text{BrN}_2$ : 473.0648 ( $\text{M}+\text{H}$ ) $^+$ , found 473.0647.

### Synthesis and characterization of **3a** and **3b**

**3a:** Pd(PPh<sub>3</sub>)<sub>4</sub> (0.004 mmol) was added to a well degassed solution of 10-(4-bromophenyl)-9-phenyl-9H-pyreno[4,5-d]imidazole (**2**) (0.4 mmol), 4-(1,2,2-triphenylvinyl)phenylboronic acid pinacol ester (0.48 mmol), K<sub>2</sub>CO<sub>3</sub> (1.2 mmol) in a mixture of toluene (12 mL)/ ethanol (4.0 mL)/ H<sub>2</sub>O (1.0 mL). The resulting mixture was stirred at 80 °C for 24 h under argon atmosphere. After cooling, the mixture was evaporated to dryness and the residue subjected to column chromatography on silica (Hexane-DCM 25:75 in vol.) to yield the desired product **3a** as colorless powder. The compound was recrystallized from DCM:ethanol (8:2) mixtures. Yield: 89.0%. <sup>1</sup>H NMR (400 MHz, CDCl<sub>3</sub>, 25 °C): δ 9.13 (dd, 1H, *J*=1.2, 8 Hz), 8.20 (dd, 1H, *J*=1.2, 8 Hz), 8.10-8.16 (m, 2H), 8.03-8.05 (m, 2H), 7.61-7.70 (m, 8H), 7.52 (dt, 2H, *J*=4, 8 Hz), 7.34-7.41 (m, 4H), 7.02-7.14 (m, 17H) ppm; <sup>13</sup>C NMR (100 MHz, CDCl<sub>3</sub>, 25 °C): δ 150.8, 143.7, 143.7, 143.6, 143.2, 141.3, 140.8, 140.4, 138.9, 138.0, 137.8, 135.2, 132.2, 131.8, 131.7, 131.4, 131.3, 130.2, 129.9, 129.6, 129.2, 128.9, 127.9, 127.9, 127.8, 127.7, 127.6, 127.5, 126.5, 126.5, 126.4, 126.3, 126.1, 125.3, 124.5, 124.3, 123.5, 122.8, 122.4, 119.8, 117.9, 0.00 ppm; HRMS (ESI): calcd. for C<sub>55</sub>H<sub>36</sub>N<sub>2</sub>: 725.2951 (M+H)<sup>+</sup>, found 725.2954.

**3b:** Pd(PPh<sub>3</sub>)<sub>4</sub> (0.004 mmol) was added to a well degassed solution of 10-(4-bromophenyl)-9-phenyl-9H-pyreno[4,5-d]imidazole (**2**) (0.4 mmol), 2-(4-pinacolatoboronphenyl)-3,3-diphenylacrylonitrile (0.48 mmol), K<sub>2</sub>CO<sub>3</sub> (1.2 mmol) in a mixture of toluene (12 mL)/ ethanol (4.0 mL)/ H<sub>2</sub>O (1.0 mL). The resulting mixture was stirred at 80 °C for 24 h under argon atmosphere. After cooling, the mixture was evaporated to dryness and the residue subjected to column chromatography on silica (Hexane-DCM 15:85 in vol.) to yield the desired product **3b** as greenish yellow powder. The compound was recrystallized from DCM:ethanol (8:2) mixtures. Yield: 73.0 %. <sup>1</sup>H NMR (400 MHz, CDCl<sub>3</sub>, 25 °C): δ 9.13 (dd, 1H, *J*=1.2, 8 Hz), 8.10-8.22 (m, 3H), 8.03-8.06 (m, 2H), 7.62-7.73 (m, 8H), 7.53 (d, 2H, *J*= 8 Hz), 7.70-7.49 (m, 8H), 7.31-7.34 (m, 2H), 7.21-7.29 (m, 3H), 7.05-7.07 (m, 2H) ppm; <sup>13</sup>C NMR (100 MHz, CDCl<sub>3</sub>, 25 °C): δ 157.8, 140.4, 140.2, 140.0, 139.1, 138.8, 134.1, 132.2, 131.7, 130.8, 130.3, 130.2, 130.0, 129.8, 129.2, 129.1, 128.9, 128.5, 128.4, 128.0, 127.6, 126.9, 126.7, 126.4, 125.3, 124.6, 124.4, 123.6, 122.9, 122.4,

120.0, 119.8, 118.0, 111.1, 0.00 ppm; HRMS (ESI): calcd. for C<sub>50</sub>H<sub>31</sub>N<sub>3</sub>+H<sup>+</sup>: 674.2591 (M+H)<sup>+</sup>, found 674.2599.

### Fluorescence quantum yields ( $\Phi_F$ )

The fluorescence quantum yields of AIE study ( $\Phi_F$ ) were calculated using 9,10-diphenylanthracene as standard in various THF-water mixtures by the steady-state comparative method.<sup>20</sup>

$$\Phi_F = \Phi_{st} \times S_u/S_{st} \times A_{st} / A_u \times n_{Du}^2/n_{Dst}^2$$

Where  $\Phi_F$  is the emission quantum yield of the sample,  $\Phi_{st}$  is the emission quantum yield of the standard,  $A_{st}$  and  $A_u$  represent the absorbance of the standard and sample at excitation wavelength, respectively. The  $S_{st}$  and  $S_u$  are the integrated emission band areas of the standard and sample, respectively, and  $n_{Dst}$  and  $n_{Du}$  are the solvent refractive index of the standard and sample. The u and st refer to the unknown and standard, respectively.

## 5.4. Conclusion

In summary, we have designed and synthesized pyrenoimidazoles **3a** and **3b** by the Pd-catalyzed Suzuki cross-coupling reaction of bromopyrenoimidazole **2** with 4-(1,2,2-triphenylvinyl)phenylboronic acid pinacol ester and 2-(4-pinacolatoboronphenyl)-3,3-diphenylacrylonitrile. The single crystal structure and packing diagram of **3a** reveals twisted conformation and absence of strong  $\pi$ --- $\pi$  stacking in pyrene units which results in fluorescent solids. The strong aggregation induced emission (AIE) and different AIE behavior was observed for **3a** and **3b**. The **3b** shows different colored emission at different water fraction which can be ascribed to the different sized nanoaggregates formation. The pyrenoimidazoles **3a** and **3b** exhibit reversible mechanochromic behavior with color contrast between blue and green. The solid state absorption, emission and powder XRD study reveals that, the transformation of twisted crystalline state to planar amorphous state is the main cause for mechanochromism in pyrenoimidazoles **3a** and **3b**. The optoelectronic applications of these materials are currently ongoing in our laboratory.

**Note:** This is copyrighted material from Royal Society of Chemistry, *J. Mater. Chem. C*, 2015, 3, 9981-9988 (DOI: 10.1039/C5TC02181B).

## 5.5. References

- [1] Forrest S R. (2003), The road to high efficiency organic light emitting devices, *Org. Electron.*, 4, 45–48 (DOI: 10.1016/j.orgel.2003.08.014).
- [2] Saragi T. P. I., Spehr T., Siebert A., Fuhrmann-Lieker T., Salbeck J. (2007), Spiro compounds for organic optoelectronics, *Chem. Rev.*, 107, 1011–1065 (DOI: 10.1021/CR0501341).
- [3] McGehee M D., Heeger A J. (2000), Semiconducting (conjugated) polymers as materials for solid-state lasers, *Adv. Mater.*, 12, 1655–1668 (DOI: 10.1002/1521-4095(200011)12:22<1655::AID-ADMA1655>3.0.CO;2-2).
- [4] Samuel I. D. W., Turnbull G A. (2007), Organic semiconductor lasers, *Chem. Rev.*, 107, 1272–1295 (DOI: 10.1021/CR050152I).
- [5] Xu H., Chen R., Sun Q., Lai W., Su Q., Huang W., Liu X., Eley D D., Tang C W., Slyke S A Van., et al. (2014), Recent progress in metal–organic complexes for optoelectronic applications, *Chem. Soc. Rev.*, 43, 3259 (DOI: 10.1039/c3cs60449g).
- [6] Zaumseil J., Sirringhaus H. (2007), Electron and ambipolar transport in organic field-effect transistors, *Chem. Rev.*, 107, 1296–1323 (DOI: 10.1021/CR0501543).
- [7] Cicoira F., Santato C. (2007), Organic Light Emitting Field Effect Transistors: Advances and Perspectives, *Adv. Funct. Mater.*, 17, 3421–3434 (DOI: 10.1002/adfm.200700174).
- [8] Liu X Y., Bai D R., Wang S. (2006), Charge-transfer emission in nonplanar three-coordinate organoboron compounds for fluorescent sensing of fluoride, *Angew. Chemie*, 118, 5601–5604 (DOI: 10.1002/ange.200601286).
- [9] Chi Z., Zhang X., Xu B., Zhou X., Ma C., Zhang Y., Liu S., Xu J., Pucci A., Cuia F D., et al. (2012), Recent advances in organic mechanofluorochromic materials, *Chem. Soc. Rev.*, 41, 3878 (DOI: 10.1039/c2cs35016e).

- [10] Sagara Y., Kato T. (2009), Mechanically induced luminescence changes in molecular assemblies, *Nat. Chem.*, 1, 605–610 (DOI: 10.1038/nchem.411).
- [11] Luo X., Li J., Li C., Heng L., Dong Y Q., Liu Z., Bo Z., Tang B Z. (2011), Reversible switching of the emission of diphenyldibenzofulvenes by thermal and mechanical stimuli, *Adv. Mater.*, 23, 3261–3265 (DOI: 10.1002/adma.201101059).
- [12] Dong Y., Xu B., Zhang J., Tan X., Wang L., Chen J., Lv H., Wen S., Li B., Ye L., et al. (2012), Piezochromic luminescence based on the molecular aggregation of 9,10-Bis(( E )-2-(pyrid-2-yl)vinyl)anthracene, *Angew. Chemie Int. Ed.*, 51, 10782–10785 (DOI: 10.1002/anie.201204660).
- [13] Davis D A., Hamilton A., Yang J., et al. (2009), Force-induced activation of covalent bonds in mechanoresponsive polymeric materials, *Nature*, 459, 68–72 (DOI: 10.1038/nature07970).
- [14] Lee Y O., Pradhan T., Yoo S., Kim T H., Kim J., Kim J S. (2012), Enhanced electrogenerated chemiluminescence of phenylethynylpyrene derivatives: Use of weakly electron-donating group as a substituent, *J. Org. Chem.*, 77, 11007–11013 (DOI: 10.1021/jo3010974).
- [15] Figueira-Duarte T M., Müllen K. (2011), Pyrene-based materials for organic electronics, *Chem. Rev.*, 111, 7260–7314 (DOI: 10.1021/cr100428a).
- [16] J. R. Lakowicz, *Principles of Fluorescence Spectroscopy*, Plenum press, New York, 1999.
- [17] J. B. Birks, *Photophysics of Aromatic Molecules*, Wiley-Interscience, London, 1970.
- [18] Dhokale B., Jadhav T., Mobin S M., Misra R.(2015), Synergistic effect of donors on tetracyanobutadine (TCBD) substituted ferrocenyl pyrenes, *RSC Adv.*, 5, 57692–57699 (DOI: 10.1039/C5RA11433K).
- [19] T. Forster and K. Kasper, *Z. Phys. Chem.* 1954, 1, 275.
- [20] J. B. Birks, D. J. Dyson and I. H. Munro, *Proc. R. Soc. London Ser. A* 1963, 275, 575.
- [21] K. A. Zachariasse, *Trends Photochem. Photobiol.* 1994, 3, 211.
- [22] Moorthy J. N., Natarajan, P., Venkatakrisnan P., Huang D.-F., Chow

- T. J. (2007), Steric inhibition of  $\pi$ -stacking: 1,3,6,8-tetraarylpyrenes as efficient blue emitters in organic light emitting diodes (OLEDs), *Org. Lett.*, 9, 5215–5218 (DOI: 10.1021/OL7023136).
- [23] Sonar P., Soh M S., Cheng Y H., Henssler J T., Sellinger A. (2010), 1,3,6,8-Tetrasubstituted pyrenes: solution-processable materials for application in organic electronics, *Org. Lett.*, 12, 3292–3295 (DOI: 10.1021/ol1007179).
- [24] Sotoyama W., Sato H., Kinoshita M., Takahashi T., Matsuura A., Kodama J., Sawatari N., Inoue H. (2003), 45.3: Tetra-substituted pyrenes: new class of blue emitter for organic light-emitting diodes, *SID Symp. Dig. Tech. Pap.*, 34, 1294 (DOI: 10.1889/1.1832523).
- [25] Figueira-Duarte T M., Simon S C., Wagner M., Druzhinin S I., Zachariasse K A., Müllen K. (2008), Polypyrene Dendrimers, *Angew. Chemie Int. Ed.*, 47, 10175–10178 (DOI: 10.1002/anie.200803408).
- [26] Figueira-Duarte T M., Del Rosso P G., Trattnig R., Sax S., List E J W., Müllen K. (2010), Designed suppression of aggregation in polypyrene: toward high-performance blue-light-emitting diodes, *Adv. Mater.*, 22, 990–993 (DOI: 10.1002/adma.200902744).
- [27] Hu J., Era M., Elsegood M R J., Yamato T. (2010), Synthesis and photophysical properties of pyrene-based light-emitting monomers: highly pure-blue-fluorescent, cruciform-shaped architectures, *European J. Org. Chem.*, 2010, 72–79 (DOI: 10.1002/ejoc.200900806).
- [28] Zöphel L., Beckmann D., Enkelmann V., Chercka D., Rieger R., Müllen K., Duan L A., Hou L D., Lee T W., Qiao J A., et al. (2011), Asymmetric pyrene derivatives for organic field-effect transistors, *Chem. Commun.*, 47, 6960 (DOI: 10.1039/c1cc11827g).
- [29] Luo J., Xie Z., Lam J W Y., Cheng L., Tang B Z., Chen H., Qiu C., Kwok H S., Zhan X., Liu Y., et al. (2001), Aggregation-induced emission of 1-methyl-1,2,3,4,5-pentaphenylsilole, *Chem. Commun.*, 397, 1740–1741 (DOI: 10.1039/b105159h).
- [30] Li Y., Liu T., Liu H., Tian M-Z., Li Y. (2014), Self-assembly of intramolecular charge-transfer compounds into functional molecular systems, *Acc. Chem. Res.*, 47, 1186–1198 (DOI: 10.1021/ar400264e).
- [31] Dong Y., Lam J W Y., Qin A., Liu J., Li Z., Tang B Z., Sun J. and

- Kwok H S. (2007), Aggregation-induced emissions of tetraphenylethene derivatives and their utilities as chemical vapor sensors and in organic light-emitting diodes, *Appl. Phys. Lett.*, 91, 11111 (DOI: 10.1063/1.2753723).
- [32] Huang J., Yang X., Wang J., Zhong C., Wang L., Qin J., Li Z., Tang C W., Vanslyke S A., Baldo M A., et al. (2012), New tetraphenylethene-based efficient blue luminophors: aggregation induced emission and partially controllable emitting color, *J. Mater. Chem.*, 22, 2478–2484 (DOI: 10.1039/C1JM14054J).
- [33] Zhao N., Yang Z., Lam J W Y., Sung H H Y., Xie N., Chen S., Su H., Gao M., Williams I D., Wong K S., et al. (2012), Benzothiazolium-functionalized tetraphenylethene: an AIE luminogen with tunable solid-state emission, *Chem. Commun.*, 48, 8637 (DOI: 10.1039/c2cc33780k).
- [34] Wang J., Mei J., Hu R., Sun J Z., Qin A. Tang B Z. (2012), Click synthesis, aggregation-induced emission, *e / z* isomerization, self-organization, and multiple chromisms of pure stereoisomers of a tetraphenylethene-cored luminogen, *J. Am. Chem. Soc.*, 134, 9956–9966 (DOI: 10.1021/ja208883h).
- [35] Wang S., Oldham Jr J. W., Hudack Jr A. R., Bazan C. G. (2000), Synthesis, morphology, and optical properties of tetrahedral oligo(phenylenevinylene) materials, *J. Am. Chem. Soc.*, 122, 5695–5709 (DOI: 10.1021/JA992924W).
- [36] Yuan W Z., Gong Y., Chen S., Shen X Y., Lam J W Y., Lu P., Lu Y., Wang Z., Hu R., Xie N., et al. (2012), Efficient solid emitters with aggregation-induced emission and intramolecular charge transfer characteristics: molecular design, synthesis, photophysical behaviors, and oled application, *Chem. Mater.*, 24, 1518–1528 (DOI: 10.1021/cm300416y).
- [37] Yuan W Z., Tan Y., Gong Y., Lu P., Lam J W Y., Shen X Y., Feng C., Sung H H-Y., Lu Y., Williams I D., et al. (2013), Synergy between twisted conformation and effective intermolecular interactions: strategy for efficient mechanochromic luminogens with high contrast, *Adv. Mater.*, 25, 2837–2843 (DOI: 10.1002/adma.201205043).

- [38] Gong Y., Tan Y., Liu J., Lu P., Feng C., Yuan W Z., Lu Y., Sun J Z., He G., Zhang Y., et al. (2013), Twisted D- $\pi$ -A solid emitters: efficient emission and high contrast mechanochromism, *Chem. Commun.*, 49, 4009 (DOI: 10.1039/c3cc39243k).
- [39] Jadhav T., Dhokale B., Mobin S M., Misra R., Sagara Y., Kato T., Davis D A., Hamilton A., Yang J L., Cremar L D., et al. (2015), Mechanochromism and aggregation induced emission in benzothiazole substituted tetraphenylethylenes: a structure function correlation, *RSC Adv.*, 5, 29878–29884 (DOI: 10.1039/C5RA04881H).
- [40] Gautam P., Maragani R., Mobin S M., Misra R., Chi Z., Zhang X., Xu B., Zhou X., Ma C., Zhang Y., et al. (2014), Reversible mechanochromism in dipyridylamine-substituted unsymmetrical benzothiadiazoles, *RSC Adv.*, 4, 52526–52529 (DOI: 10.1039/C4RA09921D).
- [41] Jadhav T., Dhokale B., Misra R., Chi Z., Zhang X., Xu B., Zhou X., Ma C., Zhang Y., Liu S., et al. (2015), Effect of the cyano group on solid state photophysical behavior of tetraphenylethene substituted benzothiadiazoles, *J. Mater. Chem. C*, 3, 9063–9068 (DOI: 10.1039/C5TC01871D).
- [42] Misra R., Jadhav T., Dhokale B., Mobin S M., Sagara Y., Kato T., Davis D A., Hamilton A., Yang J L., Cremar L D., et al. (2014), Reversible mechanochromism and enhanced AIE in tetraphenylethene substituted phenanthroimidazoles, *Chem. Commun.*, 50, 9076 (DOI: 10.1039/C4CC02824D).
- [43] Yi X., Yang P., Huang D. and Zhao J. (2013), Visible light-harvesting cyclometalated Ir(III) complexes with pyreno[4,5-d]imidazole C<sup>N</sup> ligands as triplet photosensitizers for triplet-triplet annihilation upconversion, *Dye. Pigment.*, 96, 104–115 (DOI: 10.1016/j.dyepig.2012.07.020).
- [44] Zhang X., Chi Z., Xu B., Chen C., Zhou X., Zhang Y., Liu S., Xu J., Chi Z., Zhang X., et al. (2012), End-group effects of piezofluorochromic aggregation-induced enhanced emission compounds containing distyrylanthracene, *J. Mater. Chem.*, 22, 18505 (DOI: 10.1039/c2jm33140c).

- [45] Lee C., Yang W. and Parr R G. (1988), Development of the Colle-Salvetti correlation-energy formula into a functional of the electron density, *Phys. Rev. B*, 37, 785–789 (DOI: 10.1103/PhysRevB.37.785).
- [46] Becke A D. (1993), A new mixing of Hartree–Fock and local density-functional theories, *J. Chem. Phys.*, 98, 1372 (DOI: 10.1063/1.464304).

## Chapter 6

# Multi-stimuli responsive donor-acceptor tetraphenylethylene substituted benzothiadiazoles

---

---

### 6.1. Introduction

The design and synthesis of fluorescent organic solids with different emission colors have been continuously attracting the scientific community for full color displays and white light emitting devices.<sup>[1-6]</sup> In recent years, fluorescent organic solids have been extensively used in the development of environment sensitive materials with widespread applications in analytical, environmental, optical, and biochemical areas. Particularly mechanochromic and vapochromic materials have been developed for their applications in mechano-sensors, vapo-sensors, environmental monitors, chemical sensors, optical data storage, and security papers.<sup>[7-14]</sup> These applications require the efficient solid state emission.<sup>[15-16]</sup> Unfortunately, most of the organic dyes are non-fluorescent in solid state due to the notorious aggregation caused quenching (ACQ) effect.<sup>[17-21]</sup> The tetraphenylethylene (TPE) is a weak electron donor and has propeller shaped molecular structure, which overcomes the ACQ effect.<sup>[22-30]</sup> The TPE containing molecules show aggregation induced emission (AIE) and are fluorescent in the solid state.<sup>[22-30]</sup>

The photophysical properties of the donor-acceptor (D–A) molecular systems are function of the strength of donor/acceptor (D/A) groups.<sup>[31-33]</sup> The D–A system allows the fine tuning of electronic and optical properties by modification of D/A or changing one without disturbing the other.<sup>[34]</sup> A wide variety of D–A molecular systems has been explored for mechanochromism.<sup>[35-42]</sup> In order to design efficient and desirable mechanochromic materials, it is important to understand the structure–property relationship. There are still no standard guidelines to predict the mechanochromism.<sup>[43-54]</sup>

The 2,1,3-benzothiadiazole (BTD) is a strong electron acceptor owing to its high electron affinity.<sup>[55-62]</sup> Wang *et al.* and Wei *et al.* have reported symmetrical BTD-cored cyano-substituted diphenylethene derivatives for mechanochromism.<sup>[63-64]</sup> Our group is interested in the design and synthesis of TPE substituted mechanochromic materials.<sup>[65-68]</sup> The TPE substituted BTDs are rare to show mechanochromism.<sup>[69-72]</sup> In this chapter we wish to report, the TPE substituted BTDs **3–9** and the effect of D/A strength of different substituents and their substitution pattern on the photophysical, AIE, mechanochromic and vapochromic properties.<sup>[73,74]</sup> The BTDs **3–9** (Chart 6.1) are designed in such a way that; (1) In BTD **3**, symmetrically two TPE units are substituted on BTD, which forms D–A–D architecture. (2) In BTD **4** the acceptor strength is increased by incorporating one more BTD unit, which forms the symmetric D–A–A–D architecture. (3) In BTDs **5–9**, the TPE unit is fixed at one end of the BTD and the other end is systematically varied with different units like phenyl (weak donor) in **5**, tolyl (weak donor) in **6**, trifluoromethyl-phenyl (weak acceptor) in **7**, cyanophenyl (weak acceptor) in **8** and triphenyl amine (strong donor) in **9**, which forms unsymmetrical D–A–D<sub>1</sub>, D–A–A<sub>1</sub> and D–A–D<sub>2</sub> architectures. The photophysical, AIE, mechanochromic and vapochromic properties of BTDs **3–9** are tuned on the basis of the strength of D–A interaction and conjugation length.

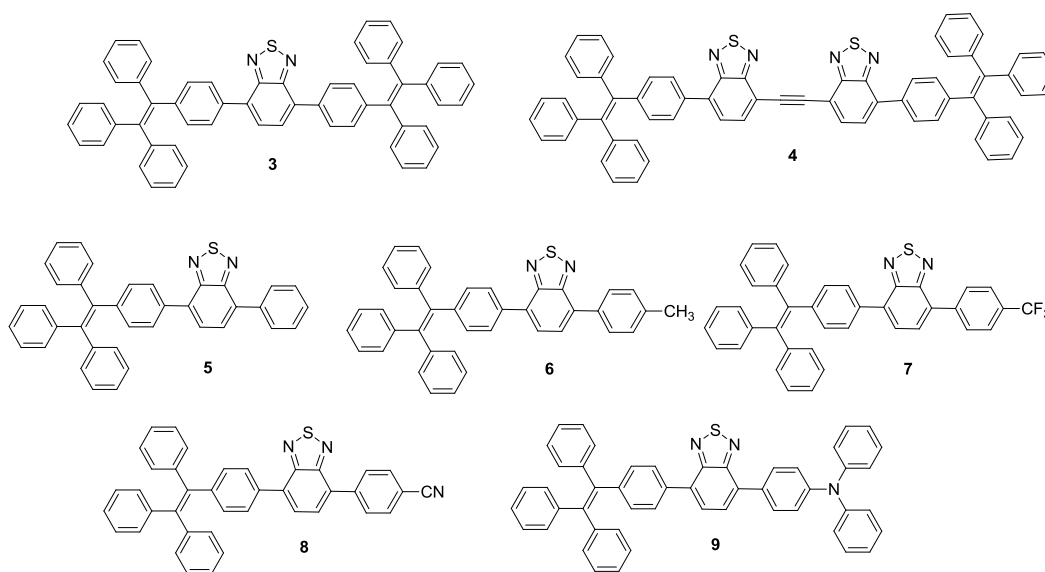
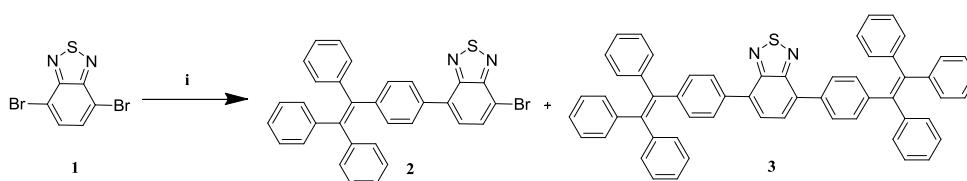


**Chart 6.1.** The TPE substituted BTDs **3–9**.

## 6.2. Results and discussion

### 6.2.1. Synthesis

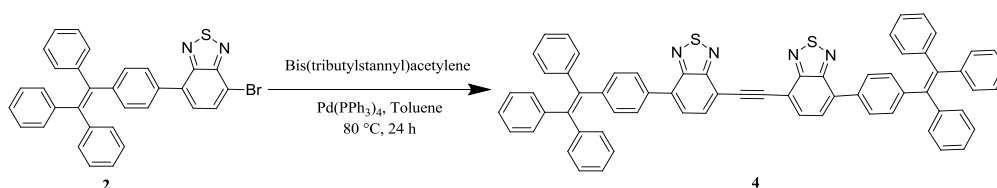
The TPE substituted BTDs **3–9** were synthesized by the Pd-catalyzed Suzuki and Stille coupling reactions. The precursor **2** was synthesized by the Pd-catalyzed Suzuki cross-coupling reaction of dibromo-BTD **1** with 0.9 equivalent of 4-(1,2,2-triphenylvinyl)phenylboronic acid pinacol ester.<sup>[72,73,75]</sup> This reaction condition resulted di-TPE substituted BTD **3** as a minor product (Scheme 6.1). The excess use of 4-(1,2,2-triphenylvinyl)phenylboronic acid pinacol ester resulted in the formation of the disubstituted BTD **3** as a major product.



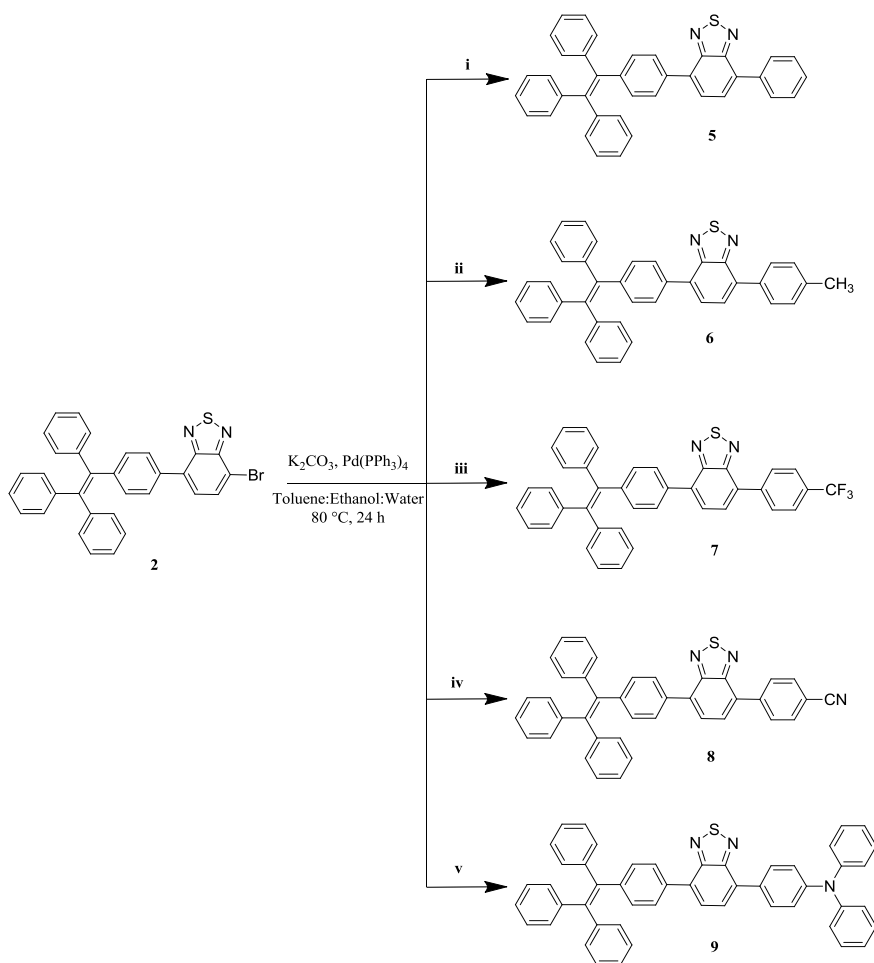
**Scheme 6.1.** Synthetic route for BTDs **2** and **3**.

(i) 4-(1,2,2-triphenylvinyl)phenylboronic acid pinacol ester,  $K_2CO_3$ ,  $Pd(PPh_3)_4$ , Toluene:Ethanol:Water, 80 °C, 24 h.

The symmetrical BTD **4** was synthesized by the Pd catalyzed Stille coupling reaction of the precursor **2** with *bis*-(tributylstannyl)acetylene in 30% yield (Scheme 6.2). The Suzuki cross-coupling reaction of the TPE substituted bromo-BTD **2** with phenylboronic acid, *p*-tolylboronic acid, (4-(trifluoromethyl)phenyl)boronic acid, 4-cyanophenylboronic acid pinacol ester and 4-(diphenylamino)phenylboronic acid pinacol ester resulted in unsymmetrical BTDs **5**, **6**, **7**, **8**, and **9** respectively in good yields (Scheme 6.3). All the BTDs **3–9** were well characterized by  $^1H$  NMR,  $^{13}C$  NMR and HRMS techniques. The BTDs **5** and **6** were also characterized by single-crystal X-ray diffraction technique.



**Scheme 6.2.** Synthetic route for BTD **4**.



**Scheme 6.3.** Synthetic route for BTDs **5**–**9**.

(i) phenylboronic acid; (ii) *p*-tolylboronic acid; (iii) (4-(trifluoromethyl)phenyl)boronic acid; (iv) 4-cyanophenylboronic acid pinacol ester; (v) 4-(diphenylamino)phenylboronic acid pinacol ester.

### 6.2.2. Single crystal X-ray diffraction studies

The crystals of the BTDs **5** and **6** were obtained by slow diffusion of ethanol into the dichloromethane solution at room temperature. The single-crystal X-ray structure of BTDs **5** and **6** are shown in Figure 6.1. The BTDs **5** and **6** crystallize in monoclinic  $I 2/c$  and triclinic  $P \bar{1}$  space groups, respectively. The crystal structure of BTD **5** shows that, the almost planar BTD core with phenyl substituent and phenyl ring of TPE unit with dihedral angles of  $8.14^\circ$  and  $13.6^\circ$  respectively. Contrary to this, the BTD **6** exhibits twisted geometry and BTD core has dihedral angles of  $57.77^\circ$  and  $53.16^\circ$  with

tolyl substituent and phenyl ring of TPE respectively. The twisted geometry of TPE unit in BTDs **5** and **6** reduces the  $\pi$ - $\pi$  stacking interaction.

**Table 6.1.** Crystal data and structure refinement for BTD **5** and **6**.

Parameter	BTD 5	BTD 6
Identification code	rm158	shelx
Empirical formula	C <sub>38</sub> H <sub>26</sub> N <sub>2</sub> S	C <sub>39</sub> H <sub>28</sub> N <sub>2</sub> S
Formula weight	542.67	556.69
Temperature	150(2) K	293(2) K
Wavelength(A)	1.5418	0.71073 Å
Crystal system, space group	Monoclinic, I 2/a	Triclinic, P -1
<i>a</i> / (Å)	17.9549(11)	5.9323(3)
<i>b</i> / (Å)	5.7818(3)	9.0092(5)
<i>c</i> / (Å)	55.027(3)	28.6842(16)
$\alpha$ / (°)	90	91.068(4)
$\beta$ / (°)	91.498(5)	90.990(4)
$\gamma$ / (°)	90	101.891(4)
Volume	5710.5(5) Å <sup>3</sup>	1499.53(14) Å <sup>3</sup>
Z, Calculated density (mg m <sup>-3</sup> )	8, 1.262	2, 1.233
Absorption coefficient /(mm <sup>-1</sup> )	1.226	0.138
F(000)	2272	584
Crystal size	0.33 x 0.26 x 0.21 mm	0.210 x 0.180 x 0.140
$\theta$ range for data collection/(°)	3.21 to 71.68	3.108 to 24.997
Reflections collected / unique	18686 / 5454 [R(int) = 0.0380]	11416 / 5252 [R(int) = 0.0419]
Completeness to theta	$\theta = 71.68$ ; 98.0 %	$\theta = 24.997$ ; 99.8%
Absorption correction	Analytical	Semi-empirical from equivalents
Max. and min. transmission	0.7829 and 0.6878	1.00000 and 0.59490
Refinement method	Full-matrix least-squares on F <sup>2</sup>	Full-matrix least-squares on F <sup>2</sup>
Data / restraints / parameters	5454 / 0 / 371	5252 / 0 / 380
Goodness-of-fit on F <sup>2</sup>	1.066	1.097
Final R indices [I>2sigma(I)]	R1 = 0.07288, wR2 = 0.2292	R1 = 0.0610, wR2 = 0.1419
R indices (all data)	R1 = 0.1152, wR2 = 0.2809	R1 = 0.0967, wR2 = 0.1647
Largest diff. peak and hole (eÅ <sup>-3</sup> )	0.467 and -0.693	0.178 and -0.257

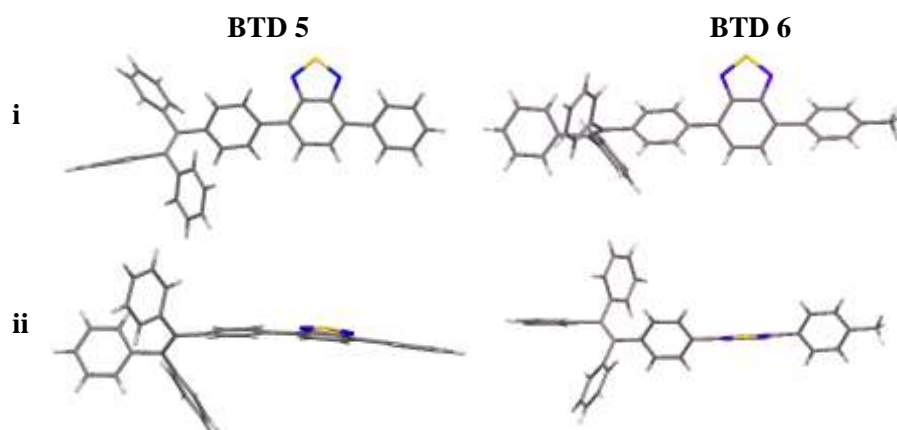


**Figure 6.1.** Crystal structure of BTDs **5** and **6** (i) Front view, (ii) Side view.

The packing diagram of BTD **5** shows strong intermolecular C–H $\cdots$ S and C–H $\cdots$  $\pi$  interactions. The intermolecular C–H $\cdots$ S (2.857 Å) interaction leads to the formation of the hydrogen bonded dimers in head-to-head fashion. These dimers are interlinked through C–H $\cdots$  $\pi$  interaction C11–H11 $\cdots$ C15 (2.866 Å) to form a 1D polymeric chain. The C–H $\cdots$  $\pi$  interaction of C11–H11 $\cdots$ C15 (2.866) leads to the cross-linking of the chains leading to formation of a 2D sheet like structure (Figure 6.2).

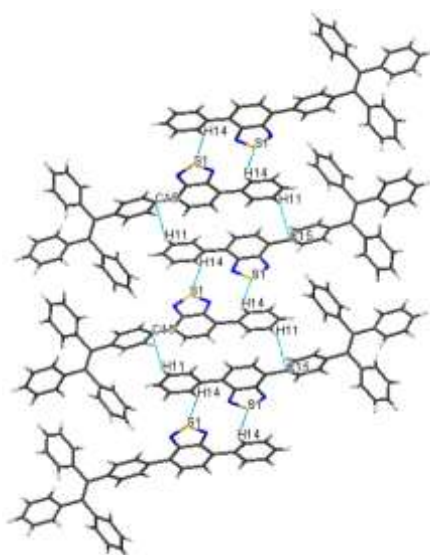


**Figure 6.2.** Crystal packing diagram of BTD **5** along *b*-axis.

The packing diagram of BTD **6** shows strong intermolecular S $\cdots$  $\pi$  and C–H $\cdots$  $\pi$  interactions. The intermolecular S $\cdots$  $\pi$  (3.654 Å) interactions lead to the formation of ladder like framework. These ladders are interlinked through

two mutual C–H··· $\pi$  interactions C23–H23···C32 (2.823 Å) to form a 2D structural sheet (Figure 6.3).

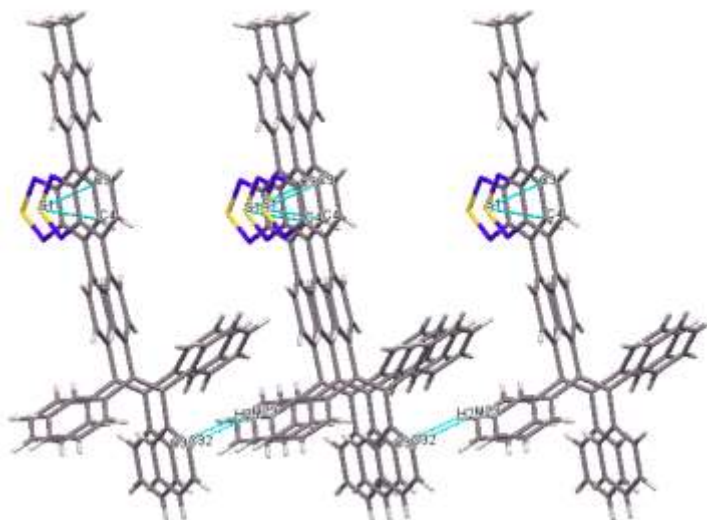


**Figure 6.3.** Crystal packing diagram of BTD **6** along tilted *a*-axis.

### 6.2.3. Thermogravimetric analysis

The thermogravimetric analysis (TGA) was performed to study the thermal stability of the BTDs **3–9** and thermograms are shown in Figure 6.4. The BTDs **3–9** exhibit high thermal stability. The decomposition temperatures ( $T_d$ , temperature at which 10% weight loss occurs during heating), for the BTDs **3–9** were found in between 346–503 °C. The trend in thermal stability follows order **4** > **3** > **9** > **8** > **6** > **5** > **7**, which shows that the symmetrical BTDs **3** and **4** are thermally more stable compared to unsymmetrical BTDs **5–9**.

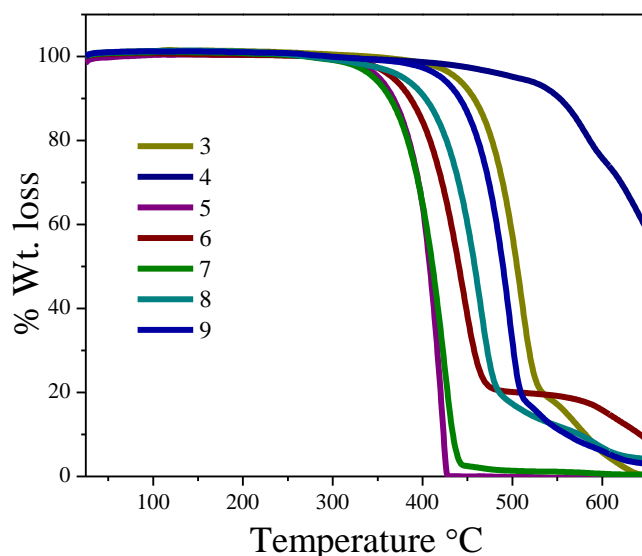


**Figure 6.4.** Thermogravimetric analysis of the BTDs **3–9**, measured at a heating rate of  $10\text{ }^{\circ}\text{C}/\text{min}$  under nitrogen atmosphere.

#### 6.2.4. Theoretical calculations

The density functional theory (DFT) calculations were performed at the B3LYP/6-31G(d) level to understand the geometry and electronic structure of the BTDs **3–9**. The energy optimized structures show twisted geometry of TPE and triphenylamine units. The contours of the HOMO and LUMO of BTDs **3–9** are shown in Figure 6.5. The HOMO orbitals are localized over TPE, and benzo part of the BTD unit in BTDs **3–8**, whereas in BTD **9** it is localized on the triphenylamine and benzo part of the BTD unit. The distribution of HOMO in BTDs **3–8** show that the TPE is a strong electron donor unit than the phenyl and tolyl units. The distribution of HOMO orbital of BTD **9** reveals that the incorporation of strong electron donating group (triphenylamine) decreases the contribution of TPE unit in the HOMO. The LUMO orbitals of BTDs **3–9** are localized on the BTD and phenyl or cyano-phenyl units, which indicate the acceptor nature of BTD and cyano-phenyl units.

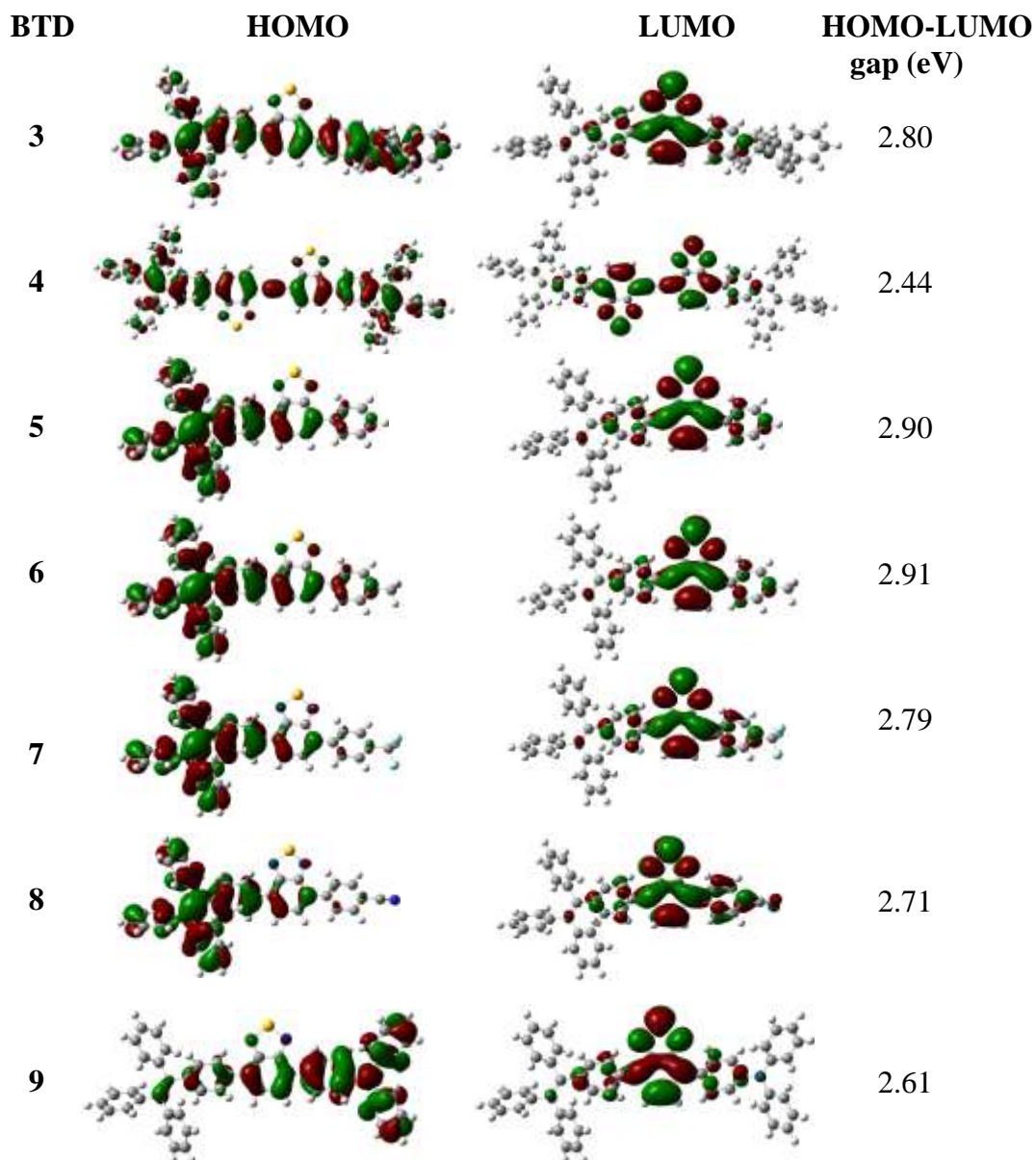


**Figure 6.5.** Frontier molecular orbitals HOMO and LUMO of the BTDs **3–9**.

The energy level diagram of the frontier orbitals are shown in Figure 6.6 which shows; (1) The incorporation of additional BTD unit stabilizes LUMO energy level by keeping HOMO level constant, results in decreased band gap and red shift in absorption spectra of BTD **4**, (2) The 4-(trifluoromethyl)phenyl and cyanophenyl units in unsymmetrical BTDs **7** and **8** stabilizes both HOMO and LUMO energy levels but stabilization of LUMO level is more pronounced compared to HOMO which results in decreased HOMO-LUMO gap, (3) The introduction of strong electron donating moiety destabilizes both the HOMO and LUMO, and extent of destabilization of

HOMO is more pronounced than the LUMO which results in decreased HOMO-LUMO gap in BTD **9**.

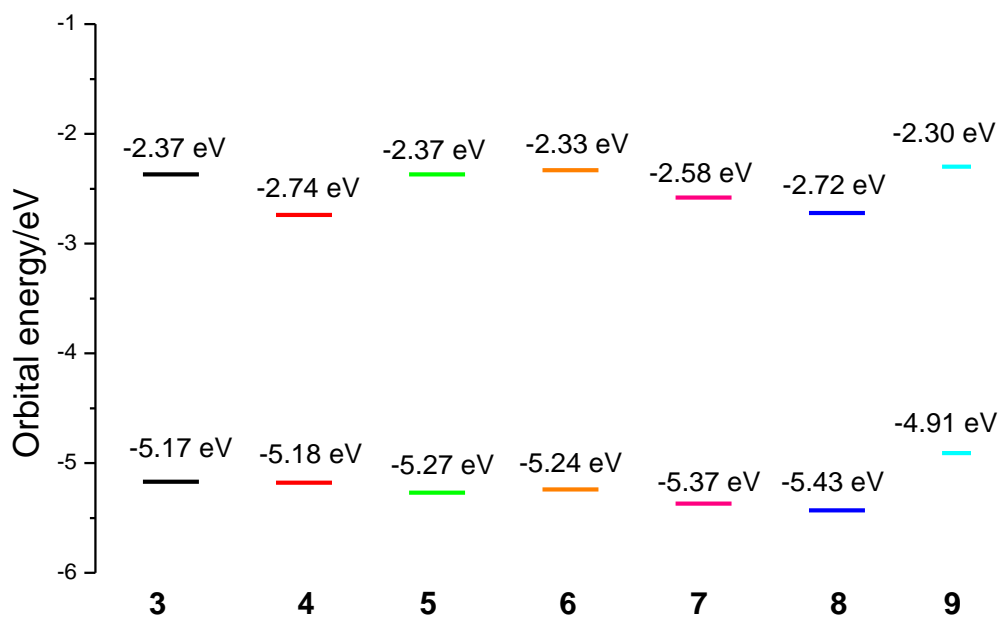


**Figure 6.6.** Correlation diagram showing the HOMO, and LUMO energies of the BTDs **3–9**, as determined at the B3LYP/6-31G(d) level.

### 6.2.5. Photophysical properties

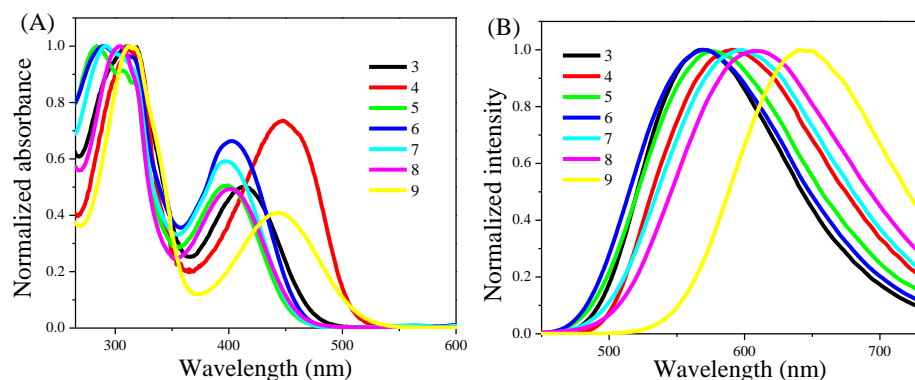


**Figure 6.7.** (A) Normalized absorption spectra and (B) Fluorescence spectra of BTDs **3–9** recorded in dichloromethane.

The UV–vis absorption and fluorescence spectra of BTDs **3–9** were recorded in dichloromethane (Figure 6.7), and the data are summarized in Table 6.2. The BTDs **3–9** exhibit strong absorption band between 260–350 nm

corresponding to  $\pi \rightarrow \pi^*$  transition and another band between 360–460 nm corresponding to charge transfer (CT) transition.<sup>[75]</sup> The BTD **4** shows red shifted CT band due to two strong electron withdrawing BTD units which increases the acceptor strength and results in strong D–A system. The BTD **9** exhibits red shifted absorption followed the BTD **4**, due to strong D–A interaction between TPA and BTD, reflecting the strong electron donating ability of TPA compared to TPE. All the BTDs **3–9** are highly fluorescent with quantum yields ~20%. The fluorescence spectra in dichloromethane (Figure 6.7) show nice tuning of emission ranging from 570 – 645 nm. The trend in the emission maxima follows the order **9** > **8** > **7** > **4** > **5** > **6** ~ **3**.

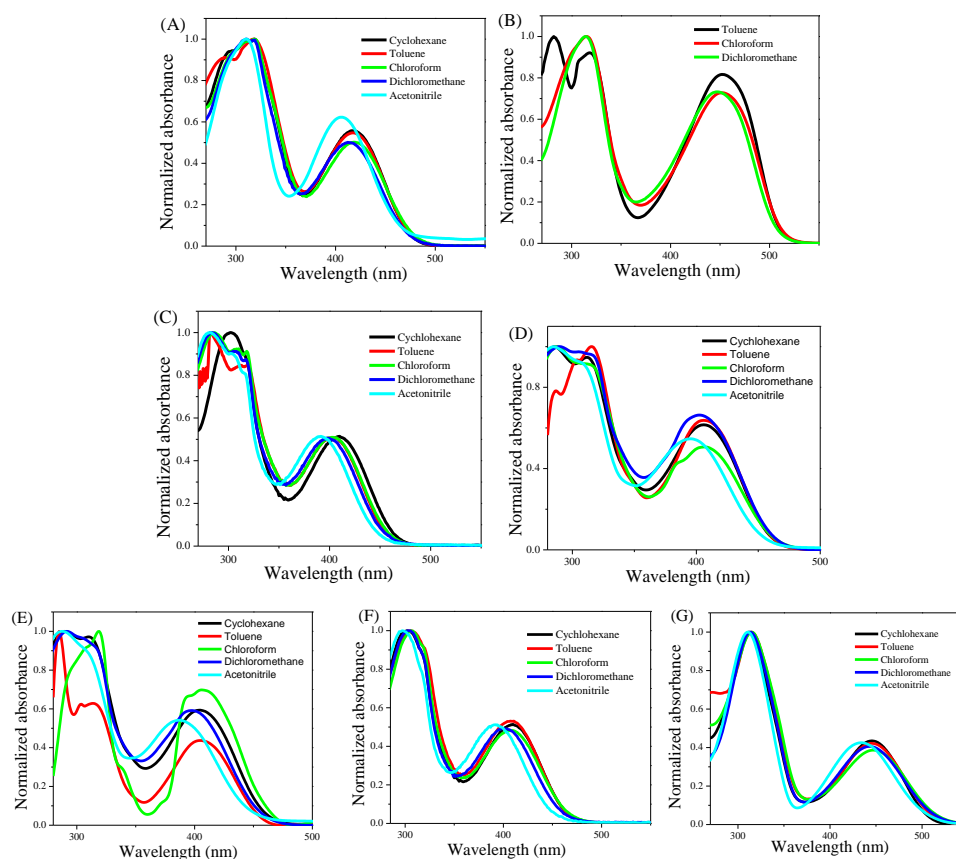


**Figure 6.8.** Normalized absorption spectra of BTDs **3**(A), **4**(B), **5**(C), **6**(D), **7**(E), **8**(F) and **9**(G) in different solvents with different polarities.

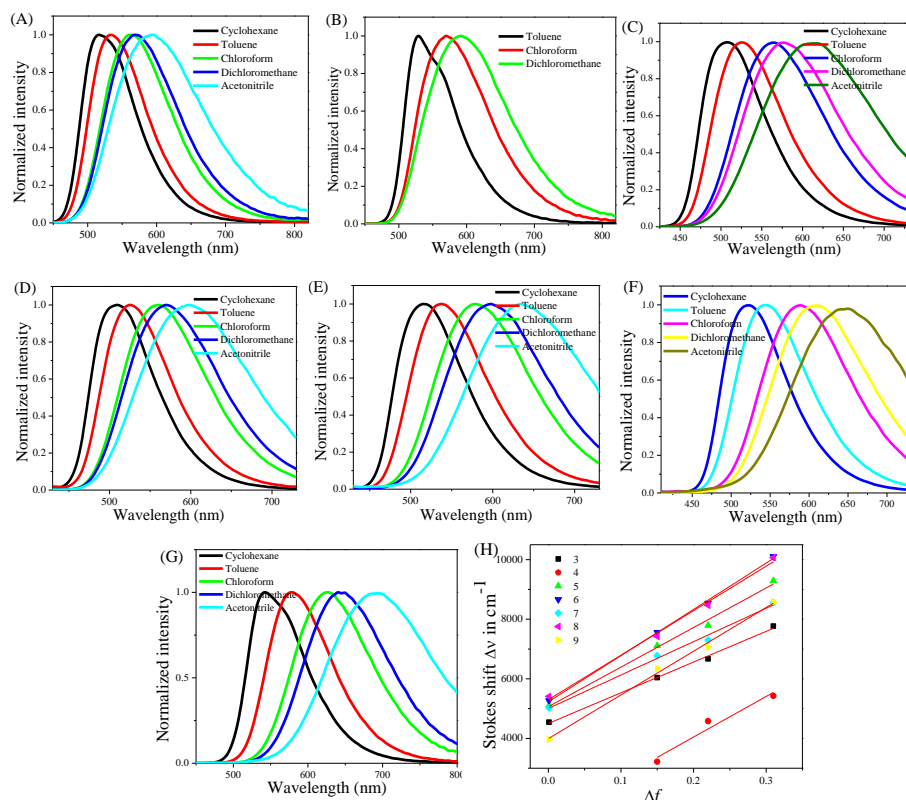


**Figure 6.9.** Photoluminescence spectra of BTDs **3**(A), **4**(B), **5**(C), **6**(D), **7**(E), **8**(F) and **9**(G) in different solvents with different polarities (concentration =  $1 \times 10^{-5}$  M, excitation = 370 nm). (H) Stokes Shift ( $\Delta\nu$ ) of BTDs **3–9** as a function of the solvent polarity parameter ( $\Delta f$ ).

The spectral properties of D–A molecules are highly sensitive towards solvent polarity. In order to study the solvatochromism, solvents of various polarities (cyclohexane, toluene, chloroform, dichloromethane and acetonitrile) were selected, and the absorption and emission spectra were recorded (Figure 6.8 and 6.9). The solvatochromic data are summarized in Table 6.2. The absorption and emission spectra of BTD **4** was not recorded in cyclohexane and acetonitrile due to its insolubility. In polar solvents, the absorption spectra of BTDs **3–9** show slight blue shifted CT band. The fluorescence spectra show large red shift and decreased fluorescence quantum yield with increasing solvent polarity from cyclohexane to acetonitrile, reflecting the larger charge separation and higher dipole moment in the excited state than in the ground state. The solvent dependence of absorption and emission was further confirmed by the Lippert-Mataga plot, which shows a linear correlation of the Stokes shift with solvent polarity (Figure 6.9). The trend in the slope of Lippert-Mataga plot follows the order, **8** > **9** > **7** > **4** > **6** >

**5** > **3** (Table 6.3) which reveals highest sensitivity of unsymmetrical BTD **8** towards solvent polarity.

**Table 6.2.** Photophysical properties of BTDs **3–9** in different solvents.

<b>BTDs</b>	<b>Solvents</b>	$\lambda_{\text{abs.}}(\text{nm})$	$\lambda_{\text{em.}}(\text{nm})$	<b>Stokes Shift(<math>\text{cm}^{-1}</math>)</b>
<b>3</b>	Cyclohexane	418	516	4544
	Toluene	418	534	5197
	Chloroform	419	561	6041
	Dichloromethane	413	570	6670
	Acetonitrile	406	593	7767
<b>4</b>	Toluene	452	529	3220
	Chloroform	452	570	4580
	Dichloromethane	448	592	5430
<b>5</b>	Cyclohexane	406	510	5023
	Toluene	407	526	5559
	Chloroform	406	560	6773
	Dichloromethane	403	571	7300
	Acetonitrile	396	599	8558
<b>6</b>	Cyclohexane	404	517	5410
	Toluene	405	538	6104
	Chloroform	404	579	7420
	Dichloromethane	398	598	8466
	Acetonitrile	387	634	10067
<b>7</b>	Cyclohexane	404	509	5106
	Toluene	403	527	5838
	Chloroform	403	565	7114
	Dichloromethane	399	579	7791
	Acetonitrile	391	614	9289
<b>8</b>	Cyclohexane	410	523	5270
	Toluene	408	545	6161
	Chloroform	408	590	7560
	Dichloromethane	401	610	8544
	Acetonitrile	392	649	10102
<b>9</b>	Cyclohexane	446	542	3971
	Toluene	446	578	5120
	Chloroform	448	626	6347
	Dichloromethane	443	645	7070
	Acetonitrile	434	691	8570

**Table 6.3.** Slopes of Lippert-Mataga plot for the BTDs **3–9**.

<b>BTDs</b>	<b>Slope</b>
<b>3</b>	10298
<b>4</b>	13608
<b>5</b>	10499
<b>6</b>	13268
<b>7</b>	13871
<b>8</b>	15506
<b>9</b>	14664

Generally, the TPE containing molecules are AIE active and are non-fluorescent in solution and highly fluorescent in the aggregated state. However, BTDs **3–9** are highly fluorescent both in solution and in aggregated state. The BTDs **3–9** are highly soluble in THF and poorly soluble in water. The solutions of BTDs **3–9** in different THF and water percentage were prepared to study the AIE. The AIE property of BTDs **3–9** was studied by using fluorescence spectroscopy (Figure 6.10).

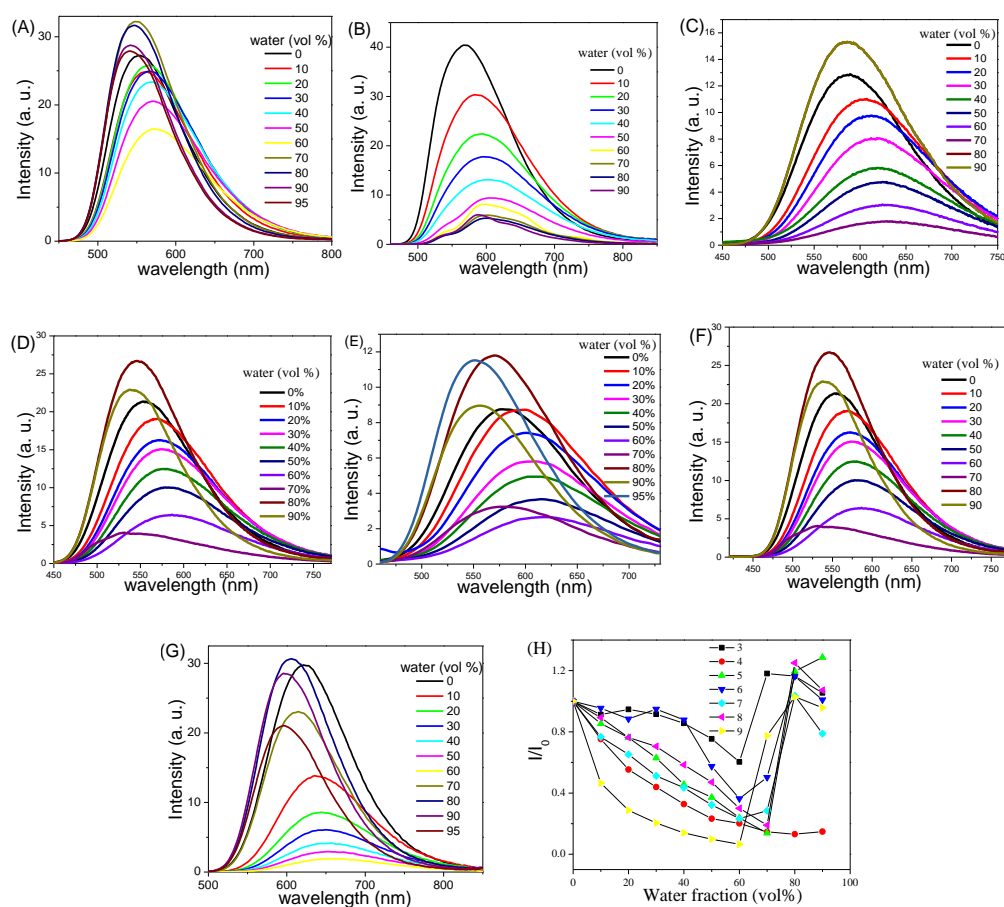


**Figure 6.10.** Fluorescence spectra of BTDs **3**(A), **4**(B), **5**(C), **6**(D), **7**(E), **8**(F) and **9**(G) in THF–Water mixtures with different water fractions (10  $\mu$ M). (H) Plot of fluorescence intensity (PL) vs. % of water fraction ( $f_w$ ). Luminogen concentration: 10  $\mu$ M; intensity calculated at  $\lambda_{\text{max}}$  of BTDs **3–9**.

The BTDs **3–9** show distinct response in different THF and water percentage. The fluorescence spectra of BTDs **3–9** show gradual red shift at low water percentage (<60%) with decrease in fluorescence intensity. This is due to the gradual increase of solvent polarity with increase in water

percentage. At high water percentage (>60%) the emission spectra of BTDs **3**, **5**, **6**, **7**, **8** and **9** show blue shifted emission with enhanced intensity, however the BTD **4** shows decreased emission intensity. The solubility of the BTDs **3–9** decreases at higher water percentage (60–90%) and forms nanoaggregates. In the aggregated form molecular rotation ceases and leads to enhanced emission in BTDs **3**, **5**, **6**, **7**, **8** and **9**. The AIE study reveals that at lower water percentages emission is controlled by solvent polarity, whereas at higher water percentage AIE dominates over solvent polarity. The photograph of the AIE study of representative BTD **9** clearly indicates the solvent polarity and AIE dependent emission behavior (Figure 6.11). The synthesized BTDs **3–9** show tunable solid state emission ranging from 470–600 nm. The solids emit blue, green, orange and orange red color under UV illumination (Figure 6.11).

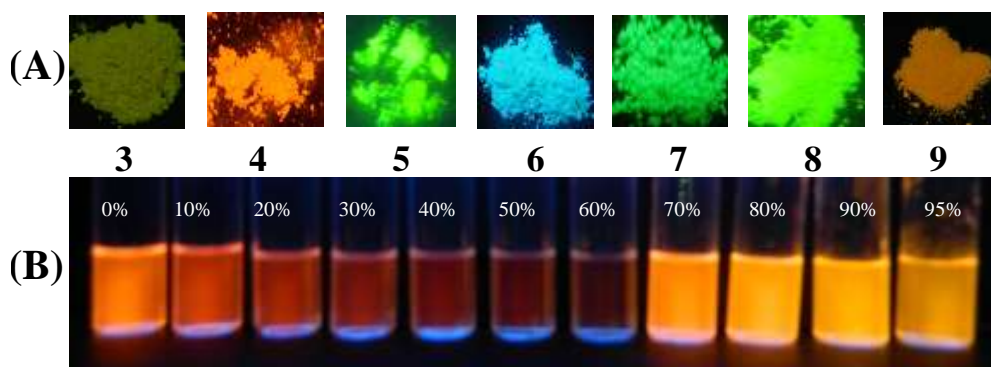


**Figure 6.11.** (A) Photograph of synthesized solid of BTDs **3–9** under 365 nm UV illumination. (B) Photograph of BTD **9** in THF–water mixtures with different water fractions (10  $\mu$ M) under 365 nm UV illumination.

### 6.2.6. Mechanochromic property

The mechanochromic property of the BTDs **3–9** was investigated by emission spectroscopy and their emission behaviors with respect to various stimuli are shown in Figure 6.12, and data are tabulated in Table 6.4. The pristine form of BTDs **3–9** show greenish yellow (522 nm), orange red (598 nm), green (526 nm), blue (471 nm), green (512), green (521 nm) and orange (572 nm) emissions, respectively (Figure 6.12). Upon grinding with the mortar pestle, all the BTDs show different mechanochromic behavior. After grinding, the BTDs **3–9** show lime green (536 nm), orange red (601 nm), green (526), green (534), yellow (547 nm), yellow (565 nm) and orange red (599 nm)

emissions respectively. The BTDs **3–9** exhibit grinding induced spectral shift ( $\Delta\lambda$ ) of 14 nm, -3 nm, 0 nm, 35 nm, 63 nm, 44 nm and 27 nm respectively, which reveals that BTDs **3, 6, 7, 8** and **9** exhibit mechanochromism, whereas mechanochromism was absent in BTDs **4** and **5**.

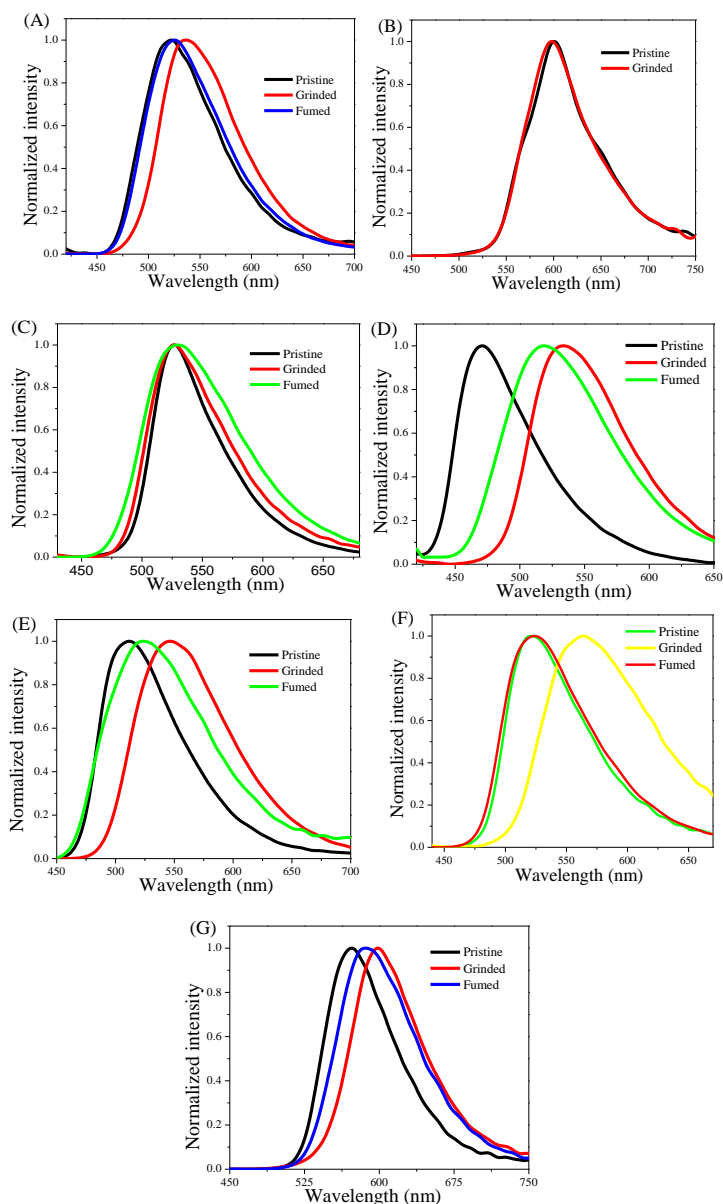


**Figure 6.12.** Emission spectra of **3(A)**, **4(B)**, **5(C)**, **6(D)**, **7(E)**, **8(F)** and **9(G)** as Pristine, Grinded and Fumed solids and photographs taken under 365 nm UV illumination.

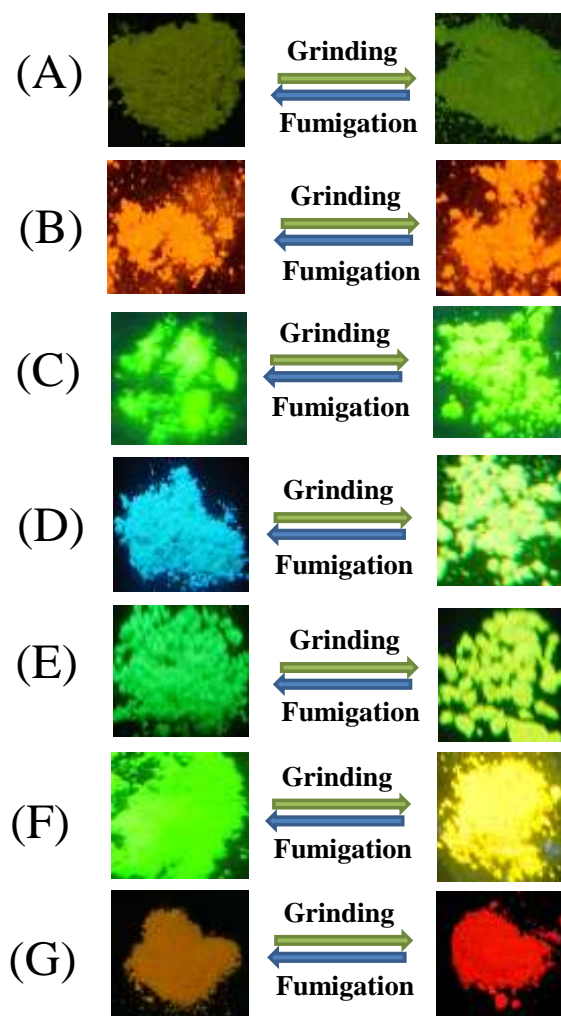


**Figure 6.13.** photograph taken under 365 nm UV illumination of BTDs **3**(A), **4**(B), **5**(C), **6**(D), **7**(E), **8**(F) and **9**(G) as pristine and ground solids.

To know more about conjugation and electronic structure before and after grinding, the BTDs **3–9** were also studied by using absorption spectroscopy (Figure 6.14) and data are tabulated in Table 6.4. The BTDs **3**, **6**, **7**, **8** and **9** show red shifted absorption bands upon grinding which indicate enhanced conjugation or increased D–A interaction. However, after grinding BTDs **4** and **5** does not show any recognizable change in the absorption spectrum (Figure 6.14), reflecting no change in the conjugation. The comparison of absorption and emission properties of BTDs **3–9** reveal that the mechanochromism is due to the increase in effective conjugation and strength of donor–acceptor interaction before and after grinding.

**Table 6.4.** Absorption and emission wavelengths of solid BTDs **3–9** under various external stimuli.

BTDs	Emission			Absorption	
	$\lambda_{\text{Pristine}}$ (nm)	$\lambda_{\text{Grinded}}$ (nm)	$\Delta\lambda$ (nm) <sup>a</sup>	$\lambda_{\text{Pristine}}$ (nm)	$\lambda_{\text{Grinded}}$ (nm)
<b>3</b>	522	536	14	395-475	415-515
<b>4</b>	598	601	-3	400-470	400-470
<b>5</b>	521	521	0	410-495	420-510
<b>6</b>	471	534	63	426-447	416-506
<b>7</b>	512	547	35	433-484	433-487
<b>8</b>	526	565	44	390-515	390-550
<b>9</b>	572	599	27	415-560	450-590

<sup>a</sup> Grinding-induced spectral shift,  $\Delta\lambda = \lambda_{\text{Grinded}} - \lambda_{\text{Pristine}}$ .

The BTDs **5** and **6** have almost similar electronic structures but both exhibit different absorption and emission behavior. The BTD **6** exhibits mechanochromism with 63 nm spectral shift in emission, whereas mechanochromism was absent in BTD **5**. The absorption and emission wavelengths in grinded form are in similar region but in pristine forms they are in different region (Table 6.4) which indicates that the huge difference in the mechanochromism is due to the difference in their pristine forms. The different absorption and emission in the pristine form of BTDs **5** and **6** can be explained with the help of their single crystal structures. The single crystal structure of BTD **5** exhibits almost planar geometry of phenyl, BTD and phenyl ring of TPE whereas BTD **6** shows twisted geometry. The twisted geometry of BTD **6** decreases the conjugation and results blue shift in absorption and emission. After grinding of BTD **6**, there might be possibility to form planar geometry like BTD **5** which result in comparable conjugation and electronic structures which leads to the absorption and emission in similar region.

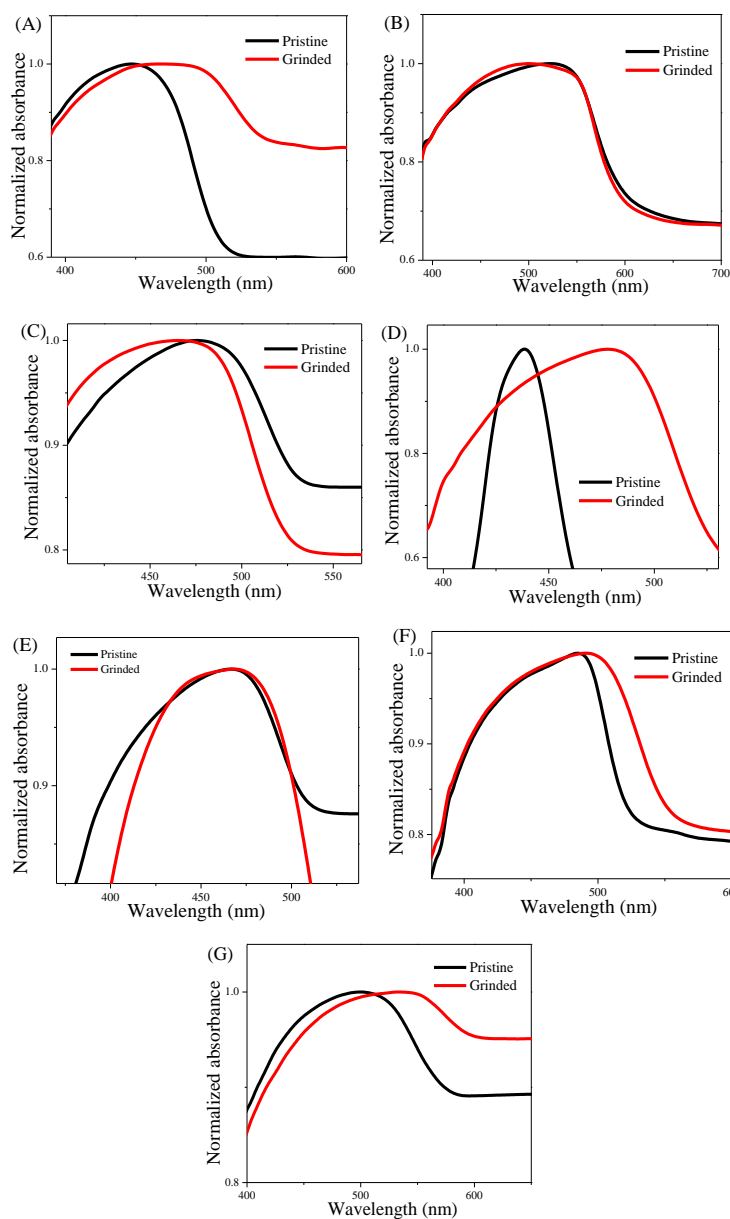


**Figure 6.14.** Absorption spectra of BTDs **3** (A), **4** (B), **5** (C), **6** (D), **7** (E), **8** (F) and **9** (G) as pristine and grinded solids.

The study of mechanochromic property shows the design of unsymmetrically substituted BTDs with D–A–A<sub>1</sub> architecture as the best strategy for developing good mechanochromic materials based on BTD. The crystal structures and photophysical properties of BTDs **5** and **6** reveal the key role of twisting in the molecular backbone for mechanochromism.

To support the planarization caused mechanochromism in BTD **6**, we performed the single point energy calculation at the B3LYP/6-31G(d) level on BTD **5** and BTD **6**. The calculations were carried out by keeping the structural

parameters (like bond lengths, bond angles and dihedral angles) same as their crystal structures. Further the **BTD 6** was taken in same geometry as the crystal structure of **BTD 5**. The main differences in two structures of **BTD 6** are dihedral angles only. We studied the effect of planarity (dihedral angle) on the energy levels of **BTD 6**. The twisted **BTD 6** is denoted as **BTD 6T** and planar **BTD 6** is denoted as **BTD 6P**. The Figure 6.15 shows HOMO and LUMO energy levels of the **BTDs 5, 6T** and **6P**. The comparison of energy levels of **BTD 5** with **BTD 6P** and **BTD 6T** reveals that, the **BTD 6P** shows almost similar energy levels with **BTD 5** whereas in **BTD 6T** the HOMO is stabilized and the LUMO is destabilized. This results in almost equal HOMO-LUMO gap values for **BTD 5** and **BTD 6P** whereas **BTD 6T** have higher HOMO-LUMO gap value. The low HOMO-LUMO gap value for **BTD 6P** than **BTD 6T** supports the planarization induced red shift in absorption and emission of **BTD 6**.

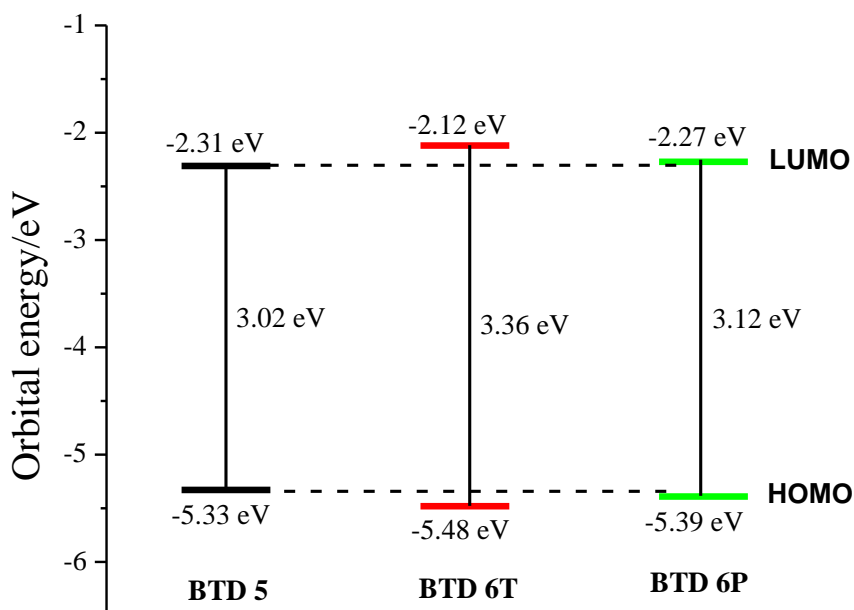


**Figure 6.15.** Correlation diagram showing the HOMO, LUMO and HOMO-LUMO gap energies of **BTD 5**, twisted **BTD 6** (**BTD 6T**) and planar **BTD 6** (**BTD 6P**), determined at the B3LYP/6-31G(d) level.

The reversible nature of mechanochromism was studied by annealing or solvent vapor fumigation. To achieve the original color of grinded **BTDs 3, 6** and **7** required annealing temperatures 220 °C, 205 °C and 205 °C respectively for 30 minutes or fumigation with hexane vapor for 2 minutes.

The BTD **8** required annealing at 80 °C for 5 minutes or fumigation of hexane vapor for 2 minutes. The BTD **7** shows irreversible mechanochromism through annealing, whereas fumigation of hexane vapors for 2 minutes show partial reversibility and emits at 586 nm. The reversibility study reveals excellent reversible mechanochromism in BTD **8** compared to other BTDs.

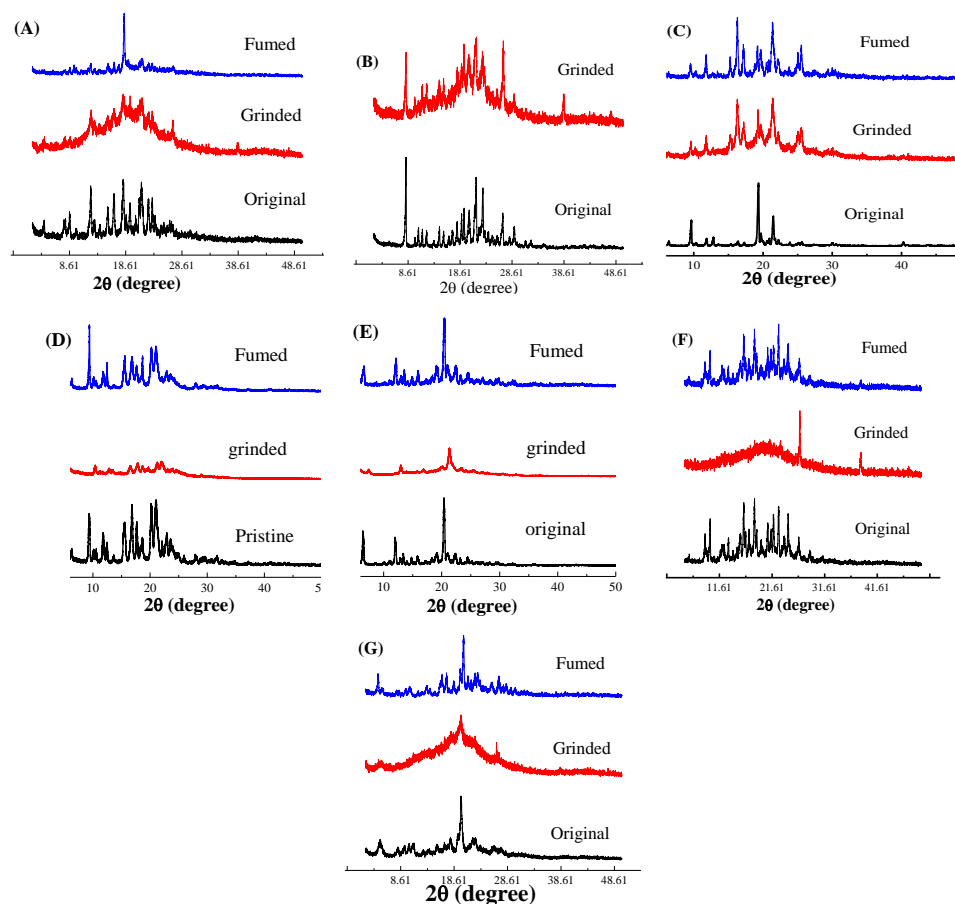


**Figure 6.16.** Powder XRD patterns of BTDs **3** (A), **4** (B), **5** (C), **6** (D), **7** (E), **8** (F) and **9** (G) in the state of as-prepared solid, after grinding and solvent fumigation treatment.

Further, different solid states (pristine, grinded and fumigated) of BTDs **3–9** were studied by powder X-ray diffraction (XRD). The pristine state of BTDs **3–9** exhibit sharp diffraction peaks in XRD, indicating their crystalline nature (Figure 6.16). After grinding BTDs **3**, **6**, **7**, **8** and **9**, the sharp peaks in pristine form disappear and broad diffuse bands were observed which reflects the amorphous nature of solid. The sharp diffraction peaks in BTDs **4** and **5** did not completely vanish. The grinded powder of BTDs **3**, **6**, **7**,

**8** and **9** when fumigated with solvent vapor regains the sharp diffraction peaks, which suggests the amorphous powder restored to its crystallinity after solvent fumigation. The powder XRD studies suggest that the mechanochromism in BTDs **3**, **6**, **7**, **8** and **9** is associated with the morphology change from the crystalline state to the amorphous state and *vice versa*.

### 6.2.7. Vapochromic property

During the synthesis of BTDs **3–9** one interesting phenomenon was observed. The BTDs **3–9** form different colored solids with different solvents. The literature survey reveals that, this phenomenon of changing color on interaction with different solvent vapors or solvents is called vapochromism.<sup>[76,77]</sup> Particularly, in the synthesis of BTD **6** we have observed this phenomenon predominantly, when we dried the solution of BTD **6** in hexane we observed light green solid whereas from dichloromethane solution green solid was obtained. To explore more about this phenomenon, we exposed the solid to different solvents and we observed that the color change is a reversible process. The fluorescence spectra of these two solids show huge difference, light green solid (from hexane/ethanol) emits at 476 nm (blue light) whereas green solid (from DCM) emits at 542 nm (green light). This study inspired us to investigate the vapochromic behavior of all the BTDs, which reveals the different extent of vapochromism in BTDs **3–9**. To study the vapochromic behavior we selected two volatile solvents hexane and dichloromethane. The emission responses of BTDs **3–9** were recorded after exposure with hexane and dichloromethane (Figure 6.17) and the corresponding data is tabulated in Table 6.5. The pristine solids of BTDs **3–9** on exposure to dichloromethane vapors show red shift in the emission wavelengths, further exposing these red shifted solids to hexane vapors once again recovers to the original emission wavelengths. The BTDs **3**, **4**, **5**, **6**, **7**, **8** and **9** exhibit solvent vapor induced spectral shift ( $\Delta\lambda$ ) of 0 nm, 5 nm, 20 nm, 66 nm, 17 nm, 40 nm and 10 nm respectively, which reveals that BTDs **6** and **8** exhibit strong vapochromism. The BTDs **6** and **8** show good naked eye vapochromism under 365 nm UV illumination which is shown in the photograph taken under 365 nm UV illumination (Figure 6.18). The BTDs **6**

and **8** show sky blue (476 nm) and green (528 nm) emission under hexane vapors when excited at 365 nm UV illumination, which upon exposure to DCM vapors show prominent emission color change to green (542 nm) and yellow (564 nm) respectively. The vapochromism results are consistent with the mechanochromism and show same type of emission changes.

**Table 6.5.** Emission wavelengths of solid BTDs **3–9** after exposure to hexane and dichloromethane vapors.

BTDs	Emission ( $\lambda$ nm)		$\Delta\lambda$ (nm) <sup>a</sup>
	Hexane	DCM	
<b>3</b>	517	517	0
<b>4</b>	590	595	5
<b>5</b>	526	546	20
<b>6</b>	476	542	66
<b>7</b>	520	537	17
<b>8</b>	528	568	40
<b>9</b>	570	580	10

<sup>a</sup> Solvent vapor induced spectral shift,  $\Delta\lambda = \lambda_{\text{DCM}} - \lambda_{\text{Hexane}}$ .

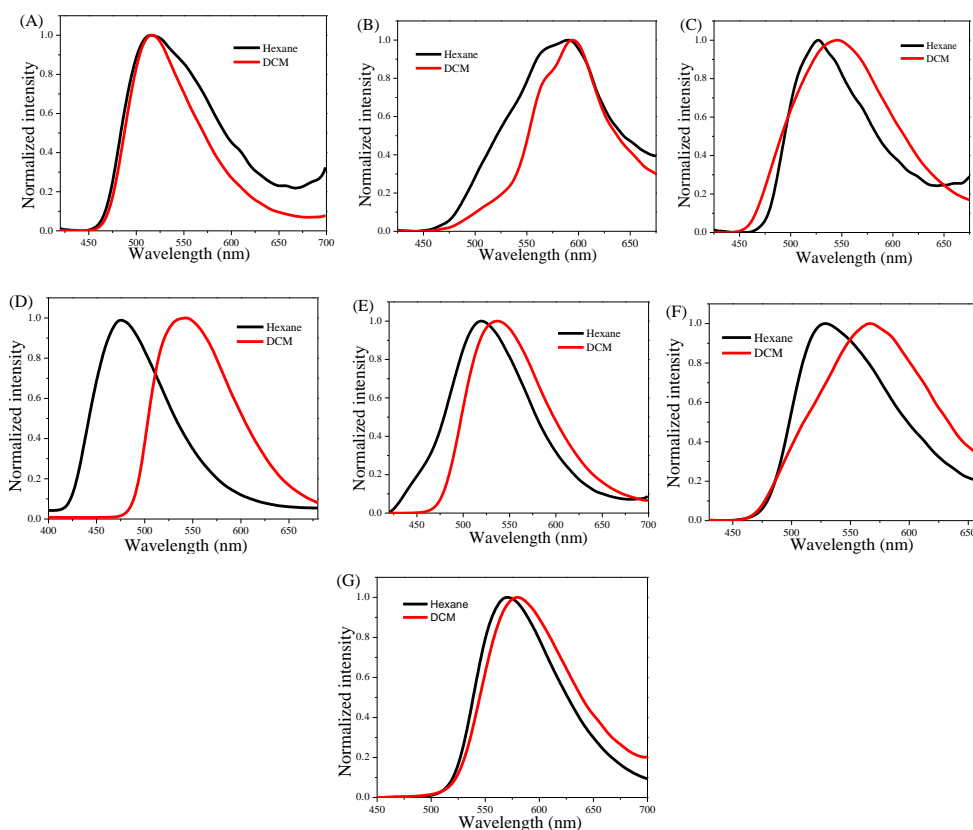


**Figure 6.17.** Emission spectra of BTDs **3** (A), **4** (B), **5** (C), **6** (D), **7** (E), **8** (F) and **9** (G) as solids from Hexane and dichloromethane (DCM).

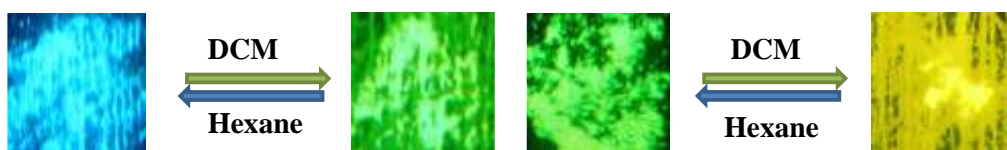


**Figure 6.18.** Photographs of BTD **6** (left) and BTD **8** (right) as solids from Hexane and dichloromethane under 365 nm UV illumination.

To understand more about the vapochromism and its correlation with mechanochromism, we performed the scanning electron microscopy (SEM) and powder X-ray diffraction (PXRD) studies for BTD **6** (Figure 6.19). Two thin films of BTD **6** were prepared on a glass slide by slow evaporation of solution of BTD **6** in hexane and dichloromethane. The morphology and crystalline nature of these thin films were studied by SEM and PXRD studies. The SEM study reveals that the BTD **6** in hexane showed a rod like morphology. On the other hand the sample in DCM did not lead to the formation of any ordered structures. The PXRD study of these two films revealed that the BTD **6** in hexane shows crystalline nature whereas in DCM it shows amorphous nature. The mechanochromic and vapochromic studies of BTD **6** by PXRD show the morphology change from the crystalline state to the amorphous state and *vice versa*. The conversion of crystalline to amorphous is partial in mechanochromism due to non-homogeneous grinding whereas vapochromism shows complete conversion.

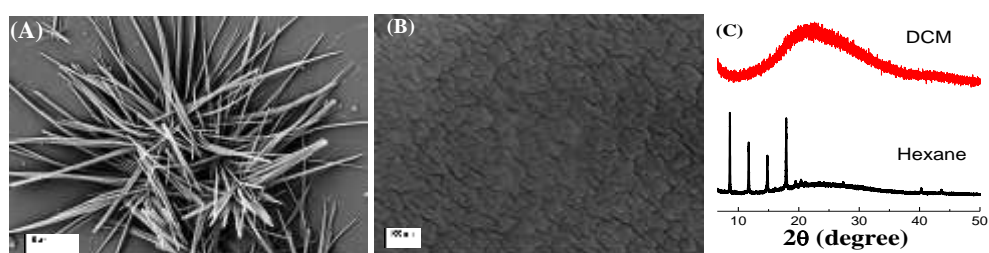


**Figure 6.19.** The SEM of thin films of BTD **6** from (A) Hexane solution and from (B) DCM solution; (C) PXRD graph of thin films of BTD **6** from Hexane solution and DCM.

### 6.3. Experimental section

#### Synthesis and characterization of intermediate 2:

**BTD 2:** Pd(PPh<sub>3</sub>)<sub>4</sub> (0.01 mmol) was added to a well degassed solution of dibromo-BTD (**1**) (0.2 mmol), 4-(1,2,2-triphenylvinyl)phenylboronic acid pinacol ester (0.2 mmol), K<sub>2</sub>CO<sub>3</sub> (0.8 mmol) in a mixture of toluene (32 mL)/ ethanol (4.0 mL)/ H<sub>2</sub>O (4.0 mL). The resulting mixture was stirred at 80 °C for 24 h under argon atmosphere. After cooling, the mixture was evaporated to dryness and the residue subjected to column chromatography on silica (Hexane-DCM 60:40 in vol.) to yield the desired product **2** as yellow powder. Yield: 53.0 %. <sup>1</sup>H NMR (400 MHz, CDCl<sub>3</sub>, 20 °C): δ 7.88 (d, 1H, *J* = 8 Hz), 7.70 (d, 1H, *J* = 8 Hz), 7.55 (d, 1H, *J* = 8 Hz), 7.03-7.19 (m, 17H) ppm; <sup>13</sup>C NMR (100 MHz, CDCl<sub>3</sub>, 20 °C): δ 153.9, 153.0, 144.2, 143.6, 143.5, 143.5, 141.6, 140.3, 134.4, 133.5, 132.2, 131.7, 131.4, 131.3, 131.3, 128.3, 128.0, 127.8, 127.7, 127.6, 126.6, 126.5, 126.5, 112.8, 0.0 ppm; HRMS (ESI): calcd. for C<sub>32</sub>H<sub>21</sub>BrN<sub>2</sub>S: 545.0682 (M+H)<sup>+</sup>, found: 545.0653.

#### Synthesis and characterization of BTD 4:

**BTD 4:** Pd(PPh<sub>3</sub>)<sub>4</sub> (0.01 mmol) and Bis(tributylstannyl)acetylene (0.4 mmol) was added to a well degassed solution of **2** (0.8 mmol) in toluene (25 mL). The resulting mixture was stirred at 80 °C for 24 h under argon atmosphere. After cooling, the mixture was evaporated to dryness and the residue subjected to column chromatography on silica (Hexane-DCM 30:70 in vol.) to yield the desired product **4** as orange red powder. Yield: 36.0 %; mp: above 250 °C. <sup>1</sup>H NMR (400 MHz, CDCl<sub>3</sub>, 20 °C): δ 8.01 (d, 2H, *J* = 8 Hz), 7.81 (d, 4H, *J* = 8 Hz), 7.73 (d, 2H, *J* = 8 Hz), 7.21 (d, 4H, *J* = 8 Hz), 7.05-7.13 (m, 30H) ppm; HRMS (ESI): calcd. for C<sub>66</sub>H<sub>42</sub>N<sub>4</sub>S<sub>2</sub>: 977.2743 (M+Na)<sup>+</sup>, found: 977.2766.

#### Synthesis and characterization of BTDs 5-9:

**BTD 5:** Pd(PPh<sub>3</sub>)<sub>4</sub> (0.005 mmol) was added to a well degassed solution of **2** (0.1 mmol), phenylboronic acid (0.12 mmol), K<sub>2</sub>CO<sub>3</sub> (0.4 mmol) in a mixture of toluene (20 mL)/ ethanol (4.0 mL)/ H<sub>2</sub>O (4.0 mL). The resulting mixture was stirred at 80 °C for 24 h under argon atmosphere. After cooling, the mixture was evaporated to dryness and the residue subjected to column chromatography on silica (Hexane-DCM 85:15 in vol.) to yield the desired product **5** as greenish yellow powder. Yield: 75.0 %; mp: 213-215 °C. <sup>1</sup>H NMR (400 MHz, CDCl<sub>3</sub>, 20 °C): δ 7.95 (d, 2H, *J* = 8 Hz), 7.74-7.79 (m, 4H),

7.55 (t, 2H,  $J=8$  Hz), 7.46 (t, 1H,  $J=8$  Hz), 7.05-7.21 (m, 17H) ppm;  $^{13}\text{C}$  NMR (100 MHz,  $\text{CDCl}_3$ , 20 °C):  $\delta$  154.2, 153.9, 143.8, 143.7, 143.6, 143.6, 141.5, 140.5, 137.4, 135.2, 133.1, 132.8, 131.6, 131.5, 131.4, 131.3, 129.2, 128.6, 128.4, 128.3, 128.1, 127.9, 127.8, 127.7, 127.6, 126.6, 126.5, 126.5, 0.0 ppm; HRMS (ESI): calcd. for  $\text{C}_{38}\text{H}_{26}\text{N}_2\text{S}$ : 565.1733 ( $\text{M}+\text{Na}$ ) $^+$ , found 565.1709.

**BTD 6:**  $\text{Pd}(\text{PPh}_3)_4$  (0.005 mmol) was added to a well degassed solution of **2** (0.1 mmol), *p*-tolylboronic acid (0.12 mmol),  $\text{K}_2\text{CO}_3$  (0.4 mmol) in a mixture of toluene (20 mL)/ ethanol (4.0 mL)/  $\text{H}_2\text{O}$  (4.0 mL). The resulting mixture was stirred at 80 °C for 24 h under argon atmosphere. After cooling, the mixture was evaporated to dryness and the residue subjected to column chromatography on silica (Hexane-DCM 80:20 in vol.) to yield the desired product **6** as light green powder. Yield: 79.0 %; mp: 213-215 °C.  $^1\text{H}$  NMR (400 MHz,  $\text{CDCl}_3$ , 20 °C):  $\delta$  7.85 (d, 2H,  $J=8$  Hz), 7.72-7.79 (m, 4H), 7.35 (d, 2H,  $J=8$  Hz), 7.05-7.21 (m, 17H), 2.45 (s, 3H) ppm;  $^{13}\text{C}$  NMR (100 MHz,  $\text{CDCl}_3$ , 20 °C):  $\delta$  154.2, 153.9, 143.7, 143.7, 143.6, 141.5, 140.5, 138.3, 135.3, 134.6, 133.2, 132.5, 131.6, 131.5, 131.4, 129.3, 129.1, 128.3, 127.9, 127.8, 127.7, 127.6, 126.6, 126.5, 126.5, 21.3, 0.0 ppm; HRMS (ESI): calcd. for  $\text{C}_{39}\text{H}_{28}\text{N}_2\text{S}$ : 557.2046 ( $\text{M}+\text{H}$ ) $^+$ , found 557.2097.

**BTD 7:**  $\text{Pd}(\text{PPh}_3)_4$  (0.005 mmol) was added to a well degassed solution of **2** (0.1 mmol), (4-(trifluoromethyl)phenyl)boronic acid (0.12 mmol),  $\text{K}_2\text{CO}_3$  (0.4 mmol) in a mixture of toluene (20 mL)/ ethanol (4.0 mL)/  $\text{H}_2\text{O}$  (4.0 mL). The resulting mixture was stirred at 80 °C for 24 h under argon atmosphere. After cooling, the mixture was evaporated to dryness and the residue subjected to column chromatography on silica (Hexane-DCM 80:20 in vol.) to yield the desired product **7** as green powder. Yield: 81.0 %; mp: 216-215 °C.  $^1\text{H}$  NMR (400 MHz,  $\text{CDCl}_3$ , 20 °C):  $\delta$  8.08 (d, 2H,  $J=8$  Hz), 7.78-7.81 (m, 6H), 7.21 (d, 2H,  $J=8$  Hz), 7.05-7.13 (m, 15H) ppm;  $^{13}\text{C}$  NMR (100 MHz,  $\text{CDCl}_3$ , 20 °C):  $\delta$  153.9, 153.9, 144.1, 143.7, 143.6, 143.6, 141.6, 140.9, 140.4, 134.9, 133.9, 131.7, 131.4, 131.4, 131.3, 129.5, 128.6, 128.4, 127.8, 127.7, 127.7, 127.6, 126.6, 126.5, 126.5, 125.5, 125.5, 0.0 ppm; HRMS (ESI): calcd. for  $\text{C}_{39}\text{H}_{25}\text{F}_3\text{N}_2\text{S}$ : 633.1583 ( $\text{M}+\text{Na}$ ) $^+$ , found 633.1571.

**BTD 8:**  $\text{Pd}(\text{PPh}_3)_4$  (0.005 mmol) was added to a well degassed solution of **2** (0.1 mmol), 4-cyanophenylboronic acid pinacol ester (0.12 mmol),  $\text{K}_2\text{CO}_3$  (0.4 mmol) in a mixture of toluene (20 mL)/ ethanol (4.0 mL)/  $\text{H}_2\text{O}$  (4.0 mL). The

resulting mixture was stirred at 80 °C for 24 h under argon atmosphere. After cooling, the mixture was evaporated to dryness and the residue subjected to column chromatography on silica (Hexane-DCM 50:50 in vol.) to yield the desired product **8** as greenish yellow powder. Yield: 55.0 %; mp: 165-168 °C. <sup>1</sup>H NMR (400 MHz, CDCl<sub>3</sub>, 20 °C): δ 8.10 (d, 2H, *J* = 8 Hz), 7.77-7.84 (m, 6H), 7.21 (d, 2H, *J* = 8 Hz), 7.05-7.13 (m, 15H) ppm; <sup>13</sup>C NMR (100 MHz, CDCl<sub>3</sub>, 20 °C): δ 153.9, 153.6, 144.3, 143.6, 143.5, 141.8, 141.6, 140.3, 134.7, 134.3, 132.3, 131.7, 131.4, 131.4, 131.3, 130.7, 129.8, 128.8, 128.4, 127.7, 127.6, 126.6, 126.5, 126.5, 118.8, 111.7, 58.5, 0.0 ppm; HRMS (ESI): calcd. for C<sub>39</sub>H<sub>25</sub>N<sub>3</sub>S: 590.1661 (M+Na)<sup>+</sup>, found 590.1662.

**BTD 9:** Pd(PPh<sub>3</sub>)<sub>4</sub> (0.005 mmol) was added to a well degassed solution of **2** (0.1 mmol), 4-(diphenylamino)phenylboronic acid pinacol ester (0.12 mmol), K<sub>2</sub>CO<sub>3</sub> (0.4 mmol) in a mixture of toluene (20 mL)/ ethanol (4.0 mL)/ H<sub>2</sub>O (4.0 mL). The resulting mixture was stirred at 80 °C for 24 h under argon atmosphere. After cooling, the mixture was evaporated to dryness and the residue subjected to column chromatography on silica (Hexane-DCM 50:50 in vol.) to yield the desired product **9** as orange powder. Yield: 61.0 %; mp: 171-174 °C. <sup>1</sup>H NMR (400 MHz, CDCl<sub>3</sub>, 20 °C): δ 7.87 (d, 2H, *J* = 8 Hz), 7.71-7.79 (m, 4H), 7.29 (t, 4H, *J* = 8 Hz), 7.05-7.22 (m, 25H) ppm; <sup>13</sup>C NMR (100 MHz, CDCl<sub>3</sub>, 20 °C): δ 148.0, 147.5, 143.7, 143.7, 141.4, 140.5, 135.3, 132.6, 132.1, 131.6, 131.5, 131.4, 130.9, 129.9, 129.3, 128.3, 128.0, 127.8, 127.7, 127.6, 127.3, 126.6, 126.5, 126.4, 124.9, 123.3, 122.9, 0.0 ppm; HRMS (ESI): calcd. for C<sub>50</sub>H<sub>35</sub>N<sub>3</sub>S: 709.2546 (M+H)<sup>+</sup>, found 709.2542.

#### 6.4. Conclusion

In conclusion, we have synthesized thermally stable tetraphenylethylene substituted benzothiadiazoles **3–9** with varying D–A interaction. The solution and solid-state optical properties of BTDs **3–9** were modulated *via* D/A substituents and the arrangement of the substituents. The BTDs **3–9** exhibit tunable fluorescence in both solution and solid state from blue to red color. The BTDs **3–9** show strong solvatochromism and the BTD **8** shows highest solvent dependent emission. The AIE study reveals that at low water percentages emission was controlled by solvent polarity and show red shift

with decrease in intensity, whereas at high water percentages AIE dominates over solvent polarity and shows enhanced emission.

The BTDs **3**, **6**, **7**, **8** and **9** exhibit reversible mechanochromism and vapochromism whereas mechanochromism and vapochromism were absent in the BTDs **4** and **5**. Particularly, the BTDs **6** and **8** show stimuli responses with good color contrast from blue to green and green to yellow with spectral shift ( $\Delta\lambda$ ) of 63 nm and 44 nm, respectively. The solid state absorption of pristine and grinded forms of BTDs **3–9** reveal enhanced conjugation or/and increased D–A interaction is origin of the mechanochromism. The crystal structure and theoretical study of BTD **6** reveals that the conversion of twisted to planar structure is accountable for good color contrast mechanochromism. The powder x-ray diffraction (PXRD) study reveals that the morphological change between thermodynamically stable crystalline phase to the metastable amorphous state and *vice versa* is associated with mechanochromism and vapochromism. The study reveals the important role of twisting in the molecular backbone, nature of substituent and way of substitution in deciding the photophysical and stimuli responsive properties of TPE substituted BTDs. The best strategies for developing good stimuli responsive materials are the use of unsymmetrically substituted BTDs with D–A–A<sub>1</sub> architecture and twisted molecular architecture. The results presented here will be helpful in designing new BTD based stimuli responsive smart materials.

**Note:** This is copyrighted material from American Chemical Society, *J. Phys. Chem. C*, 2016, 120, 24030–24040 (DOI: 10.1021/acs.jpcc.6b09015) and Royal Society of Chemistry, *J. Mater. Chem. C*, 2015, 3, 9063–9068 (DOI: 10.1039/C5TC01871D).

## 6.5. References

- [1] Forrest S R. (2003), The road to high efficiency organic light emitting devices, *Org. Electron.*, 4, 45–8 (DOI: 10.1016/j.orgel.2003.08.014).
- [2] Farinola G M., Ragni R. (2011), Electroluminescent materials for white organic light emitting diodes., *Chem. Soc. Rev.*, 40, 3467–82

- (DOI: 10.1039/c0cs00204f).
- [3] Saragi T. P. I., Spehr T., Siebert A., Fuhrmann-Lieker T., Salbeck J. (2007), Spiro Compounds for Organic Optoelectronics, *Chem. Rev.*, 107, 1011–1065 (DOI: 10.1021/CR0501341).
- [4] Duan L., Qiao J., Sun Y., Qiu Y. (2011), Strategies to Design Bipolar Small Molecules for OLEDs: Donor-Acceptor Structure and Non-Donor-Acceptor Structure, *Adv. Mater.*, 23, 1137–44 (DOI: 10.1002/adma.201003816).
- [5] Zhu M., Yang C., Tang C W., VanSlyke S A., Kamtekar K T., Monkman A P., Bryce M R., Farinola G M., Ragni R., Chi Y., et al. (2013), Blue fluorescent emitters: design tactics and applications in organic light-emitting diodes, *Chem. Soc. Rev.*, 42, 4963 (DOI: 10.1039/c3cs35440g).
- [6] Sheats., Antoniadis., Hueschen., Leonard., Miller., Moon., Roitman. and Stocking. (1996), Organic Electroluminescent Devices, *Science*, 273, 884–8.
- [7] Sun H., Liu S., Lin W., Zhang K Y., Lv W., Huang X., Huo F., Yang H., Jenkins G., Zhao Q., et al. (2014), Smart responsive phosphorescent materials for data recording and security protection., *Nat. Commun.*, 5, 3601 (DOI: 10.1038/ncomms4601).
- [8] Woodall C H., Beavers C M., Christensen J., Hatcher L E., Intissar M., Parlett A., Teat S J., Reber C., Raithby P R. (2013), Hingeless Negative Linear Compression in the Mechanochromic Gold Complex [(C<sub>6</sub>F<sub>5</sub>Au)<sub>2</sub>(μ-1,4-diisocyanobenzene)], *Angew. Chemie*, 125, 9873–6 (DOI: 10.1002/ange.201302825).
- [9] Dong Y., Xu B., Zhang J., Tan X., Wang L., Chen J., Lv H., Wen S., Li B., Ye L., et al. (2012), Piezochromic Luminescence Based on the Molecular Aggregation of 9,10-Bis(( E ))-2-(pyrid-2-yl)vinyl)anthracene, *Angew. Chemie*, 124, 10940–3 (DOI: 10.1002/ange.201204660).
- [10] Kim H-J., Whang D R., Gierschner J., Lee C H., Park S Y. (2015), High-Contrast Red-Green-Blue Tricolor Fluorescence Switching in Bicomponent Molecular Film, *Angew. Chemie*, 127, 4404–7 (DOI: 10.1002/ange.201411568).

- [11] Sagara Y., Kato T. (2008), Stimuli-Responsive Luminescent Liquid Crystals: Change of Photoluminescent Colors Triggered by a Shear-Induced Phase Transition, *Angew. Chemie*, 120, 5253–6 (DOI: 10.1002/ange.200800164).
- [12] Krikorian M., Liu S., Swager T M. (2014), Columnar Liquid Crystallinity and Mechanochromism in Cationic Platinum(II) Complexes, *J. Am. Chem. Soc.*, 136, 2952–5 (DOI: 10.1021/ja4114352).
- [13] Larsen M B., Boydston A J. (2013), “Flex-Activated” Mechanophores: Using Polymer Mechanochemistry To Direct Bond Bending Activation, *J. Am. Chem. Soc.*, 135, 8189–92 (DOI: 10.1021/ja403757p).
- [14] Sagara Y., Kato T. (2009), Mechanically induced luminescence changes in molecular assemblies, *Nat. Chem.*, 1, 605–10 (DOI: 10.1038/nchem.411).
- [15] Ning Z., Chen Z., Zhang Q., Yan Y., Qian S., Cao Y., Tian H. (2007), Aggregation-induced Emission (AIE)-active Starburst Triarylamine Fluorophores as Potential Non-doped Red Emitters for Organic Light-emitting Diodes and Cl<sub>2</sub> Gas Chemodosimeter, *Adv. Funct. Mater.*, 17, 3799–807 (DOI: 10.1002/adfm.200700649).
- [16] Kwon M S., Gierschner J., Yoon S-J., Park S Y. (2012), Unique Piezochromic Fluorescence Behavior of Dicyanodistyrylbenzene Based Donor-Acceptor-Donor Triad: Mechanically Controlled Photo-Induced Electron Transfer (eT) in Molecular Assemblies, *Adv. Mater.*, 24, 5487–92 (DOI: 10.1002/adma.201202409).
- [17] Birks, J. B. *Photophysics of Aromatic Molecules*; Wiley: London, U.K., **1970**
- [18] Förster T., Kasper K. (1954), Ein Konzentrationsumschlag der Fluoreszenz., *Zeitschrift für Phys. Chemie*, 1, 275–7 (DOI: 10.1524/zpch.1954.1.5\_6.275).
- [19] Jayanty S., Radhakrishnan T P. (2004), Enhanced Fluorescence of Remote Functionalized Diaminodicyanoquinodimethanes in the Solid State and Fluorescence Switching in a Doped Polymer by Solvent Vapors, *Chem. - A Eur. J.*, 10, 791–7 (DOI: 10.1002/chem.200305123).
- [20] Malkin, J. *Photophysical and Photochemical Properties of Aromatic*

- Compounds*; CRC: Boca Raton, FL, **1992**.
- [21] Henry J. T., Jerome L. M., Wim T. K., James A. M., Judith H., Scott W., Isaac R., Watts K., (2005), Enhanced Photoluminescence from Group 14 Metalloles in Aggregated and Solid Solutions, *Inorg. Chem.*, 44, 2003–2011 (DOI: 10.1021/IC049034O).
- [22] Dong Y., Lam J W Y., Qin A., Liu J., Li Z., Tang B Z., Sun J., Kwok H S. (2007), Aggregation-induced emissions of tetraphenylethene derivatives and their utilities as chemical vapor sensors and in organic light-emitting diodes, *Appl. Phys. Lett.*, 91, 11111 (DOI: 10.1063/1.2753723).
- [23] Huang J., Yang X., Wang J., Zhong C., Wang L., Qin J., Li Z. (2012), New tetraphenylethene-based efficient blue luminophors: aggregation induced emission and partially controllable emitting color, *J. Mater. Chem.*, 22, 2478–84 (DOI: 10.1039/C1JM14054J).
- [24] Zhao N., Yang Z., Lam J W Y., Sung H H Y., Xie N., Chen S., Su H., Gao M., Williams I D., Wong K S., et al. (2012), Benzothiazolium-functionalized tetraphenylethene: an AIE luminogen with tunable solid-state emission, *Chem. Commun.*, 48, 8637 (DOI: 10.1039/c2cc33780k).
- [25] Wang J., Mei J., Hu R., Sun J Z., Qin A., Tang B Z. (2012), Click Synthesis, Aggregation-Induced Emission, *E / Z* Isomerization, Self-Organization, and Multiple Chromisms of Pure Stereoisomers of a Tetraphenylethene-Cored Luminogen, *J. Am. Chem. Soc.*, 134, 9956–66 (DOI: 10.1021/ja208883h).
- [26] Zhao N., Li M., Yan Y., Lam J W Y., Zhang Y L., Zhao Y S., Wong K S., Tang B Z. (2013), A tetraphenylethene-substituted pyridinium salt with multiple functionalities: synthesis, stimuli-responsive emission, optical waveguide and specific mitochondrion imaging, *J. Mater. Chem. C*, 1, 4640 (DOI: 10.1039/c3tc30759j).
- [27] Xu B., Xie M., He J., Xu B., Chi Z., Tian W., Jiang L., Zhao F., Liu S., Zhang Y., et al. (2013), An aggregation-induced emission luminophore with multi-stimuli single- and two-photon fluorescence switching and large two-photon absorption cross section, *Chem. Commun.*, 49, 273–5 (DOI: 10.1039/C2CC36806D).
- [28] Xu B., Chi Z., Zhang X., Li H., Chen C., Liu S., Zhang Y., Xu J.

- (2011), A new ligand and its complex with multi-stimuli-responsive and aggregation-induced emission effects, *Chem. Commun.*, 47, 11080 (DOI: 10.1039/c1cc13790e).
- [29] Lin Y., Chen G., Zhao L., Yuan W Z., Zhang Y., Tang B Z. (2015), Diethylamino functionalized tetraphenylethenes: structural and electronic modulation of photophysical properties, implication for the CIE mechanism and application to cell imaging, *J. Mater. Chem. C*, 3, 112–20 (DOI: 10.1039/C4TC02161D).
- [30] Luo J., Xie Z., Lam J W Y., Cheng L., Tang B Z., Chen H., Qiu C., Kwok H S., Zhan X., Liu Y., et al. (2001), Aggregation-induced emission of 1-methyl-1,2,3,4,5-pentaphenylsilole, *Chem. Commun.*, 397, 1740–1 (DOI: 10.1039/b105159h).
- [31] Wang J-L., Xiao Q., Pei J. (2010), Benzothiadiazole-Based D- $\pi$ -A- $\pi$ -D Organic Dyes with Tunable Band Gap: Synthesis and Photophysical Properties, *Org. Lett.*, 12, 4164–7 (DOI: 10.1021/ol101754q).
- [32] Zhang H., Wan X., Xue X., Li Y., Yu A. and Chen Y. (2010), Selective Tuning of the HOMO-LUMO Gap of Carbazole-Based Donor-Acceptor-Donor Compounds toward Different Emission Colors, *European J. Org. Chem.*, 2010, 1681–7 (DOI: 10.1002/ejoc.200901167).
- [33] Bureš F., Schweizer W B., May J C., Boudon C., Gisselbrecht J-P., Gross M., Biaggio I., Diederich F. (2007), Property Tuning in Charge-Transfer Chromophores by Systematic Modulation of the Spacer between Donor and Acceptor, *Chem. - A Eur. J.*, 13, 5378–87 (DOI: 10.1002/chem.200601735).
- [34] Misra R., Gautam P. and Mobin S M. (2013), Aryl-Substituted Unsymmetrical Benzothiadiazoles: Synthesis, Structure, and Properties, *J. Org. Chem.*, 78, 12440–52 (DOI: 10.1021/jo402111q).
- [35] Guo Z-H., Jin Z-X., Wang J-Y., Pei J. (2014), A donor–acceptor–donor conjugated molecule: twist intramolecular charge transfer and piezochromic luminescent properties, *Chem. Commun.*, 50, 6088 (DOI: 10.1039/c3cc48980a).
- [36] Wei J., Liang B., Cheng X., Zhang Z., Zhang H., Wang Y. (2015), High-contrast and reversible mechanochromic luminescence of a D- $\pi$ -

- A compound with a twisted molecular conformation, *RSC Adv.*, 5, 71903–10 (DOI: 10.1039/C5RA12050K).
- [37] Qi Q., Qian J., Tan X., Zhang J., Wang L., Xu B., Zou B., Tian W. (2015), Remarkable Turn-On and Color-Tuned Piezochromic Luminescence: Mechanically Switching Intramolecular Charge Transfer in Molecular Crystals, *Adv. Funct. Mater.*, 25, 4005–10 (DOI: 10.1002/adfm.201501224).
- [38] Shen X Y., Wang Y J., Zhao E., Yuan W Z., Liu Y., Lu P., Qin A., Ma Y., Sun J Z., Tang B Z. (2013), Effects of Substitution with Donor–Acceptor Groups on the Properties of Tetraphenylethene Trimer: Aggregation-Induced Emission, Solvatochromism, and Mechanochromism, *J. Phys. Chem. C*, 117, 7334–47 (DOI: 10.1021/jp311360p).
- [39] Zhang X., Chi Z., Xu B., Chen C., Zhou X., Zhang Y., Liu S., Xu J. (2012), End-group effects of piezofluorochromic aggregation-induced enhanced emission compounds containing distyrylanthracene, *J. Mater. Chem.*, 22, 18505–18513 (DOI: 10.1039/c2jm33140c).
- [40] Xue S., Liu W., Qiu X., Gao Y. Yang W. (2014), Remarkable Isomeric Effects on Optical and Optoelectronic Properties of *N* - Phenylcarbazole-Capped 9,10-Divinylanthracenes, *J. Phys. Chem. C*, 118, 18668–75 (DOI: 10.1021/jp505527f).
- [41] Sun J., Dai Y., Ouyang M., Zhang Y., Zhan L., Zhang C. (2015), Unique torsional cruciform  $\pi$ -architectures composed of donor and acceptor axes exhibiting mechanochromic and electrochromic properties, *J. Mater. Chem. C*, 3, 3356–63 (DOI: 10.1039/C4TC02046D).
- [42] Gong Y., Tan Y., Liu J., Lu P., Feng C., Yuan W Z., Lu Y., Sun J Z., He G., Zhang Y. (2013), Twisted D– $\pi$ –A solid emitters: efficient emission and high contrast mechanochromism, *Chem. Commun.*, 49, 4009 (DOI: 10.1039/c3cc39243k).
- [43] Zhang X., Chi Z., Xu B., Jiang L., Zhou X., Zhang Y., Liu S., Xu J. (2012), Multifunctional organic fluorescent materials derived from 9,10-distyrylanthracene with alkoxy endgroups of various lengths, *Chem. Commun.*, 48, 10895 (DOI: 10.1039/c2cc36263e).

- [44] Sase M., Yamaguchi S., Sagara Y., Yoshikawa I., Mutai T., Araki K. (2011), Piezochromic luminescence of amide and ester derivatives of tetraphenylpyrene—role of amide hydrogen bonds in sensitive piezochromic response, *J. Mater. Chem.*, 21, 8347 (DOI: 10.1039/c0jm03950k).
- [45] Kunzelman J., Kinami M., Crenshaw B R., Protasiewicz J D., Weder C. (2008), Oligo(p-phenylene vinylene)s as a “New” Class of Piezochromic Fluorophores, *Adv. Mater.*, 20, 119–22 (DOI: 10.1002/adma.200701772).
- [46] Nguyen N D., Zhang G., Lu J., Sherman A E., Fraser C L. (2011), Alkyl chain length effects on solid-state difluoroboron  $\beta$ -diketonate mechanochromic luminescence, *J. Mater. Chem.*, 21, 8409 (DOI: 10.1039/c1jm00067e).
- [47] Sagara Y., Mutai T., Yoshikawa I., Araki K. (2007), Material Design for Piezochromic Luminescence: Hydrogen-Bond-Directed Assemblies of a Pyrene Derivative, *J. Am. Chem. Soc.*, 129, 1520–1521 (DOI: 10.1021/JA0677362).
- [48] Han T., Zhang Y., Feng X., Lin Z., Tong B., Shi J., Zhi J., Dong Y. (2013), Reversible and hydrogen bonding-assisted piezochromic luminescence for solid-state tetraaryl-but-1,3-diene, *Chem. Commun.*, 49, 7049 (DOI: 10.1039/c3cc42644k).
- [49] Zhang Y., Han T., Gu S., Zhou T., Zhao C., Guo Y., Feng X., Tong B., Bing J., Shi J., et al. (2014), Mechanochromic Behavior of Aryl-Substituted But-1,3-Diene Derivatives with Aggregation Enhanced Emission, *Chem. - A Eur. J.*, 20, 8856– 8861 (DOI: 10.1002/chem.201403132).
- [50] Davis R., Kumar N. S. S., Abraham S., Suresh C. H., Rath N. P., Tamaoki N., Das S. (2008), Molecular Packing and Solid-State Fluorescence of Alkoxy-Cyano Substituted Diphenylbutadienes: Structure of the Luminescent Aggregates, *J. Phys. Chem. C*, 112, 2137–2146 (DOI: 10.1021/JP710352M).
- [51] Kumar N S S., Varghese S., Rath N P., Das S. (2008), Solid State Optical Properties of 4-Alkoxy-pyridine Butadiene Derivatives: Reversible Thermal Switching of Luminescence, *J. Phys. Chem. C*,

- 112, 8429–37 (DOI: 10.1021/jp800298b).
- [52] Kumar N S S., Varghese S., Suresh C H., Rath N P., Das S. (2009), Correlation between Solid-State Photophysical Properties and Molecular Packing in a Series of Indane-1,3-dione Containing Butadiene Derivatives, *J. Phys. Chem. C*, 113, 11927–35 (DOI: 10.1021/jp902482r).
- [53] Thomas R., Varghese S., Kulkarni G U. (2009), The influence of crystal packing on the solid state fluorescence behavior of alkyloxy substituted phenyleneethynylenes, *J. Mater. Chem.*, 19, 4401 (DOI: 10.1039/b902937k).
- [54] Liu Q., Liu W., Yao B., Tian H., Xie Z., Geng Y., Wang F. (2007), Synthesis and Chain-Length Dependent Properties of Monodisperse Oligo(9,9-di-n-octylfluorene-2,7-vinylene)s, *Macromolecules*, 40, 1851–1857 (DOI: 10.1021/MA0628073).
- [55] Sakurai H., Ritonga M. T. S., Shibatani H., Hirao T. (2005), Synthesis and Characterization of p-Phenylenediamine Derivatives Bearing an Electron-Acceptor Unit, *J. Org. Chem.*, 70, 2754–2762 (DOI: 10.1021/JO048324J).
- [56] Dhanabalan A., van Duren J K J., van Hal P A., van Dongen J L J., Janssen R A J. (2001), Synthesis and Characterization of a Low Bandgap Conjugated Polymer for Bulk Heterojunction Photovoltaic Cells, *Adv. Funct. Mater.*, 11, 255–62 (DOI: 10.1002/1616-3028(200108)11:4<255::AID-ADFM255>3.0.CO;2-I).
- [57] Zhang M., Tsao H N., Pisula W., Yang C., Mishra A K., Müllen K. (2007), Field-Effect Transistors Based on a Benzothiadiazole–Cyclopentadithiophene Copolymer, *J. Am. Chem. Soc.*, 129, 3472–3473 (DOI: 10.1021/JA0683537).
- [58] Chen S., Li Y., Yang W., Chen N., Liu H., Li Y. (2010), Synthesis and Tuning Optical Nonlinear Properties of Molecular Crystals of Benzothiadiazole, *J. Phys. Chem. C*, 114, 15109–15 (DOI: 10.1021/jp103159b).
- [59] Shi C., Yao Y., Yang Y., Pei Q. (2006), Regioregular Copolymers of 3-Alkoxythiophene and Their Photovoltaic Application, *J. Am. Chem. Soc.*, 128, 8980–8986 (DOI: 10.1021/JA061664X).

- [60] Hou Q., Zhou Q., Zhang Y., Yang W., Yang R., Cao Y. (2004), Synthesis and Electroluminescent Properties of High-Efficiency Saturated Red Emitter Based on Copolymers from Fluorene and 4,7-Di(4-hexylthien-2-yl)-2,1,3-benzothiadiazole, *Macromolecules*, 37, 6299– 6305 (DOI: 10.1021/MA049204G).
- [61] Zhu Z., Waller D., Gaudiana R., Morana M., Mühlbacher D., Scharber M., Brabec C. (2007), Panchromatic Conjugated Polymers Containing Alternating Donor/Acceptor Units for Photovoltaic Applications, *Macromolecules*, 40, 1981– 1986 (DOI: 10.1021/MA062376O).
- [62] Justin Thomas K R., Lin J T., Velusamy M., Tao Y-T., Chuen C-H. (2004), Color Tuning in Benzo[1,2,5]thiadiazole-Based Small Molecules by Amino Conjugation/Deconjugation: Bright Red-Light-Emitting Diodes, *Adv. Funct. Mater.*, 14, 83–90 (DOI: 10.1002/adfm.200304486).
- [63] Gautam P., Maragani R., Mobin S M., Misra R. (2014), Reversible mechanochromism in dipyridylamine-substituted unsymmetrical benzothiadiazoles, *RSC Adv.*, 4, 52526–9 (DOI: 10.1039/C4RA09921D).
- [64] Dou C., Chen D., Iqbal J., Yuan Y., Zhang H., Wang Y. (2011), Multistimuli-Responsive Benzothiadiazole-Cored Phenylene Vinylene Derivative with Nanoassembly Properties, *Langmuir*, 27, 6323–9 (DOI: 10.1021/la200382b).
- [65] Zhang X., Ma Z., Yang Y., Zhang X., Jia X., Wei Y. (2014), Fine-tuning the mechanofluorochromic properties of benzothiadiazole-cored cyano-substituted diphenylethene derivatives through D–A effect, *J. Mater. Chem. C*, 2, 8932–8 (DOI: 10.1039/C4TC01457J).
- [66] Misra R., Jadhav T., Dhokale B., Mobin S M. (2014), Reversible mechanochromism and enhanced AIE in tetraphenylethene substituted phenanthroimidazoles, *Chem. Commun.*, 50, 9076 (DOI: 10.1039/C4CC02824D).
- [67] Jadhav T., Dhokale B., Mobin S M., Misra R. (2015), Mechanochromism and aggregation induced emission in benzothiazole substituted tetraphenylethylenes: a structure function correlation, *RSC Adv.*, 5, 29878–84 (DOI: 10.1039/C5RA04881H).

- [68] Jadhav T., Dhokale B., Mobin S M., Misra R. (2015), Aggregation induced emission and mechanochromism in pyrenoidiazoles, *J. Mater. Chem. C*, 3, 9981–8 (DOI: 10.1039/C5TC02181B).
- [69] Jadhav T., Dhokale B., patil Y., Misra R. (2015), Aggregation induced emission and mechanochromism in tetraphenylethene substituted pyrazabole, *RSC Adv.*, 5, 68187–91 (DOI: 10.1039/C5RA12697E).
- [70] Li S., Shang Y., Zhao E., Kwok R T K., Lam J W Y., Song Y., Tang B Z. (2015), Color-tunable and highly solid emissive AIE molecules: synthesis, photophysics, data storage and biological application, *J. Mater. Chem. C*, 3, 3445–51 (DOI: 10.1039/C4TC02691H).
- [71] Li H., Chi Z., Zhang X., Xu B., Liu S., Zhang Y., Xu J., (2011), New thermally stable aggregation-induced emission enhancement compounds for non-doped red organic light-emitting diodes, *Chem. Commun.*, 47, 11273 (DOI: 10.1039/c1cc14642d).
- [72] Zhao Z., Deng C., Chen S., Lam J W Y., Qin W., Lu P., Wang Z., Kwok H S., Ma Y., Qiu H., et al. (2011), Full emission color tuning in luminogens constructed from tetraphenylethene, benzo-2,1,3-thiadiazole and thiophene building blocks, *Chem. Commun.*, 47, 8847 (DOI: 10.1039/c1cc12775f).
- [73] Jadhav T., Dhokale B., Misra R., Chi Z., Zhang X., Xu B., Zhou X., Ma C., Zhang Y., Liua S., et al. (2015), Effect of the cyano group on solid state photophysical behavior of tetraphenylethene substituted benzothiadiazoles, *J. Mater. Chem. C*, 3, 9063–8 (DOI: 10.1039/C5TC01871D).
- [74] Jadhav T., Dhokale B., Patil Y., Mobin S M., Misra R. (2016), Multi-Stimuli Responsive Donor–Acceptor Tetraphenylethylene Substituted Benzothiadiazoles, *J. Phys. Chem. C*, 120, 24030–40 (DOI: 10.1021/acs.jpcc.6b09015).
- [75] Misra R., Gautam P., Jadhav T. and Mobin S M. (2013), Donor–Acceptor Ferrocenyl-Substituted Benzothiadiazoles: Synthesis, Structure, and Properties, *J. Org. Chem.*, 78, 4940–8 (DOI: 10.1021/jo4005734).
- [76] Röck F., Barsan N., Weimar U. (2008), Electronic Nose: Current Status and Future Trends, *Chem. Rev.*, 108, 705–725 (DOI: 10.1021/cr07001a001).

10.1021/CR068121Q).

- [77] Zhang X., Li B., Chen Z-H., Chen Z-N. (2012), Luminescence vapochromism in solid materials based on metal complexes for detection of volatile organic compounds (VOCs), *J. Mater. Chem.*, 22, 11427 (DOI: 10.1039/c2jm30394a).

## Chapter 7

# Aggregation induced emission and mechanochromism in tetraphenylethene substituted pyrazabole

---

---

### 7.1. Introduction

In recent years research on design and synthesis of organic molecules exhibiting AIE and mechanochromism has gained momentum due to their applications in mechano-sensors, optical data storage, and security papers.<sup>[1-6]</sup> Molecular systems exhibiting strong solid state fluorescence and high color contrast are essential for mechanochromism.<sup>[7]</sup> The conventional organic fluorescent dyes are non-fluorescent in solid state due to the notorious effect called aggregation caused quenching (ACQ).<sup>[8-10]</sup> Tang et al. has introduced the concept of aggregation induced emission (AIE) to overcome the ACQ.<sup>[11-14]</sup> Generally, the propeller-like conformation of AIE active molecules restrict tight packing in the aggregated state, which minimizes the chance of intermolecular  $\pi$ - $\pi$  stacking and results in highly fluorescent solid.<sup>[11-14]</sup>

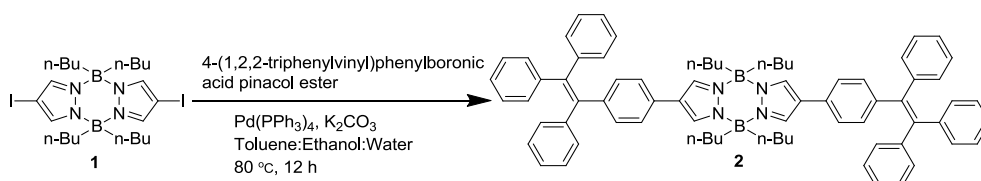
The tetraphenylethene is AIE active molecule and widely studied for numerous applications.<sup>[15-20]</sup> However, there is huge space for developing TPE-based functional materials. The TPE derivatives, containing electron donor as well as acceptor moieties have been used to develop piezochromic, mechanochromic, vapochromic, thermochromic and solvatochromic materials.<sup>[15-22]</sup> Our group is involved in design and synthesis of mechanochromic materials.<sup>[23-25]</sup> Earlier chapters, we have shown that the TPE substituted phenanthroimidazole, pyrenoimidazoles and benzothiadiazole can be used as mechanochromic materials. The literature reveals that, variety of weak acceptor units (phenanthroimidazole, benzothiazole, aldehyde and triazolyl units) have been attached to weak donor TPE for synthesizing mechanochromic materials.<sup>[23-26]</sup> We were interested to see the effect of TPE substitution on the pyrazabole.

The organoboron compounds are of great interest due to their potential applications in OLEDs, organic photovoltaics (OPVs), organic field effect transistor (OFET), and NLO materials.<sup>[27-31]</sup> Pyrazabole is a class of organoboron compound, which is synthesized by condensation of two pyrazole units with tri-*n*-butylboranes. The pyrazabole act as a weak acceptor and has been explored for variety of applications such as liquid crystalline material, multiphoton absorption, and luminescent polymers.<sup>[32-37]</sup> Recently we have reported high two photon absorption (2PA) and three photon absorption (3PA) in ferrocenyl substituted pyrazaboles.<sup>[38]</sup>

Herein, we have attached TPE unit on the pyrazabole through single bond and explored its AIE and mechanochromic properties. The TPE substituted pyrazabole exhibits strong blue colored emission upon aggregation, and highly reversible mechanochromism between blue and green color.

## 7.2. Results and discussion

### 7.2.1. Synthesis



**Scheme 7.1.** Synthetic route for the TPE substituted pyrazabole **2**.

The TPE substituted pyrazabole **2** was synthesized by the Pd-catalyzed Suzuki cross-coupling reaction of 2,6-diiodopyrazabole with the 4-(1,2,2-triphenylvinyl)phenylboronic acid pinacol ester in 45% yield (Scheme 7.1). The precursors 2,6-diiodopyrazabole and 4-(1,2,2-triphenylvinyl)phenylboronic acid pinacol ester were synthesized by reported procedures.<sup>[38,39]</sup> The TPE substituted pyrazabole was well characterized by usual spectroscopic techniques.

### 7.2.2. Thermogravimetric analysis

Thermo gravimetric analysis (TGA) of TPE substituted pyrazabole show good thermal stability with thermal decomposition temperature ( $T_d$ ) at

307 °C corresponding to 5% weight loss under nitrogen atmosphere (Figure 7.1).

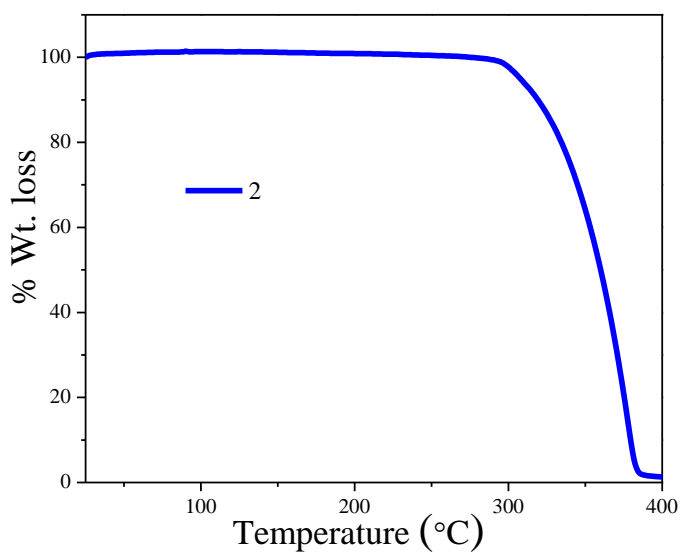


**Figure 7.1.** Thermogravimetric analysis of **2**, measured at a heating rate of 10 °C/ min under nitrogen atmosphere.

### 7.2.3. Theoretical calculations

In order to understand the geometrical structure of the pyrazabole **2**, computational calculation was performed using density functional theory (DFT) at the B3LYP/6-31G(d) level using the Gaussian 09 program.<sup>[40,41]</sup> The energy minimized structure of the pyrazabole **2** show twisted geometry for TPE unit, while pyrazabole core show planar geometry (Figure 7.2). The central core of pyrazabole show chair conformation. The pyrazabole and TPE units are non-planar with dihedral angle of 27° between pyrazabole and phenyl of TPE.

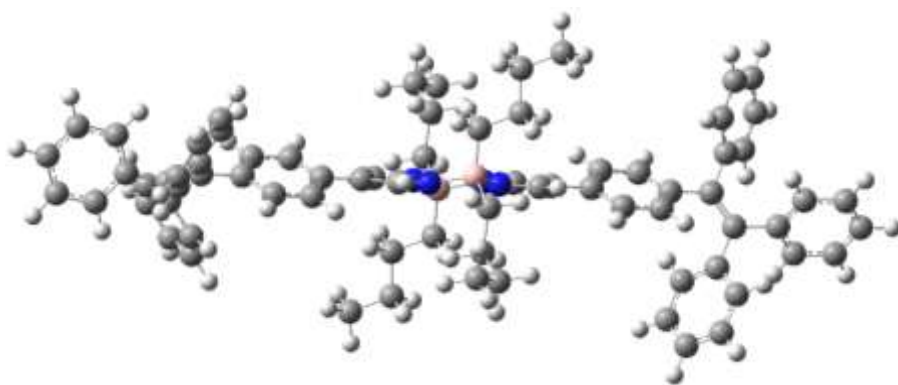


**Figure 7.2.** Energy optimized structure of pyrazabole **2** at the B3LYP/6-31G (d) level.

#### 7.2.4. Photophysical properties

The electronic absorption spectra of the TPE substituted pyrazabole **2** exhibit absorption band between 250-380 nm. The TPE substituted pyrazabole **2** is weakly fluorescent in solution, due to free molecular rotations of phenyl rings of tetraphenylethylene unit. The AIE property of TPE substituted pyrazabole was studied by absorption and fluorescence spectroscopy (Figure 7.3, Figure 7.4). The TPE substituted pyrazabole is highly soluble in tetrahydrofuran (THF) and insoluble in water, therefore the small aggregate particles were prepared by increasing the water fraction in the THF–water mixture. In pure THF solution the TPE substituted pyrazabole **2** exhibit poor fluorescence quantum yield, which remains constant until the molecules start aggregating significantly (AIE effect). The fluorescence of TPE substituted pyrazabole in THF:water mixture remains constant upto the 60% water fraction ( $f_w$ ) and above 60%  $f_w$  molecules started aggregating with enhanced fluorescence. At 90% water fraction the fluorescence intensity was enhanced by 578 fold (Figure 7.3). The photograph of **2** in THF–water mixtures with different water fractions under 365 nm UV illumination shows the AIE behavior (Figure 7.3). The study of absorption behavior of AIE show noticeable change after 60% water fraction, and started to show light scattering of the nanoaggregate suspension in the THF–water mixtures (Figure 7.4).

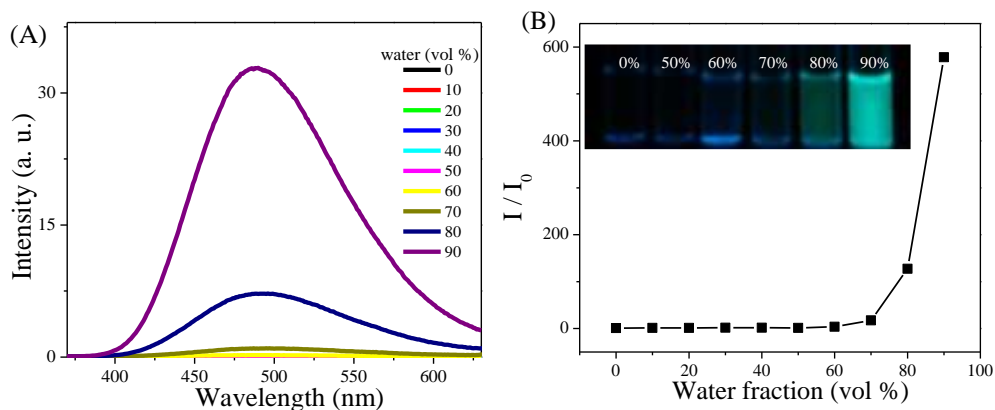


**Figure 7.3.** (A) Fluorescence spectra of pyrazabole **2** in THF-water mixtures with different water fractions, (B) Plot of Photoluminescence intensity (PL) vs % of water fraction ( $f_w$ ). Luminogen concentration:  $10 \mu\text{M}$ ; excitation wavelength:  $340 \text{ nm}$ ; intensity calculated at  $\lambda_{\text{max}}$ . Inset photograph of **2** in THF-water mixtures with different water fractions ( $10 \mu\text{M}$ ) under  $365 \text{ nm}$  UV illumination.

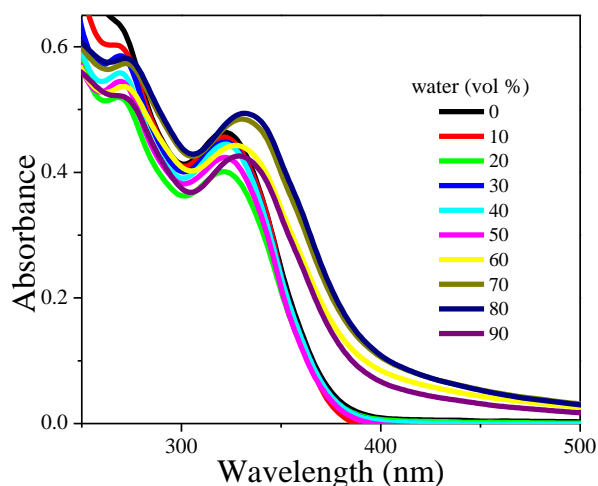


**Figure 7.4.** UV-Vis absorption spectra of **2** in THF-water mixtures with different water fractions.

In order to determine the dimensions of the nano-aggregates formed, the nanoaggregates at 90% water fraction ( $f_w$ ) were studied with the help of dynamic light scattering (DLS) and scanning electron microscopy (SEM). The DLS study shows the average hydrodynamic diameter of  $180 \text{ nm}$  for nano-aggregates (Figure 7.5). The SEM study reveals rectangular sized nanoaggregates were formed with average size of  $\sim 115 \text{ nm}$ . These studies confirm the formation of nanoaggregates at 90% ( $f_w$ ).

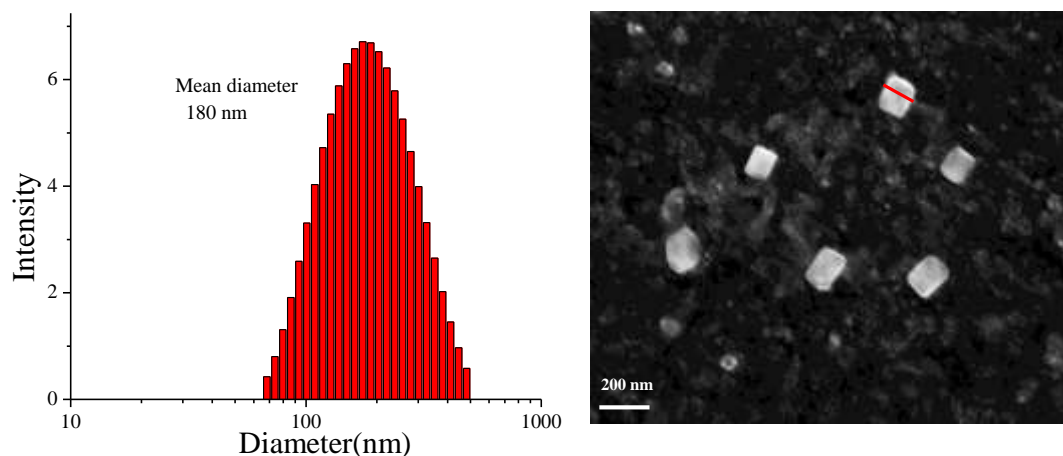


**Figure 7.5.** The particle size distributions of **2** in THF–water mixture (10:90, v:v) (Left) and SEM image (right).

### 7.2.5. Mechanochromic property

The mechanochromic properties of TPE substituted pyrazabole **2** was explored by the emission studies. The pristine form of **2** emits blue light at 453 nm which upon grinding using a spatula or a pestle exhibits drastic 44 nm change in the emission behavior and emits green light at 497 nm (Figure 7.6). This color contrast mechanochromic effect of TPE substituted pyrazabole **2** can be reverted to its original color either by annealing or fuming with dichloromethane vapor. The grinded form of **2** upon annealing at 150 °C for 5 min or fuming with dichloromethane vapor for 4 min restored the original blue emission. This reversible mechanochromic behavior can be repeated between blue and green emission and proves these stimuli does not cause any chemical change (Figure 7.6).

In order to understand the mechanism of mechanochromism in TPE substituted pyrazabole **2** powder X-ray diffraction (PXRD) analysis was performed (Figure 7.7). The pristine form of pyrazabole **2** exhibit intense and sharp diffraction peaks reflecting the crystalline behavior. Upon grinding pyrazabole **2** show weak and diffused diffraction peaks suggesting the transition to amorphous state. The grinded form of pyrazabole **2** when subjected to heating or fuming, the sharp diffraction peaks were observed again indicating the transformation of amorphous state of sample to crystalline state. This result concludes that the mechanochromism in pyrazabole **2** is

associated with the morphological change from the crystalline state to the amorphous state and *vice versa*.

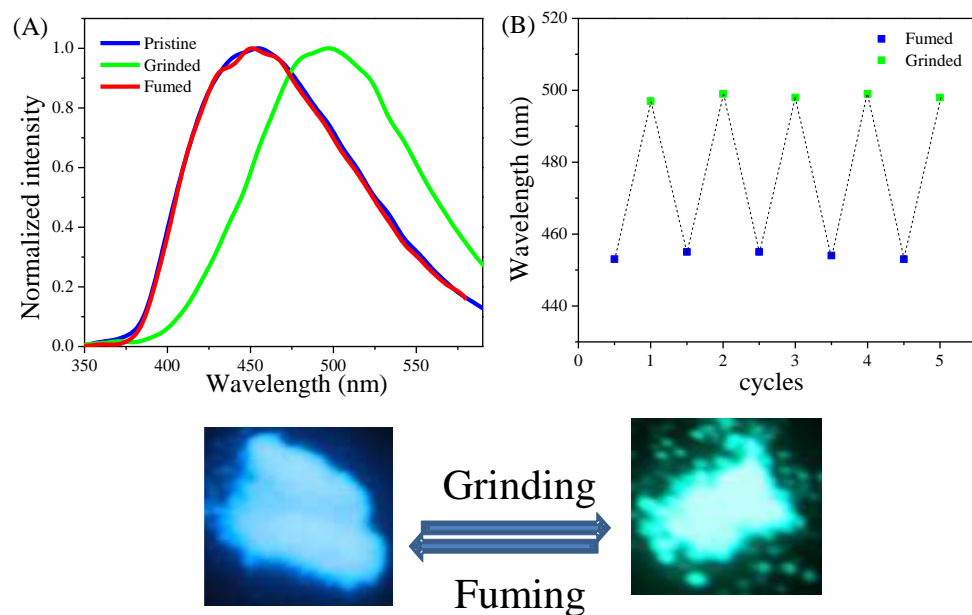


**Figure 7.6.** (A) Emission spectra of **2** as pristine, grinded and fumed solids; Photograph taken under 365 nm UV illumination. (B) Repeated switching of the solid-state fluorescence of **2** by repeated grinding and fuming cycles.

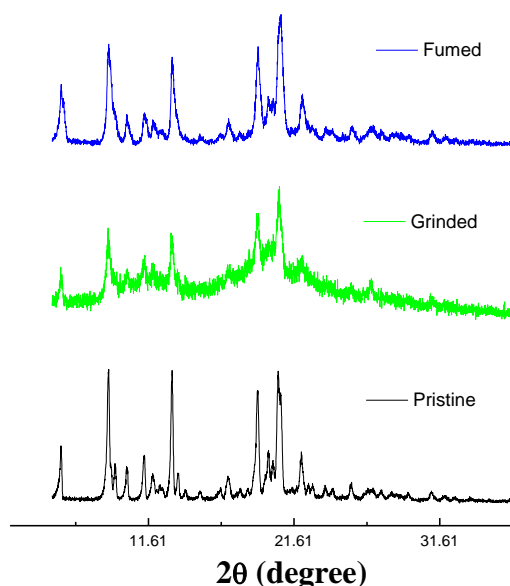


**Figure 7.7.** PXRD curves of **2** in pristine, grinded and fumed form.

### 7.3. Experimental section

#### Synthesis and characterization of TPE substituted pyrazabole **2**:

Pd(PPh<sub>3</sub>)<sub>4</sub> (0.004 mmol) was added to a well degassed solution of 2,6-diiodopyrazabole (**1**) (0.4 mmol), 4-(1,2,2-triphenylvinyl)phenylboronic acid

pinacol ester (0.48 mmol), K<sub>2</sub>CO<sub>3</sub>(1.2 mmol) in a mixture of toluene (12 mL)/ ethanol (4.0 mL)/ H<sub>2</sub>O (1.0 mL). The resulting mixture was stirred at 80 °C for 24 h under argon atmosphere. After cooling, the mixture was evaporated to dryness and the residue subjected to column chromatography on silica to yield the desired product **2** as colorless powder. The compound was recrystallized from DCM:ethanol (8:2) mixtures. Yield: 42.0%. <sup>1</sup>H NMR (400 MHz, CDCl<sub>3</sub>, 25 °C): δ 7.75 (s, 4H), 7.30 (d, 4H, *J*=4 Hz), 7.02-7.17 (m, 34H), 1.13-1.19 (m, 8H), 0.65-0.82 (m, 28H) ppm; <sup>13</sup>C NMR (100 MHz, CDCl<sub>3</sub>, 25 °C): δ 143.7, 143.7, 143.6, 142.7, 141.1, 140.3, 132.0, 131.4, 131.3, 130.1, 129.2, 127.8, 127.7, 127.6, 126.5, 126.5, 126.4, 124.8, 122.7, 27.5, 26.2, 14.1, 0.00 ppm.

#### 7.4. Conclusion

In summary, we have designed and synthesized AIE active mechanochromic TPE substituted pyrazabole **2** by the Pd-catalyzed Suzuki cross-coupling reaction. The geometry optimized structure shows twisted geometry of TPE unit. The AIE study reveals remarkable 578 folds enhancement in the emission intensity at 90% water fraction. The TPE substituted pyrazabole **2** show highly reversible mechanochromism between blue and green light with 44 nm grinding induced spectral shift. The powder XRD results indicate the transformation from crystalline to amorphous state is responsible for mechanochromism. The results obtained here will help in design of new mechanochromic molecules for various optoelectronic applications.

**Note:** This is copyrighted material from Royal Society of Chemistry, *RSC Adv.*, 2015, 5, 68187-68191 (DOI: 10.1039/C5RA12697E).

#### 7.5. References

[1] Chi Z., Zhang X., Xu B., Zhou X., Ma C., Zhang Y., Liu S., Xu J.

- (2012), Recent advances in organic mechanofluorochromic materials, *Chem. Soc. Rev.*, 41, 3878 (DOI: 10.1039/c2cs35016e).
- [2] Sagara Y., Kato T. (2009), Mechanically induced luminescence changes in molecular assemblies, *Nat. Chem.*, 1, 605–610 (DOI: 10.1038/nchem.411).
- [3] Davis D. A., Hamilton A., Yang J., *et al.* (2009), Force-induced activation of covalent bonds in mechanoresponsive polymeric materials, *Nature*, 459, 68–72 (DOI: 10.1038/nature07970).
- [4] Dong Y., Xu B., Zhang J., Tan X., Wang L., Chen J., Lv H., Wen S., Li B., Ye L., *et al.* (2012), Piezochromic luminescence based on the molecular aggregation of 9,10-Bis(( *E* )-2-(pyrid-2-yl)vinyl)anthracene, *Angew. Chemie Int. Ed.*, 51, 10782–10785 (DOI: 10.1002/anie.201204660).
- [5] Luo X., Li J., Li C., Heng L., Dong Y Q., Liu Z., Bo Z., Tang B. Z. (2011), Reversible switching of the emission of diphenyldibenzofulvenes by thermal and mechanical stimuli, *Adv. Mater.*, 23, 3261–3265 (DOI: 10.1002/adma.201101059).
- [6] Dhokale B., Jadhav T., Mobin S. M., Misra R. (2015), *Meso* alkynylated tetraphenylethylene (TPE) and 2,3,3-triphenylacrylonitrile (TPAN) substituted BODIPYs, *J. Org. Chem.*, 80, 8018–8025 (DOI: 10.1021/acs.joc.5b01117).
- [7] Kwon M. S., Gierschner J., Yoon S-J., Park S. Y. (2012), Unique piezochromic fluorescence behavior of dicyanodistyrylbenzene based donor-acceptor-donor triad: Mechanically controlled photo-induced electron transfer (eT) in molecular assemblies, *Adv. Mater.*, 24, 5487–5492 (DOI: 10.1002/adma.201202409).
- [8] J. B. Birks, *Photophysics of Aromatic Molecules*, Wiley, London, U.K, 1970.
- [9] Jayanty S., Radhakrishnan T. P. (2004), Enhanced fluorescence of remote functionalized diaminodicyanoquinodimethanes in the solid state and fluorescence switching in a doped polymer by solvent vapors, *Chem. - A Eur. J.*, 10, 791–797 (DOI: 10.1002/chem.200305123).
- [10] Henry J. T., Jerome L. M., Wim T. K., James A. M., Judith H., Scott W., Isaac R., Watts K., (2005), Enhanced photoluminescence from

- group 14 metalloles in aggregated and solid solutions, *Inorg. Chem.*, 2005, 44, 2003–2011 (DOI: 10.1021/IC049034O).
- [11] Luo J., Xie Z., Lam J W Y., Cheng L., Tang B Z., Chen H., Qiu C., Kwok H S., Zhan X., Liu Y., *et al.* (2001), Aggregation-induced emission of 1-methyl-1,2,3,4,5-pentaphenylsilole, *Chem. Commun.*, 397, 1740–1741 (DOI: 10.1039/b105159h).
- [12] Li Y., Liu T., Liu H., Tian M-Z., Li Y. (2014), Self-assembly of intramolecular charge-transfer compounds into functional molecular systems, *Acc. Chem. Res.*, 47, 1186–1198 (DOI: 10.1021/ar400264e).
- [13] Liu H., Xu J., Li Y., Li Y. (2010), Aggregate nanostructures of organic molecular materials, *Acc. Chem. Res.*, 43, 1496–1508 (DOI: 10.1021/ar100084y).
- [14] Hong Y., Lam J W Y., Tang B Z. (2011), Aggregation-induced emission, *Chem. Soc. Rev.*, 40, 5361 (DOI: 10.1039/c1cs15113d).
- [15] Dong Y., Lam J. W. Y., Qin A., Liu J., Li Z., Tang B. Z., Sun J., Kwok H. S. (2007), Aggregation-induced emissions of tetraphenylethene derivatives and their utilities as chemical vapor sensors and in organic light-emitting diodes, *Appl. Phys. Lett.*, 91, 11111 (DOI: 10.1063/1.2753723).
- [16] Huang J., Yang X., Wang J., Zhong C., Wang L., Qin J., Li Z. (2012), New tetraphenylethene-based efficient blue luminophors: aggregation induced emission and partially controllable emitting color, *J. Mater. Chem.*, 22, 2478–2484 (DOI: 10.1039/C1JM14054J).
- [17] Zhao N., Yang Z., Lam J. W. Y., Sung H. H. Y., Xie N., Chen S., Su H., Gao M., Williams I. D., Wong K. S., *et al.* (2012), Benzothiazolium-functionalized tetraphenylethene: an AIE luminogen with tunable solid-state emission, *Chem. Commun.*, 48, 8637 (DOI: 10.1039/c2cc33780k).
- [18] Zhao N., Li M., Yan Y., Lam J. W. Y., Zhang Y. L., Zhao Y. S., Wong K. S., Tang B. Z. (2013), A tetraphenylethene-substituted pyridinium salt with multiple functionalities: synthesis, stimuli-responsive emission, optical waveguide and specific mitochondrion imaging, *J. Mater. Chem. C*, 1, 4640 (DOI: 10.1039/c3tc30759j).
- [19] Xu B., Xie M., He J., Xu B., Chi Z., Tian W., Jiang L., Zhao F., Liu S.,

- Zhang Y., *et al.* (2013), An aggregation-induced emission luminophore with multi-stimuli single- and two-photon fluorescence switching and large two-photon absorption cross section, *Chem. Commun.*, 49, 273–275 (DOI: 10.1039/C2CC36806D).
- [20] Xu B., Chi Z., Zhang X., Li H., Chen C., Liu S., Zhang Y., Xu J. (2011), A new ligand and its complex with multi-stimuli-responsive and aggregation-induced emission effects, *Chem. Commun.*, 47, 11080–11082 (DOI: 10.1039/c1cc13790e).
- [21] Shen X. Y., Wang Y. J., Zhao E., Yuan W. Z., Liu Y., Lu P., Qin A., Ma Y., Sun J. Z., Tang B. Z. (2013), Effects of substitution with donor–acceptor groups on the properties of tetraphenylethene trimer: aggregation-induced emission, solvatochromism, and mechanochromism, *J. Phys. Chem. C*, 117, 7334–7347 (DOI: 10.1021/jp311360p).
- [22] Xu B., He J., Mu Y., Zhu Q., Wu S., Wang Y., Zhang Y., Jin C., Lo C., Chi Z., *et al.* (2015), Very bright mechanoluminescence and remarkable mechanochromism using a tetraphenylethene derivative with aggregation-induced emission, *Chem. Sci.*, 6, 3236–3241 (DOI: 10.1039/C5SC00466G).
- [23] Misra R., Jadhav T., Dhokale B., Mobin S. M. (2014), Reversible mechanochromism and enhanced AIE in tetraphenylethene substituted phenanthroimidazoles, *Chem. Commun.*, 50, 9076 (DOI: 10.1039/C4CC02824D).
- [24] Jadhav T., Dhokale B., Mobin S. M., Misra R. (2015), Mechanochromism and aggregation induced emission in benzothiazole substituted tetraphenylethylenes: a structure function correlation, *RSC Adv.*, 5, 29878–29884 (DOI: 10.1039/C5RA04881H).
- [25] Gautam P., Maragani R., Mobin S. M., Misra R. (2014), Reversible mechanochromism in dipyridylamine-substituted unsymmetrical benzothiadiazoles, *RSC Adv.*, 4, 52526–52529 (DOI: 10.1039/C4RA09921D).
- [26] Wang J., Mei J., Hu R., Sun J. Z., Qin A., Tang B. Z. (2012), Click synthesis, aggregation-induced emission, *e / z* isomerization, self-organization, and multiple chromisms of pure stereoisomers of a

- tetraphenylethene-cored luminogen, *J. Am. Chem. Soc.*, 134, 9956–9966 (DOI: 10.1021/ja208883h).
- [27] Christopher D. E., Marder T. B., (2004), Applications of three-coordinate organoboron compounds and polymers in optoelectronics, *Chem. Mater.*, 16, 4574–4585 (DOI: 10.1021/CM0495717).
- [28] Jäkle F. (2006), Lewis acidic organoboron polymers, *Coord. Chem. Rev.*, 250, 1107–1121 (DOI: 10.1016/j.ccr.2006.01.007).
- [29] Rao Y-L., Wang S. (2011), Four-coordinate organoboron compounds with a  $\pi$ -conjugated chelate ligand for optoelectronic applications, *Inorg. Chem.*, 50, 12263–12274 (DOI: 10.1021/ic200658v).
- [30] Hudson Z. M., Wang S. (2009), Impact of donor–acceptor geometry and metal chelation on photophysical properties and applications of triarylboranes, *Acc. Chem. Res.*, 42, 1584–1596 (DOI: 10.1021/ar900072u).
- [31] Jäkle F. (2010), Advances in the synthesis of organoborane polymers for optical, electronic, and sensory applications, *Chem. Rev.*, 110, 3985–4022 (DOI: 10.1021/cr100026f).
- [32] Barberá J., Giménez R., Serrano J. L. (1994), Pyrazaboles: New room-temperature columnar liquid crystals, *Adv. Mater.*, 6, 470–472 (DOI: 10.1002/adma.19940060605).
- [33] Barberá J., Giménez R., Serrano J. L. (2000), Mesogenic pyrazaboles: synthesis, properties, and structural characterization, *Chem. Mater.*, 12, 481–489 (DOI: 10.1021/CM991120C).
- [34] Cavero E., Lydon D. P., Uriel S., de la Fuente M. R., Serrano J. L., Giménez R. (2007), Roof-shaped pyrazaboles as a structural motif for bent-core liquid crystals, *Angew. Chemie*, 119, 5267–5269 (DOI: 10.1002/ange.200700820).
- [35] Cavero E., Fuente M R de la., Beltrán E., Romero P., Serrano J L., Giménez R. (2007), Bent-core liquid crystals from roof-shaped boron coordination compounds: synthesis, characterization, dielectric, and electro-optic studies, *Chem. Mater.*, 19, 6230–6239 (DOI: 10.1021/cm702129s).
- [36] Jäkle F., Priermeier T., Wagner M. (1996), Synthesis, structure, and dynamic behavior of *ansa*-ferrocenes with pyrazabole bridges,

- Organometallics*, 15, 2033–2040 (DOI: 10.1021/om9509305).
- [37] Herdtweck E., Jäkle F., Opromolla G., Spiegler M., Wagner M., Zanello P. (1996), Structural features and electrochemical properties of ansa-ferrocenes with pyrazabole bridges, (DOI: 10.1021/OM960722S).
- [38] Jadhav T., Maragani R., Misra R., Sreeramulu V., Rao D. N., Mobin S. M. (2013), Design and synthesis of donor–acceptor pyrazabole derivatives for multiphoton absorption, *Dalt. Trans.*, 42, 4340 (DOI: 10.1039/c3dt33065f).
- [39] Hu R., Maldonado J. L., Rodriguez M., Deng C., Jim C. K. W., Lam J. W. Y., Yuen M. M. F., Ramos-Ortiz G., Tang B. Z., He G. S., *et al.* (2012), Luminogenic materials constructed from tetraphenylethene building blocks: Synthesis, aggregation-induced emission, two-photon absorption, light refraction, and explosive detection, *J. Mater. Chem.*, 22, 232–240 (DOI: 10.1039/C1JM13556B).
- [40] Parr R. G., Yang W. (1995), Density-Functional Theory of the Electronic Structure of Molecules, *Annu. Rev. Phys. Chem.*, 46, 701–728 (DOI: 10.1146/annurev.pc.46.100195.003413).
- [41] Lee C., Yang W., Parr R. G. (1988), Development of the Colle-Salvetti correlation-energy formula into a functional of the electron density, *Phys. Rev. B*, 37, 785–789 (DOI: 10.1103/PhysRevB.37.785).



# Chapter 8

## Conclusions and scope for future work

---

### 8.1. Conclusions

In recent years tetraphenylethylene based luminogens have gained immense attention of scientific community.<sup>[1]</sup> The TPE based luminogens show aggregation induced emission property and they are highly fluorescent in the solid state. We have synthesized various TPE substituted phenanthroimidazoles, pyrenoimidazoles, benzothiadiazoles and pyrazabole. We have successfully synthesized various fluorescent coloured solids and studied their AIE and mechanochromism. We have proposed that the planarization induced enhanced conjugation is responsible for the mechanochromism and also change from crystalline to amorphous form is associated with the mechanochromism.

In chapter 3, we have designed and synthesized high color contrast mechanochromic tetraphenylethene substituted phenanthroimidazoles **3a** and **3b**. The powder XRD results indicate the destruction of solid state packing from crystalline to amorphous state is responsible for mechanochromism. The cyano-group in phenanthroimidazole improves the thermal stability and enhances the AIE. The single crystal X-ray and packing analysis reveals that hydrogen bonding and strong supramolecular interactions are responsible for AIEE in **3b**.<sup>[2]</sup>

In Chapter 4, the TPE substituted phenanthroimidazoles **3a–3d** were synthesized by Pd-catalyzed Suzuki cross-coupling reaction. The phenanthroimidazoles **3a–3d** show good thermal stability and introduction of cyano-group helps to improve thermal stability. The phenanthroimidazoles **3a–3d** are weakly emissive in solutions whereas strong emission was observed in the aggregated state due to the aggregation induced emission (AIE). The reversible mechanochromism with good color contrast between blue and green color was observed in all phenanthroimidazoles **3a–3d**. It is shown that the

changing the end group is effective strategy to tune the solid state emission and mechanochromism.<sup>[3]</sup>

In chapter 5, we have designed and synthesized pyrenoimidazoles **3a** and **3b** by the Pd-catalyzed Suzuki cross-coupling reaction of bromopyrenoimidazole **2** with 4-(1,2,2-triphenylvinyl)phenylboronic acid pinacol ester and 2-(4-pinacolatoboronphenyl)-3,3-diphenylacrylonitrile. The single crystal structure and packing diagram of **3a** reveals twisted conformation and absence of strong  $\pi$ --- $\pi$  staking in pyrene units which results in fluorescent solids. The strong aggregation induced emission (AIE) and different AIE behavior was observed for **3a** and **3b**. The **3b** shows different colored emission at different water fraction which can be ascribed to the different sized nanoaggregates formation. The pyrenoimidazoles **3a** and **3b** exhibit reversible mechanochromic behavior with color contrast between blue and green. The solid state absorption, emission and powder XRD study reveals that, the transformation of twisted crystalline state to planar amorphous state is the main cause for mechanochromism in pyrenoimidazoles **3a** and **3b**.<sup>[4]</sup>

In chapter 6, we have synthesized thermally stable tetraphenylethylene substituted benzothiadiazoles **3-9** with varying D-A interaction. The solution and solid-state optical properties of BTDs **3-9** were modulated *via* D/A substituents and the arrangement of the substituents. The BTDs **3-9** exhibit tunable fluorescence in both solution and solid state from blue to red color. The AIE study reveals that at low water percentages emission was controlled by solvent polarity and show red shift with decrease in intensity, whereas at high water percentages AIE dominates over solvent polarity and shows enhanced emission.

The BTDs **3**, **6**, **7**, **8** and **9** exhibit reversible mechanochromism and vapochromism whereas mechanochromism and vapochromism were absent in the BTDs **4** and **5**. Particularly, the BTDs **6** and **8** show stimuli responses with good color contrast from blue to green and green to yellow with spectral shift ( $\Delta\lambda$ ) of 63 nm and 44 nm, respectively. The solid state absorption of pristine and grinded forms of BTDs **3-9** reveal enhanced conjugation or/and increased D-A interaction is origin of the mechanochromism. The crystal structure and theoretical study of BTD **6** reveals that the conversion of twisted to planar structure is accountable for good color contrast mechanochromism. The

powder x-ray diffraction (PXRD) study reveals that the morphological change between thermodynamically stable crystalline phase to the metastable amorphous state and *vice versa* is associated with mechanochromism and vapochromism. The study reveals the important role of twisting in the molecular backbone, nature of substituent and way of substitution in deciding the photophysical and stimuli responsive properties of TPE substituted BTDs.<sup>[5,6]</sup>

In chapter 7, we have designed and synthesized AIE active mechanochromic TPE substituted pyrazabole **2** by the Pd-catalyzed Suzuki cross-coupling reaction. The geometry optimized structure shows twisted geometry of TPE unit. The AIE study reveals remarkable 578 folds enhancement in the emission intensity at 90% water fraction. The TPE substituted pyrazabole **2** show highly reversible mechanochromism between blue and green light with 44 nm grinding induced spectral shift. The powder XRD results indicate the transformation from crystalline to amorphous state is responsible for mechanochromism.<sup>[7]</sup>

## 8.2. Scope for future work

The thesis highlights the smart methodology of synthesizing highly luminescent solids based on TPE derivatives. Further, they mechanochromic properties were explored. Depending upon their conjugation length and strength of donor-acceptor interaction, solid state emission properties were tuned successfully from blue to red color. We have propose that the planarization induced enhanced conjugation is responsible for the mechanochromism and also change from crystalline to amorphous form is associated with the mechanochromism. Thus, we have described AIE and mechanochromic properties of various TPE substituted derivatives. By understanding the AIE and mechanism of mechanochromism in various TPE derivatives many more fluorescent solids can be developed of desired properties.

The imidazole based donor-acceptor molecules have been used in developing blue OLEDs due to their charge carrier mobility. Lee *et al.* and Yang *et al.* have shown phenanthroimidazole- $\pi$ -triphenylamine derivatives

can be efficiently used for development of non-doped blue OLEDs.<sup>[8,9]</sup> The synthesis of solid state fluorescent material is one of the good methods to increase the efficiency of the devices. The tetraphenylethene (TPE) has been widely explored for AIE phenomenon and used to develop OLED materials.<sup>[10]</sup> So, we can use these TPE derivatives in the development of efficient OLEDs.<sup>[11]</sup>

Recently, TPE substituted BTDs were reported for bio-imaging applications.<sup>[12]</sup> Thus the reported TPE substituted BTDs in this thesis can also be promising candidates for bios-imaging applications.

## References

- [1] Mei J., Leung N. L. C., Kwok R. T. K., Lam J. W. Y., Tang B. Z. (2015), Aggregation-Induced Emission: Together We Shine, United We Soar!, *Chem. Rev.*, 115, 11718–940 (DOI: 10.1021/acs.chemrev.5b00263).
- [2] Misra R., Jadhav T., Dhokale B., Mobin S. M. (2014), Reversible mechanochromism and enhanced AIE in tetraphenylethene substituted phenanthroimidazoles. *Chem. Commun.*, 50, 9076-9078 (DOI: 10.1039/C4CC02824D).
- [3] Jadhav T., Choi J. M., Lee J. Y., Dhokale B., Mobin S. M., Misra R. (2016), Effect of end-groups on mechanochromism and electroluminescence in tetraphenylethylene substituted phenanthroimidazoles. *J. Phys. Chem. C*, 120, 18487–18495 (DOI: 10.1021/acs.jpcc.6b06277).
- [4] Jadhav T., Dhokale B., Mobin S. M., Misra R. (2015), Aggregation induced emission and mechanochromism in pyrenoimidazoles. *J. Mater. Chem. C*, 3, 9981-9988 (DOI: 10.1039/C5TC02181B).
- [5] Jadhav T., Dhokale B., Misra R. (2015), Effect of the cyano group on solid state photophysical behavior of tetraphenylethene substituted benzothiadiazoles. *J. Mater. Chem. C*, 2015, 3, 9063-9068 (DOI: 10.1039/C5TC01871D).
- [6] Jadhav T., Dhokale B., Patil Y., Mobin S. M., Misra R. (2016), Multi-Stimuli Responsive Donor–Acceptor Tetraphenylethylene Substituted Benzothiadiazoles, *J. Phys. Chem. C*, 120, 24030–40 (DOI:

- 10.1021/acs.jpcc.6b09015).
- [7] Jadhav T., Dhokale B., Patil Y., Misra R. (2015), Aggregation induced emission and mechanochromism in tetraphenylethene substituted pyrazabole. *RSC Adv.*, 5, 68187-68191 (DOI: 10.1039/C5RA12697E).
- [8] Zhang S., Li W., Yao L., Pan Y., Shen F., Xiao R., Yang B., Ma Y. (2013), Enhanced proportion of radiative excitons in non-doped electro-fluorescence generated from an imidazole derivative with an orthogonal donor-acceptor structure, *Chem. Commun.*, 49, 11302 (DOI: 10.1039/c3cc47130f).
- [9] Zhang Y., Lai S-L., Tong Q-X., Lo M-F., Ng T-W., Chan M-Y., Wen Z-C., He J., Jeff K-S., Tang X-L., et al. (2012), High Efficiency Nondoped Deep-Blue Organic Light Emitting Devices Based on Imidazole- $\pi$ -triphenylamine Derivatives, *Chem. Mater.*, 24, 61-70 (DOI: 10.1021/cm201789u).
- [10] Yang J., Huang J., Li Q., Li Z. (2016), Blue AIEgens: approaches to control the intramolecular conjugation and the optimized performance of OLED devices, *J. Mater. Chem. C*, 4, 2663-84 (DOI: 10.1039/C5TC03262H).
- [11] Jadhav T., Choi J. M., Lee J. Y., Dhokale B., Misra R. (2016), Non-doped blue organic light emitting devices based on tetraphenylethylene- $\pi$ -imidazole derivatives, *Org. Electron.*, 37, 448-52 (DOI: 10.1016/j.orgel.2016.07.009).
- [12] Feng G., Tay C Y., Chui Q X., Liu R., Tomczak N., Liu J., Tang B Z., Leong D T., Liu B. (2014), Ultrabright organic dots with aggregation-induced emission characteristics for cell tracking, *Biomaterials*, 35, 8669-77 (DOI: 10.1016/j.biomaterials.2014.06.023).